304243-R00017
Revision B

ITER WIDE ANGLE VIEWING SYSTEM PROJECT

55.GA SYSTEM DESIGN DESCRIPTION FOR UWAVS-35 (UP2, 8, 11, AND 14)

Sponsored by Oak Ridge National Laboratory
c/o Princeton Plasma Physics Laboratory

Under Subcontract No: S013437

Prepared by General Atomics
PO Box 85608
San Diego, CA 92186-5608

GA PROJECT 30424

Released 2024/12/04

Released 2024/12/04

GENERAL ATOMICS

REVISION HISTORY

Revision	Date	Description of Changes
A	2024/07/18	Initial Release
B	See Watermark	Comments received by ITER Organization and recorded in IDM have been addressed individually and are tabulated in Appendix C.

POINT OF CONTACT INFORMATION

PREPARED BY:			
Name	**Position**	**Email**	**Phone**
Sean McCartney	Engineer	Sean.McCartney@ga.com	858-455-6652
APPROVED BY:			
Name	**Position**	**Email**	**Phone**
Ramon Thomson	Quality Engineer	Ramon.Thomson@ga.com	858-455-9268
Sean McCartney	Lead Engineer	Sean.McCartney@ga.com	858-248-6652
Anthony Gattuso	Program Manager	Anthony.Gattuso@ga.com	858-455-2910

Released 2024/12/04

Released 2024/12/04

TABLE OF CONTENTS

REVISION HISTORY ..... **II**
POINT OF CONTACT INFORMATION ..... **II**
ACRONYMS ..... **X**
1 INTRODUCTION **1**
1.1 Purpose 1
1.2 Scope 1
1.3 Definitions 2
2 REQUIREMENTS **5**
3 SAFETY **8**
4 DESIGN ARCHITECTURE **10**
4.1 Global Design Architecture 10
4.2 Functional Architecture 11
4.3 Subsystem Design Architecture 14
5 DESIGN METHODOLOGY **19**
5.1 Requirements 19
5.2 Optical Model 19
5.3 Mechanical Design Approach 20
5.4 Skeleton Design Methodology 20
6 SUBSYSTEM DESIGN DESCRIPTIONS **22**
6.1 Front End Optical Modular System 22
6.2 Interspace Optics Tube 29
6.3 Bioshield Optical Labyrinth 30
6.4 Back End Optics and Cameras 31
7 SYSTEM PERFORMANCE **34**
7.1 Optical Performance 34
7.2 IR Measurement 34
7.3 Visible Measurement 36
7.4 Tolerances Analysis 36
7.5 STOP Analysis 41
7.6 Active Alignment 51
8 CALIBRATION **53**
8.1 Calibration Strategy 53
8.2 Back-end Calibration Design 54
8.3 Transmission Filament Design 55
9 MIRROR CLEANING RF DESIGN **58**
9.1 Mirror Cleaning System RF Design Overview 58
9.2 Prematcher 60
9.3 RF Generator and Active Matching Network 61
9.4 Notch Filter 62
9.5 Transmission Lines 64
10 INSTRUMENTATION AND CONTROL ARCHITECTURE **68**
11 INTERFACES **70**
12 ASSEMBLY STRATEGY **72**

Released 2024/12/04
Released 2024/12/04

12.1 Installation Sequence 72
12.2 Factory Assembly 73
12.3 Factory Qualification Testing....74
12.4 Onsite Assembly....78
12.5 Alignment Method....80
12.6 Alignment Requirement Verification....83
12.7 Port Plug Testing at PPTF 84
12.8 Onsite Testing and Commissioning....85

13 REMOTE HANDLING 87

13.1 Remote Handling Compatibility Assessment....87
13.2 Plant Definition 88
13.3 Task Definition Forms....89

14 RISK ANALYSIS....91

14.1 Fire Assessment....91
14.2 Visible Species Measurements....95
14.3 Heat Flux Measurement....96
14.4 Front-to-End Calibration (F2E)....96
14.5 Ghost Images 96
14.6 Neutron Damage of Ceramics....97
14.7 Stepper Motors Selection....99
14.8 MIC Coax Thermo-nuclear Load....103
14.9 Mirror Cleaning Long-term Redeposition 104
14.10 RF Transmission Loss 105
14.11 DSM Surface Tolerances....106
14.12 In-Vessel Mirror Fabrication....107
14.13 In-Vacuum Mirror Module Fabrication....107
14.14 In-Vessel Mirror Module Stability 107
14.15 Ex-Vessel Condensation....108
14.16 Blackbody Heat Management....108
14.17 Use of Cadmium....109
14.18 Dust Protection 110

15 PROTOTYPES....112

15.1 Mirror Cleaning Prototype 112
15.2 First Mirror Prototype 123
15.3 Transmission Filament Prototype....125
15.4 Shutter Prototype....126

REFERENCES 128

APPENDIX A UWAVS SYSTEM DIAGRAMS A-1

APPENDIX B OPTICALLY SIGNIFICANT INTERFACES B-1

Released 2024/12/04

Released 2024/12/04

LIST OF FIGURES

Figure 1. Coverage of divertor from a) one UWAVS diagnostic and b) five Upper Port UWAVS diagnostics. 1
Figure 2. DET-07077-D, 55.GA CM model to USDA. 3
Figure 3. 55.GA Enovia tree for UP02 and UP08 4
Figure 4. 55.GA Enovia tree for UP11 and UP14. 4
Figure 5: 55.GA Diagnostic System. 10
Figure 6. UWAVS system architecture. 11
Figure 7. In-Vessel optics provide large FOV imager and optical relay. 12
Figure 8. Interspace mirrors provide alignment mirrors and a second optical relay 12
Figure 9. Port cell optics provide beam splitting, shaping, and correcting optics. 14
Figure 10. FEOMS decomposition and functional interfaces. 14
Figure 11. Bullnose decomposition and functional interfaces. 15
Figure 12. IOT decomposition and functional interfaces. 16
Figure 13. BOL decomposition and functional interfaces. 16
Figure 14. BEOC decomposition and functional interfaces. 17
Figure 15. UWAVS Optical Model. 19
Figure 16. CATIA optics CSKE. 20
Figure 17. PPAD and PCAD references linked to UPP RSKE. 21
Figure 18. PCAD virtual coordinate system established 11 degrees off axis of PPAD. 21
Figure 19. FEOMS modules and optics in the DSM. 22
Figure 20. UWAVS-35 Bullnose assembly (Front Mirror Unit). 23
Figure 21. In-vessel shutter architecture 24
Figure 22. In-vessel shutter cross-sectional view. 25
Figure 23. Shutter operational states (a) Full closed, (b) Full open, (c) Closed internal state, (d) Open internal state. 26
Figure 24. FEOMS mirror module design 27
Figure 25. Beam path through A30 mirror modules 28
Figure 26. Exploded views of A30 mirror modules a) A30M1 and b) A30M2 28
Figure 27. Exploded views of A30 mirror modules a) A30M3 and b) A30M4 28
Figure 28. IOT subsystem (a-b) in context and (c) isolated with primary assemblies annotated. 29
Figure 29. BOL between the IOT (left) and the BEOC (right). 30
Figure 30. BOL dogleg with light beam visible (left) top-down view of dogleg layout (right). 31
Figure 31. Back-End Optics and Cameras (doors removed for clarity). 32
Figure 32. BEOC main optical layout. 33
Figure 33. IR measurement data flow and processing scheme. 35
Figure 34. UWAVS mirror module interfaces to DSM. 43
Figure 35. FEA and RBM contributions to spot size increment by component and for assemblies 45
Figure 36. IR-1 Camera objective with the materials listed 50
Figure 37. Example calibration timeline 54

Released 2024/12/04
Released 2024/12/04

Figure 38. Calibration optical layout 55
Figure 39. Preliminary transmission filament design 56
Figure 40. Comparison of filament light source positions and light back to sensor. 57
Figure 41. Filament on shutter blade inside the Bullnose. 57
Figure 42. Simplified RF mirror cleaning system schematic. 59
Figure 43 Mechanical assembly of the bullnose with key RF components identified. 59
Figure 44. The fixed prematcher board layout (left) with the signal trace shown in brown and ground plane shown in gray. Calculated S-parameters of the prematcher. 61
Figure 45 Commercial 60 MHz, 1 kW RF generator. 61
Figure 46 Active Matching Network and Smith chart for 1 of the 3 available tuning ranges 62
Figure 47 Compact NF Assembly.....63
Figure 48 HFSS Analysis of the compact NF with the slider at the middle position. 64
Figure 49 Technical data for the selected ex-vessel coaxial cable type.....65
Figure 50. Illustration of plant layout showing cubicle locations and anticipated cable runs for RF transmission lines. 66
Figure 51. Illustration of the instrumentation and controls for 55.GA single port 68
Figure 52. 55.GA design breakdown into subsystems.....69
Figure 53. UWAVS installation process sequence. 72
Figure 54. FEOMS mirror modules subassemblies 73
Figure 55. FEOMS mirror modules mechanical inspection 73
Figure 56. Assembled bullnose used for validation of mirror cleaning system. 74
Figure 57. Shutter assembly setup on a test bench.....75
Figure 58. FEOMS setup for optical axis verification. 76
Figure 59. FEOMS transmitted wavefront verification.....76
Figure 60. IOT imaging performance test configuration.....77
Figure 61. IOT distortion and magnification test configuration. 77
Figure 62. a) Exploded and b) assembled pictorial views of the FEOMS within the DSM. 79
Figure 63. Installation sequence of ex-vessel subsystems in the Interspace and Port Cell.....80
Figure 64. Laser tracker and nest mounted spherical mounted retroreflectors (SMRs) 81
Figure 65. Example laser tracker metrology of (a) PCSS frame, (b) tenant location on PCSS, and (c) ISS and PCSS installed in Upper Port. 82
Figure 66. Laser tracker with (a) T-probe stylus used with (b) integrated fiducials.....82
Figure 67. ISS and PCSS trolley SMR locations for final subsystem positional requirements verification. 83
Figure 68. Optical axis alignment test configuration for the installed FEOMS. 83
Figure 69. Imaging performance test configuration for the installed FEOMS. 84
Figure 70. Image performance verification of (a) IOT using an interferometer and (b) BEOC using fiber lasers mounted to a curved fiducial. 84
Figure 71. Fishbone diagram of perquisites for System Commissioning 86
Figure 72. Breakdown of the UWAVS-35 Remote Handling Documents. 87
Figure 73. Removal of the A20 mirror module. 89
Figure 74. Port Cell loading conditions in case of fire. 92
Figure 75. Volumetric swelling in Alumina due to neutron fluence (E > 0.1MeV) 98

Released 2024/12/04
Released 2024/12/04

Figure 76. Radiation hardened stepper motors integrated onto the A40M2 mirror assembly. 100
Figure 77. Max body forces imposed on magnetic components due to the ITER magnetic field during a plasma shot (17MA-DINA2019-01). a) X,Y, Z components b) magnitude 101
Figure 78. Bullnose with MIC9 coax 104
Figure 79. Illustration showing benefit of relocating UP02 and UP17 RF generators to NE Shielded Corner. 106
Figure 80. Thermal calibration temperature plot of internal ambient air temperature taken at IR blackbody source location. 108
Figure 81. Surface temperature plots for thermal calibration of (a) IR blackbody source and (b) IR cameras. 109
Figure 82. UWAVS ISS-PCSS shroud (a) in bioshield (b) components and size. 110
Figure 83. Mirror Cleaning Prototype hardware. 112
Figure 84. Comparison of the Prototype Bullnose (left) to the UWAVS-35 Bullnose (right). 113
Figure 85. The prototype Bullnose with key elements identified. 114
Figure 86. Comparison of the prototype mirror (left) with the UWAVS-35 A10 mirror (right). 115
Figure 87. Detailed view of the prototype mirror assembly. 115
Figure 88. Cross-section view of the prototype mirror assembly. 116
Figure 89. RF connection between the mirror and the prematcher PCB. 116
Figure 90. S-Shaped NF (left) and C-Shaped NF with VCR fittings (right). 117
Figure 91. NF performance when tee onto a 50 ohm transmission line. 118
Figure 92. Prototype bullnose with the NF in its rotated orientation. 118
Figure 93. Measured smith chart of mockup notch filter (red line) with HFSS results overlayed (green line). Note impedance values are given normalized to 50 ohms. 121
Figure 94. Plasma Impedance measurement diagram 123
Figure 95. Reflectivity of Pt coated specimens before and after simulated steam ingress event showing minimal loss of reflectivity. 124
Figure 96. Diffuse and specular reflectivity of Pt coated samples before and after mirror cleaning showing minimal degradation. 124
Figure 97. Prototype test apparatus a) conceptual layout b) existing hardware. 125
Figure 98. Representation of filament life cycle test. 126
Figure 99. UWAVS system architecture. A-1
Figure 100. FEOMS decomposition and functional interfaces. A-2
Figure 101. Bullnose decomposition and functional interfaces. A-3
Figure 102. IOT decomposition and functional interfaces. A-4
Figure 103. BOL decomposition and functional interfaces. A-5
Figure 104. BEOC decomposition and functional interfaces. A-6
Figure 105. Simplified RF mirror cleaning system schematic. A-7
Figure 106. Illustration of the instrumentation and controls for 55.GA single port A-8
Figure 107. UWAVS installation process sequence. A-9

Released 2024/12/04
Released 2024/12/04

LIST OF TABLES

Table 1. Applicable CAD Models. 2
Table 2. Annex-B Measurement Parameter Overview with Conditions and Required Accuracies for Primary Measurements 5
Table 3. Annex-B Measurement Parameter Overview with Conditions and Required Accuracies for Secondary Measurements 6
Table 4. Diagnostic System Classifications per Annex B 8
Table 5. Overview of key optical performance requirements 34
Table 6. Generic DSM mechanical tolerances 37
Table 7. Critical DSM interface tolerances 37
Table 8. ISS and PCSS Installation Tolerances 37
Table 9. UWAVS component tolerances 38
Table 10. Optic tolerance budget 40
Table 11. Overview of UWAVS tolerance analyses and results (Vis-1 channel) 41
Table 12. Imaging resolution error contribution by tolerances for all channels 41
Table 13. Displacements and rotations at module attachment points 42
Table 14. Mirror Displacements and Rotations 43
Table 15. A20 and A30 Mirror Displacement and Rotation Estimates. 43
Table 16. Spot size increment due to surface FEA and RBM 45
Table 17. List of IOT materials used in thermal analysis 46
Table 18. List of IOT optic materials and thickness 46
Table 19. Effect of IOT thermal expansion on spot size 47
Table 20. List of Material and CTE as used in Zemax Simulations 48
Table 21. RMS Spot Radius Increment for BEOC at 37°C with and without A40 Active Alignment 48
Table 22. RMS spot increment for the IR-1 channel at 37°C, with and without compensation 49
Table 23. Thermal compensators for VIS-1 and IR-1 channels 50
Table 24. Final system compensator range for IR-1 and Vis-1 channels 51
Table 25. RMS Spot Radius Increment for Operational Load 51
Table 26. Overview of active alignment system Analysis Results 52
Table 27. Estimated Cable Lengths and Associated Power Loss 67
Table 28. 55.GA Interface Sheets 70
Table 29. 55.GA Piping & Instrumentation Diagrams 71
Table 30. 55.GA Cabling Diagrams 71
Table 31. 55.GA Process Flow Diagrams 71
Table 32. 55.GA Single Line Diagrams 71
Table 33. PPTF Test Sequence 85
Table 34. List of UWAVS-35 Remote Handling Task Definition Forms 89
Table 35. IOT Quantified Materials and Melting Points 92
Table 36. BOL Quantified Materials and Melting Points 93
Table 37. BEOC Quantified Materials and Melting Points 93

Released 2024/12/04
Released 2024/12/04

Table 38. IOT Combustible materials within the Port Cell Interspace 94
Table 39. BOL Combustible materials within the Port Cell Interspace 94
Table 40. BEOC Combustible materials within the Port Cell.....94
Table 41. Ceramic Materials used in Bullnose 99
Table 42. Body forces on the A40 mirror actuator assemblies.....102
Table 43. Estimated mass of Co in UWAVS system due to stepper motors 103
Table 44. Improvement to Cable Runs by Relocating RF Generators 106
Table 45. Optically significant interfaces of the FEOMS B-1
Table 46. Optically significant interfaces of the IOT..... B-2
Table 47. Optically significant interfaces of the BEOC..... B-3

Released 2024/12/04

Released 2024/12/04

ACRONYMS

Acronym	Description
AE	Algorithms and External Data
ALARA	As Low as Reasonably Achievable
BE	Back End
BEOC	Back End Optics & Cameras
BOL	Bioshield Optical Labyrinth
BP-HiPIMS	Bipolar High Power Impulse Magnetron Sputtering
CDA	Clean Dry Air
COTS	Commercial-Off-the-Shelf
CP	Closure Plate
CSKE	Component Skeleton
DFW	Diagnostic First Wall
DSM	Diagnostic Shield Module
EM	Electromagnetic
F2E	Front-to-End
FEOMS	Front End Optical Modular Systems
FDR	Final Design Review
FMU	First Mirror Unit
HCC	Hard Core Components
HCF	Hot Cell Facility
HFSS	High Frequency Simulation Software
IO	ITER Organization
IOT	Interspace Optics Tube
ISS	Interspace Support Structure
PC	Port Cell
PC-I	Port Cell Interspace
PCSS	Port Cell Support Structure
PDR	Preliminary Design Review
PIC	Protection Important Component
PID	Piping & Instrumentation Diagram
PPTF	Port Plug Test Facility

Released 2024/12/04
Released 2024/12/04

Acronym	Description
PSKE	Positional Skeleton
QC	Quality Class
RH	Remote Handling
RSKE	Reference Skeleton
SDD	System Design Description
SDDR	Shut Down Dose Rate
SI	International System of Units
TCS	Test and Conditioning State
TCWS	Tokamak Cooling Water System
TM	Transmission Monitoring
UPP	Upper Port Plug
UWAVS	Upper Wide Angle Viewing System
UWS	Universal Work Station
VV	Vacuum Vessel
WFE	Wavefront Error

Released 2024/12/04

Released 2024/12/04

1 INTRODUCTION

The 55.GA Upper Port Wide Angle Viewing System (UWAVS) images the divertor surface in sections and provides machine protection (monitoring for overheating of surfaces), plasma control (basic and advanced), and physics measurement roles. UWAVS is located in UP 2/8 (RFDA), UP 11/14 (USDA) and UP 17 (EUDA). The UWAVS coverage of the divertor is shown in Figure 1.

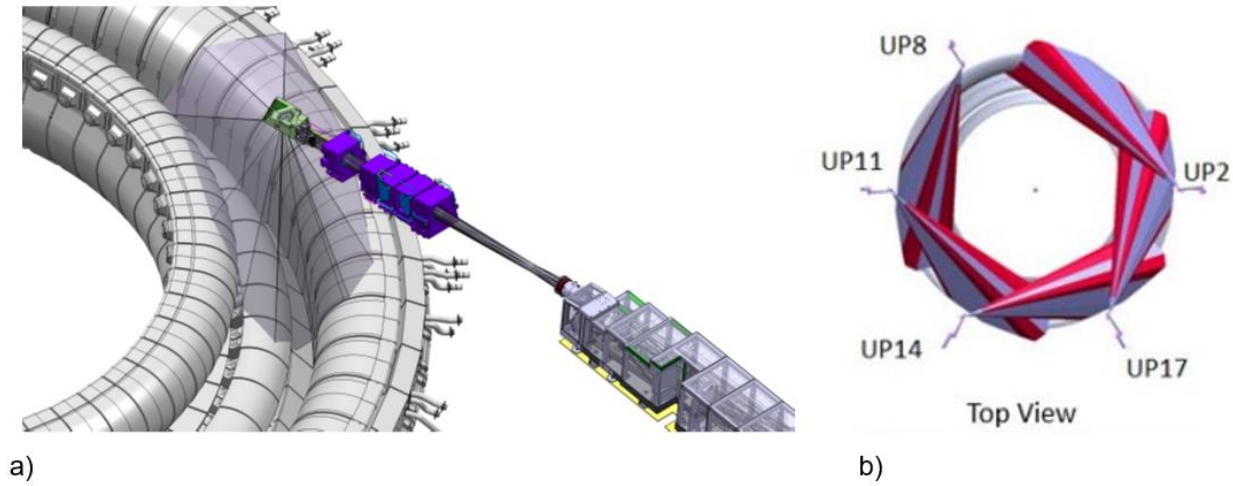

Figure 1. Coverage of divertor from a) one UWAVS diagnostic and b) five Upper Port UWAVS diagnostics.

1.1 Purpose

This document provides the System Design Description (SDD) of the 55.GA diagnostic system at the preliminary design phase of the program.

1.2 Scope

This document provides high-level definitions of the UWAVS-35 system architecture, functions, decomposition, and performance. This document does not include discussion of the UWAVS-17 system. However, the ex-vessel systems are designed to be common for both UWAVS-17 and UWAVS-35 designs. This report does not include a summary of the Structural Integrity Reports ([1], [2]).

The high-level summaries in the SDD reference additional documents that include further detail into the optical design, mechanical design, I&C architecture, system integration, assembly and verification testing strategy. The report also includes content not captured in other documentation including general safety considerations, details of the RF mirror cleaning design, status of prototype activities, and a risk analysis.

Released 2024/12/04
Released 2024/12/04

1.3 Definitions

1.3.1 Units

The units of the international system (SI) are used unless otherwise stated.

1.3.2 Coordinate Systems

Coordinate system references are consistent with the ITER Tokamak Global Coordinate System [3] unless otherwise stated.

1.3.3 Geometry

The official configuration management (CM) models provided by USDA for all 55.GA ports is listed in Table 1 below and shown for reference in Figure 2. Table 1 also lists the native 55.GA CAD geometry and versions referenced throughout this report.

Table 1. Applicable CAD Models.

Model	CAD File
55.GA CM model to USDA	DET-07077-D_CMM_DIR_12-7-2023
Baseline Optical Model in CATIA	TNO2022_V010_42_20221209_SOLID_BEAM.CATPart, A.4
CATIA skeleton of optics elements	UWAVS_OPTICS_ELEMENTS_CSKE.CATPart, A.23
FEOMS CATIA files	UWAVS_FEOMS_SUBYSYSTEM_ASSY.CATProduct, A.75
Bullnose CATIA files	UWAVS35_BULLNOSE_ASSY.CATProduct, A.7
IOT CATIA File	UWAVS_IOT_SUBYSYSTEM_ASSY.CATProduct, A.192
BOL CATIA File	UWAVS_BOL_SUBYSYSTEM_ASSY.CATProduct, A.26
BEOC CATIA File	UWAVS_BEOC_SUBSYSTEM_ASSY.CATProduct, A.40
Upper Port Plug CSKE references	15_52_55_UPORT_PLUG_RSKE#2P38ES-Y.CATPART

Released 2024/12/04
Released 2024/12/04

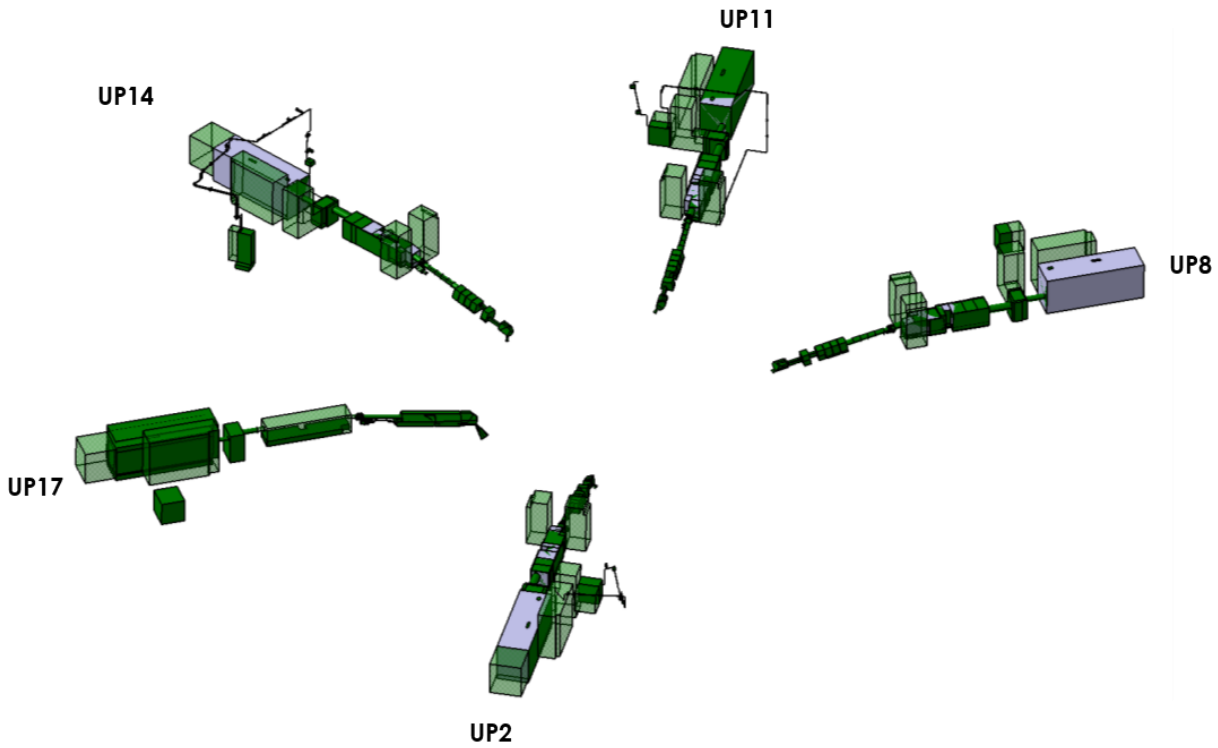

Figure 2. DET-07077-D, 55.GA CM model to USDA.

1.3.4 ENOVIA Trees

The associated ENOVIA tree geometry for the 55.GA at PDR are shown below for UP02 and UP08 in Figure 3, and UP11 and UP14 in Figure 4.

Released 2024/12/04

Released 2024/12/04

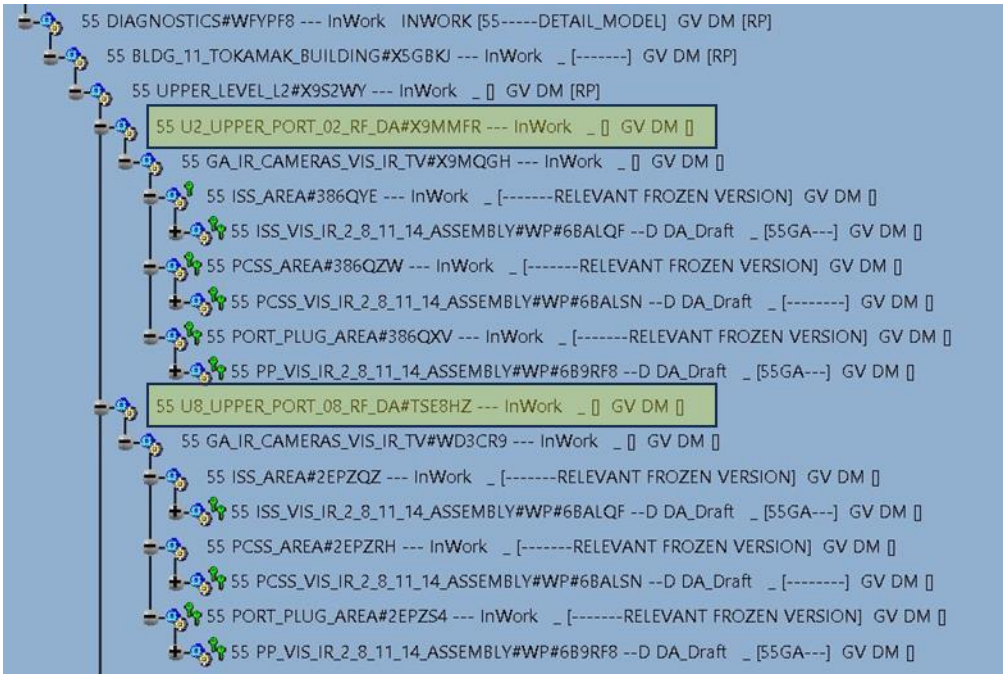

Figure 3. 55.GA Enovia tree for UP02 and UP08

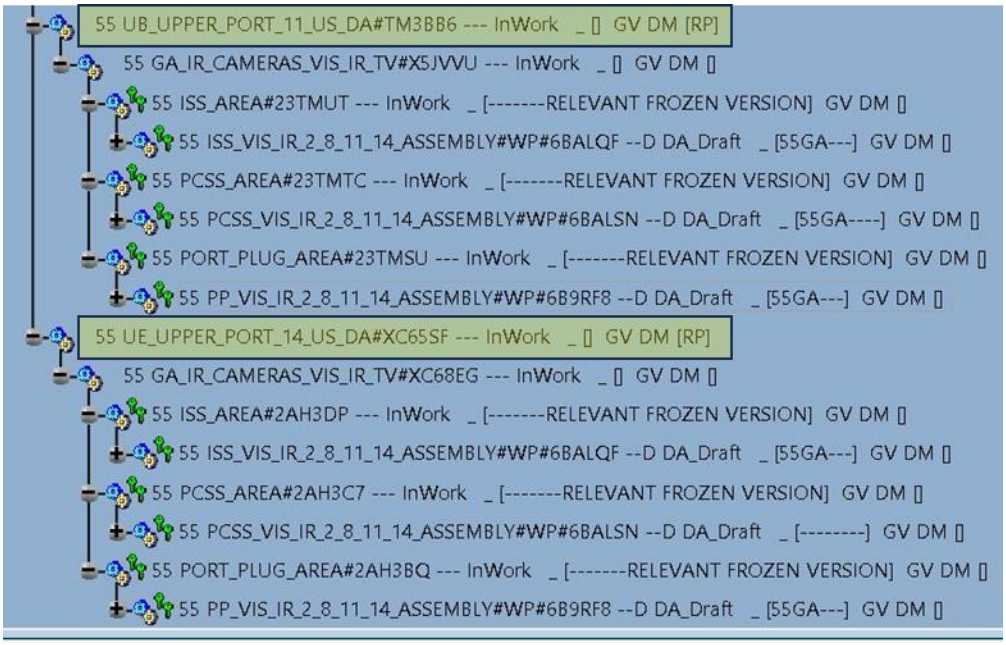

Figure 4. 55.GA Enovia tree for UP11 and UP14.

Released 2024/12/04

Released 2024/12/04

2 REQUIREMENTS

55.GA diagnostic measurement parameters are essentially the stakeholder requirements that drive the design of the system. 55.GA measurement roles are described in the Sub-System Requirement Document sSRD-55.GA (IR Cameras: Vis/IR TV (Upper) [4]), and in the 55.GA PA Annex B [5]. Detailed description and analysis are provided in 55.GA UWAVS-35 System Detailed Performance Definition [6].

Table 2 provides an overview of the primary role measurements of the 55.GA diagnostic. In addition, it indicates which parameters are determined directly by the UWAVS system and which measurement parameters require additional processing and interpretation. In the latter case, measurement algorithms are not yet available and assumed to be provided later by ITER. Hence the accuracy of these measurement parameters cannot be established at this stage.

Table 2. Annex-B Measurement Parameter Overview with Conditions and Required Accuracies for Primary Measurements

DiagSyst_Name	DiagRoleName	RoleName	MeasName	ParameterName	ConditionName	RangeValue	TimeFreq Resol	SpatialWave	Accuracy
55.GA	Primary	1a.1 MP	16. Divertor operational parameters	Max. surface temperature	-	200 - 3600°C	2 ms	-	10%
55.GA	Primary	1a.1 MP	17. First wall (FW) visible image & wall temperature	FW Surface luminance	All heating ports, upper strike region, dome, baffle. > 50 % of rest, evenly distributed.	40 -1E5 cd / m2	10 ms	3 mm	30 % absolute, 1% relative
55.GA	Primary	1a.2 BC	17. First wall (FW) visible image & wall temperature	FW Surface temperature	All heating ports, upper strike region, dome, baffle. > 50 % of rest, evenly distributed.	200 - 3600°C	10 ms	5 mm	20°C
55.GA	Primary	1b. AC	38. Heat loading profile in divertor	Power load	Default	0.1 - 25 MW m-2	2 ms	3mm	0.1
55.GA	Primary	1b. AC	38. Heat loading profile in divertor	Power load	Disruption	0.02 - 5 GW m-2	0.02 ms	3 mm	0.2
55.GA	Primary	1b. AC	38. Heat loading profile in divertor	Surface temperature	-	1000 - 3600 °C	0.02 ms	3 mm	0.1
55.GA	Primary	1b. AC	38. Heat loading profile in divertor	Surface temperature	-	200 - 1000 °C	2 ms	3 mm	0.1
55.GA	Primary	2. PHY	17. First wall (FW) visible image & wall temperature	FW surface temperature during ELMs	6 % of each blanket row, dome and baffles	400 - 3600°C	20 us	5 mm	20°C

Derived from the UWAVS IR and Vis data using calibration factors and assumptions on the surface emissivity

Derived from the UWAVS IR data and other diagnostic measurements. Requires engineering development from ITER IO sources.

Table 3 provides an overview of the measurements with supplementary or back-up roles for the UWAVS diagnostic.

Released 2024/12/04
Released 2024/12/04

Table 3. Annex-B Measurement Parameter Overview with Conditions and Required Accuracies for Secondary Measurements

DiagSyst_Name	DiagRoleName	RoleName	MeasName	ParameterName	ConditionName	RangeValue	TimeFreq Resol	SpatialWave	Accuracy
55.GA	Back Up	1a.2 BC	35. Impurity and D,T influx in divertor	GD, GT	-	1E19 - 1E25 at s-1	1 ms	50 mm	0.3
55.GA	Back Up	1a.1 MP	35. Impurity and D,T influx in divertor	GBe, GC, GW	-	1E17 - 1E22 at s-1	1 ms	50 mm	0.3
55.GA	Back Up	1a.1 MP	14. H-mode, ELMs and L-H mode transition indicator	ELM Da bursts	Main plasma	-	20 ms	one site	-
55.GA	Back Up	1a.2 BC	14. H-mode, ELMs and L-H mode transition indicator	L-H Da step	Main plasma	-	20 ms	-	-
55.GA	Supplementary	1a.2 BC	02. Plasma position and shape	Divertor channel location (r dir.)	Ip > 3 MA	-	10 ms	-	10 mm
55.GA	Supplementary	1a.2 BC	02. Plasma position and shape	Divertor channel location (r dir.)	Ip quench	-	10 ms	-	20 mm
55.GA	Supplementary	1b. AC	31. Escaping alphas and fast ions	First wall flux, Non-Alphas	Default	0.001 - 0.2 MW m-2	100 ms	a/10 along poloidal direction	0.1
55.GA	Supplementary	1b. AC	31. Escaping alphas and fast ions	First wall flux, Non-Alphas	Transients	0.01 - 2 MW m-2	10 ms	a/10 along poloidal direction	0.3
55.GA	Supplementary	2. PHY	31. Escaping alphas and fast ions	First wall flux, Alphas	Default	0.01 - 2 MW m-2	100 ms 0.1ms**	a/10 along poloidal direction	0.1
55.GA	Supplementary	2. PHY	31. Escaping alphas and fast ions	First wall flux, Alphas	Transients	0.1 - 20 MW m-2	10 ms	a/10 along poloidal direction	0.3
55.GA	Supplementary	1a.1 MP	12. Impurity species monitoring	Cu Influx	-	5E17 - 2E21 s-1	-	-	-
55.GA	Supplementary	1a.2 BC	12. Impurity species monitoring	Extrinsic (Ne, Ar, Kr) influx	-	5E18 - 8E21 s-1	-	-	-
55.GA	Supplementary	1a.1 MP	12. Impurity species monitoring	W influx	-	5E16 - 2E20 s-1	-	-	-

Derived from spectral line intensities measured by UWAVS using specialized atomic physics codes and other measurements. ITER should calculate this measurement.

More definition needed….actual L-H transition will be difficult to detect although occurrence of ELMs is achievable.

Requires magnetic equilibrium reconstruction and input from magnetics and possibly MSE and thermal profiles (Te and Ne). UWAVS cannot satisfy this requirement.

UWAVS can detect local heating, but it will not be known if due to escaping alphas and other particle without correlation with other diagnostic data. ITER should calculate this measurement.

Released 2024/12/04

Released 2024/12/04

For species influx measurement, UWAVS inherently provides a line integrated intensity measurement, based on a single spectral line integrated intensity. This will be the target deliverable data for UWAVS. To determine species influx a combination of plasma model, plasma measurement data, and 3D-tomography are required. The calibration factors are needed to derive the absolute line intensities from the raw signals provided by UWAVS.

Determining the heat load and particle fluxes requires additional input from IO. UWAVS will provide wall radiance and temperature as the inputs for determination of the heat flux. These measurements will be addressed during the final design phase.

Released 2024/12/04

Released 2024/12/04

3 SAFETY

The 55.GA design follows the Project Requirements [7] and Safety Roombook [8] guidelines for general safety objectives, occupational safety (ALARA), zoning, and Protection/Safety Important Component (PIC/SIC) classifications. The 55.GA in-vessel and ex-vessel subsystems are separated by two primary confinement barriers consisting of 1) a double-window assembly for transmission of light, and 2) a valve box for pneumatic application of an in-vessel shutter. All the opto-mechanical hardware is located within the Vacuum Vessel (VV), Interspace, and Port Cell. Therefore, secondary barrier components associated with penetrations from the Port Cell to Gallery, and Gallery to Diagnostic Hall are not within the scope of 55.GA. PIC/SIC components and assemblies from Annex [5] are summarized in Table 4 and classified per [9]

Table 4. Diagnostic System Classifications per Annex B

Subsystem Description	Diagnostic Component	Safety Class	Seismic Class	Quality Class	Vacuum Class
Window	Primary Vac Double Window Assembly	SIC-1 (Confinement)	SC1(S)	QC-1	VQC-1
Window	SVS Connections	SIC-1 (Confinement)	SC1(SF)	QC-1	VQC-1
Port Plug Seal Plate system	1st isolation valve for gas feed close to closure plate	SIC-1 (Confinement)	SC1	QC-1	VQC-1
Port Plug Seal Plate system	2nd valve further away from closure plate	SIC-1 (Confinement)	SC1	QC-1	VQC-1

The SIC-1 double-window assembly is an IO design for 55.GA and controlled with an interface sheet [10]. The confinement barrier must withstand 2 bar differential peak pressure, seismic, electromagnetic, and accident loads, in additional to thermal loading from nuclear heating, bakeout, and fire accident temperatures per the load specification [11]. The window assembly is continuously monitored by PBS.31.SV for possible leaks. In addition, the temperature rise due to ECH loads on the windows is monitored for overheating on the external housing by 55.NW and the I&C port integrator systems (PBS.55.Q0/U0).

An in-vessel, pneumatically actuated shutter utilizes a valve box assembly, located in the Port Cell alcove, with two redundant SIC-1 safety valves to operate and protect the vacuum from the positive pressure of the pneumatic shutter actuation. The gas valve box (GVB) also includes two SIC-2 isolated controls for each SIC-1 valve. The GVB provides the double confinement barriers required per vacuum handbook [12]. Refer to Piping and Instrumentation Diagrams (PID) for the SIC-1 an SIC-2 shutter actuation GVB. The GVB design is out of scope for this PDR.

Released 2024/12/04
Released 2024/12/04

The sensors for monitoring the SIC systems components are defined in the PID for each port [13], [14], [15], and [16]. The independence of the SIC-1 control valves are indicated by the Train A and Train B designation in the Cabling diagram for each port [17], [18], [19], and [20].

Fire sectors within the Tokamak Building segregate regions between the Port Cell and Gallery, and Gallery to Diagnostic Hall, and are classified as SIC-2. For 55.GA, the design and qualification of penetrations for these boundaries fall under the primary responsibility of port integrators and IO. However, 55.GA supports designs of safety critical components and penetrations by selecting IO approved cables [21] and interface sheets to ensure adequate safety measures are established. A preliminary fire assessment of 55.GA components per the ITER Fire Safety Approach document [22] is included in section 14.1.

Radioactive waste management encompasses the systematic handling, treatment, storage, and disposal of materials that contain radioactive elements. 55.GA is designed to operate such that it minimizes radioactive waste by selection of approved ITER materials, the use of nuclear shielding materials to minimize exposure, and the use of a modular design architecture to ease waste management during decommissioning [23].

Released 2024/12/04

Released 2024/12/04

4 DESIGN ARCHITECTURE

4.1 Global Design Architecture

UWAVS 55.GA architecture is based on a modular approach that includes key physical and functional subsystems both inside and outside of the Vacuum Vessel (VV) as shown in Figure 5.

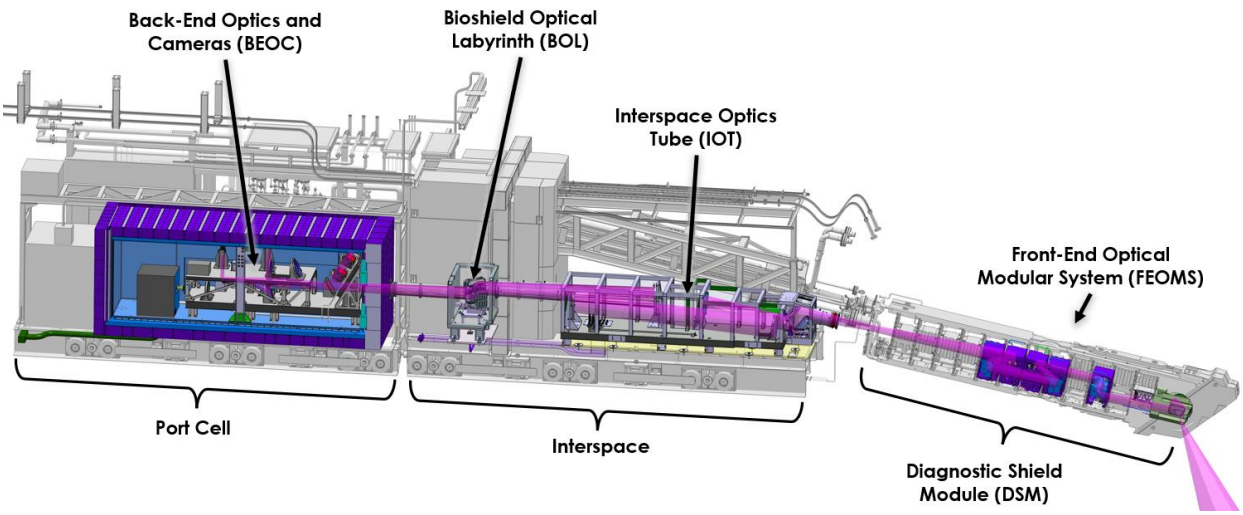

Figure 5: 55.GA Diagnostic System.

In-vessel mirrors mounted in actively-cooled assemblies make up the Front End Optical Modular System (FEOMS), and install in the Diagnostic Shield Module (DSM) that inserts into the Upper Port Plug (UPP) and ultimately, the VV. They are designed mounted on removable mirror modules that are compatible with remote handling (RH) equipment in the hot cell. The vacuum window is the final in-vessel optic. The two tilted sapphire windows provide the required double barrier safety protection at the vacuum boundary as discussed in Section 3.

The interspace subsystems comprise of the Interspace Optical Tube (IOT) and the Bioshield Optical Labyrinth (BOL). The IOT includes two actuated mirrors to provide active beam steering and correct for thermal deformations of the VV. The aft dog legs in the IOT relay the image from the FEOMS through the BOL to the BEOC. The BOL serves as the final dog leg with two tip and tilt gimbals that provide coarse alignment of IOT to BEOC. The BOL is housed inside the bio shield wall.

The BEOC subsystem encloses beam splitting, shaping, and correcting optics for camera imaging. It includes two visible and two infrared cameras and optical paths. It houses calibration source equipment and RF matching electronics. The BEOC is surrounded with protective shielding layers to absorb neutron, gamma, and electromagnetic radiation to protect sensitive electronics.

Released 2024/12/04
Released 2024/12/04

Figure 6 (landscape version in Figure 99 of APPENDIX A) shows the UWAVS system architecture and key interfaces. Color codes and line types are noted in the legend.

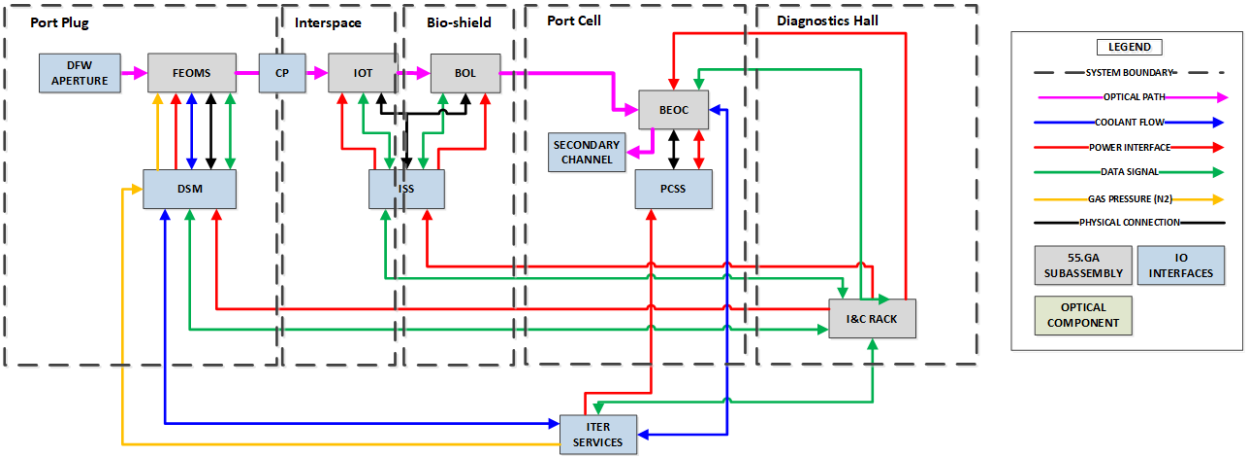

Figure 6. UWAVS system architecture.

4.2 Functional Architecture

Very similar with the physical architecture, the functional architecture of the system can be decomposed into functional subsystems.

4.2.1 Functions of In-Vessel Optics

The in-vessel optics, collectively known as the FEOMS, primarily act as the large field of view (FOV) imager and an optical relay. The diverter is initially imaged through an 18 mm aperture by two off-axis spherical mirrors, A10-M1 and A10-M2. These mirrors image the large FOV to the space just beyond A10-M2. A10-M1 and A10-M2 exist in a volume with direct exposure to the ITER plasma and A10-M1 has an unimpeded line of sight to the plasma. Following the A10 mirror group is an optical dog-leg, A20-M1 and A20-M2. These mirrors provide a break in the neutron line of sight, so shielding can be installed to reduce nuclear loads on downstream optics. Since A10-M1 and A10-M2 form the divertor image directly after A10-M2, an optical relay is needed to transfer the image further downstream, towards the cameras. This function is performed by the A30 mirror group, which consists of 4 mirrors and serves to correct some of the aberrations caused by the divertors tilted orientation. Finally, the FEOMS is sealed inside the UPP with a pair of wedged sapphire vacuum windows (A35 VW1/ A35 VW2). All mirrors inside the FEOMS are made from ITER grade stainless steel and are water cooled. A10-M1 and A10-M2 are coated with a platinum metal coating, to aid in longevity of repeated plasma cleanings, while remaining mirrors are coated in a protected aluminum coating. An image of the FEOMS optics and beam path are shown in Figure 7.

Released 2024/12/04
Released 2024/12/04

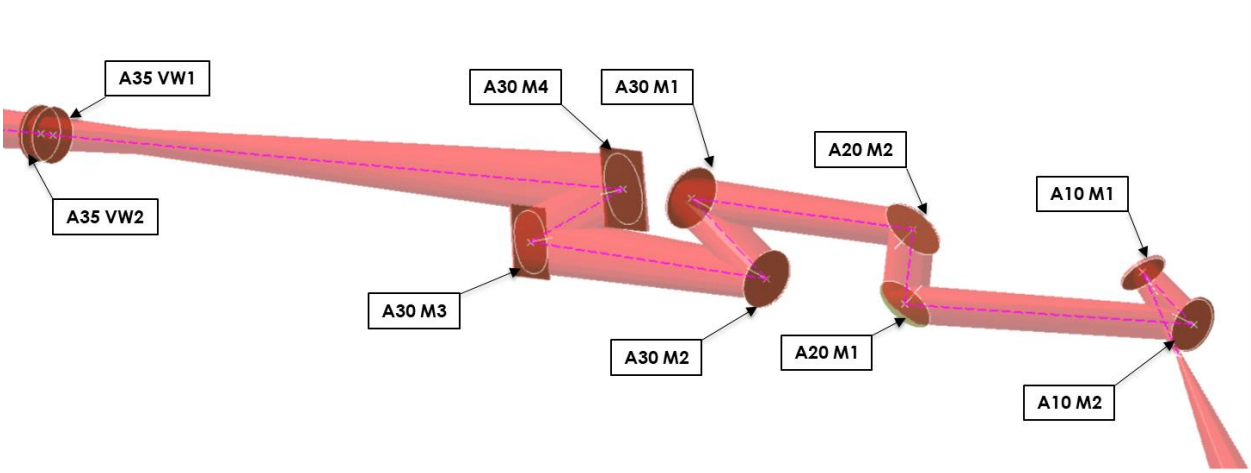

Figure 7. In-Vessel optics provide large FOV imager and optical relay.

4.2.2 Functions of Interspace Optics

After the light leaves the VV and port plug enclosure, it enters the IOT. First, a set of flat, remote actuated, dog-leg mirrors (A40-M1 and A40-M2) provide the means to compensate for thermal expansion in the VV, as well as another opportunity to shield downstream optics from neutron streaming. Next, a set of four mirrors in the A50 mirror group relay the image from the FEOMS in the VV, to the BEOC in the Port Cell (PC). These mirrors also provide additional corrections to the beam, to compensate for upstream aberrations. Leaving the IOT, the beam passes through the BOL. Here, a set of flat, remote actuated mirrors, A60-M1 and A60-M2, provide the means for aligning the IOT to the BEOC. This dogleg sits in the bioshield, again utilizing the offset beam path to provide neutron shielding to downstream optics and electronics. These mirrors are not integrated into an active control loop; they only provide a user determined update to system alignment. An image of the IOT mirrors and beam path are shown in Figure 8.

Released 2024/12/04

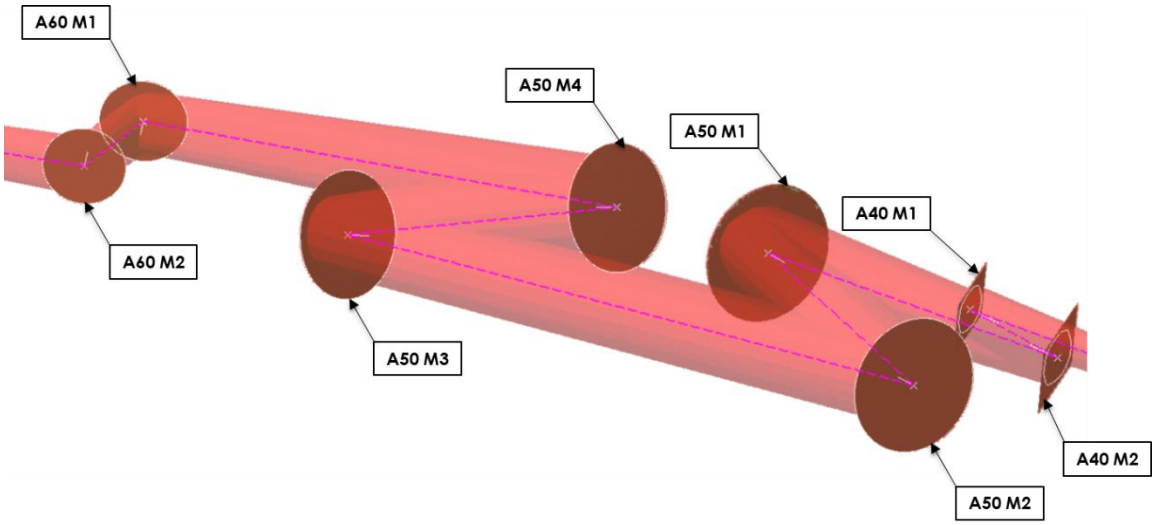

Figure 8. Interspace mirrors provide alignment mirrors and a second optical relay

Released 2024/12/04

4.2.3 Functions of Port Cell Optics

Within the BEOC there are a series of common optics before the chromatic split between the infrared and visible channels. First, a thin sapphire window (A70W1) is used for correcting chromatic aberration induced by the sapphire vacuum windows in the UPP. Next, another thin sapphire beam splitter (A70S1) is used introduce the calibration sources and respective optical legs. Finally, the dichroic beamsplitter A70S2, a fused silica optic, splits the infrared from the visible channels, with the infrared reflecting off the first surface and the visible transmitting through the optic. The entire BEOC enclosure is shielded to reduce neutron, gamma, and electromagnetic radiation incident upon sensitive electronics.

The infrared channel starts with a compound field lens, comprised of A80-L1 and A80-L2, optimized to reduce pupil aberration at the cold stop of the infrared cameras. Here, the two infrared channels are split with another dichroic A80-S1, a silicon optic splitting lower band from higher band, with the lower band reflecting off the beamsplitter and the higher band transmitting. Each infrared channel then reflects off a gold coated N-BK7 fold mirror, towards the infrared imager lens, A80-M1 and A90A for the low IR band, and A80-M2 and A90B for the high band. These compound lenses are identical for each infrared channel and consist of 7 individual lenses assembled into a lens tube. In the low infrared band, the imaging lens is followed by two filters A90A-W1 and A90A-W2. The specifics of these filters are not finalized, one is allocated for low IR bandpass filter, the other is allocated for a neutral density filter if needed. Filters in the high IR band are similar, A90B-W1 and A90B-W2, with the bandpass filter passing only the spectrum of interest. Finally, infrared light passes through the cold stop of the IR cameras, then to the sensor.

Similarly to the infrared channels, the two visible channels pass through a common achromatic doublet lens (A100-L1/2) before splitting into the two visible channels. This doublet helps correct chromatic aberrations over the large visible range (400-750nm) and limit beam size further downstream in the visible channel. The visible beamsplitter, A100-S1, splits the two visible channels, with the reflected path going towards the high resolution visible channel, and the transmitted path going towards the high speed visible channel. Each channel utilizes a silver coated folding mirror, A100-M1 for the high resolution channel, and A100-M2 for the high speed channel. Each channel has a set of 3 filter wheels after the fold mirrors. Two of the filter wheels contain spectral filters to enable isolating specific elemental spectral lines. The third wheel contains a series of increasing attenuation neutral density filters to aid keeping intensities within the dynamic range of the cameras. After spectral filtering and intensity normalization, each visible channel has a compound lens optimized for different magnifications, A110A for the high resolution channel and A110B for the high speed channel. An image of the BEOC optics and beam path are shown in Figure 9.

Released 2024/12/04
Released 2024/12/04

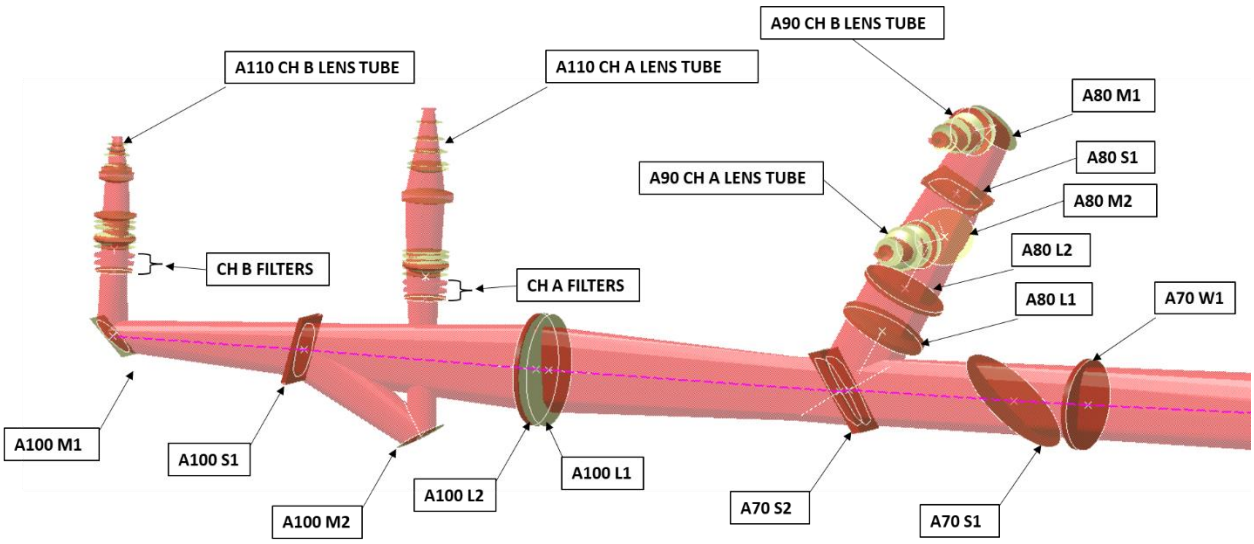

Figure 9. Port cell optics provide beam splitting, shaping, and correcting optics.

4.3 Subsystem Design Architecture

55.GA subsystems can also be decomposed further using the modular approach.

The FEOMS consists of six different subassemblies that support and house water cooled focusing mirrors. The first two mirrors are housed in the First Mirror Unit (FMU) or Bullnose, nested inside the Diagnostic First Wall (DFW). This assembly mounts into a cavity at the front of the DSM. Figure 10 (landscape version in Figure 100 of APPENDIX A) shows the FEOMS block diagram that highlights function, decomposition, and interfaces. Color codes and line types are noted in the legend.

Released 2024/12/04

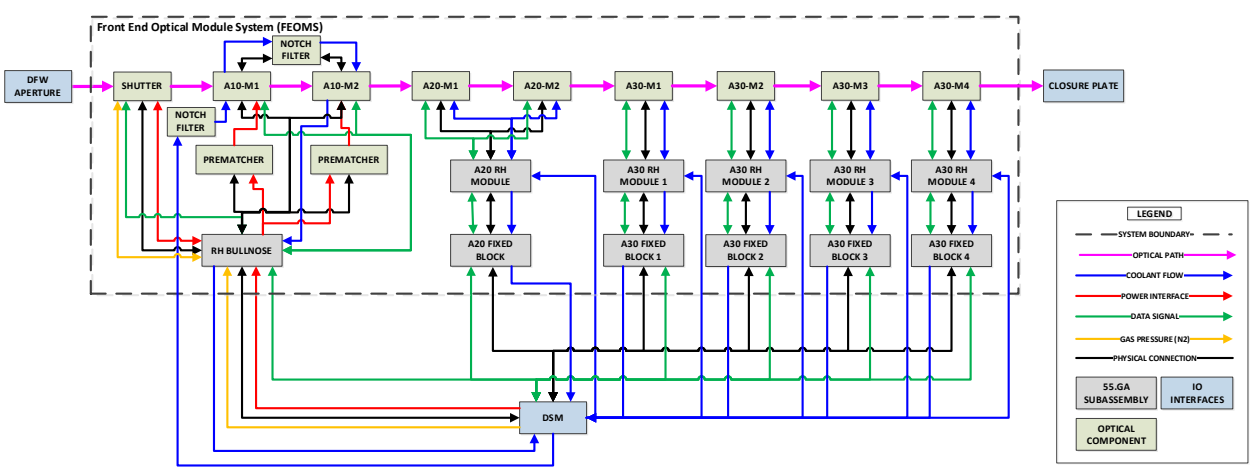

Figure 10. FEOMS decomposition and functional interfaces.

Two additional groups of water-cooled mirror assemblies are located behind shielding panels nested between the DSM partitions that comprise the rest of the front-end optical module

Released 2024/12/04

assemblies. These serve as the support structure for the in-vessel optical doglegs that relay the image through the rest of the DSM, backfill, and shielding.

The A20 group consists of two water cooled mirrors located in the same module in DSM bay 2 forming the first optical dogleg.

The A30 group consists of four modules each containing a single water-cooled mirror in a zigzag configuration spanning DSM bay 4 through 7. The architecture of each module is similar, though each requires a unique design to accommodate the beam path shape, position, and direction.

The Bullnose is the front mirror unit that houses the A10 small hole imaging mirrors. These mirrors act as wide-angle imagers that collimate a beam back to the rest of the FEOMS. The aperture is small to minimize contamination from exposure to the plasma. A shutter is also mounted on the back of the aperture and closed as required for protection during events such as Glow Discharge Conditioning (GDC), Ion Cyclotron Wall Conditioning (ICWC), and Electron Cyclotron Wall Conditioning (ECWH). UWAVS is capable of transmission monitoring between shots and the first two mirror units are designed with in-situ RF plasma cleaning capability. Figure 11 (landscape version in Figure 101 of APPENDIX A) shows the UWAVS Bullnose block diagram that highlights function, decomposition, and interfaces. Color codes and line types are noted in the legend.

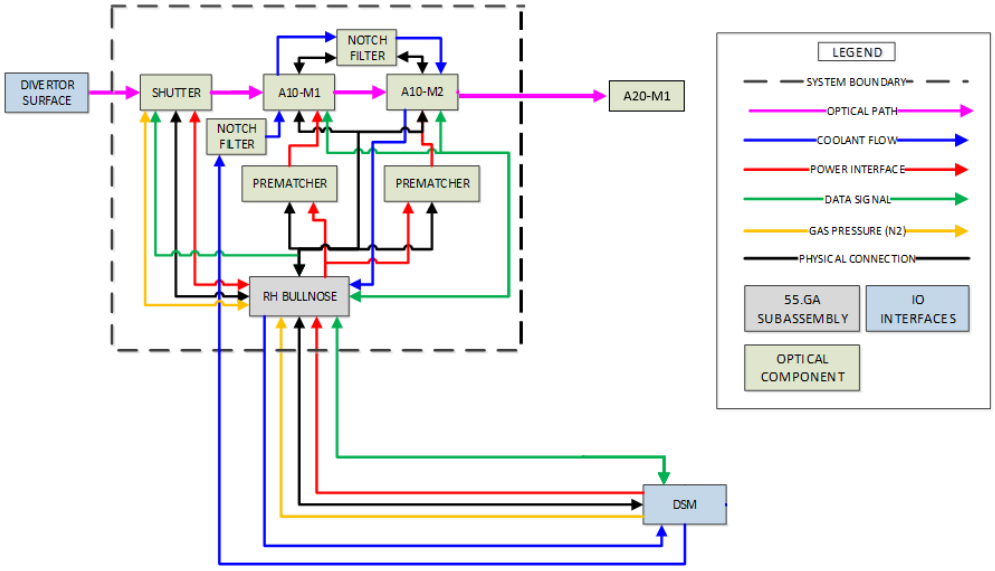

Figure 11. Bullnose decomposition and functional interfaces.

The IOT subsystem resides in the Interspace, supported by the Interspace Support Structure (ISS). At the fore end (Tokamak Global Coordinate System, TGCS negative X-direction), the IOT resides immediately next to the UPP Closure Plate (CP) and provides a mechanically passive interface with the VV window. At the aft end, the IOT projects the UWAVS line of sight into the

Released 2024/12/04
Released 2024/12/04

BOL subsystem. Surrounding the IOT will be shielding, other diagnostic equipment, and various forms of ITER infrastructure. Figure 12 (landscape version in Figure 102 of APPENDIX A) shows the IOT subsystem block diagram that highlights function, decomposition, and interfaces. Color codes and line types are noted in the legend.

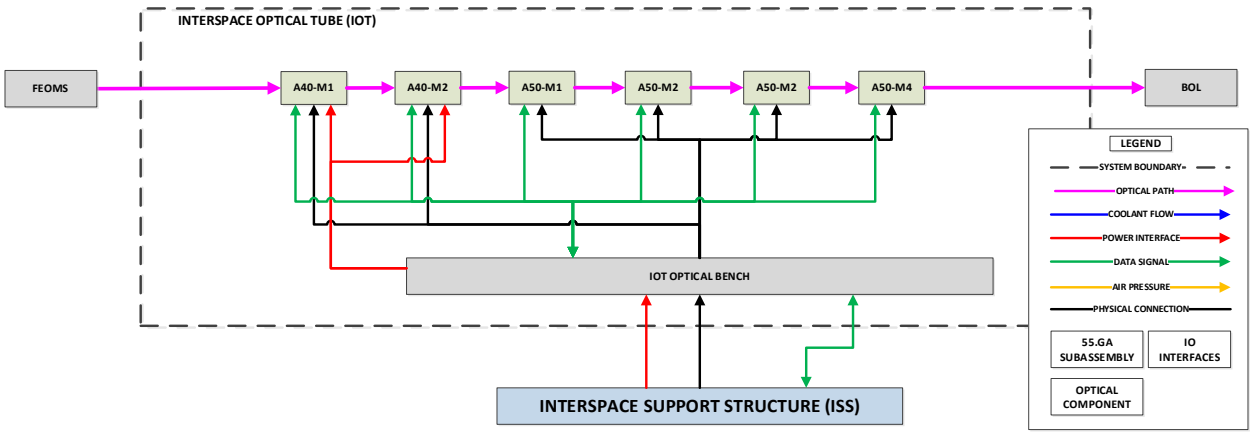

Figure 12. IOT decomposition and functional interfaces.

The BOL sits within the Bioshield and maintains alignment between the IOT and BEOC after maintenance periods when the ISS or Port Cell Support Structure (PCSS) are reinstalled. This is done using two actuated mirror mount assemblies. The two assemblies also create an optical dogleg within the Bioshield to reduce neutron streaming through the 55.GA diagnostic beam path. Figure 13 (landscape version in Figure 103 of APPENDIX A) shows the BOL subsystem block diagram that highlights function, decomposition, and interfaces. Color codes and line types are noted in the legend.

Released 2024/12/04

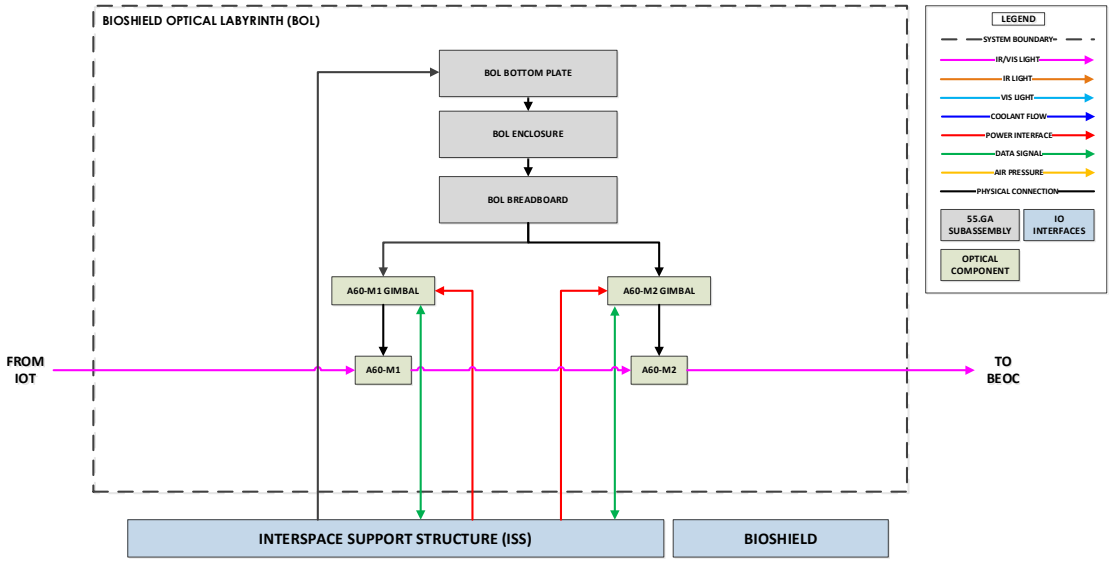

Figure 13. BOL decomposition and functional interfaces.

Released 2024/12/04

The BEOC is located behind the Bioshield in the Port Cell (PC), the BEOC mounts to the Port Cell Support Structure (PCSS) via an interface plate and shielded enclosure designed to protect the sensitive electronics and optics from radiation and contamination ingress.

Light enters the BEOC through a shielded shroud from the Bioshield Optical Labyrinth (BOL) and passes through a series of windows and mirrors that split the full spectral range into two wavelength bands (Visible and IR). Both IR and visible legs of the optical system consist of two cameras, and have lens doublets and respective fold mirrors and energy splitters to separate the light into two required camera channels. Finally, the wavelength bands are focused onto camera detectors via IR and visible lens arrays. The BEOC also houses calibration sources and optics.

Figure 14 (landscape version in Figure 104 of APPENDIX A) shows the BEOC subsystem block diagram that highlights function, decomposition, and key mechanical, optical, electrical, and cooling interfaces. Color codes and line types are noted in the legend.

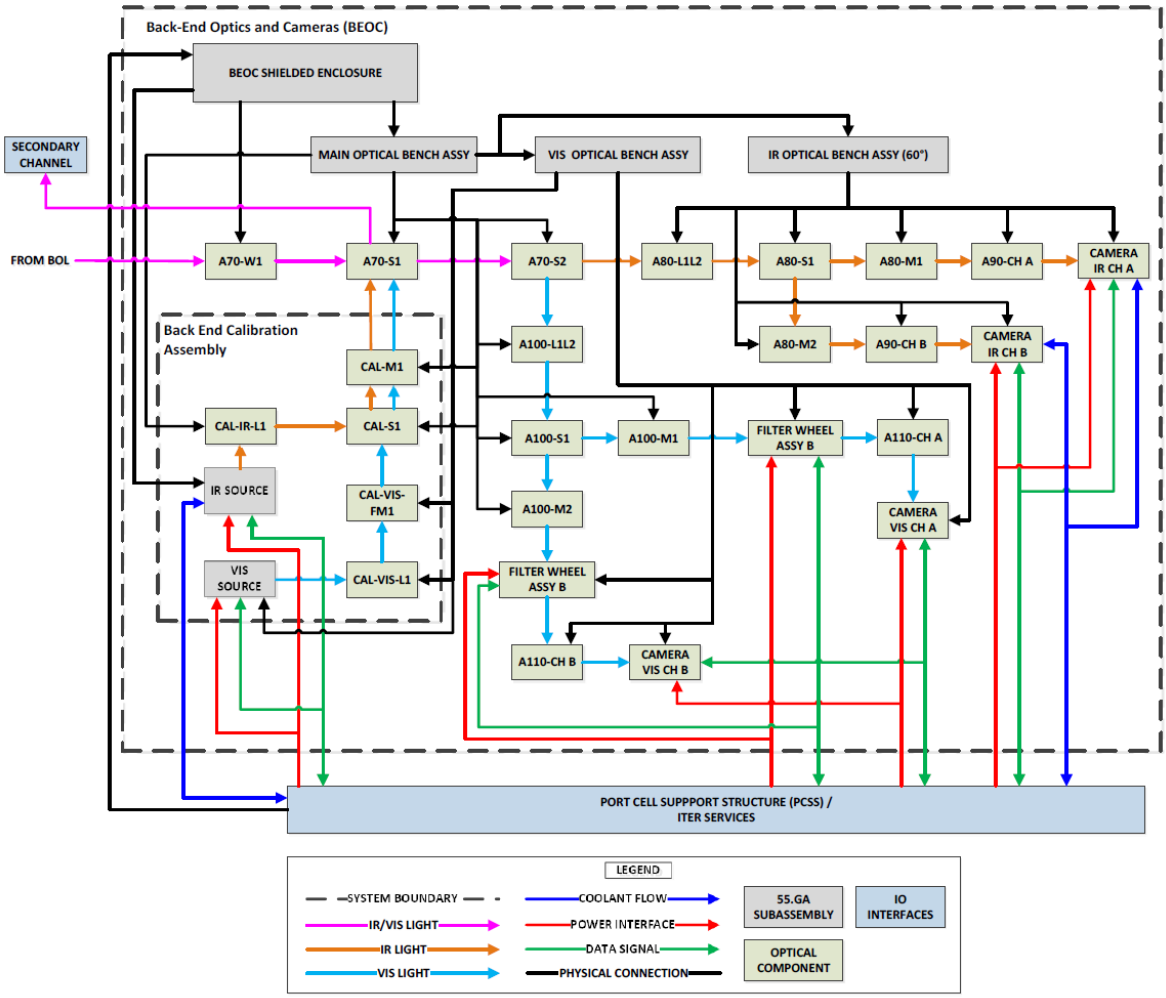

Figure 14. BEOC decomposition and functional interfaces.

Released 2024/12/04
Released 2024/12/04

The modular architecture provides several key benefits. It provides initial FAT testing to be done at a modular level. This helps pinpoint alignment and assembly issues early in fabrication and verification tests. It also supports decommissioning requirements.

Released 2024/12/04

Released 2024/12/04

5 DESIGN METHODOLOGY

5.1 Requirements

The Design Compliance Matrix (DCM) [24] tabulates how each requirement in the Sub-System Requirements Document (sSRD) [4] is met at the preliminary design.

The Technical Data List (TDL) is used to address all required IO applicable documents that are used throughout the design to meet requirements of the sSRD [4].

The ITER Vacuum Handbook [12] is used to guide vacuum component design and will be leveraged through fabrication. The Material Design Handbook [25] is used to establish a common source of material data. 55.GA leverages the SDC-IC [26] and the associated materials design limit data [27] for in-vessel, and the RCC-MRx [28] for ex-vessel design verification analysis.

The ITER cable catalogue [29] cables and in-vessel connectors [30] are leveraged throughout the design to meet requirements of vacuum, radiation exposure, fire risks.

5.2 Optical Model

The optical model provides the starting point for mechanical design and integration. Optics are designed inside the 55.GA. space claim with optimized prescriptions to meet diagnostic performance, and typically sized 5-10% larger than the beam path. The margin reduces risk in performance losses from mechanical tolerances and thermal displacements that occur during operation. The system of optics is designed to minimize aberrations for both for both visible light (400-700nm) and mid-wave infrared light (3-4.5µm). The baseline optical model includes all optics of the diagnostic from the first in vessel mirror back to the cameras. The optical model is referenced in section 1.3.3, and shown in Figure 15.

Released 2024/12/04

Released 2024/12/04

Figure 15. UWAVS Optical Model.

5.3 Mechanical Design Approach

Once the baseline optical design is established the UWAVS mechanical designs take form to support the optics and provide system functions and meet load specification requirements. Parametric links are used for locating optical mounts and design of subsequent interfacing structures and mechanisms.

5.4 Skeleton Design Methodology

The design approach for developing the UWAVS subsystems is to utilize skeleton hierarchy per [31] in conjunction with IO space claim models to locate and design optical mounts and support structures. The optics Component Skeleton (CSKE) contains the beam path and mirror S1 surfaces as shown in Figure 16.

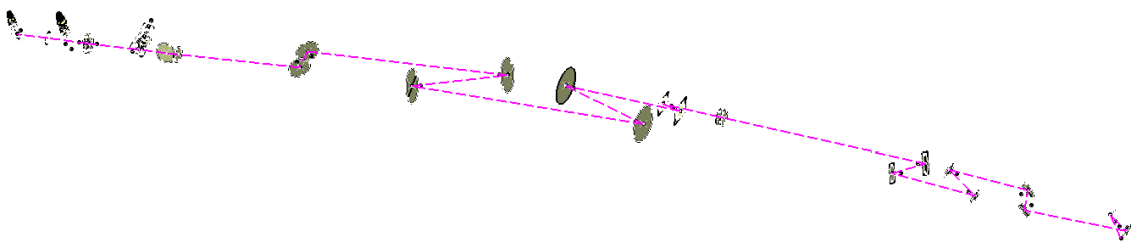

Figure 16. CATIA optics CSKE.

Key IO interfaces are critical to established positional constraints of the UWAVS design. The UPP Reference Skeleton (RSKE) contains key orientation and positioning planes. These elements setup the FEOMS, IOT, BOL, and BEOC CSKEs which publish the driving elements for the aperture cutouts, captured fastener locations, and mirror orientation planes for each subsystem. Figure 17 shows UPP CSKE references (see Table 1) and Figure 18 shows the Port Plug Assembly Datum (PPAD) and Port Cell Assembly Datum (PCAD) in reference to IOT and FEOMS subassemblies.

Released 2024/12/04
Released 2024/12/04

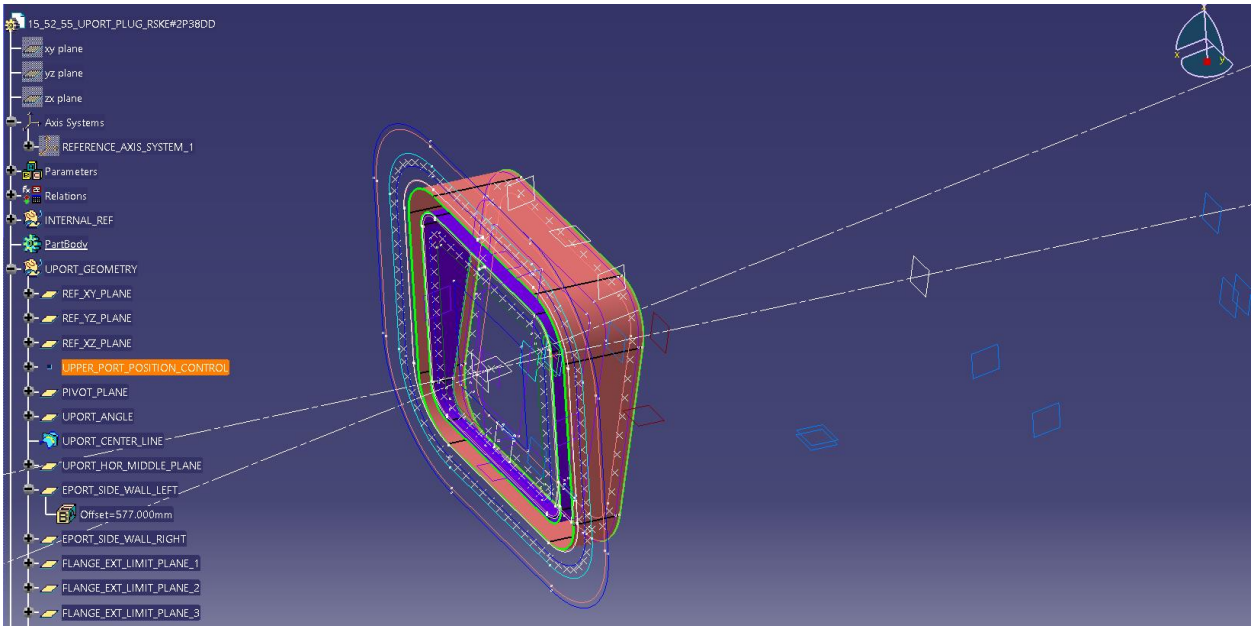

Figure 17. PPAD and PCAD references linked to UPP RSKE.

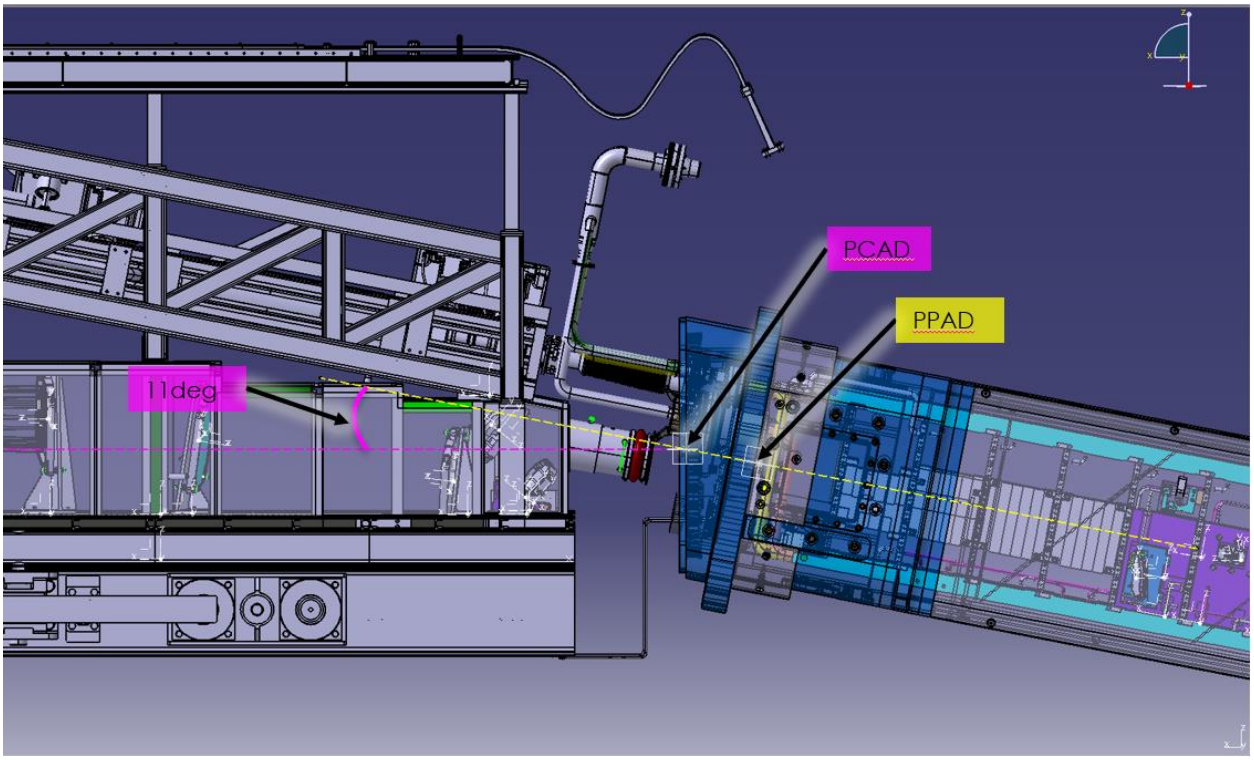

Figure 18. PCAD virtual coordinate system established 11 degrees off axis of PPAD.

Key 55.GA interfaces such as fasteners are established using Positioning Skeletons (PSKE) to minimize mate errors. RSKEs can be used to leverage the same approach for pipes and fastener interfaces with Port Integrators in final design.

Released 2024/12/04
Released 2024/12/04

6 SUBSYSTEM DESIGN DESCRIPTIONS

High level summaries of each 55.GA subsystem components and functions are included in the following sections (6.1-6.4). Detailed design descriptions and interfaces for each are discussed in the associated technical design descriptions and referenced as appropriate.

6.1 Front End Optical Modular System

The primary function of the FEOMS subsystem is to image a wide angle view of the divertor surface through a pinhole aperture of the DFW, and relay that image through a zigzag of dog leg mirror pairs back to the ex-vessel optics and cameras.

The mirrors are mounted on removable mirror modules that are compatible with remote handling tools in the hot cell in case maintenance is required. The modules also aid in neutron and gamma ray absorption and function as shielding. The mirror modules and where they reside in the DSM are shown in Figure 19.

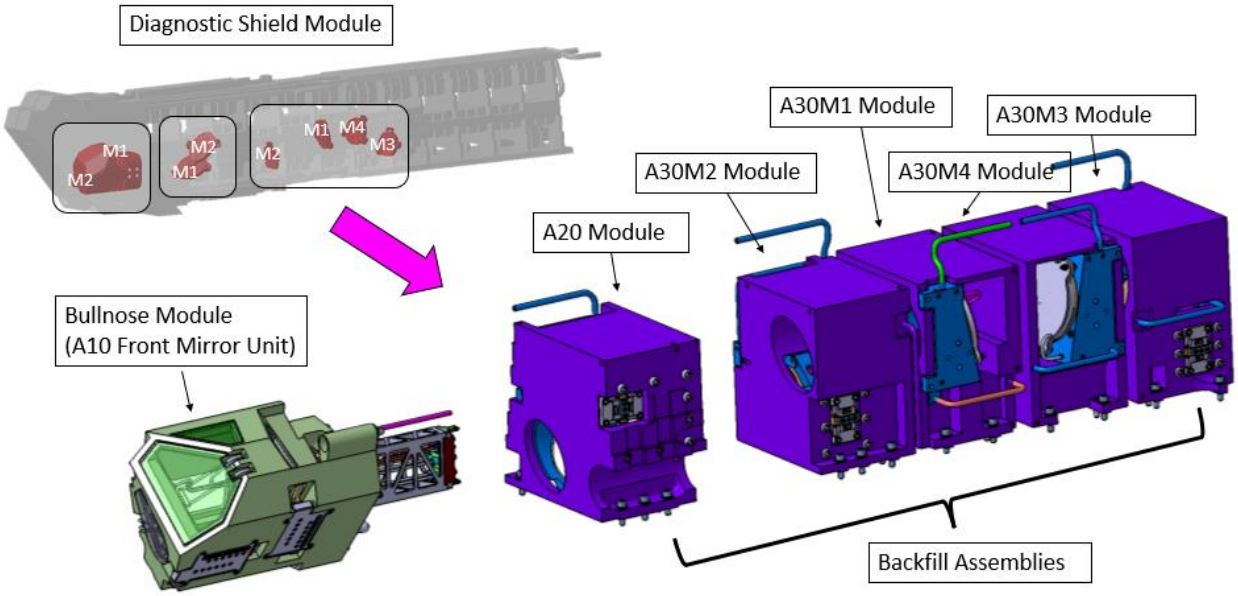

Figure 19. FEOMS modules and optics in the DSM.

6.1.1 Bullnose

A detailed design description is available in the 55.GA Bullnose Technical Design Description (TDD) [32] The related structural assessment of the design is documented in both structural integrity report [1], and in more detail in the 55.GA Bullnose calculation note [33].

The Bullnose (Front Mirror Unit) depicted in Figure 20 contains the A10 mirror group and the system aperture. Wide-angle light enters the system through the aperture at the lower front end

Released 2024/12/04
Released 2024/12/04

of the bullnose and reflects off the A10M1 and A10M2 mirror assemblies before exiting through the rear. Both A10 mirrors include a Radio Frequency (RF) cleaning system which allows for the removal of contaminates via plasma sputtering. RF power is fed to the mirrors through a series of mineral insulated cables (MIC) and through a RF pre-matcher printed circuit board (PCB) located directly behind them. Leakage of the RF power through the cooling water feed pipes is prevented through the use of a notch filter assembly mounted on the side of the housing. Additional details of the RF design are captured in Section 9. The housing consists of a machined block with gun drilled water channels throughout to manage the thermal load. A pneumatic shutter allows the aperture to be closed and resistive filaments are located on the back of the shutter blade for transmission monitoring. The bullnose is remotely handled for installation, featuring alignment pins on the back surface, and mounting with four large, forward facing RH bolts. Interfaces for cooling water, pneumatic, and electrical connections are established at the rear of the bullnose.

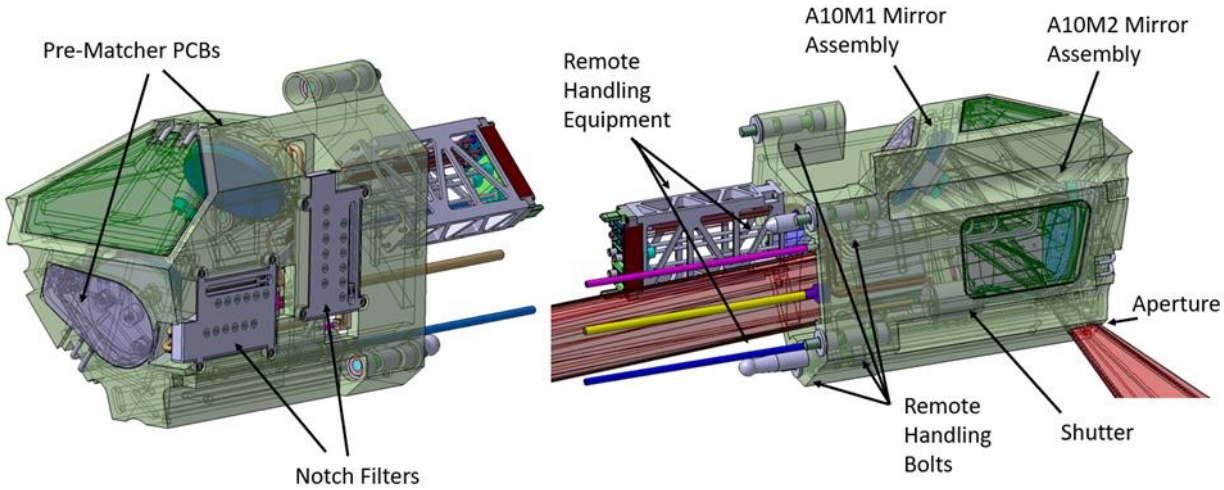

Figure 20. UWAVS-35 Bullnose assembly (Front Mirror Unit).

6.1.2 In-Vessel Shutter

A detailed design description is available in the 55.GA Shutter TDD [34]. The related structural assessment of the design is documented in both structural integrity report [1], and in more detail in the 55.GA in-vessel shutter calculation note [35].

The in-vessel shutter sits behind the aperture of the bullnose and protects the first two in-vessel mirrors from contamination during events such as Glow Discharge Conditioning (GDC), Ion Cyclotron Wall Conditioning (ICWC), and Electron Cyclotron Wall Conditioning (ECWH).

Sitting on the base of the bullnose, the shutter is primarily comprised of a pneumatic actuator weldment which drives a linkage arm holding the aperture blade. The design utilizes a preload

Released 2024/12/04
Released 2024/12/04

spring coupled with the bellow to realize a non-actuated aperture open state. Upon pressurization of the pneumatic actuator chamber, the bellow hydraulic area coupled with restrained axial movement drives a center pintle to initiate movement of the linkage arm through kinematic joints. The linkage arm holds the aperture blade which fully obstructs the aperture opening within the bullnose structure thereby protecting the mirrors and sensitive components internal to the bullnose. Figure 21 depicts the in-vessel shutter without the transmission source and the power cables.

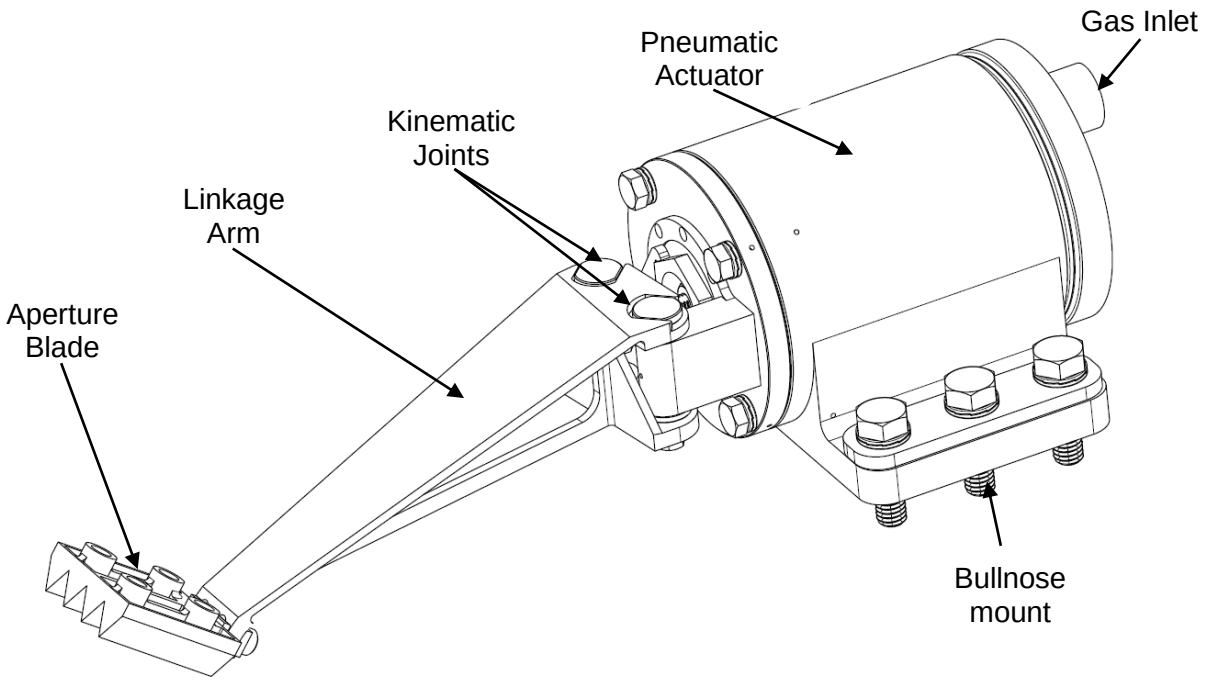

Figure 21. In-vessel shutter architecture

The in-vessel shutter is designed to use a gas control box concept from Diagnostic 55.E2 to drive the pneumatic bellow actuator. Movement of the actuator uses the pressure differential across a thin-walled bellow which is constrained such that its hydraulic area creates an axial force which drives the pintle motion shown in Figure 22. The calculated thermal environment [35], allows passive cooling of the shutter assembly, which captures some of the active cooling of the bullnose through mounting of the actuator housing. Component materials are chosen in accordance with [12] and based on actual testing results of similarly designed shutters within in-vessel Tokamak environments.

Released 2024/12/04
Released 2024/12/04

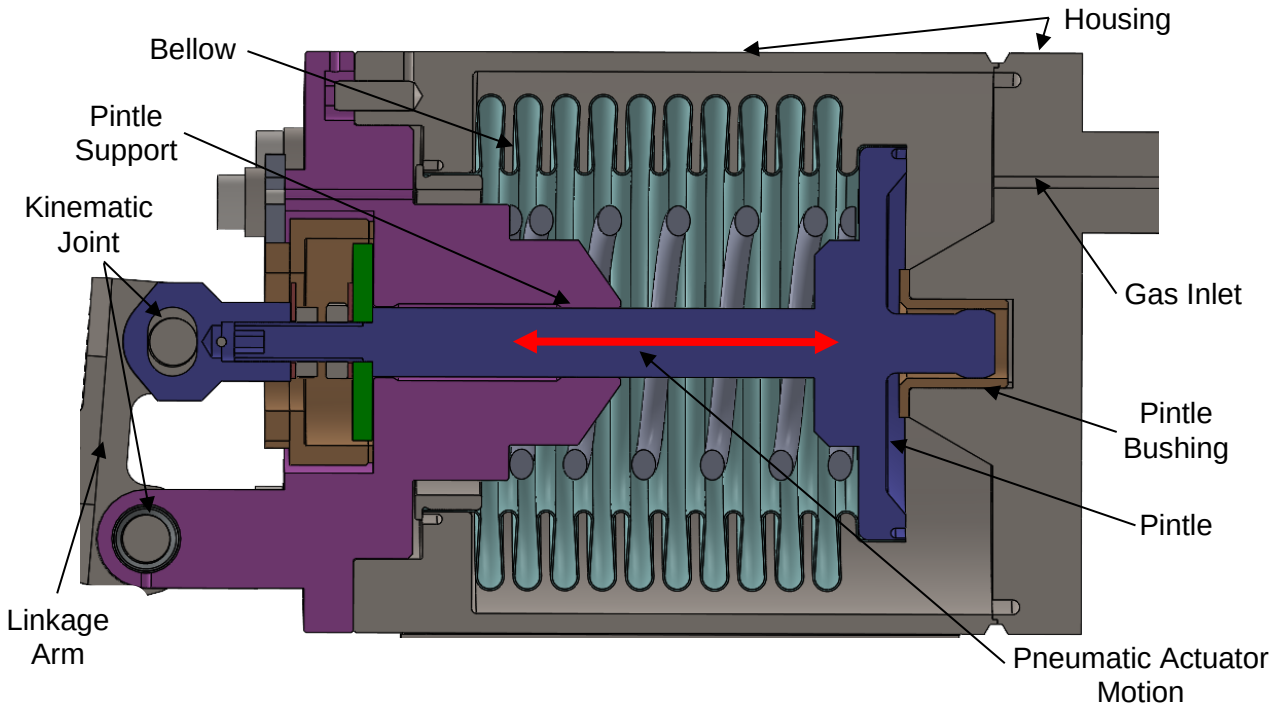

Figure 22. In-vessel shutter cross-sectional view.

Internal to the bellow, the actuator pressure is the base pressure of VQC1 Tokamak components, 10^{-7}-10^{-4} Pa (10^{-12}-10^{-9} bar). The hydraulic chamber created by the actuator housing and the bellow wall is connected to the gas inlet line. Gas line pressurization during shutter open condition is at 0.1 bar (10^{3} Pa). When pressurized to 2.0 bar (200kPa), the bellow compresses thereby axially moving the pintle to displace a single kinematic joint within the linkage arm. This linear displacement is translated to a rotational movement of the linkage arm thereby moving the aperture blade through a nominal 33.0mm range that provides line of sight coverage of the bullnose aperture opening and unobstructed view of the bullnose aperture opening. The range of motion is shown in Figure 23.

Released 2024/12/04
Released 2024/12/04

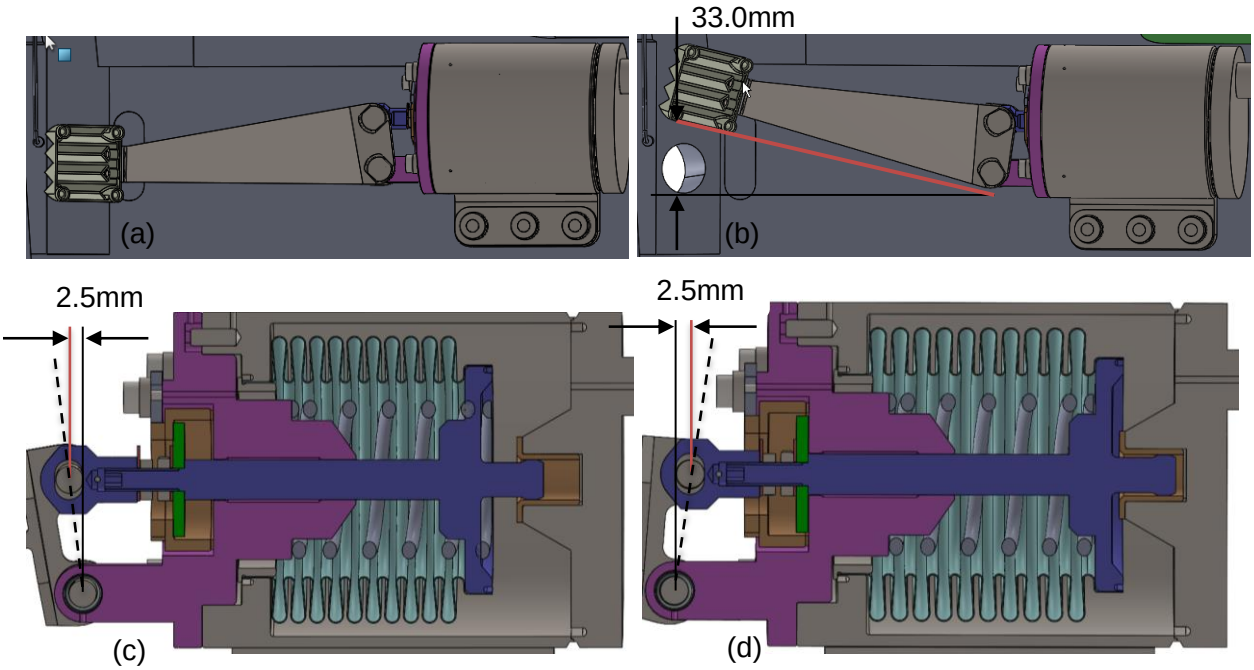

Figure 23. Shutter operational states (a) Full closed, (b) Full open, (c) Closed internal state, (d) Open internal state.

The shutter design pictured in Figure 22 satisfies multiple design requirements by protecting the bellow through restricting its range of motion and by biasing the design to fail open through multiple failure modes. The housing weldment protects the bellow to meet ITER Vacuum Handbook [12] criteria. Exception to a double wall bellow requiring a monitored interspace is accepted since the gas system contains redundant SIC-1 and SIC-2 safety valves. In the case of a bellow failure, the system is contained and protected by the safety valves. The shutter remains inoperable but fails open due to the double redundant spring setup provided by the bellow and internal compression spring.

6.1.3 Front End Optical Modules

A detailed design description is available in the 55.GA FEOMS TDD [36]. The related structural assessment of the design is documented in both structural integrity report [1], and in more detail in the 55.GA FEOMS calculation note [37].

The rest of the in-vessel mirror assemblies are designed leveraging a common modular architecture and described here as mirror module assemblies. Although sometimes referred to as shielding or backfill modules, the primary UWAVS function is optical. The basic assembly consists of a fixed module and, a removable module that supports one or two mirrors (see A20 example in Figure 24). All three major components are actively cooled to manage thermo-nuclear heat

Released 2024/12/04
Released 2024/12/04

loads. The mirrors are attached to the removable modules using an adjustable kinematic mechanism to achieve fine tip/tilt positioning. The kinematic mechanism is cooled only through conduction out to the interfaces.

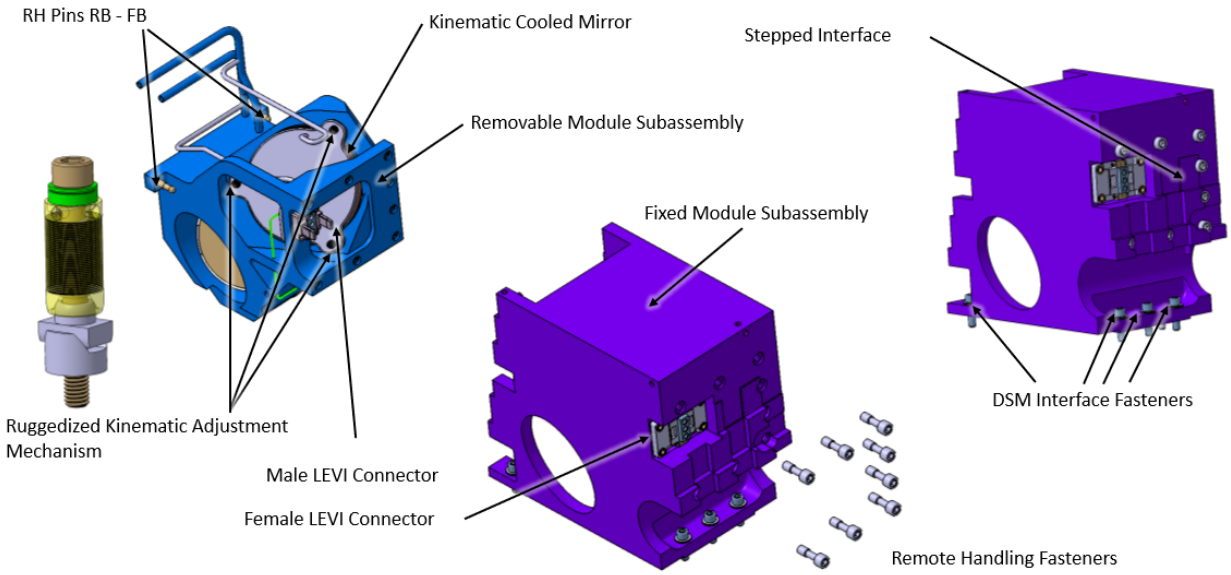

Figure 24. FEOMS mirror module design

The mirror modules are comprised of removable modules and fixed modules. The removable modules are Remote Handling (RH) compatible for maintenance and replacement. The fixed modules are not RH compatible or maintainable and are permanently bolted to the DSM floor interface. Both the fixed and removable modules, interface with the DSM shielding panels on one side and are designed with stepped interfaces to minimize direct streaming of neutrons.

While the A20 Module consists of two mirror mounts and an optical dogleg managed within the one bay module, each A30 module has a single mirror mount, and the optical dog legs are created in pairs of modules. The apertures in and out of each module are sized appropriately to clear the optical beam through each bay, as shown in Figure 25.

Released 2024/12/04
Released 2024/12/04

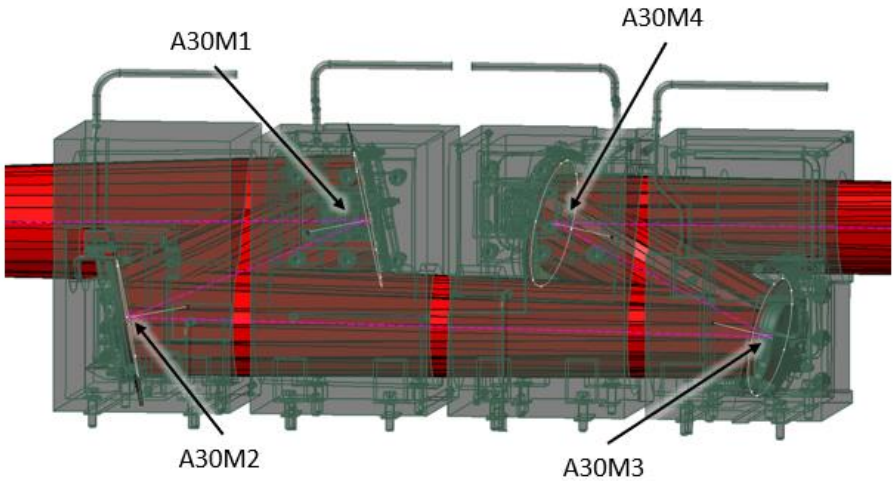

Figure 25. Beam path through A30 mirror modules

Exploded views of all A30 mirror module designs are shown in Figure 26 and Figure 27.

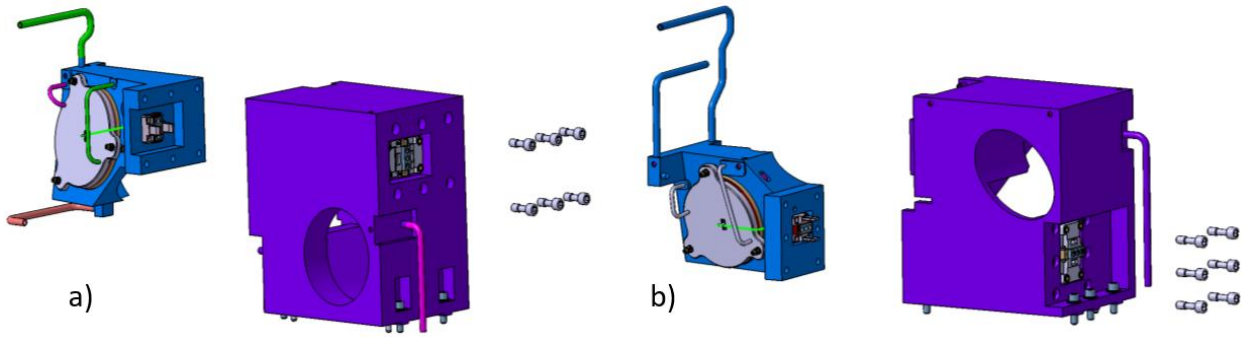

Figure 26. Exploded views of A30 mirror modules a) A30M1 and b) A30M2

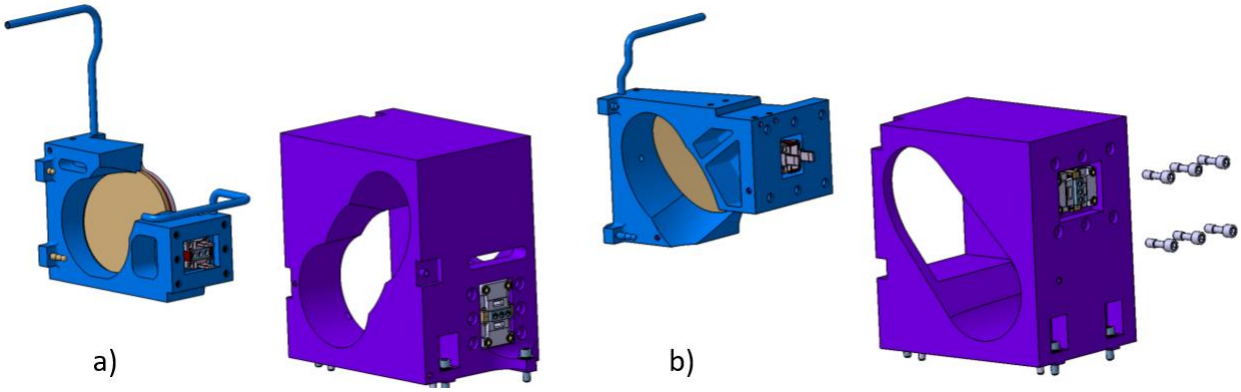

Figure 27. Exploded views of A30 mirror modules a) A30M3 and b) A30M4

Released 2024/12/04
Released 2024/12/04

6.2 Interspace Optics Tube

A detailed design description is available in the 55.GA IOT TDD [38]. The related structural assessment of the design is documented in both structural integrity report [2], and in more detail in the 55.GA IOT calculation note [39].

The key purpose of the IOT assembly is to provide active beam steering to compensate VV thermal displacements during operation and function as an optical relay, as well as a neutronic dogleg.

The IOT consists of five primary assemblies: the A40 mirror group assembly, A50 mirror group assembly, interface plate assembly, optical bench, and enclosure assembly, and IOT services assembly. Figure 28 shows the IOT subsystem and highlights the primary assemblies.

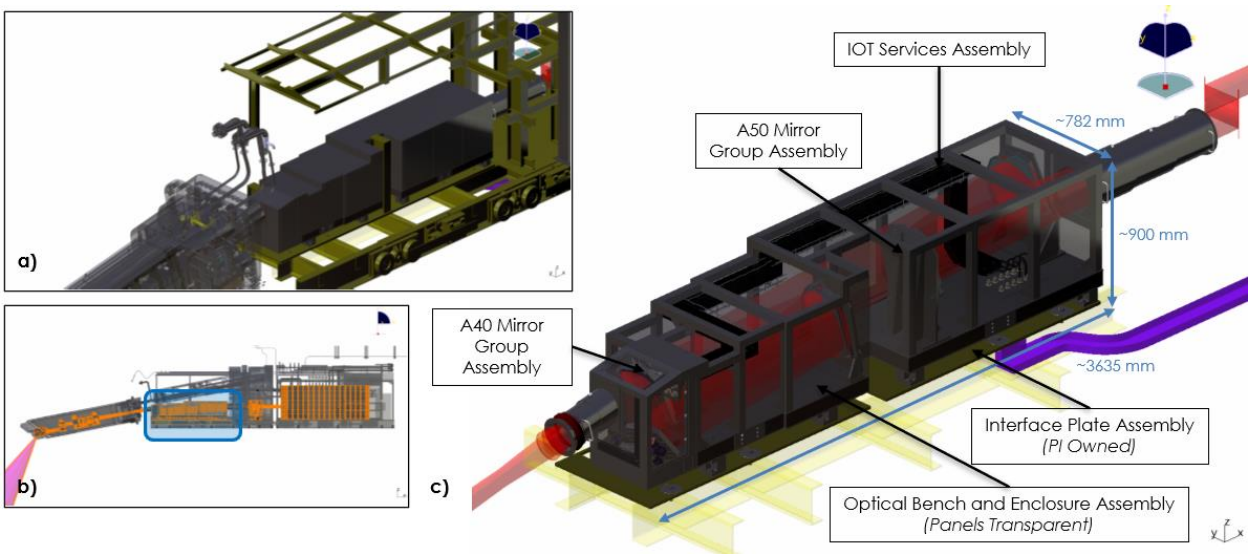

Figure 28. IOT subsystem (a-b) in context and (c) isolated with primary assemblies annotated.

The A40 mirror group assembly provides active alignment to compensate for relative thermal displacement of the VV during operation. The A40 mirror group consists of two parallel flat mirrors, actuated in a combined five degrees of freedom: tip and tilt on both mirrors and piston on A40-M2. Both A40 mirrors are constrained to a holding cell via preloaded flexures, which directly oppose precision-machined reference pads.

The A50 mirror group assembly consists of four large mirrors with variable surface shapes, which provide an optical relay, as well as neutronic dogleg. Like the A40 mirrors, the A50 mirrors are constrained via preloaded flexures and reference pads. Additionally, each A50 mirror is mounted via a 3-point, ruggedized kinematic mount which allows for fine adjustment of tip, tilt, and piston during initial assembly and alignment. The kinematic mounts will be locked in place for the operational lifespan after initial alignment.

Released 2024/12/04
Released 2024/12/04

The interface plate assembly facilitates the interface between the IOT and ISS and allows for initial installation alignment to compensate for gross ISS absolute installation tolerances. The optical bench and enclosure assembly provides the primary structural support for the IOT mirror groups, as well as protection from contamination and stray light sources. The IOT services assembly routes electrical power and signal from the ISS interface point to necessary locations within the subsystem. The IOT services assembly also provides disconnect points for both subsystem and component installation and maintenance events.

6.3 Bioshield Optical Labyrinth

A detailed design description is available in the 55.GA BOL TDD [40]. The related structural assessment of the design is documented in both structural integrity report [2], and in more detail in the 55.GA IOT calculation note [41].

The BOL sits within the Bioshield and maintains alignment between the IOT and BEOC after maintenance periods when the Interspace ISS or PCSS are reinstalled. This is done using two actuated mirror mount assemblies. The two assemblies also create an optical dogleg within the Bioshield to reduce neutron streaming through the 55.GA diagnostic beam path. The A60 mirror assemblies are secured to a breadboard in an enclosure that prevents the ingress of dust and stray light. The enclosure is secured to a subsystem bottom plate through four legs. The bottom plate features alignment pucks that allow the subsystem to be aligned to the ISS or PPAD virtual datum at installation. Figure 29 shows a rendering of the BOL between IOT and BEOC with a visible light beam. Figure 29 shows the BOL subsystem block diagram that highlights function, decomposition, and interfaces. Color codes and line types are noted in the legend.

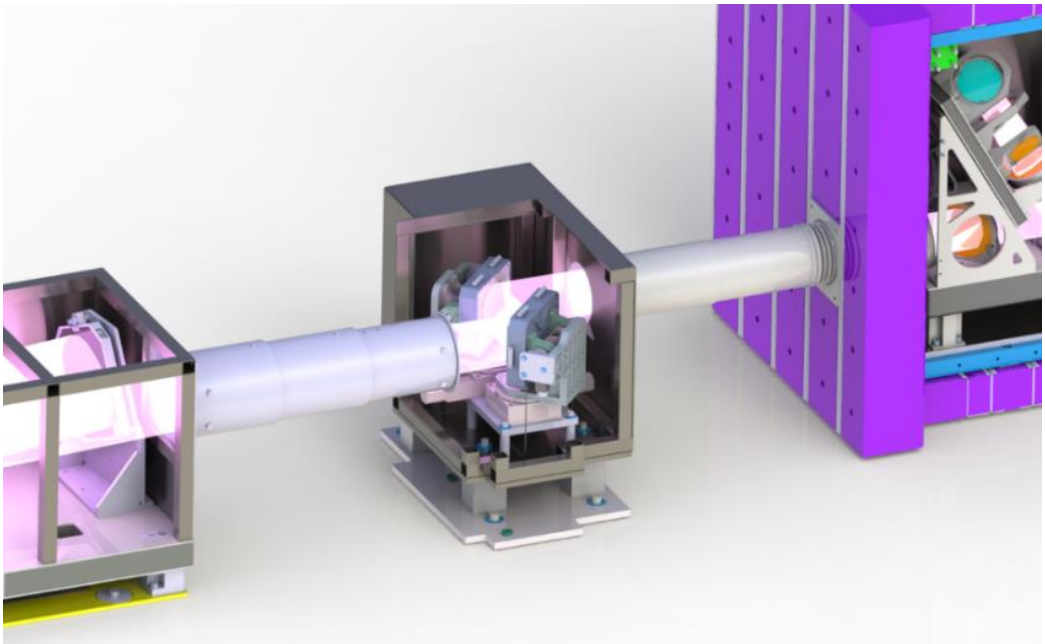

Figure 29. BOL between the IOT (left) and the BEOC (right).

Released 2024/12/04
Released 2024/12/04

The primary function of the BOL is to relay the light beam through the Bioshield with a labyrinth/dogleg to minimize the radiation exposure to workers in the Port Cells. The BOL provides two additional functions. First, it steers the 55.GA light beam to maintain alignment between the IOT on the ISS and the BEOC on the PCSS after removal and reinstallation of either support structure with a minimum angular step size of 0.25 µrad. Second, it provides closed interface assemblies to enshroud the light beam from external light and contaminate dust between the IOT and the BEOC.

The BOL dogleg to reduce neutron streaming is shown in Figure 30. The aperture is 220 mm and the offset is 186 mm. This dogleg allows visible and IR light to pass through the subsystem while reducing harmful radiation through the system.

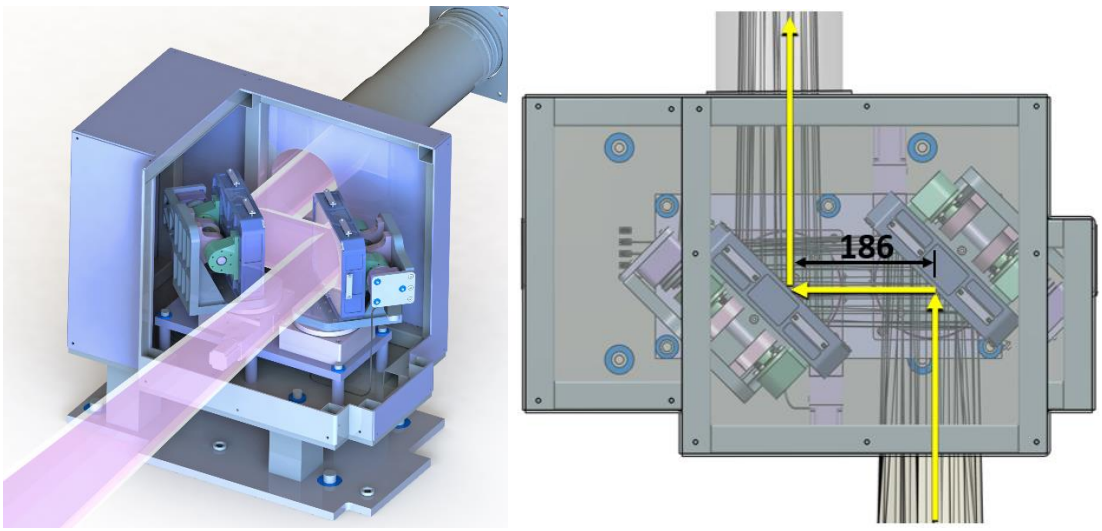

Figure 30. BOL dogleg with light beam visible (left) top-down view of dogleg layout (right).

Released 2024/12/04

Released 2024/12/04

6.4 Back End Optics and Cameras

A detailed design description is available in the 55.GA BEOC TDD [42]. The related structural assessment of the design is documented in both structural integrity report [2], and in more detail in the 55.GA BEOC calculation note [43].

The BEOC serves as the last UWAVS optical subsystem containing conditioning optics and the infrared (IR) and visible cameras. Located behind the Bioshield in the Port Cell, the BEOC mounts to the Port Cell Support Structure (PCSS) via an interface plate and shielded enclosure designed to protect the sensitive electronics and optics from radiation and contamination ingress.

Light enters the BEOC through a shielded shroud from the BOL and passes through a series of windows and mirrors that split the full spectral range into two wavelength bands (Visible and IR). Both IR and visible legs of the optical system consist of two cameras, lens doublets, fold mirrors

and energy splitters to separate the light into two required camera channels. Finally, the wavelength bands are focused onto camera detectors via IR and visible lens arrays.

As seen in Figure *31*, the BEOC consists of the optical relay system, the optical bench assembly, and the shielded enclosure. The optical bench assembly supports the optical relay system while the shielded enclosure protects the optics and sensitive electronics from radiation and contamination. The BEOC is mated to the PCSS via an interface plate which allows in-plane translation to adjust for large initial installation tolerances within the Port Cell.

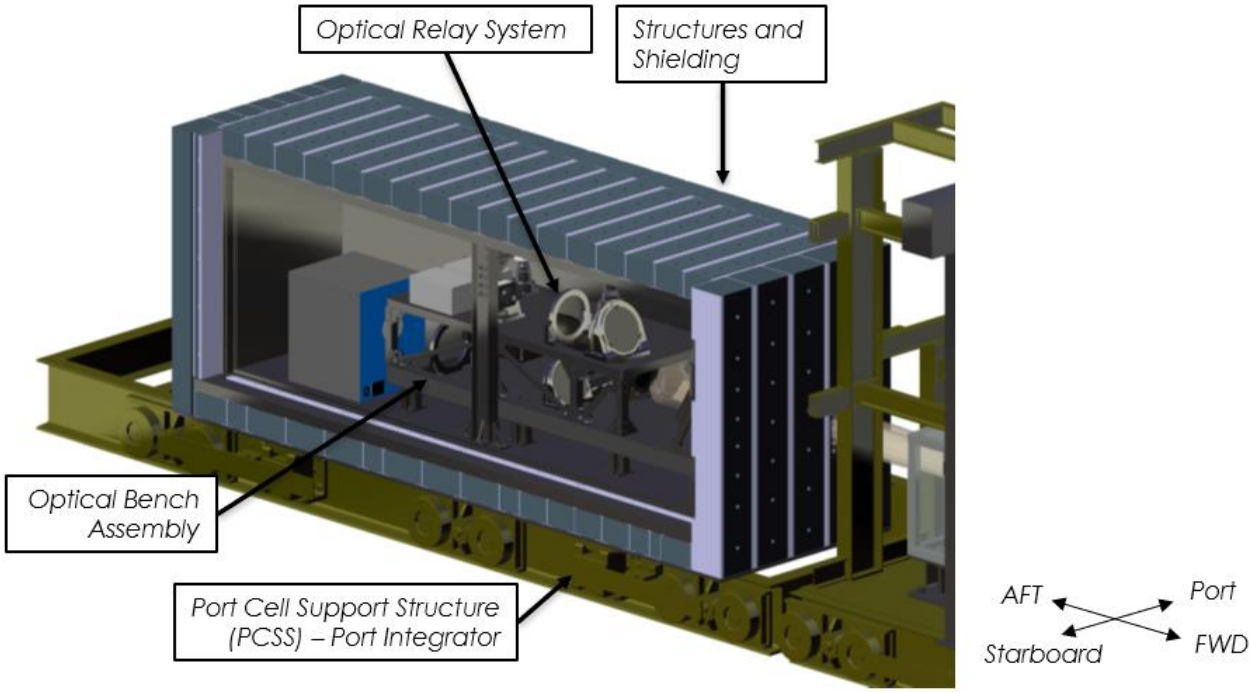

Figure 31. Back-End Optics and Cameras (doors removed for clarity).

The optical relay system shown in Figure 32 is comprised of the A70, A80, A90, A100, A110 optics groups, a pair of filter wheel assemblies, the IR and visible cameras, and the calibration system. The A70 optics group is a set of large windows, beam splitters, and folding mirrors that condition and separate the IR and visible light beams. The A80 optics group consists of a field lens, beam splitter and folding mirrors to direct the two IR frequency band beams to their appropriate cameras. The A90 optics consist of two identical lens tubes to focus an image for the two IR cameras. The A100 optics group consists of an achromatic doublet to correct the color aberration, a beam splitter, and folding mirrors to direct the visible light beams to the two visible cameras. The A110 optics are a set of two lens tubes containing different optics that form an image for the Channel A and Channel B visible cameras.

Released 2024/12/04
Released 2024/12/04

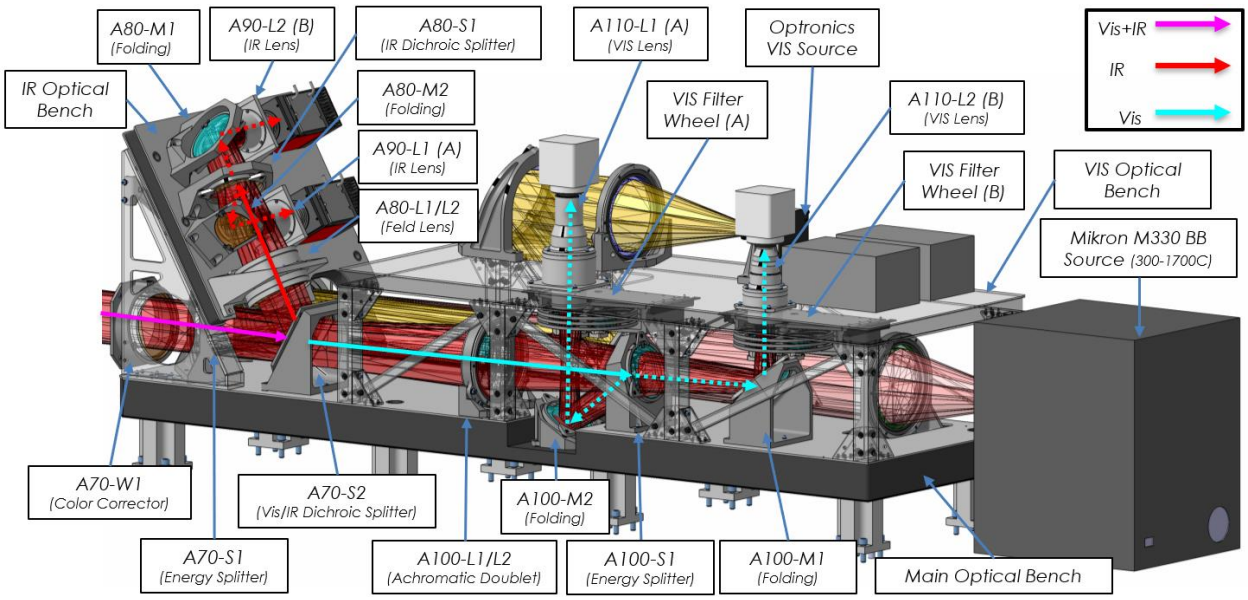

Figure 32. BEOC main optical layout.

To ensure accurate IR and visible measurements, a calibration assembly is also nested in the shielded enclosure. The calibration system consists of a set of lens and fold mirrors that bring light from a black body (IR) or integrating sphere (visible) into the into the beam path via the A70-S1 splitter.

A modular, actuated filter wheel assembly be placed containing filters to isolate 10 frequency bands is placed in front of the lens tube for the observation of specific elements as well as a set of neutral density filters. These filter wheel assembly modules are accessible for replacement in the event of a failure or should alternate filters be desired.

The BEOC is exposed to lesser radiation and lower temperatures than the IOT and BOL but not an inconsequential amount. The BEOC is enclosed in layers of shielding to minimize radiation and electromagnetic (EM) exposure, protecting electronics and cameras inside.

Released 2024/12/04
Released 2024/12/04

7 SYSTEM PERFORMANCE

7.1 Optical Performance

The 55.GA optical system performances are described in detail in the UWAVS-35 Optical Model Results [44] and the 55.GA UWAVS-35 System Detailed Performance Definition [6]. A summary of the key performance parameters is provided below in Table 5. This comprises coverage, imaging resolution and system optical transmission. Here green is compliant, yellow is near compliant and red indicates a non-compliance to the requirement.

Table 5. Overview of key optical performance requirements

	REQUIREMENT	VIS	IR	PERFORMANCE	NOTES
Optical system	Spatial Coverage	65 % of the outer divertor target 60% of the outer baffle 15 % of the inner baffle 45 % of the dome area		63% 60% 17% 38%	<1% vignetting FoV reported: Divertor target close, Dome limited by inner baffle & viewing angle
	Wavelength Range	400-700 nm	3-5 µm	Yes	Visible band ok. 55.GL extension to 850nm is tbd. IR→ use 3-4.5 µm due to VW absorption & emission > 4.5 µm
	Transmission	3-7%	10%	Vis: 0.9-5.9% IR: 18-40%	Visible light: Mainly for short wavelengths (<450nm) IR: more light than required
	Spectral Resolution	H-alpha, Be, C, Cu, Ne, Ar, Kr, W, D, T	2 bands (3.0-3.5 µm & 4.0-4.5µm)	Yes	Spectral resolution determined by filters Visible ~1nm bandwidth IR: 500nm width band filter in 3-4.5 µm range recommended
	Spatial Resolution @ 10.3 m /object plane	3mm	5mm	Vis: 3mm IR: 5mm	Requirement changed: - FWHM of PSF (before 30% MTF) - In object plane (before in plane ⊥ to LOS)
	Spatial Resolution @ 12 m ⊥ to LOS	3mm		Vis: 3.6mm	Requirement for visible imaging MP049 changed: - 12m working distance (10m before)

7.2 IR Measurement

Temperature and radiative flux are the core measurements for the infrared measurement parameters. A well calibrated infrared sensor converts detector counts in the image plane to wall temperature in the object plane. This conversion includes a number of computational and corrective steps, but critically depends on the emissivity of the target under observation. If the emissivity is known, or does not change, a single channel thermal measurement can be used to produce the IR measurement parameters, see Section 7.2.1. Unfortunately, surface emissivity is expected to change in an unpredictable manner. For this reason, a two color approach will be used to periodically update an emissivity map of the target (Section 7.2.2). Single color temperatures and heat flux measurements will still use a fast single color approach, but the emissivity of the surface will be determined by a slow two-color measurement. For a more detailed description of infrared measurement process, see [6].

7.2.1 Single color approach

Single color temperature measurements must include a number of different processing steps in order to accurately determine the temperature of in the object plane (see Figure 33). First a

Released 2024/12/04
Released 2024/12/04

detector must be properly characterized such that signal count can be converted to optical intensity. Knowing the spectral transmission of the system, the optical intensity is converted to spectral radiance in the measurement band. Then through a series of optical and background corrections, and a tokomak image map conversion, a wall radiance map is produced. Finally, the emissivity map is applied to produce a temperature map of the divertor.

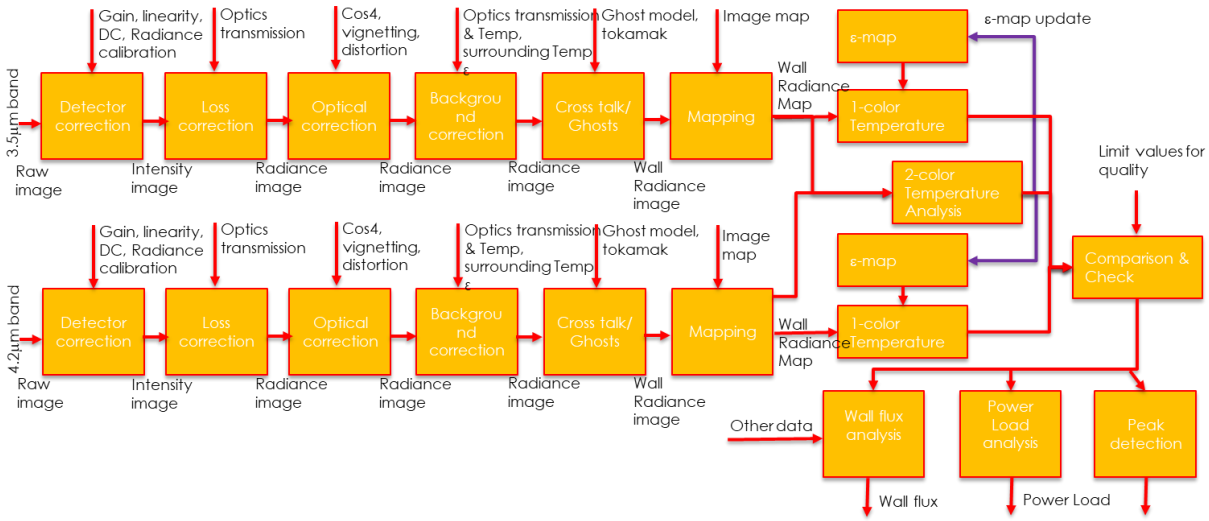

Figure 33. IR measurement data flow and processing scheme.

7.2.2 Two color approach

To accurately infer divertor temperature, the emissivity of the divertor's surface must be known and the optical system's spectral response must be calibrated via a known source (e.g., blackbody). In addition, background radiation levels must be considered. The tungsten (or any other metallic) ITER divertor and wall presents some complications due to the induced error that may result from reflections from these surfaces.

The emissivity of the tungsten divertor is much less than unity and depends on the history of the surface, such as the initial polishing, later erosion by plasma, possible deposition of other materials, and possible surface melting. To provide greater accuracy, the emissivity is obtained by the 55.GA system by using a two-color measurement. Two IR cameras each view the same target surface in distinct wavebands and each infers a single-color temperature, and the ratio of luminosities is used to infer a two-color temperature. By comparing the temperature of each single-color measurement with the two-color measurement, the emissivity of each one-color systems can be corrected to yield corrected single-color temperatures. This approach is described in detail in [6].

The high reflectivity of the tokomak interior can produce a relatively uniform background from light scattered or reflected into the entrance aperture from locations other than the primary viewed

Released 2024/12/04
Released 2024/12/04

area. In addition, a ghost images can result from stray reflections and corrupt image data. A comprehensive strategy to deal with these issues remains to be formulated and reviewed during final design phase.

7.3 Visible Measurement

Unlike the infrared measurements focusing on thermal imaging, the visible measurements are primarily concerned with integrated species concentration measurements, and the converting of those into radiative influx measurements. Using spectral lines associated with elemental energy state transitions, and a set of narrow spectral filters, a well calibrated imaging system can determine the line integrated intensity of specific species in the plasma. The divertor area is imaged onto the visible sensors; each pixel effectively collecting a cone of emitted light between the divertor and the aperture. Light collected from any location in this cone is indistinguishable from light emitted at any other location in this cone. Wall emission and Bremsstrahlung radiation become a primary driver for accurately measuring the species line integrated intensities and influx. For a detailed description of this visible measurement process and challenges, see [6].

7.4 Tolerances Analysis

Component, assembly, and interface tolerances have a direct impact on the optical alignment and ultimately contribute to optical performance of the UWAVS diagnostic. Tolerances are assessed during the preliminary design phase to identify worst offenders and to establish component design architectures. A preliminary tolerance stack-up for all assembly structures and optical mounts in the UWAVS subsystems and components is complete. The tolerance data is used to assess impact on the optical performance.

Only a high-level explanation of the assumptions and results are summarized here. A more detailed explanation of assumptions and tolerances for critical interfaces are documented in [45]. The results of the mechanical tolerance impact on performance are summarized in [44].

7.4.1 External Interface Tolerances

Per building the tolerance chain [46] the UPP has tolerances associated with its installation. However, the DSM is shimmed inside the UPP and the UPP positional tolerances are not included in the tolerances analysis. Therefore, the shimmed DSM positional tolerances (Generic DSM Mechanical Tolerances from [46]) are included in the tolerance analysis and listed in Table 6 [46] for reference.

Released 2024/12/04
Released 2024/12/04

Table 6. Generic DSM mechanical tolerances

Description	Units	NOM	MAX	MIN	NOTES
Toroidal displacement	mm	0.000	1.260	-0.350	dy
Poloidal displacement	mm	0.000	0.120	-0.790	dz
Radial displacement	mm	0.000	0.500	-0.100	dx
Toroidal rotation	deg	0.000	0.060	-0.060	Rx
Poloidal rotation	deg	0.000	0.013	-0.013	Ry
Radial rotation	deg	0.000	0.080	-0.080	Rz

These tolerances establish the possible positions and rotations of the DSM installed in the port plug. The tolerances of the DSM interface bays must be included separately. They establish the bay-to-bay positional tolerances of each mirror module of the FEOMS. Table 7 includes the assumed tolerances used in the tolerance analysis.

Table 7. Critical DSM interface tolerances

Description	Units	Tolerance (profile or true position)	Notes/Remarks
DSM surface profile	mm	0.60	Optical analysis indicates tighter tolerances are required to meet system performance
DSM/FEOMS Mirror Module locating pin positions	mm	0.050	Cylindrical control, MMC

The ex-vessel ISS and PCSS support structure installation tolerances are provided in [47] and listed in Table 8 [47] for reference. UWAVS is designed with integrated alignment features to mitigate the installation uncertainty/tolerances of the supporting structures (i.e., ISS, PCSS).

Table 8. ISS and PCSS Installation Tolerances

Description	Absolute	Reproducibility
Toroidal Location	+/- 20 mm	+/- 5 mm
Poloidal Location	+/- 5 mm	+/- 1 mm
Radial Location	+/- 5 mm	+/- 1 mm
Horizontal Tilt	+/- 1 mrad	+/- 1 mrad

Released 2024/12/04
Released 2024/12/04

Description	Absolute	Reproducibility
Vertical Tilt	+/- 1 mrad	+/- 1 mrad
Radial Tilt	+/- 1 mrad	+/- 1 mrad

The large absolute tolerances can be mitigated by tighter positioning of interface plates during on-site assembly. See details from onsite assembly plan [48] regarding interface plate positioning. Generally, most mirrors feature a second level of either manual or actuated adjustability, but the individual mirror adjustment can only be used in reference to the optical table and local datum fiducials. Optics cannot be adjusted to accommodate ISS/PCSS tolerances.

7.4.2 Component and Assembly Tolerances

UWAVS component tolerances are rolled up as standard mechanical tolerances leveraging minimum and maximum values, profile, or positional tolerances according to guidelines from machinery handbook [49], Commercial-Off-the-Shelf (COTS) data sheets, and engineering judgement. The assumptions are categorized by size and type of component. Critical UWAVS component tolerances used for the mechanical stack up are listed in Table 9 below.

Table 9. UWAVS component tolerances

Interface Type	Value
Holes	
Bolt hole diameter - 1.0mm thru 3.2mm	+0.10 / -0.02 mm
Bolt hole diameter - 3.3mm thru 6.4mm	+0.13 / -0.02 mm
Bolt hole diameter - 6.5mm thru 12.7mm	+0.15 / -0.02 mm
Bolt hole diameter - 12.8mm thru 19.1mm	+0.20 / -0.02 mm
Bolt hole diameter - 19.2mm thru 25.0mm	+0.25 / -0.02 mm
Bolt hole diameter - 25.1mm thru 50.0mm	+0.30 / -0.02 mm
Press fits - 2mm to 3mm	-0.012 / -0.028 mm
Press fits - 4mm to 6mm	-0.011 / -0.031 mm
Locational Clearance fit - 1mm to 3mm	+0.016 / +0.000 mm
Locational Clearance fit - 4mm to 6mm	+0.020 / +0.000 mm
Locational Clearance fit - 12mm to 30mm	+0.029 / +0.000 mm
A10 Bullnose locating pin diameter	+/- 0.015 mm
A20/A30 Module locating pin diameter	+0.018 / -0.007 mm
Surfaces	
Optical Bench Surfaces - metric	+/- .10 mm per 600 mm Square
Optical Bench Surfaces - standard	+/- .004"per 24" Square

Released 2024/12/04
Released 2024/12/04

Interface Type	Value
DSM surface roughness	6.30 µm
DSM surface profile	0.60 mm
Machined Surface - Standard	+/- .250 mm (~.010")
Machined Surface - Precision	+/- .025 mm (~.001")
Critical Interfaces	
Pin positional tolerance - Large structures (i.e., DSM floor)	+/- 0.025 mm
Pin positional tolerance - Small structures (i.e., Mirror Assy)	+/- 0.013 mm
Tapped hole positional tolerance - Critical	+/- 0.063 mm
Thru hole positional tolerance - Critical	+/- 0.063 mm
Resolution of kinematic adjustment	+/- 0.016 mm
Laser tracker Distance Accuracy (16um +0.8um/m)	+/- 0.009 mm
Laser tracker Angle Accuracy (20um +5um/m)	+/- 0.010 mm

In-vessel tolerances are rolled up to each mirror and reported back to the DSM origin. Optically significant interfaces of the FEOMS are listed in Table 45 of APPENDIX B and evaluated explicitly in the sensitivity analysis to highlight worst offenders.

Ex-vessel tolerances are rolled up to each optic and reported back through the optical benches and ultimately the PCSS origin. Optically significant interfaces located ex-vessel are listed in Table 46 (IOT) and Table 47 (BEOC) of APPENDIX B and are evaluated explicitly in the sensitivity analysis to highlight worst offenders.

7.4.3 Optic Tolerances

Optical surface roughness and profile tolerances that impact Wavefront Error (WFE) are managed with a top-down performance budget established at the middle of the spectral band. Typically, the cost benefit associated with refining large optic profile and surface tolerances beyond industry standards is not justified. The spot sizes associated with the industry standards for optics of similar size and complexity are used to establish the overall budget for the optic shape errors and surface quality and listed in Table 10 for reference [6].

Released 2024/12/04
Released 2024/12/04

Table 10. Optic tolerance budget

Error Contributor	Vis 1	Vis 2	IR 1	IR 2
	400-730nm	400-730nm	3-4.5mm	3-4.5mm
	RMS spot size radius [mm] @ Det.	RMS spot size radius [mm] @ Det.	RMS spot size radius [mm] @ Det.	RMS spot size radius [mm] @ Det.
2. Realization optics	**1.9**	**1.1**	**1.6**	**1.6**
FEOMS	1.4	0.9	1.1	1.1
IOT	0.9	0.6	0.8	0.7
BEOC	0.7	0.4	0.8	0.8

7.4.4 Results of Analysis

Sensitivity analysis identifies the impact on the performance of individual misalignments of each assembly and component. It identifies which tolerance elements have the biggest impact on the final performance and proposes mitigation actions.

Monte Carlo simulations generates a series of full system models, where all the mechanical interfaces are misaligned inside the anticipated tolerance envelope and uniformly distributed. Compensators are aligned using the alignment resolution values based on the mechanical designs.

Tolerance analyses uses the increment of the root mean square (RMS) spot radius as the measure of performance. The Monte Carlo analysis is performed separately for the UWAVS subsystems, and full system performance is extrapolated from these simulations by adding the individual contributions in quadrature.

As the Vis-1 channel has the highest complexity and the most stringent optical requirements, all tolerance simulations have been performed for this channel. For the common and mirror-based sections, i.e. FEOMS and IOT modules, there is no direct impact to the tolerance analysis due to the selection of this channel. In the BEOC, using this channel is deemed to be a conservative approach, which will help determine the required production and alignment technology. Similar tolerance values will be acceptable for the other imaging channels.

Released 2024/12/04
Released 2024/12/04

Results of the tolerance analysis of Vis-1 channel compared to requirements can be seen in Table 11. In order to meet performance budgets, the alignment tolerance of the A110 optical tube had to be reduce to +/-15µm.

Table 11. Overview of UWAVS tolerance analyses and results (Vis-1 channel)

Analysis	Description	Main outcome	Requirements
FEOMS	RMS spot size increment	1.7µm	1.7µm
IOT	RMS spot size increment	1.36µm	1.4µm
BEOC	RMS spot size increment	1.8µm	1.8µm

With the proposed tolerances the imaging resolution can be achieved. Using 95% certainty, the resulting spot size increment for all the channels can be found in Table 12.

Table 12. Imaging resolution error contribution by tolerances for all channels

Error Contributor	Vis 1	Vis 2	IR 1	IR 2
	400-730nm	400-730nm	3-4.5µm	3-4.5µm
	RMS spot size radius [µm] @ Det.	RMS spot size radius [µm] @ Det.	RMS spot size radius [µm] @ Det.	RMS spot size radius [µm] @ Det.
4. Alignment and integration	**2.8**	**1.9**	**2.3**	**2.3**
FEOMS	1.7	1.2	1.4	1.4
IOT	1.4	0.9	1.1	1.1
BEOC	1.8	1.2	1.4	1.4

Spot size increment on vis-2, IR-1 and IR-2 channels is extrapolated from the results on channel vis-1. Spot increment is defined as the product of vis-1 channel spot radius increment and the quotient of the studied channel magnification and vis-1 channel magnification.

7.5 STOP Analysis

Structural Thermal Optical Performance (STOP) analysis assesses the optical system performance loss due to displacements and rotations that occur under operational loads. After applying the operational loads, the active alignment system is allowed to correct the system alignment, after which the resulting impact on the imaging is assessed. Full detail of the STOP analysis is summarized and documented in the optical model report [44]. A high-level explanation of the process and results are summarized here.

Released 2024/12/04
Released 2024/12/04

7.5.1 FEOMS

Due to its close position to the core of the reactor, the FEOMS is exposed to the highest thermal and mechanical loads which may induce optic deformations. The stresses and resulting displacements and rotations are caused by the following contributors:

1. Thermal expansion caused by CTE mismatch of materials.
2. Mechanical stress caused by the cooling channel pressure under the optical surfaces.
3. Thermal stress caused by temperature gradients.
4. Mechanical stress caused by gravity and preload.

The STOP analysis combines these different contributors and calculates the resulting optical surface deformations as well as surface and module displacements. Module displacements caused by larger structure deformation (like the VV and UPP) need to be added manually at the interfaces.

A full STOP analysis was performed on the FEOMS. Displacements of the UWAVS modules and mirrors are calculated based on a fixed reference point on the DSM. DSM displacements at interfaces between the UWAVS modules and the DSM are also needed for proper system modeling. Using a set of point cloud data DSM deformations during plasma operation are used to generate nodal displacements. Average displacements and rotations for the UWAVS module interface points and are listed in Table 13.

Table 13. Displacements and rotations at module attachment points

Component	X	Y	Z	Theta X	Theta Y	Theta Z
	mm	mm	mm	deg	deg	deg
Bullnose	-0.93145	5.90E-02	0.28859	1.74E-03	3.48E-02	1.21E-03
Bay 2	-0.23947	1.09E-02	-0.13986	-2.41E-06	3.36E-02	-1.49E-04
Bay 4	0.38007	4.58E-02	-0.37512	2.34E-03	2.33E-02	-1.27E-03
Bay 5	0.68719	2.95E-02	-0.46212	1.90E-03	2.29E-02	-1.80E-03
Bay 6	1.0055	3.80E-02	-0.56513	3.63E-04	2.38E-02	-9.11E-04
Bay 7	1.3098	6.15E-02	-0.64803	-2.58E-04	2.23E-02	-7.65E-04

Displacements are in the ITER Tokamak Global Coordinate System, include the operational heat load only and do not include gravity. This data provides the interface.

Released 2024/12/04
Released 2024/12/04

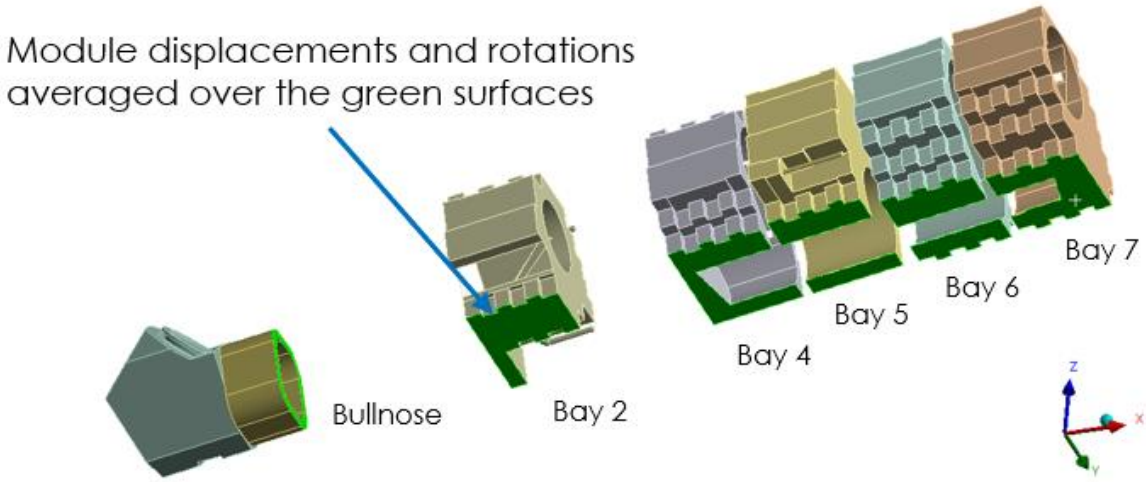

Figure 34. UWAVS mirror module interfaces to DSM.

Separate analyses are used to estimate the contributions of mirror displacements and rotations within each mirror module in the DSM. Table 14 and Table 15 summarize the estimated mirror displacements and rotations under operational load conditions (THO) with thermal expansion effects included. The displacements and rotations are extracted from the deformable point masses defined by each mirror surface. Mirror surface displacement and rotation data are mapped into an optical model for Structural Thermal Optical Performance (STOP) analysis.

Table 14. Mirror Displacements and Rotations

Mirror	ΔX	ΔY	ΔZ	ΔθX	ΔθY	ΔZ
	mm	mm	mm	deg	deg	deg
A10M1	-0.303515	-0.038995	0.038874	-0.000007	-0.000300	0.000837
A10M2	-0.583751	0.079586	-0.301953	-0.000722	-0.002457	0.003454

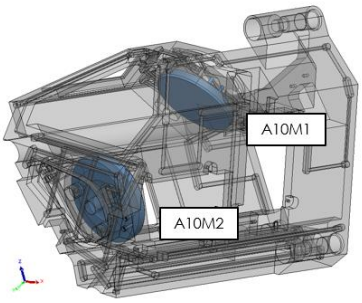

Table 15. A20 and A30 Mirror Displacement and Rotation Estimates.

Location	DX	DY	DZ	DRX	DRY	DRZ
	[mm]	[mm]	[mm]	[deg]	[deg]	[deg]
A20-M1 (I/F 4)	-0.052223	0.015579	0.180637	2.381E-03	-9.441E-03	1.678E-03
A20-M2 (I/F 4)	-0.077120	-0.120225	0.324591	-5.706E-04	-6.179E-03	5.744E-03
A30-M1 (I/F 4)	-0.198110	-0.0287`32	0.161950	-1.933E-04	1.742E-03	1.655E-03

Released 2024/12/04
Released 2024/12/04

A30-M2 (I/F 4)	-0.050905	0.085470	0.102592	-5.117E-04	-3.338E-03	-8.630E-04
A30-M3 (I/F 4)	-0.049535	0.050433	0.121921	-6.180E-04	4.998E-03	-1.861E-03
A30-M4 (I/F 4)	-0.043007	-0.064185	0.237438	2.813E-03	-6.250E-03	2.475E-03

The combined contribution of surface form error and rigid body motion (RBM) to the final spot size increment is shown in Table 16, and shows a small decrease on the final spot size. This is due to the optical surface power change compensation by thermal expansion of the mirrors mechanical separation. When taken together the individual contributions can increase the total spot radius increment or partially compensate one another. For example, the A10 full module increment is less than the individual contribution from A10-M1, whereas the A30 full module increment is greater than the individual mirror contributions. Figure 35 shows both the FEA and RBM contributions to spot size increment by component and for all assemblies of the FEOMS and the contribution to the full system.

Released 2024/12/04

Released 2024/12/04

Table 16. Spot size increment due to surface FEA and RBM

Component	spot radius (µm)	Spot radius increment (µm)
No FEA	1.76	NA
A10-M1	2.82	1.05
A10-M2	2.44	0.67
A10_full	2.48	0.71
A20-M1	1.81	0.05
A20-M2	1.76	-0.01
A20_full	1.89	0.13
A30-M1	2.10	0.33
A30-M2	1.92	0.15
A30-M3	2.08	0.31
A30-M4	1.87	0.11
A30-Full	3.18	1.42
Full system	3.67	1.91

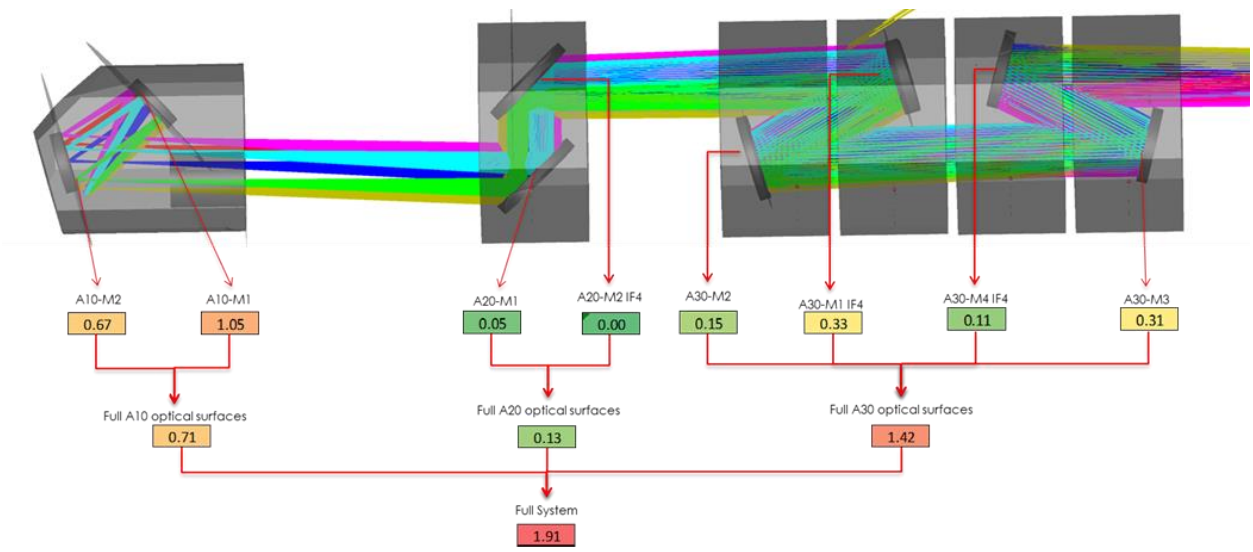

Figure 35. FEA and RBM contributions to spot size increment by component and for assemblies

7.5.2 IOT

Due to the higher thermal and mechanical stability at the IOT location, a Zemax thermal analysis of the system was performed with a uniform temperature. Zemax thermal analysis requires all surfaces to have a thermal coefficient of expansion defined. This way, the distance between two mirror surfaces can be varied due to thermal expansion of material between the mirrors.

Released 2024/12/04
Released 2024/12/04

Then, Zemax uses the CTE to calculate the variation in distance between surfaces as a function of the temperature increment from room temperature (20°C) and the working temperature. It also calculates changes in curvature for the optical surfaces due to thermal expansion.

Two thermal expansion effects are considered in this analysis:

- Variations in distance between components due to thermal expansion of the Optical Bench
- Expansion of the mirrors: Displacement of the optical surfaces with respect their mechanical assembly surface due to mirror expansion. Change of optical element optical power due to expansion.

For the IOT case, all thermal properties are defined explicitly accordingly to the list of materials shown in Table 17:

Table 17. List of IOT materials used in thermal analysis

Component	Material	TCE (µm/m °C)
BOL	Stainless steel	15.6
Optical Bench & Support (interspace between mirrors)	316L SS honeycomb and face sheets	16.0
Optical components	N-BK7	7.1

For the optical components, element thickness and material are specified according to Table 18:

Table 18. List of IOT optic materials and thickness

Group	Optic	Description	Material	Thickness (mm)
A40	M1	Active Alignment Mirror	NBK7	25
A40	M2	Active Alignment Mirror	NBK7	25
A50	M1	Relay Group Mirror	NBK7	21.38
A50	M2	Relay Group Mirror	NBK7	25
A50	M3	Relay Group Mirror	NBK7	25
A50	M4	Relay Group Mirror	NBK7	22.38
A60	M1	Labyrinth Active Mirror	NBK7	30
A60	M2	Labyrinth Active Mirror	NBK7	30

During ITER operating conditions the temperature inside the IOT is anticipated to be 52°C [50]. Simulations consider this temperature in the IOT for components from the exit of the vacuum

Released 2024/12/04
Released 2024/12/04

window located before A40 components until the exit of the IOT. Under these conditions, and if no optimization is performed, spot size in the central field will increase more than 30 microns.

If A40 is used for tip/tilt and focus compensation, performance shows an average spot increment of 0.61 microns.

Full results are listed Table 19, showing a total increment of 0.61µm for the compensated thermal range at 52°C.

Table 19. Effect of IOT thermal expansion on spot size

Field value (mm)		RMS Spot radius increment (µm)		
Field X	**Field Y**	**52°C Uncorrected**	**52°C Compensated**	**60°C Compensated**
0.00	0.00	34.13	**0.45**	0.64
0.00	2450.00	32.93	**1.25**	1.86
0.00	-2128.00	34.89	**0.53**	0.93
419.06	1281.00	33.20	**0.68**	1.06
560.40	0.00	34.11	**0.69**	0.93
1014.92	-1058.58	34.04	**0.73**	0.98
537.63	-2142.44	35.30	**0.70**	1.18
-456.84	1034.26	33.40	**0.42**	0.73
-311.35	258.37	33.94	**0.41**	0.61
-599.90	1708.28	32.89	**0.53**	0.95
-347.16	-324.55	33.97	**0.29**	0.44
118.22	-1059.53	33.97	**0.19**	0.31
Average		**33.9**	**0.61**	0.94

7.5.3 BEOC

The BEOC is located after the bio-wall in the PCSS inside an enclosure with layers of shielding materials. This implies that, as in the IOT case, the module has thermal homogeneity and high thermal and mechanical stability. Therefore, it is not required to perform a full STOP analysis to this section. In this case, only thermal analysis is performed.

Methodology is the following:

- The system is optimized for performance at 20 degrees.

Released 2024/12/04
Released 2024/12/04

- A CTE coefficient is assigned to the separation between components. CTE for mechanical components are listed in Table 20
- For the lenses, the CTE and refractive index is defined by the material.
- Temperature is increased to 37°C.
- Performances for Vis1 and IR1 channels are analyzed.
- A40 is used to correct the performance for spot size.

The list of used materials is shown in Table 20 below.

Table 20. List of Material and CTE as used in Zemax Simulations

Component	Material	CTE (µm/m °C)
Optical Bench assembly	440SS Honeycomb	10.2
A100-M1	N-BK7	7.1
Vis channels support pedestal	304SS	17.3
Vis Camera lens holder	304SS	17.3
Vis Optical lenses	Different materials	As defined by Zemax material library
IR channels support pedestal	304SS	17.3
IR Camera lens holder	304SS	17.3
IR Optical lenses	Different materials	As defined by Zemax material library

7.5.3.1 VIS-1 Channel Results

As with the IOT model, it is required to use A40 for alignment and spot optimization. Without compensation the spot size would increase by more than 30 microns. Focus compensation allows for a spot size increment of 0.6µm as shown in Table 21.

Table 21. RMS Spot Radius Increment for BEOC at 37°C with and without A40 Active Alignment

Field value (mm)		RMS spot radius increment (µm)	
Field X	Field Y	No compensation	A40-Mirror compensation
0	0	30.16	0.46
0	2450	29.35	0.92
0	-2128	31.48	0.92
419.06	1281	29.37	0.6
560.4	0	30.15	0.71

Released 2024/12/04
Released 2024/12/04

Field value (mm)		RMS spot radius increment (µm)	
Field X	**Field Y**	**No compensation**	**A40-Mirror compensation**
1014.92	-1058.58	30.22	0.86
537.63	-2142.44	32.04	1.21
-456.84	1034.26	29.53	0.37
-311.35	258.37	29.98	0.39
-599.9	1708.28	29.14	0.4
-347.16	-324.55	30.00	0.34
118.22	-1059.53	30.07	0.4
Average		**30.12**	**0.63**

7.5.3.2 IR-1 Channel Results

Thermal simulations were also performed in the same way for the IR-1 channel. In this case, the performance and active alignment compensation values are listed in Table 22.

Table 22. RMS spot increment for the IR-1 channel at 37°C, with and without compensation

Field value (mm)		RMS spot radius increment (µm)	
Field X	**Field Y**	**No compensation**	**A40-Mirror compensation**
0	0	6.45	0.63
0	2450	7.84	-0.3
0	-2128	8.42	0.47
419.06	1281	7.44	-0.14
560.4	0	6.72	0.37
1014.92	-1058.58	7.55	0.01
537.63	-2142.44	8.03	0.44
-456.84	1034.26	6.67	0.2
-311.35	258.37	6.36	0.66
-599.9	1708.28	7.27	-0.25
-347.16	-324.55	6.90	0.48
118.22	-1059.53	7.67	0.07
Average		**7.35**	**0.28**

Released 2024/12/04
Released 2024/12/04

7.5.3.3 VIS-1 and IR-1 Active Alignment Incompatibility

Inspection of the different active alignment values for IR-1 and Vis-1 shows total difference of 3.5mm in the piston compensation (see Table 23). This implies that it is not possible to use simultaneously A40 for thermal compensation of the IR and visible channels. Both channels show different thermal behavior.

Table 23. Thermal compensators for VIS-1 and IR-1 channels

Temperature	Vis-1	IR-1
A40-M2 focus	**2.4**	**-1.06**
A40-M1 X tilt	0.285	-0.15
A40-M1 Y tilt	0.003	0.02
A40-M2 X tilt	0.285	-0.14
A40-M2 Y tilt	-0.003	0.03

Generally, refractive indexes of optical materials increase with the temperature, while curvature decreases. Therefore, focal length on a positive optical system gets larger as the system heats up. This is the case for the Vis-1 channel lens tube. The objective lenses of the IR channels show different/opposite behavior. Lens materials used in the IR-1 channel are CaF2, ZnS and Silicon, see Figure 36. Here the temperature dependence of the refractive index of Silicon is four times stronger than the one of ZnS, while CaF2 shows very small negative variations of refractive index with temperature. Lens A90-L1 is the only lens with negative power and the only one made of Silicon. Since it shows the strongest variation of power with temperature, it drives the full system focal length, which decreases with the temperature.

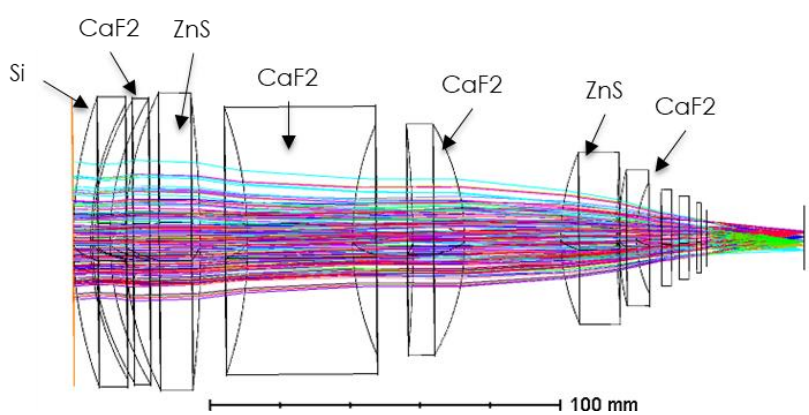

Figure 36. IR-1 Camera objective with the materials listed

As a solution for this issue, A40 is used as alignment and focus compensator for the IR-1 channel, and an extra alignment element is introduced to the visible channels. After discussions, it was

Released 2024/12/04
Released 2024/12/04

decided to use a motorized stage on the Vis channel detectors to compensate the focus difference.

The final alignment required is summarized Table 24 below.

Table 24. Final system compensator range for IR-1 and Vis-1 channels

Alignment	Vis-1	IR-1
A40-M2 focus	2.4	-1.06
A40-M1 X tilt	0.285	-0.15
A40-M1 Y tilt	0.003	0.02
A40-M2 X tilt	0.285	-0.14
A40-M2 Y tilt	-0.003	0.03
Camera focus	**-0.352**	0

7.5.4 Results of Analysis

Results for full operational load of the opto-mechanical system can be seen in Table 25. Analysis of the complete system yields a spot size increment within the issued requirement. The partially offsetting or compensating contributions between the individual modules allows this to be true despite the individual contributions for the FEOMS and IOT slightly exceeding their requirements.

Table 25. RMS Spot Radius Increment for Operational Load

Module	Rms spot size increment (µm)	Requirements (µm)
FEOMS	1.91	1.9
IOT	0.53	0.5
BEOC	0.38	0.9
Complete system	1.39	2.2

Released 2024/12/04

Released 2024/12/04

7.6 Active Alignment

In the active alignment system plan, several analyses were conducted to evaluate the required compensator ranges and resolutions while checking the impact on the footprints of the active alignment system mirrors. For a detailed description of the analysis performed, see [44]. Overview of the analyses and results are summarized in Table 26.

Table 26. Overview of active alignment system Analysis Results

Analysis	Description	Main Outcome	Remarks
Tolerance & thermal	Tip/Tilt actuator ranges	Sufficient range	
Tolerance & thermal	Focus actuator range	Tight range	Required range is not symmetric in both directions. The center of the adjustment range should be defined accordingly.
Tolerance & thermal	Tip/Tilt actuator resolution	Insufficient resolution	Finer resolution is needed to have sub pixel spot displacement
Tolerance & thermal	Focus actuator resolution	Sufficient resolution	
Tolerance	Footprint on mirrors	No vignetting	
Thermal	Footprint on mirrors	No vignetting	
Pivot position	Footprint on mirrors	No vignetting	The pivot position result in extra margin in the upper side of the mirrors
	I&C implementation		Data needed from previous processes to complete I&C flow diagram

The main outcome of this analysis is that the foreseen alignment ranges are sufficient to cope with the anticipated tolerances and vessel deformations. A40 mirror tip/tilt actuator resolution needs improvement. This is foreseen to be implemented in the final design phase.

Released 2024/12/04

Released 2024/12/04

8 CALIBRATION

8.1 Calibration Strategy

UWAVS imaging system provides real-time, simultaneous visible and infrared images of ITER divertor region via optical systems located in the UPPs of the ITER VV. The system is primarily responsible for measuring IR radiance and temperature in the MWIR part of the spectrum and chemical species line integrated emission intensity in the visible part of the spectrum. For accurate and absolute measurements of these properties, a calibration scheme was developed which accounts for all components in the measurement system. This includes sensor level, instrument level, and system level effects as well models and algorithms used in data interpretation. A detailed description of the full calibration scheme is given in the Optical Model Results [44] and Calibration Plan presentation [51], and a description of the instrumentation or signal conditioning used in the calibration is given in the Instrumentation and Control Architecture [52].

The calibration strategy includes four essential types of calibrations: Front-to-End Calibration (F2E), Back End Calibration (BE), Transmission Modeling (TM) and Algorithms and external data (AE). Each of these methods has a specific objective outlined below.

- Front-to-End Calibration provides calibrated radiance per pixel and wall temperature verification. This uses known sources, located within the ITER vessel to calibrate the system response including all effects. Separate light sources are required both for IR and visible measurements. It is essential to perform these measurements at least once in lifetime, but preferably, periodic calibration after installation, and during the long-term maintenance is applied to correct the impact of degradation of components over time. At this time, an approach to F2E calibration has not formally been confirmed by ITER for the UWAVS system, but it is expected to be necessary. Replacing front-to-end calibration by in factory testing will result in loss of measurement accuracy, but is a viable backup option if IO does not provide for the as-installed F2E calibration.
- Back End Calibration provides calibration of the visible and IR sensors and the associated optics. This includes effects such as sensor gain, linearity, background, bad pixels, etc. as well as radiance correction. Both Infrared and Visible cameras may degrade over time, so fixed visible and IR sources are implemented in the BEOC to be used periodically (e.g., in between pulses). These sources are identified in Figure 38. During initial installation and after long term maintenance, back-end calibration will need to be conducted.
- Algorithms and External Data uses physical models and algorithms to provide corrections for data interpretations. This includes correction for changes in emissivity, Bremsstrahlung background, thermal background, ghosts, and image mapping (scale, distortion, rotation, shift).

Released 2024/12/04
Released 2024/12/04

- Transmission Monitoring provides periodic measurements of the full system's optical and IR transmission to account for any degradation of the optical elements (specifically first mirrors). This is accomplished with a with a hot filament source mounted on the back of the shutter within bullnose, which creates a known radiation source for both visible and IR channels. Prototype testing is planned to validate the source performance and long-term stability. The transmission filament is described in section 8.3. It is anticipated that TM is required after every pulse (or few pulses) and before and after mirror cleaning.

Each calibration activity outlined above is expected to be conducted at specific times, either during installation, operation, short-term maintenance (STM), or long-term maintenance (LTM). An example timeline with the operation type and calibration types is shown in Figure 37.

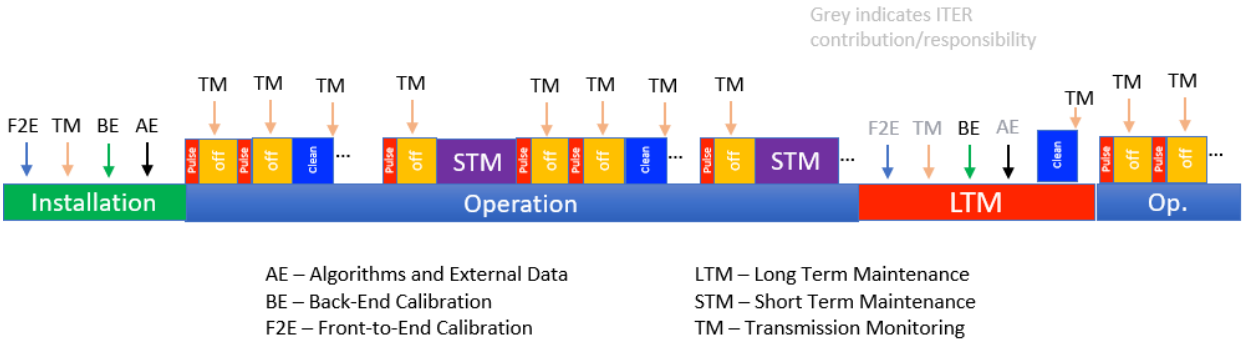

Figure 37. Example calibration timeline

8.2 Back-end Calibration Design

The calibration system consists of a set of lens and fold mirrors that bring light from a black body source (IR) or integrating sphere (visible) into the beam path via the A70 splitter. The two-level optical layout shown in Figure 38 has the visible leg mounted on the visible optical bench assembly and the IR leg mounted to the main optical bench assembly. Visible light is directed down to the main optical bench by CAL-VIS-FM1 and is combined with the IR leg via CAL-S1 dichroic splitter. The opto-mechanical construction of the calibration mounts uses the same design methods as the main optical path mounts.

Released 2024/12/04
Released 2024/12/04

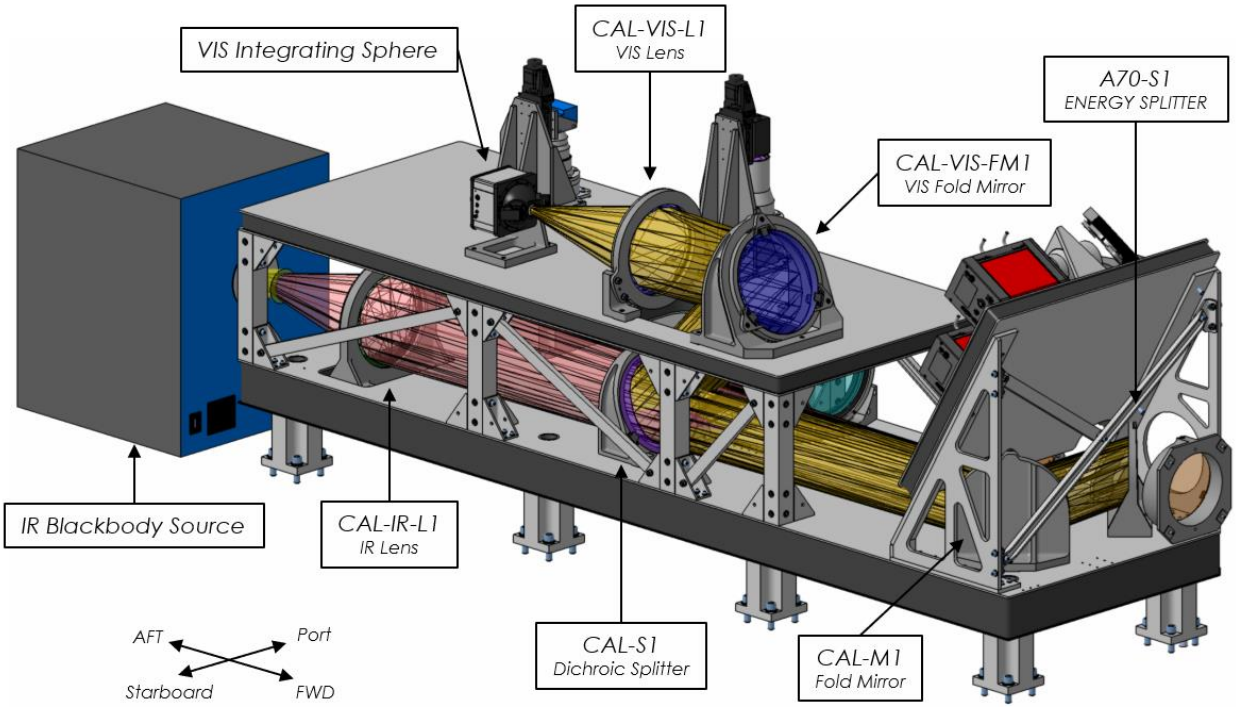

Figure 38. Calibration optical layout

8.3 Transmission Filament Design

Transmission monitoring is performed using a hot filament, serving as a light source mounted on the back of the shutter. This allows for periodic monitoring of transmission changes of the optical train. The transmission monitoring filament design needs to achieve temperatures up to 1500°C for SNR≥1000 in the visible spectrum. See additional discussion of the filament transmission monitoring approach of the Calibration section of the Optical Model Results [44]. The filament design is under development to meet the following performance specifications:

- The radiating surface shall be 20mm diameter, slightly larger than the aperture (18mm).
- Heater shall be capable of achieving external surface temperature of 1500°C on the radiator plate.
- Temperature of radiating surface shall be uniform to within 10% over the surface at steady state.
- Two heating circuits in a single housing.
- Maximum current for each heating circuit shall be 20 Amps to meet requirements of electrical feedthrough.
- Radiator plate shall be Molybdenum with a matte finish achieved by grit blasting.

Released 2024/12/04
Released 2024/12/04

- The filament will be capable of 3 operational modes:
    1. Both heaters simultaneously (normal operating mode)
    2. Heater one heater only
    3. Heater two heater only

The preliminary design concept of the heater assembly is shown below in Figure 39.

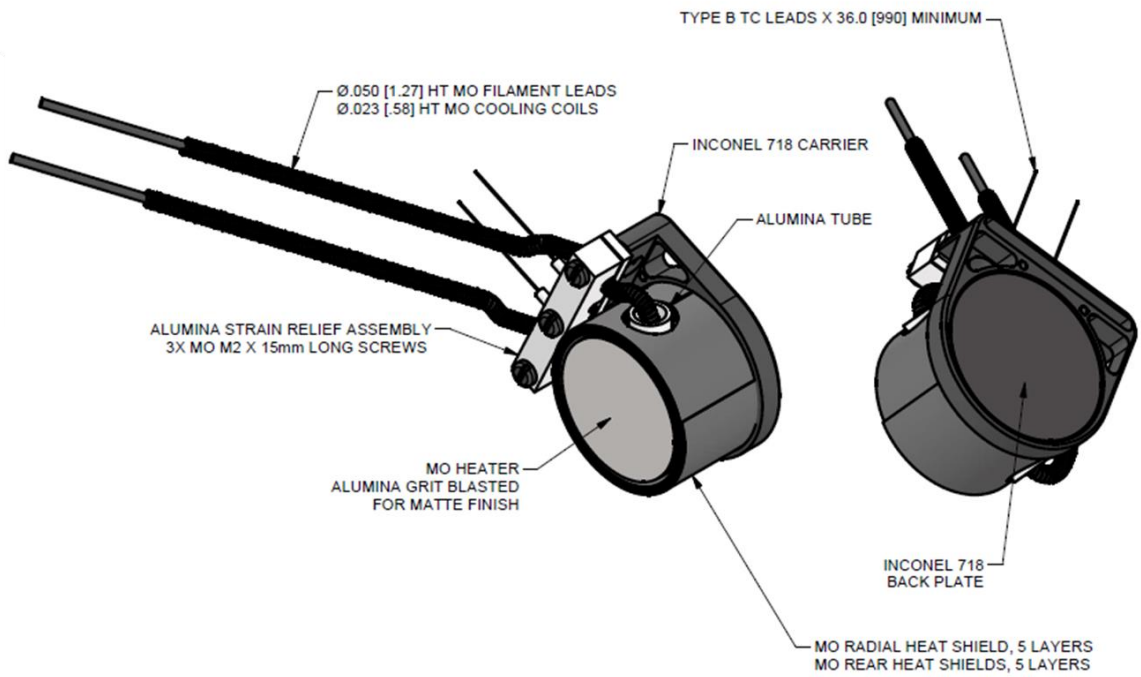

Figure 39. Preliminary transmission filament design

Annex B [5] defines multiple calibration filaments placed before and after various optics along the beam path. However, the only useful position for a transmission filament is directly on the beam path which obstructs the field of view. Analysis during preliminary design indicates filaments near the edge of the beam path do not provide light or coverage over the mirrors back to the sensor as indicated in Figure 40. Therefore, the only transmission filament in the UWAVS system resides on the back of the shutter blade.

Released 2024/12/04
Released 2024/12/04

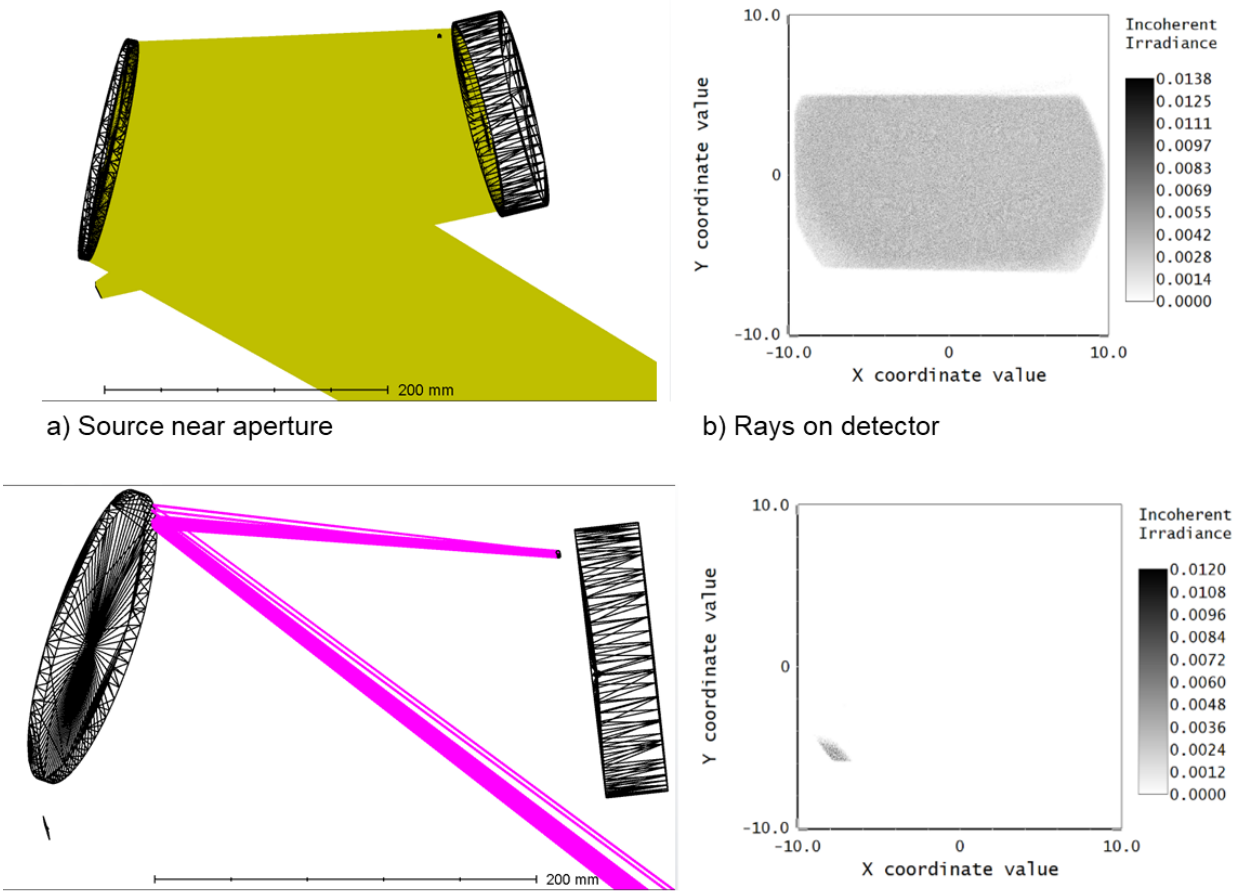

a) Source near aperture

b) Rays on detector

c) Source near edge of beam path

d) Rays on detector

Figure 40. Comparison of filament light source positions and light back to sensor.

An image of the filament on the shutter blade in front of the aperture is shown in Figure 41.

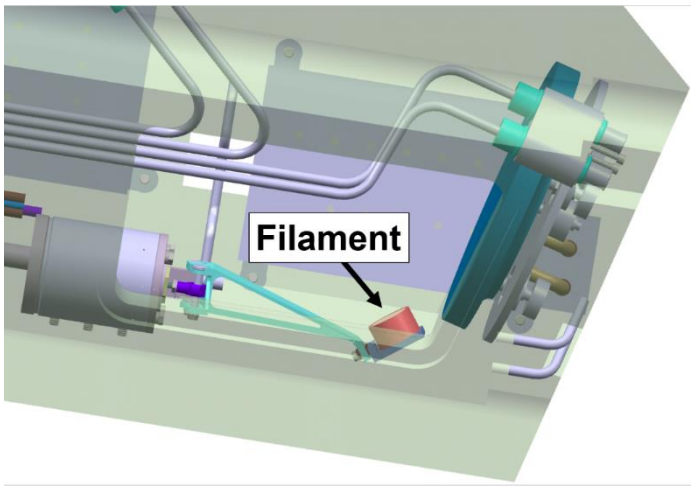

Figure 41. Filament on shutter blade inside the Bullnose.

Released 2024/12/04

Released 2024/12/04

9 MIRROR CLEANING RF DESIGN

9.1 Mirror Cleaning System RF Design Overview

The primary function of the mirror cleaning system is to provide efficient and homogenous cleaning of the first two mirrors which will experience surface contamination from exposure to the ITER plasma. This is achieved through RF plasma cleaning. A plasma sustained in the bullnose generates energetic ions impinging on the mirror's surface which eject material/ions from the mirror (sputtering). During the sputtering process both the contaminant material and mirror coating material will be removed. By adjusting the plasma's properties (gas species, pressure, ion energy, etc.) the sputtering process can be tuned to optimize the relative removal rates of the contaminants vs the mirror coating material, especially for low Z contaminants. There has been extensive research and development performed on the RF plasma cleaning methodology adopted by the UWAVS diagnostic.

The mirror cleaning system is comprised of both in-vacuum RF components, feedthroughs and ex-vessel RF power generation, tuning, and transmission components. The plasma cleaning system will support the removal of various contaminants (both low and high atomic number species), and thus must be able to operate over a range of gas species (e.g., H, He and Ar), gas pressures (1-10 Pa), and ion energies (50-200 eV). To generate sufficient ion energies, the RF power needs to meet or exceed 1 W/cm^2 at the mirror surface (~250 W total for a 170 mm diameter mirror).

A block diagram of the mirror cleaning system is shown in Figure 42 (landscape version in Figure 105 of APPENDIX A). The system is composed of two identical RF delivery systems, one for each mirror within the bullnose. Each system contains a fixed frequency (60 MHz) RF generator located in the cubicle. The RF generator feeds an active matching network located in the BEOC. The active matching network dynamically adjust to maintain proper impedance match between the RF generator and the bullnose load impedance (i.e. the combination of the prematcher, mirror plasma, and Notch Filter (NF). The output of the matching network is split, and each output is coupled to a fixed prematcher behind each mirror. The purpose of the fixed prematcher is to transform source impedance to the nominal plasma/mirror impedance. At present this impedance is unknown. Estimates can be based on previous work but with a large degree of uncertainty. Section 15.1 discusses the prototype development and planned measurements of the plasma impedance in a representative UWAVS bullnose environment. The output of the fixed prematcher is attached to the mirror. The mirror is DC grounded through the water cooling lines, so a quarter-wave or NF decouples the 60 MHz from ground by reflecting the incident power back to the local cleaning plasma.

Released 2024/12/04
Released 2024/12/04

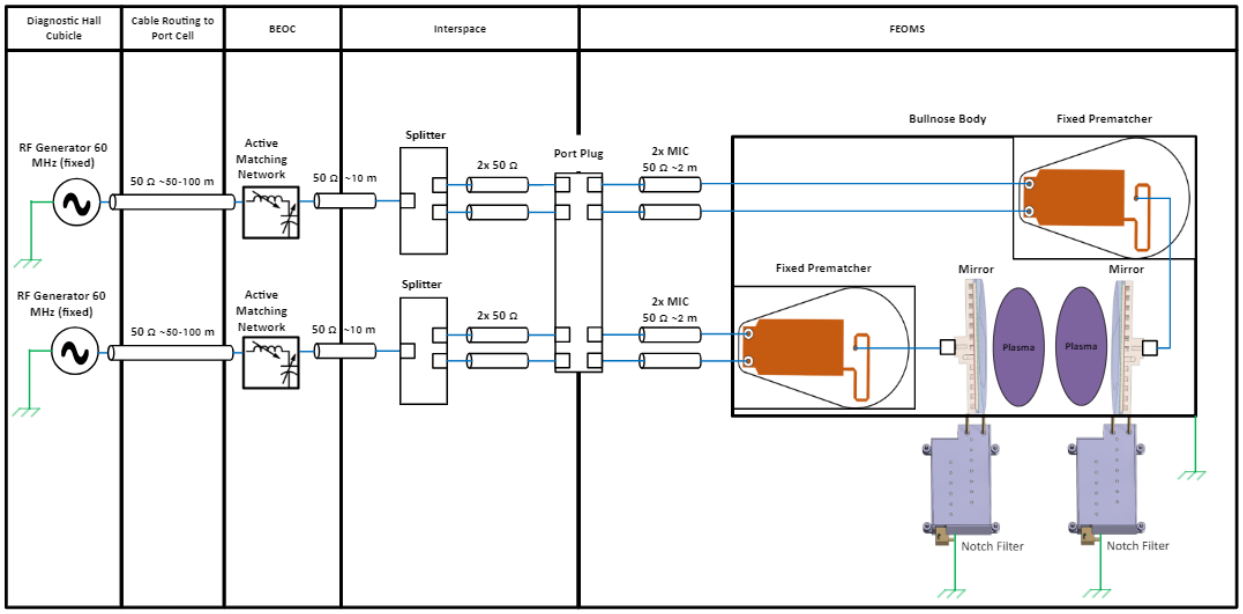

Figure 42. Simplified RF mirror cleaning system schematic.

The bullnose assembly is shown in Figure 43 with the key elements of the mirror cleaning system identified. The space constraints imposed on the bullnose require that these elements are compactly integrated into the bullnose assembly.

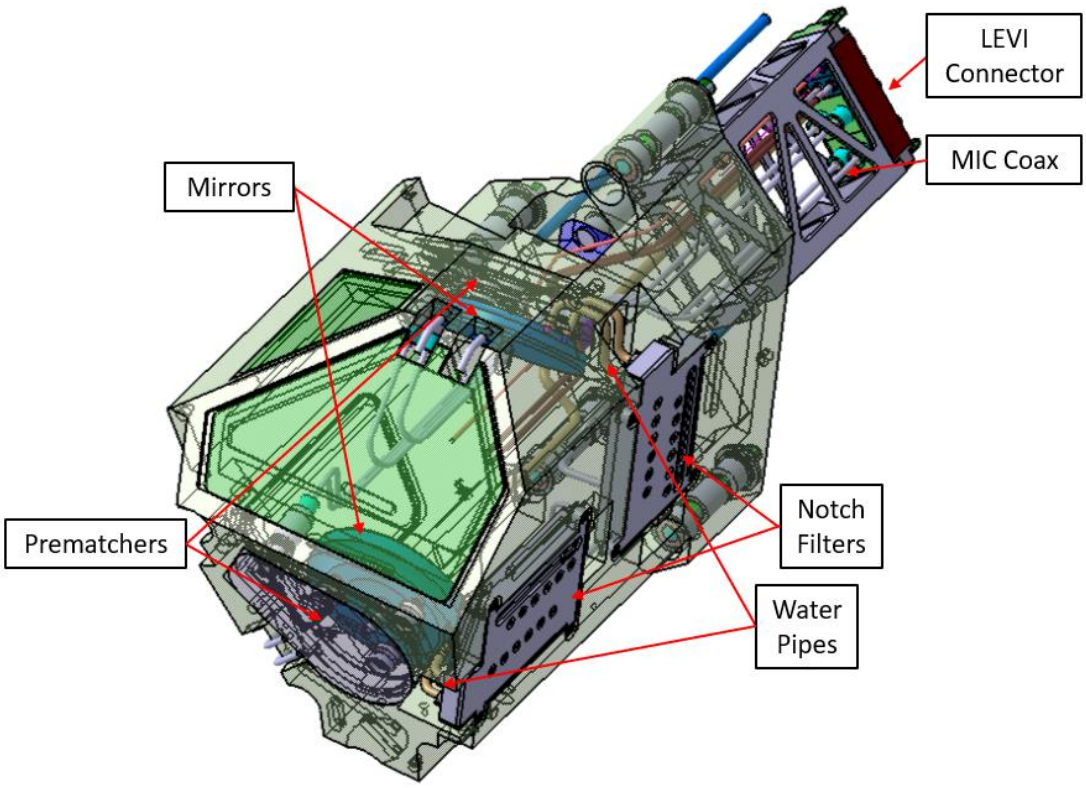

Figure 43 Mechanical assembly of the bullnose with key RF components identified.

Released 2024/12/04
Released 2024/12/04

9.2 Prematcher

Efficient RF power delivery requires that large transmission losses be mitigated, and that total transmission loss is characterized and budgeted to ensure sufficient power delivery to the plasma. If the total transmission loss is too large it will require greater input RF power and increase the likelihood of RF induced failures (e.g., arcing, heating, component failure or degradation, etc.). The transmission loss of the RF system is composed of both real or attenuation loss and rejection or mismatch loss. There will be significant loss due to the large physical length (~100 m) of the system and number of connection points. While these losses are difficult to minimize, given the length and complexity of the system, they are individually small and can be easily budgeted in the system design. A large risk to the RF system design is rejection or mismatch loss from the impedance mismatch between the 50 Ω RF source and a mostly inductive or capacitive plasma load at an electrode/mirror. In most RF driven plasma applications this matching is performed by an active matching network (further discussed in Section 9.3) placed near the impedance mismatch (i.e. mirror input). However, the ITER environment precludes the use of an active matcher near the bullnose, and instead the active matcher is located approximately 10 m away in the BEOC. This both limits the active matching network's ability to create a match over a range of load impedances and creates large Voltage Standing Wave Ratio (VSWR) over the length of the RF system between the matching network and load. High VSWR can be particularly problematic at connector locations or upstream where the RF power is highest, and RF induced failure is more likely. As such a fixed prematcher is used to match the source impedance to the nominal load (plasma+mirror) impedance at the point of mismatch. The active matcher's role is then limited to correcting for smaller deviations from the nominal plasma impedance caused by variation in the systems operating parameters (e.g., RF power, temperature, gas species, gas pressure, transient behavior, etc.).

Released 2024/12/04

The fixed prematcher is an in-vessel circuit board which is mounted within the bullnose directly behind each mirror. The current design of the prematcher was incorrectly based on an assumed load impedance of 0.6 Ω-j8.8 and optimized for operation at 60 MHz. At this time, effort has not been taken to redesign and integrate the prematcher, because the high uncertainty in the assumed impedance and the work underway to measure the true load impedance (as discussed in Section 15.1.2). The current prematcher design is shown for completeness. The reflection coefficient (S11) is designed to be less than -10 dB to provide ~87% of power to the mirror for plasma cleaning. Figure 44 shows the prematcher board layout and the calculated S-parameters corresponding to ~92% total power coupling to the load. The board is constructed on a 1 mm thick alumina substrate with 50 µm thick copper traces. Note that once the load impedance is measured and the prematcher is finalized additional modeling and/or measurements will be necessary to include the stray capacitance or inductance caused by the prematcher housing structure.

Released 2024/12/04

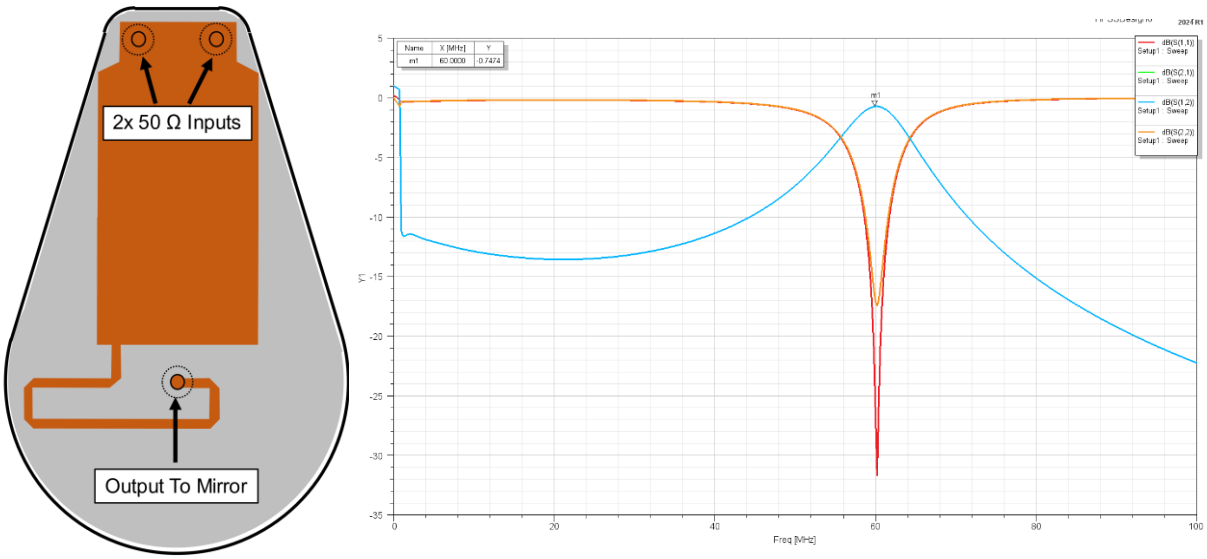

Figure 44. The fixed prematcher board layout (left) with the signal trace shown in brown and ground plane shown in gray. Calculated S-parameters of the prematcher.

9.3 RF Generator and Active Matching Network

The 60 MHz RF generator as shown in Figure 45 is located in the cubicle. The final power requirement of the RF generator has not been finalized, as it will have to account for the total transmission loss and the power required by the plasma. The total loss will be accurately determined in the FDR phase. However, at present the RF Generator is expected to be capable of at least 1 kW of power at 60 MHz. Fortunately, commercial RF generators are available in excess of 5 kW at 60 MHz. At present the prototype effort uses a Comet Cito Plus 6010, 60 MHz and 1 kW RF generator for each mirror, and similar models are available up to 6 kW.

Figure 45 Commercial 60 MHz, 1 kW RF generator.

The active matching network is located within the BEOC and transforms the source impedance (50 Ω) to the conjugate of the load impedance (typically <50 Ω) at the output. The active matcher selected for the prototype test is the Comet AGS 6020 (shown in Figure 46), which is capable of handling 2 kW at 60 MHz and generally forming matches for loads with resistive components <50 ohms and reactive components between -j50 ohms and j50 ohms. By transforming the source

Released 2024/12/04
Released 2024/12/04

impedance to the conjugate of the load, impedance power can be efficiently transferred to the load. The active matching network consist of two fixed inductors, main and shunt (with up to 3 different fixed taps), and two variable capacitors, load and tune, which are driven by servo motors. The active matching network dynamically adjusts the capacitors to minimize VSWR. The time to form a stable match from good preset values is typically less than 2 seconds. Smith charts for each of the available inductor taps are also shown in Figure 46.

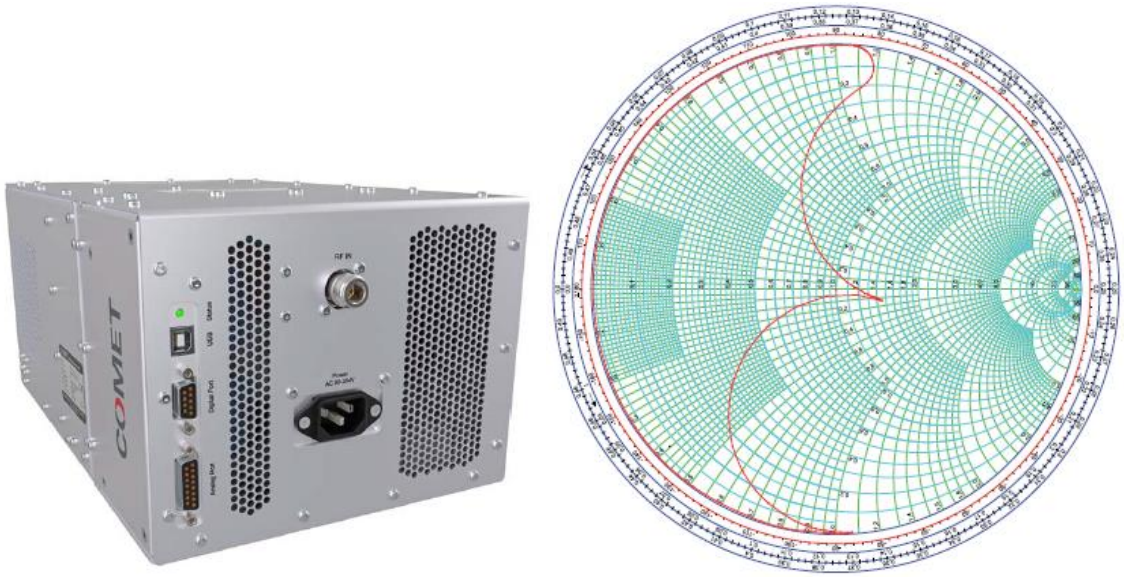

Figure 46 Active Matching Network and Smith chart for 1 of the 3 available tuning ranges

It should be noted that previous studies have found that the prematcher performance can be optimized by active tuning of the RF frequency. However, at present this is not believed to be necessary as the active matching network can still account for small impedance mismatches at the prematcher.

9.4 Notch Filter

In typical RF driven plasma cleaning applications, the electrode is electrically isolated from ground. This allows for efficient delivery of the RF power and efficient cleaning operation, as the electrode develops a self-bias which aides in the sputtering process. The bullnose of UWAVS and other ITER diagnostics are subjected to high nuclear heat loads which requires active liquid cooling of most components, including the mirrors. In addition, insulating breaks have been prohibited over concerns of their long-term reliability and high consequences associated with a coolant leak. The result is that the mirror is electrically grounded via the water-cooling lines. A quarter-wave notch filter is used to create an RF choke and isolate the RF from ground. The current NF design is shown in Figure 47. It is constructed from stainless steel and alumina components. The water flows through an “S-shaped” center conductor which enclosed in alumina

Released 2024/12/04
Released 2024/12/04

insulator to form a transmission line structure. The center conductor is shorted to ground by the slider. The slider position can be adjusted and fixed during commissioning to set the effective transmission line length to a quarter wavelength at 60 MHz.

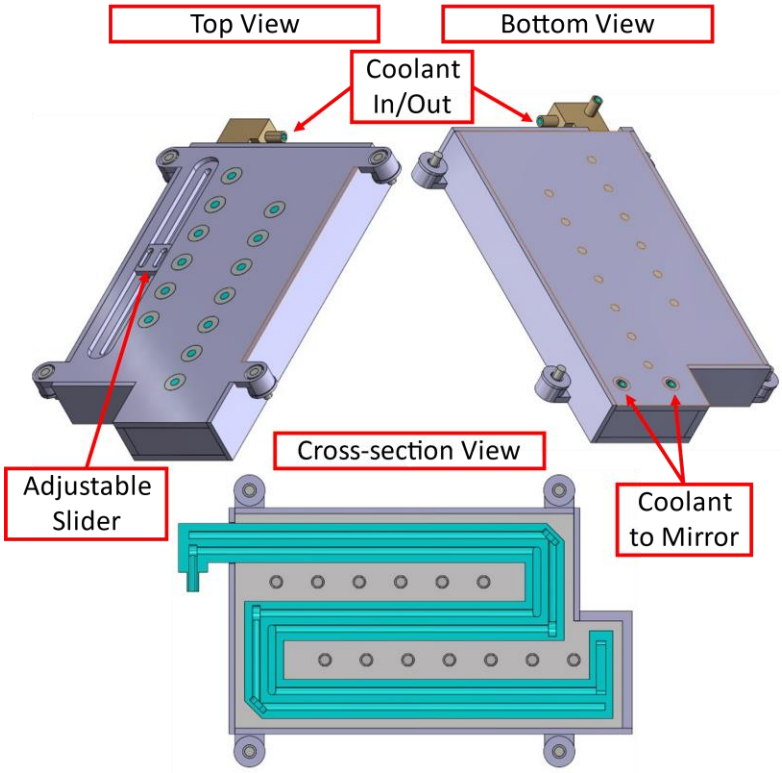

Figure 47 Compact NF Assembly

RF modeling indicates that the current compact NF design is adjustable from 40-47 MHz once the length of pipes affixing to the mirror are included. This indicates that the current compact NF is too large and will need to be reduced in total length to recenter the range at 60 MHz. Fortunately, the NF size was initially of concern, so any reduction in overall length/size will aide in the NF integration within the bullnose's allowed volume. While the NF has not been adjusted to reflect the appropriate length in the present design, the NF has been analyzed and adjusted for the prototype version discussed in Section 15.1.1. Ansys High Frequency Simulation Software (HFSS) simulations of the compact NF with the pipes attaching it to the mirror and the slider at the middle position is shown in Figure 48. The Smith chart shows that the NF does perform as a high impedance "open" circuit at the notch frequency. It should be noted that this analysis should be repeated once the NF design (including the pipes and insulation attaching it to the mirror) has been finalized. Actual performance of the NF for rejecting the 60 MHz RF will depend on the load impedance.

Released 2024/12/04
Released 2024/12/04

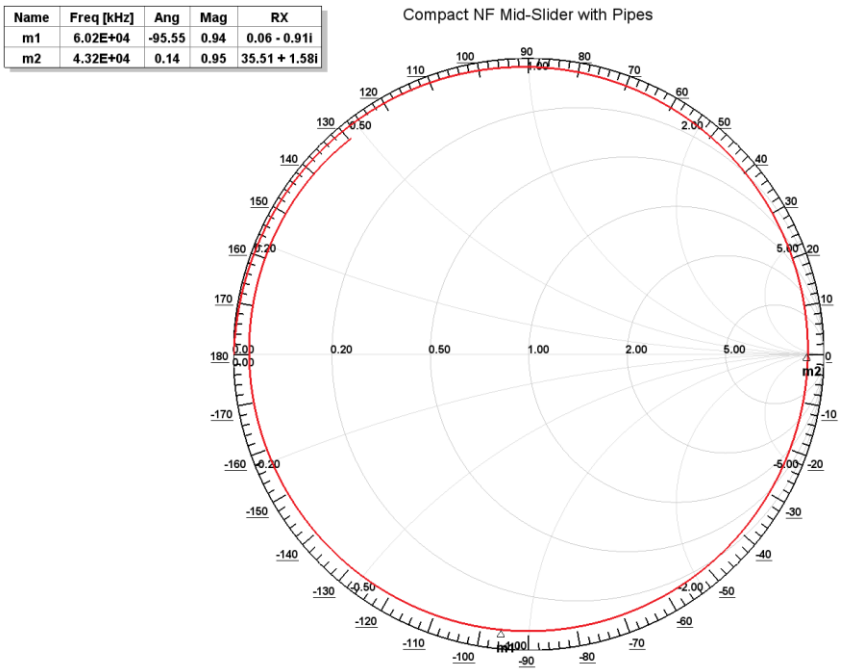

Figure 48 HFSS Analysis of the compact NF with the slider at the middle position.

9.5 Transmission Lines

The simplified schematic presented previously in Section 9.1 shows several regions where RF power is transmitted using significant lengths of coaxial cables as well as a variety of connectors, and feed-throughs. It is expected that the design and selection of components will be standardized across other PBS.55 systems including the choice of flexible coaxial cable, mineral insulated cable (MIC), vacuum feed-throughs, and connectors.

The detailed design and analysis of the UWAVS RF power transmission system from the active matching units in the BEOC to the first-mirrors in the bullnose will be pursued during final design. Furthermore, the exact routing of the cables between the diagnostic hall cubicles and port cell has yet to be determined by PBS.44 (Cable Trays) and PBS 55.NEX0 (Electrical Ex-Vessel Systems). However, it is important to conduct a preliminary estimate of the losses incurred by the long distances expected. This is accomplished by identifying likely cable routing paths, estimating the lengths of each section, and applying the appropriate loss factor for the type of cable selected.

9.5.1 Cable Selection (Ex-Vessel)

Cable selection is restricted to those published in the IO Cable Catalog [29]. However, a flexible coaxial cable has been approved specifically selected for RF mirror cleaning applications due to its low attenuation, flexibility, fire-resistance, and radiation resistance. The IO designation for this cable type is EZ0110LN although the industry trade name *is Ecoflex10 plus Heatex*. This cable

Released 2024/12/04
Released 2024/12/04

will be included in a future version of the catalog. Technical data for this cable is shown in Figure 49 below.

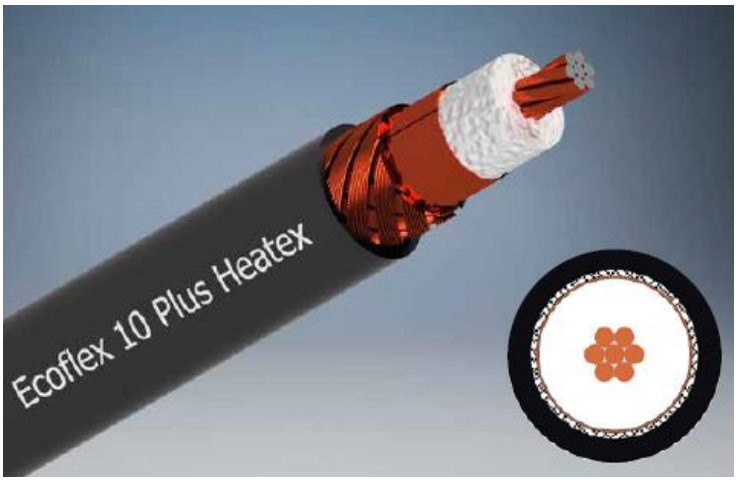

Technical data

Inner conductor	Hybrid CCA – stranded copper-clad aluminium wire
Inner conductor Ø	2,85 mm (7 x 1,0 mm, 10 AWG)
Dielectric	foamed Polyethylene (PE) with skin
Dielectric Ø	7,2 mm
Outer conductor 1	copper foil overlapped
Shielding factor	100%
Outer conductor 2	shield braiding of bare copper wires
Shielding factor	75%
Outer conductor Ø	7,9 mm
Jacket	highly flexible thermoplastic copolymer (FRNC) black
Weight	106 kg/km
Min. Bending radius	4XØ single, 8XØ repeated
Temperature range	-55 to +85°C Transport & fixed installation -40 to +85°C Flexible use
Pulling strength	600 N

Electrical data at 20°C

Capacity (1 kHz)	78 nF/km
Velocity factor	0,85
Screening attenuation 1 GHz	≥ 90 dB
DC-resistance Inner conductor	≤ 5,1 Ω/km
DC-resistance Outer conductor	6,6 Ω/km
Insulation resistance	≥ 10 GΩ*km
Test voltage DC (wire/screen)	7 kV
Max. Voltage	5 kV

Typ. Attenuation (db/100 m at 20°C)

5 MHz	0,76	1000 MHz	13,49
10 MHz	1,14	1296 MHz	15,68
50 MHz	2,66	1500 MHz	17,01
100 MHz	3,80	1800 MHz	18,91
144 MHz	4,66	2000 MHz	20,14
200 MHz	5,51	2400 MHz	22,42
300 MHz	6,94	3000 MHz	25,37
432 MHz	8,46	4000 MHz	29,55
500 MHz	9,12	5000 MHz	33,44
800 MHz	11,88	6000 MHz	37,05
		8000 MHz	44,08

Max. Power handling (W at 40°C)

10 MHz	3.100	2400 MHz	175
100 MHz	960	3000 MHz	154
500 MHz	413	4000 MHz	130
1000 MHz	285	5000 MHz	115
2000 MHz	194	6000 MHz	100
		8000 MHz	86

Figure 49 Technical data for the selected ex-vessel coaxial cable type.

Two key parameters of interest are the attenuation and maximum power handling at 60 MHz:

Attenuation: 2.94 dB/100m

Max Power: 1250 W

Released 2024/12/04
Released 2024/12/04

These values are estimated by curve fitting the published data in the frequency range 5-2000 MHz. The attenuation per 100 meters is about 3dB, equivalent to 50% power loss. The 1250 W maximum power rating is sufficient for the 1kW RF generator. However, if more power is found to be needed then additional lines will be needed as well as splitters and combiners.

9.5.2 Estimated Cable Lengths

The decision to place the RF generators in the diagnostic hall cubicles requires long transmission lines using shared cable trays routed throughout the plant managed by 55.NE. The exact routing of the cables between the diagnostic hall cubicles and port cell has yet to be determined by 55.NE. We have therefore relied on rough estimates of likely paths to each port, with distances inferred from plant layout diagrams. Figure 50, indicates likely paths from the cubicle area in the diagnostic hall (DH) to the BEOC in each port cell. The estimated cable lengths are conservative. It is also assumed that an additional 10 m of cable will be required to connect the RF active matching units in the BEOC to the CP electrical feed-through (EFT).

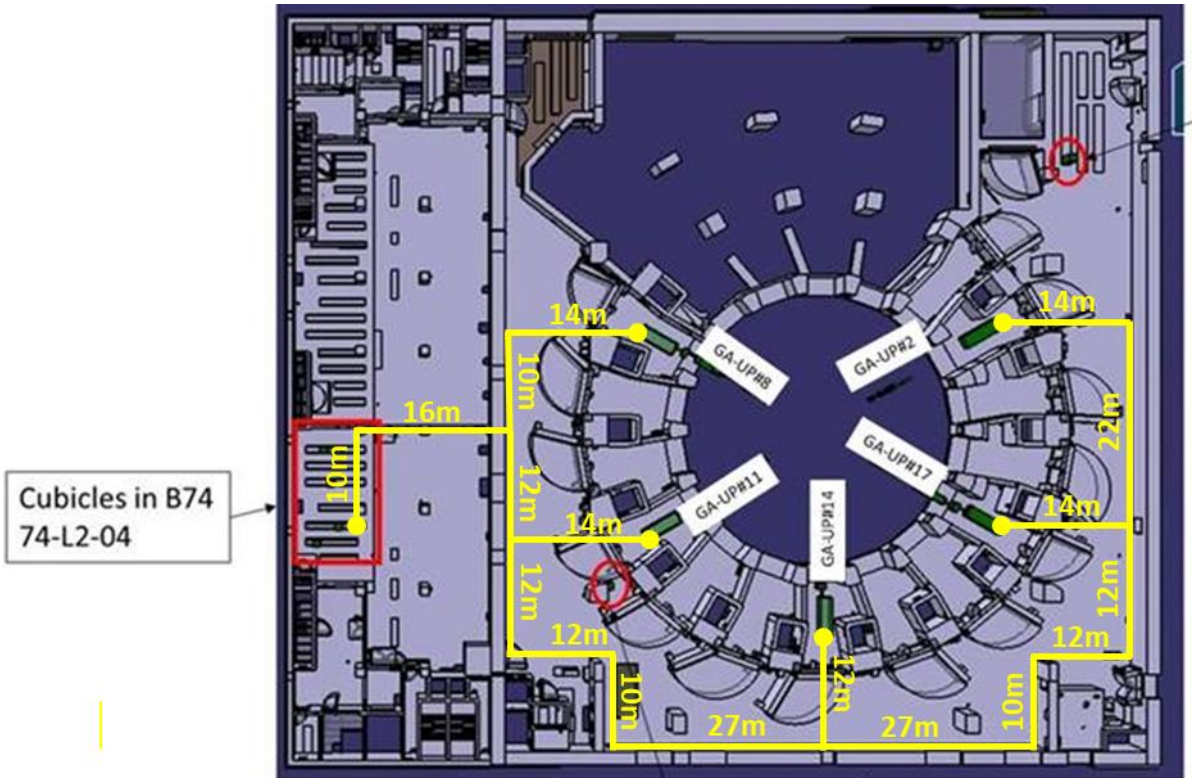

Figure 50. Illustration of plant layout showing cubicle locations and anticipated cable runs for RF transmission lines.

A tabulation of the total cable lengths, including BEOC to EFT, is presented in Table 27. The shortest cable runs are to ports UP08 and UP11, estimated to be about 60 m. For comparison,

Released 2024/12/04
Released 2024/12/04

cable distances used for similar calculations by the 55.E6 (VSRS) system has been reported as 48 m from DH to port cell. The longest distance is to port UP02 and is estimated at 206 m.

The impact of the long cable lengths on transmitted RF power is discussed as a risk in Section 14.10.

Table 27. Estimated Cable Lengths and Associated Power Loss

Port #	Est. Cable Length (m)			Atten. (dB)	Power Loss
	DH to BEOC	BEOC to EFT	Total		
UP08	50	10	60 m	1.80dB	34%
UP11	52	10	62 m	1.86dB	35%
UP14	111	10	121 m	3.63dB	57%
UP17	174	10	184 m	5.52dB	72%
UP02	196	10	206 m	6.18dB	76%

Released 2024/12/04

Released 2024/12/04

10 INSTRUMENTATION AND CONTROL ARCHITECTURE

The UWAVS System I&C is tasked to provide real-time view of the divertor region using two IR cameras and two visible cameras (2X Infratech Image IR 10300 and Emergent HT-12000/Mikrotron EoSens 4CXP respectively). Additional details on the specific camera specifications can be found in [52].

The I&C system serves primary roles in basic control, machine protection, and advanced control. UWAVS diagnostics is positioned in 5 different ports, namely, Port 02, Port 08, Port 11, Port 14, and Port 17. Notably, the instrumentation across all 5 ports is identical. Throughout the beamline, motors and sensors are strategically placed, with signals routed to and from them to the back-end optics and cameras (BEOC), and diagnostic hall, spanning over a length > 100 meters. The system has most of the equipment located in BEOC and diagnostic hall. Fast controllers, and slow controllers are in the diagnostic hall cubicles. The signals are routed via specially selected cables based on radiation and environmental exposure. An instrumentation diagram for UWAVS is shown in Figure 51 (landscape version in Figure 106 of APPENDIX A).

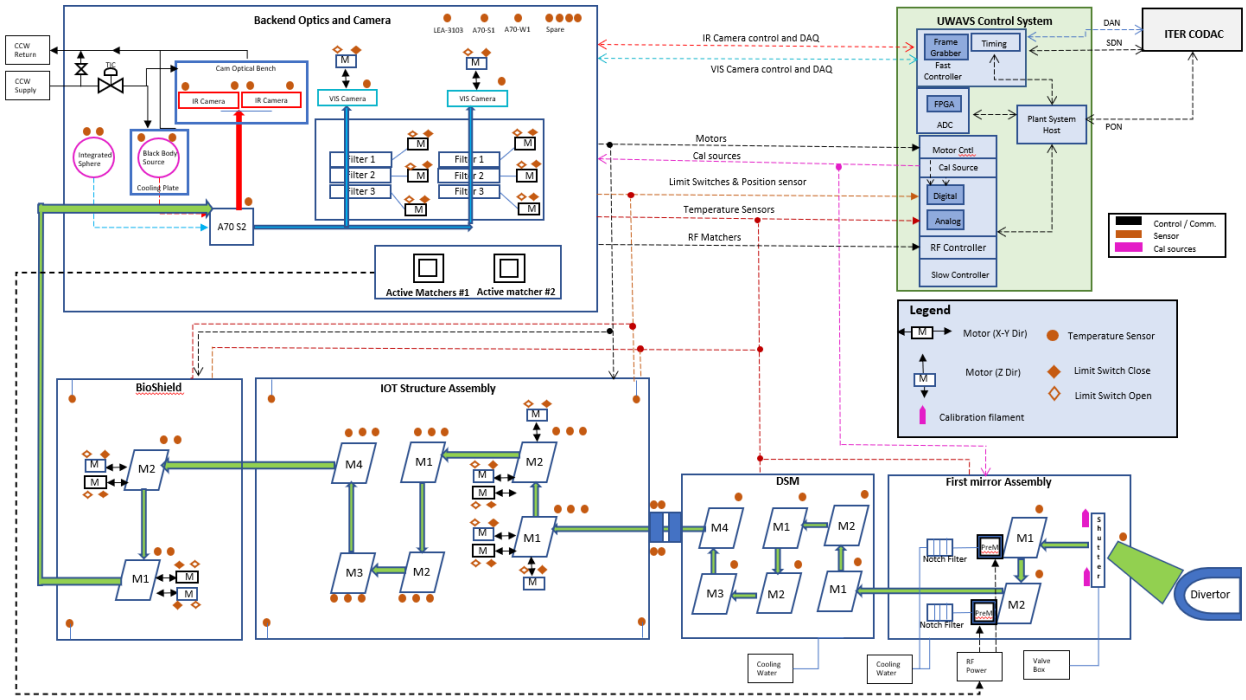

Figure 51. Illustration of the instrumentation and controls for 55.GA single port

The UWAVS Instrumentation and Control system has two hierarchical roles. At the higher level the UWAVS I&C system is required to serve the larger needs of the ITER plant system. As with other diagnostics, the UWAVS system will serve as an integrated node in the CODAC (Control, Data Access and Communication) network system as a designated ITER Plant System. At the lower level the system is required to attend to the local needs of the UWAVS electro-mechanical

Released 2024/12/04
Released 2024/12/04

and opto-electrical systems. This includes measurement, control, monitoring, calibration, and maintenance using various instruments to perform UWAVS operations such as active alignment, mirror cleaning, etc.

Each UWAVS port has independent two full sized cubicles. One full size cubicle houses fast controller with mTCA chassis and frame grabbers for high-speed, high-performance measurement, as well as the supervisory fast controller. Second full-size cubicle contains slow controller and all the controllers for COTS devices except for cameras. Slow controller is used to perform slow, low frequency I&C functions. The Plant System Host (PSH) is shared between all five UWAVS ports and currently located in the single common cubicle dedicated to all ports.

A control scheme for single port is divided in I&C subsystems that show different parts of I&C in terms of instrumentation and operation as shown in Figure 52.

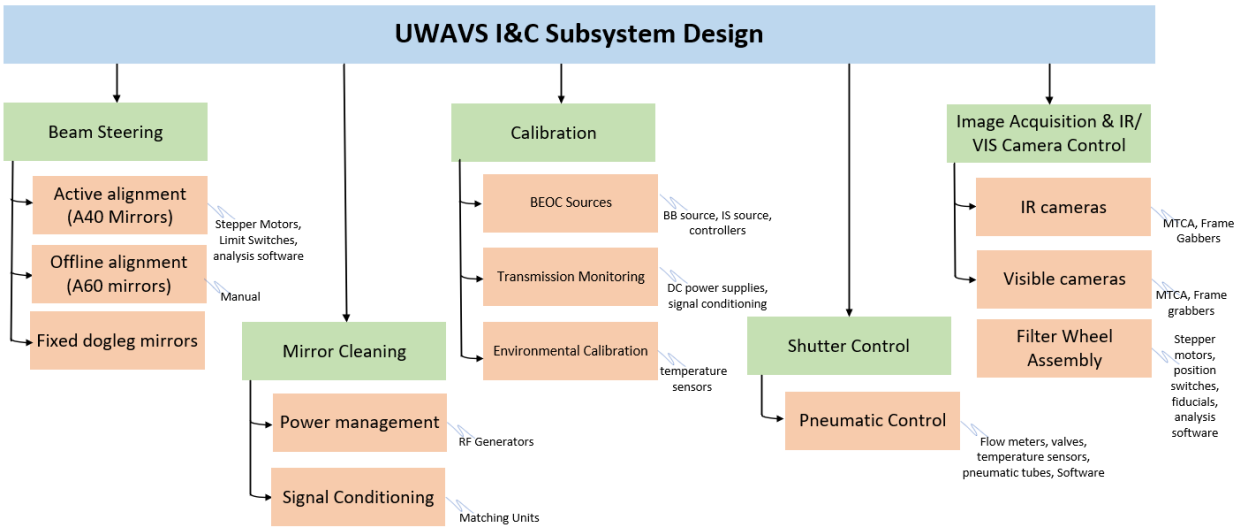

Figure 52. 55.GA design breakdown into subsystems

A complete UWAVS I&C design includes the diagrams, control schemes, I&C design decisions. The UWAVS diagrams are detailed in P&ID [53], [13], [16], [54], cabling [17], [19], [18], [20], SLD [55], [56], [57], [58], and PFD [59], [60], [61], [62]. Important aspects of UWAVS I&C design such as the cubicle layouts, head load analysis, instrument selection (BOM), software architecture, and description of I&C subsystems is documented in [52]. The function definitions, operational procedures, hardware architecture, state machine, requirements, use cases, CODAC interfaces etc. is detailed in [63], [64].

Released 2024/12/04
Released 2024/12/04

11 INTERFACES

Interface sheets relevant to the 55.GA system are given in Table 28. Piping & instrumentation diagrams (PID's) are given in Table 29. Cabling diagrams are given in Table 30. Process flow diagrams (PFD's) are given in Table 31. Single line diagrams (SLD's) are given in Table 32.

Table 28. 55.GA Interface Sheets

No.	PBS	IDM#	Title
1	18	V74XGK	IS-18.GC-55-001 Interface between the Optical Diagnostics and the Glow Discharge Cleaning
2		V7G5WY	IS-18.GI-55-002 Functional Interface between the Diagnostics "Mirror Cleaning" and the Gas Injection System
3	23	24T35Z	IS-23.06-55.GA001 Interface between HCRHS (PBS 23.06) and Diagnostic (PBS 55.GA) for Vis/IR Up (located in UPP#02)
4		8SG655	IS-23.11 (ART)-55.(C1, C2, C4, D1, E1, E2, E4, E6, EB, EC, EF, G1, G6, GA, GE)-001 calibration
5	31	RRNVCK	IS-31-55-016 Type-1 Diagnostics
6		SRJ488	IS-31-55-018 Ex-Vessel-Interspace
7		SRRHVH	IS-31-55-019 Shutter Actuation
8		SRZ7KT	IS-31-55-020 Mirror Cleaning
9	44	QVEYBM	IS-44-55-009 Interface sheet between PBS 44 and 55 for US-DA package cables
10	45	UMTL7W	IS-45-55.GA-001 Interface between PBS 45 CODAC and PBS 55.GA Upper Port Visible/Infrared wide angle viewing
11	47	XBQND7	IS-47-55.GA-050 Functional interface between IR Cameras, Vis/IR TV (Upper) and PCS
12	48	6W3NKB	IS-48.01-55.GA-001 Interface Between Vis/IR Up and central Safety System (Nuclear Safety)
13	55	SZRKME	IS-55.NW-55.GA-001
14		W38CTA	IS-55.GA-55.NE-001 Interface between Vis/IR Up (55.GA) and electrical services (55.NE)
15		3SBSAW	IS-55.GA-55.GL-001
16		X5W4BE	IS-55.U2-55.GA-001
17		X838G5	IS-55.GA-55.U8-001
18		XWR3MD	IS-55.GA-55.UB-001
19		X8XM6S	IS-55.GA-55.UE-001
20		UDQG3P	IS-55.GA-55.UH-001
21	58	WPPW3Q	IS-55-58-013 UPP Functional Tests Sequence
22	62	34GS5D	Interface Sheet (IS) between Tokamak Building (PBS 62.11) & Diagnostic Building (PBS 62.74) and Diagnostic (PBS 55)
23		357AB7	Interface Sheet (IS) between Hot Cell Building (PBS 62.21) and Diagnostic (PBS 55)
24	64	UY2DWM	IS-55-64-001 Functional Interface between Diagnostics and Radiological & Environmental Monitoring System (REMS)
25	66	VC5NWA	IS-55-66-004 Port Based Diagnostic Systems radwastes (Upper, Equatorial, Lower)

Released 2024/12/04
Released 2024/12/04

Table 29. 55.GA Piping & Instrumentation Diagrams

Port	IDM #	Title
2	PJ4JFG	55-GA-A0_IR_Cameras:_VIS/IR_TV_(Upper)_UPP02_PID
8	PJAC7P	55-GA-B0_IR_Cameras:_VIS/IR_TV_(Upper)_UPP08_PID
11	PJCAT5	55-GA-C0_IR_Cameras:_VIS/IR_TV_(Upper)_UPP11_PID
14	PHUE63	55-GA-D0_IR_Cameras:_VIS/IR_TV_(Upper)_UPP14_PID

Table 30. 55.GA Cabling Diagrams

Port	IDM #	Title
2	3QQP6T	55-GA-A0_IR_Cameras:_VIS/IR_(Upper)_UPP02_Cabling
8	3QSJ6B	55-GA-B0_IR_Cameras:_VIS/IR_TV_(Upper)_UPP08_Cabling
11	596WA5	55-GA-C0_IR_Cameras:_VIS/IR_TV_(Upper)_UPP11_Cabling
14	3QSD6R	55-GA-D0_IR_Cameras:_VIS/IR_(Upper)_UPP14_Cabling

Table 31. 55.GA Process Flow Diagrams

Port	IDM #	Title
2	3QRZQ8	55-GA-A0_IR_Cameras:_Vis/IR_TV_(Upper)_UPP02 PFD
8	FA247Z	55-GA-B0_IR_Cameras:_Vis/IR_TV_(Upper)_UPP08 PFD
11	FA49ZM	55-GA-C0_IR_Cameras:_Vis/IR_TV_(Upper)_UPP11 PFD
14	FAA8Y4	55-GA-D0_IR_Cameras:_Vis/IR_TV_(Upper)_UPP14 PFD

Table 32. 55.GA Single Line Diagrams

Port	IDM #	Title
2	RF429Q	55-GA-A0_IR_Cameras:_VIS/IR_TV_(Upper)_UPP02_SLD
8	RMEANB	55-GA-B0_IR_Cameras:_VIS/IR_TV_(Upper)_UPP08_SLD
11	RRE4X9	55-GA-C0_IR_Cameras:_VIS/IR_TV_(Upper)_UPP11_SLD
14	RY67QS	55-GA-D0_IR_Cameras:_VIS/IR_TV_(Upper)_UPP14_SLD

Released 2024/12/04
Released 2024/12/04

12 ASSEMBLY STRATEGY

12.1 Installation Sequence

Due to construction schedule, UWAVS must be assembled in stages in various sections of the building. Some of the equipment is integrated into larger structures prior to installation into the tokamak building, while some is mounted directly from interfaces on the building itself. Installation of some items cannot proceed until certain prerequisite installations are complete.

Figure 53 (landscape version in Figure 107 of APPENDIX A) outlines these installation dependencies for the complete UWAVS system. Processes with an orange arrow leading from them must be installed prior the connected process. For example, the populated DSM assembly must be installed before the Port Plug assembly can proceed followed by the populated ISS assembly. Items connected by black arrows indicate equipment that is integrated into a larger assembly often with other diagnostic systems prior to installation. Items with a green arrow leading from them are ready for installation at ITER when all prerequisites have been installed.

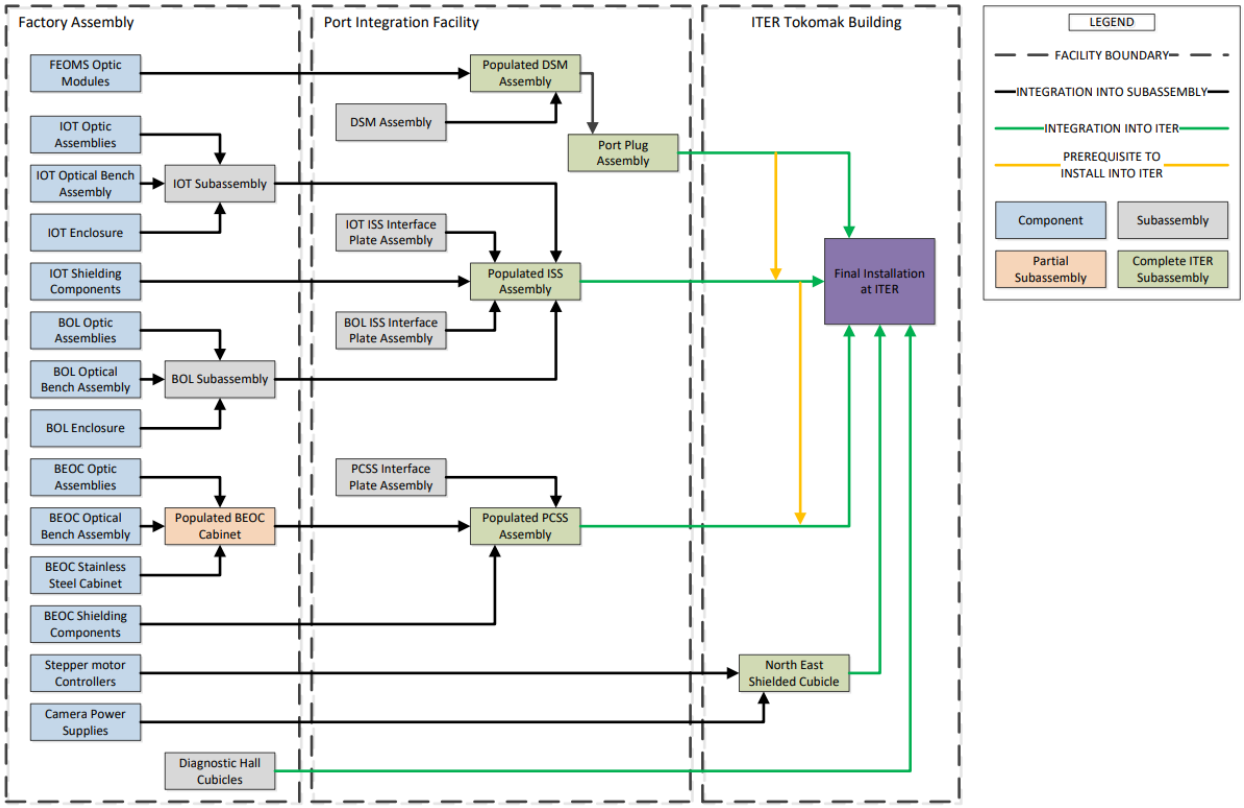

Figure 53. UWAVS installation process sequence.

Released 2024/12/04
Released 2024/12/04

12.2 Factory Assembly

Details of factory assembly will be established in final design however the high-level factory assembly has been established. Each FEOMS modules will be fully assembled (Figure 54) and mechanically inspected (Figure 55) as unit subassemblies. Then they will be installed on a DSM tooling simulator and tested as a group to verify optical performance (see Section 12.3 for additional details on factory testing).

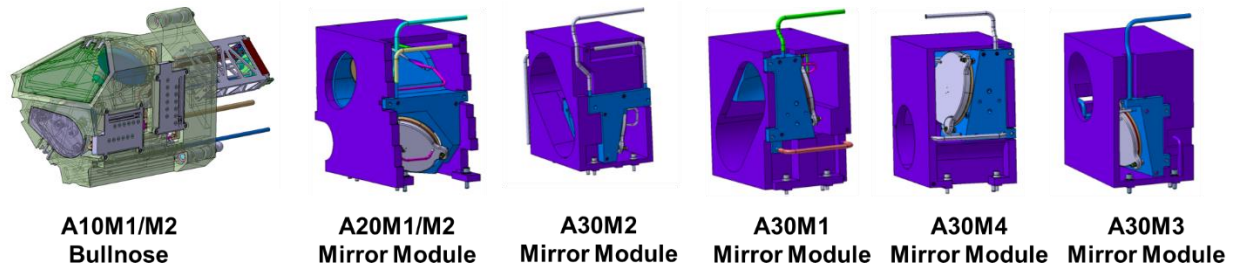

Figure 54. FEOMS mirror modules subassemblies

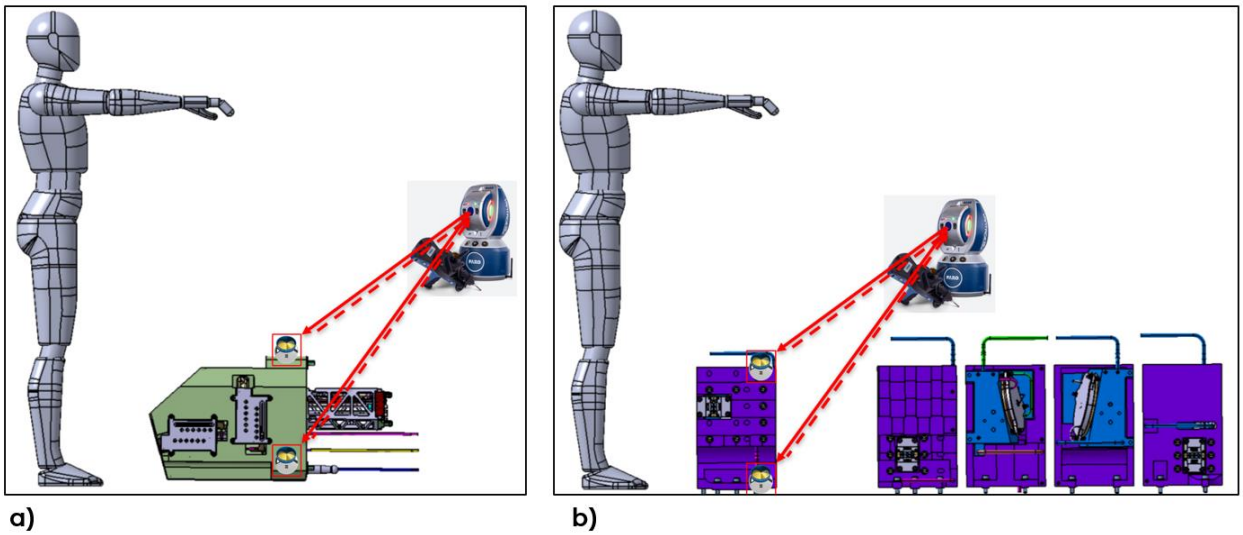

Figure 55. FEOMS mirror modules mechanical inspection

Additional details of in-vessel welds and design accommodations for manufacturing, inspection, and alignment can be found in technical design descriptions of the Bullnose [32] and the FEOMS A20-A30 mirror modules [36].

Similarly, each ex-vessel optical mount will be fully assembled and mechanically inspected as a unit subassembly. Each ex-vessel subsystem, however, will be fully assembled, aligned, and tested optically for verification as described in 12.3.

Released 2024/12/04
Released 2024/12/04

12.3 Factory Qualification Testing

Factory Qualification Testing will be done at the module and subsystem level prior to shipping to the Port Integrator Facility. Generally, qualification testing is done in five categories: component, in-vessel system, ex-vessel system, calibration, and I&C. For a detailed description of the factory qualification testing refer to UWAVS-35 Factory Qualification Test Plan [65].

All components and subassemblies shall pass quality inspections per relevant technical drawings and technical specifications. Any component containing welds shall be inspected per the ITER Vacuum Handbook [12], and components containing cooling channels shall undergo static pressure testing. Optical metrology shall be performed on all optics (or relevant samples) to measure optical properties: surface figure, transmission/reflectivity, and surface roughness in the case of metal mirrors. For mechanical components and subassemblies, all critical interfaces will be measured using laser tracker or CMM metrology and integrated into an “as-built” optical model. Surface figure and transmission/reflectivity will also be added to the “as-built” optical model. This model is used to predict optical performance and starting positions of remote alignment mirrors.

The mirror cleaning subsystem shall be tested on the assembled FEOMS bullnose to validate the integrity of the RF delivery system, see Figure 56. The bullnose is installed in a vacuum chamber and connected to an external RF system via the LEVI connector inside the vessel. A modified, representative plasma cleaning recipe is performed to ensure proper functionality of the system, without risking mirror surface quality.

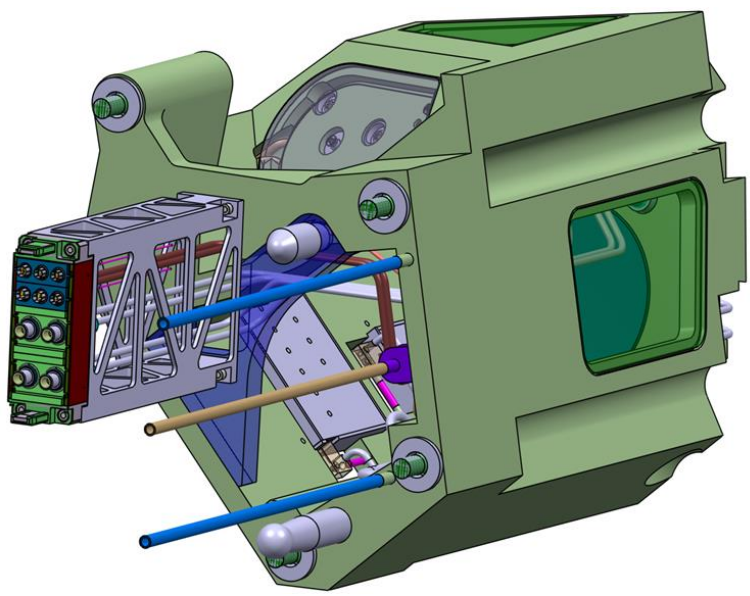

Figure 56. Assembled bullnose used for validation of mirror cleaning system.

Shutters shall be tested at in-vessel vacuum pressures under elevated temperatures to ensure actuation functionality, see Figure 57. In addition to actuation testing, the transmission monitoring

Released 2024/12/04
Released 2024/12/04

filament, located on the blade of the shutter, will be characterized. After the supplier characterizes temperature vs power consumption, the integrated filament will be testing in vacuum to verify power consumption data from supplier.

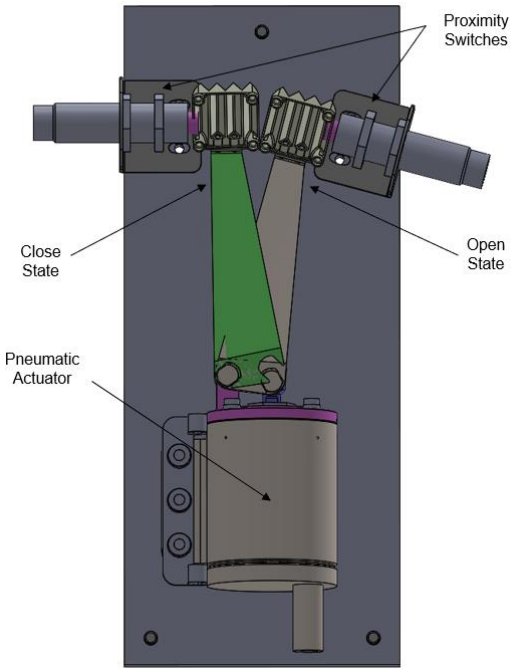

Figure 57. Shutter assembly setup on a test bench.

In-vessel components shall be aligned and verified using a DSM simulator, a fixture designed as a surrogate for the DSM. After mirror modules are assembled and metrology has been performed on critical interfaces, mirrors are adjusted to place mirror surfaces at correct positions and angles. Initially, bullnose optics A10-M1 and A10-M2 are installed the complete bullnose is installed on the DSM simulator. The optical axis is verified and subsystem level wavefront is checked against modeled performance. Once performance is verified, the remaining mirror modules are installed on the DSM simulator. Again, optical axis and subsystem transmitted wavefront are verified to ensure FEOMS component optical performance, see Figure 58 and Figure 59. Electrical connector on mirror modules shall be tested for good health connections and to ensure thermocouple functionality.

Released 2024/12/04
Released 2024/12/04

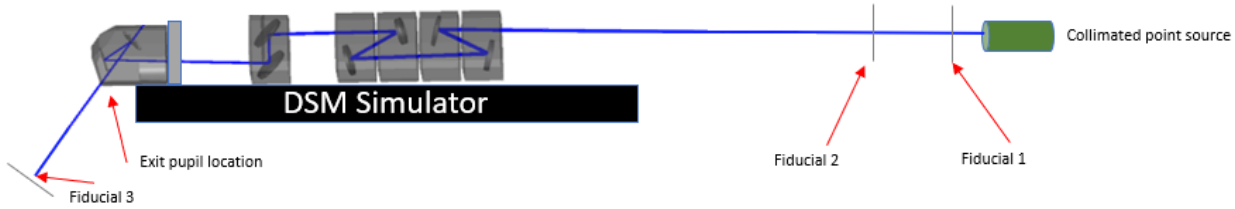

Figure 58. FEOMS setup for optical axis verification.

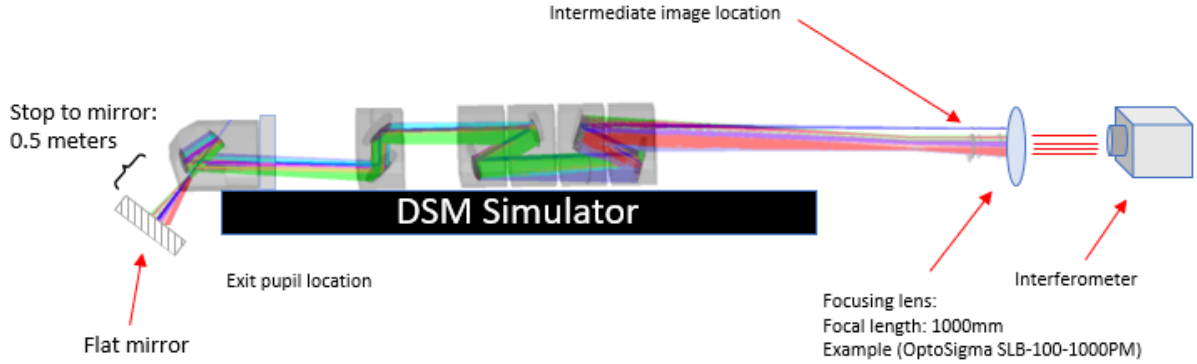

Figure 59. FEOMS transmitted wavefront verification.

The UWAVS ex-vessel section consists of the IOT, BOL, and BEOC. These subsystems are located in the interspace, bioshield labyrinth, and port cell, respectively. Unlike the in-vessel section, these subsystems are assembled and tested in the installed configuration.

IOT mirrors are comprised of two mirror groups, A40 active alignment mirrors, and A50 image relay mirrors. The active alignment mirrors are two flat mirrors used to correct alignment between the in-vessel section and the ex-vessel section, as such their positions are preset during factory alignment refined later during the On-site Testing and Commissioning Plan [66]. Tolerance analysis indicated a heightened sensitivity to mirror alignment of the A50 mirror group, so additional alignment steps are implemented to ensure performance. Each A50 mirror is manually aligned to the next downstream mirror as opposed to relying on pure mechanical positioning/tilting of the mirror surface. Once the A50 mirror group is aligned as a unit, imaging performance is verified interferometrically, checking against the modeled wavefront error, see Figure 60. Distortion and magnification are then verified, see Figure 61.

Released 2024/12/04
Released 2024/12/04

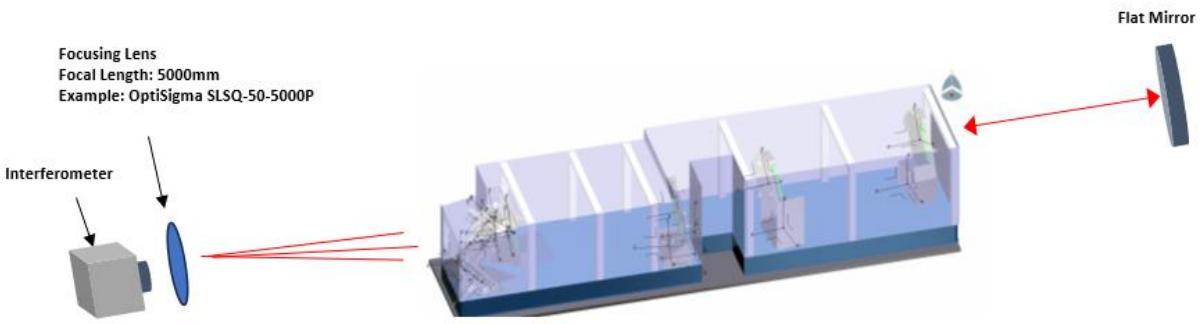

Figure 60. IOT imaging performance test configuration.

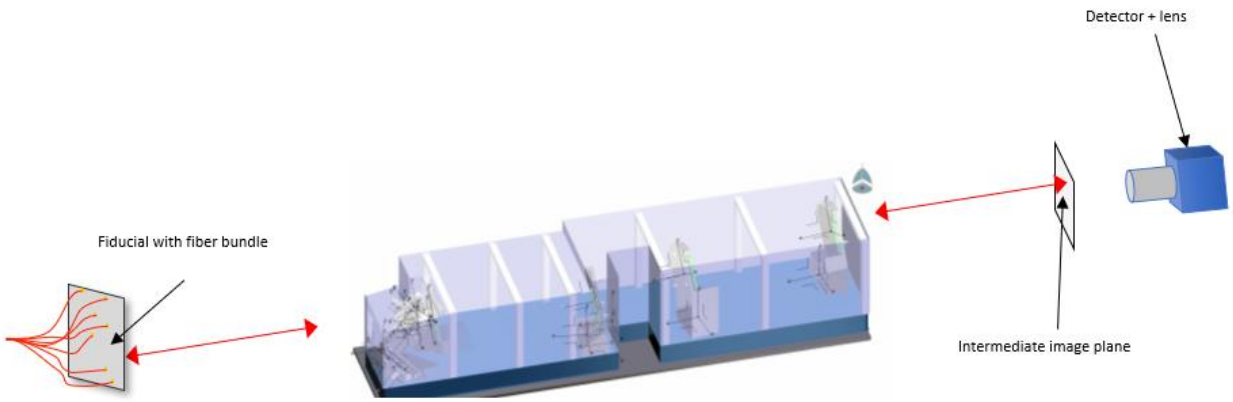

Figure 61. IOT distortion and magnification test configuration.

Much like the A40 mirror group, the A60 mirror group in the BOL is used to align the IOT to BEOC. This mirror group is a set two flat mirrors oriented in a dog-leg configuration. They are preset to a nominal position and refined during the On-Site Testing and Commissioning [66].

Optical assemblies on the BEOC are first validated in a test fixture then installed onto the BEOC optical bench. Transmitted wavefront of A90 and A110 lens barrels are first verified individually. Then, in combination with A80 field lens (IR) and A100 achromat doublet (VIS), wavefront and MTF are correlated. This enables an MTF measured in-situ to be directly correlated with imaging performance measured via transmitted wavefront. Finally, all optics are installed on the BEOC optical bench and MTF is measured for both channels.

Once all optics are installed, calibration sources in the BEOC are used to characterize and calibration both the infrared and visible channels. This entails characterizing non-uniformity correction, detector linearity, and spectral corrections.

A series of tests are preformed to verify functionality of measurement parameter algorithms and the interface between UWAVS and CODAC. Measurement parameter calculations are verified

Released 2024/12/04
Released 2024/12/04

using a set of synthetic images designed to simulate events. A mini CODAC simulator is used to verify the UWAVS/CODAC interface [67].

12.4 Onsite Assembly

This section describes the high-level on-site assembly of the UWAVS system. For detailed assembly plans for the In-vessel FEOMS and Ex-vessel subsystems, refer to [68] and [48] respectively.

12.4.1 In-vessel

The in-vessel port integration plan [68] covers the FEOMS assembly plan at the Port Integrator in detail. As a tenant the 55.GA port integration plan serves as input into the higher-level Onsite Assembly Plans [69]. The 55.GA plan does not consider other diagnostic tenants. It provides 55.GA basic needs and outlines a preliminary strategy to aid the overall port integration plan.

The FEOMS can be assembled bay-by-bay and front-to-back (radial outward direction in TGCS) within the DSM, as shown in Figure 62. Special tooling and assembly process considerations are required for the A10 Bullnose, due to its unique mounting plane and design architecture. A common design architecture and assembly process is planned for the A20 and all A30 mirror modules.

Released 2024/12/04

Released 2024/12/04

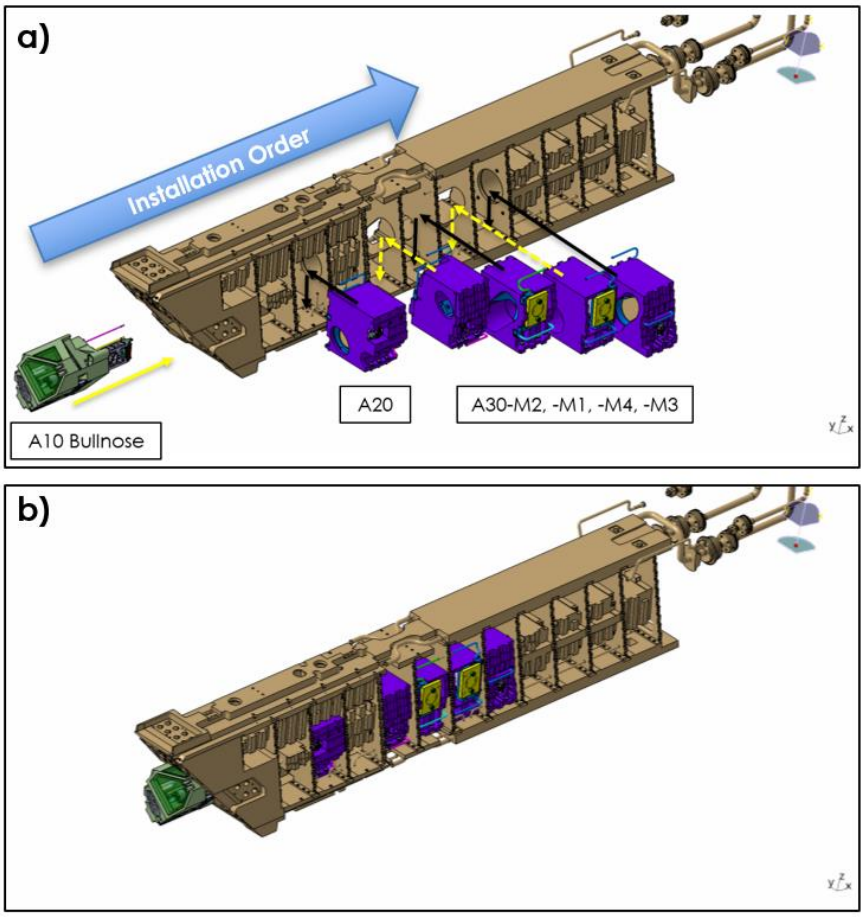

Figure 62. a) Exploded and b) assembled pictorial views of the FEOMS within the DSM.

Released 2024/12/04

12.4.2 Ex-vessel

The ex-vessel UWAVS subsystems residing in the interspace and port cell can be assembled in parallel onto their respective support structures in the PIF, however must be installed in sequence from TGCS radially outwards starting with the ISS and ending with the PCSS as seen in Figure 63.

Released 2024/12/04

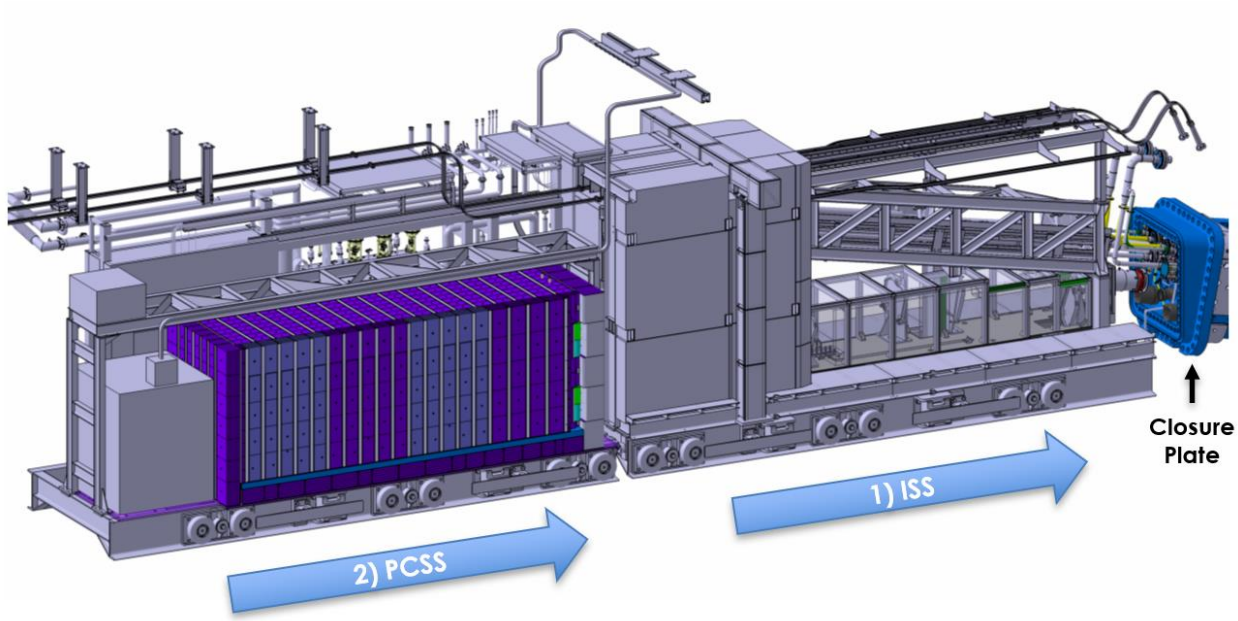

Figure 63. Installation sequence of ex-vessel subsystems in the Interspace and Port Cell.

12.4.3 Gallery

UWAVS components in the North-East shielded cubicle are shipped to the ITER facility and assembled and integrated at site. These shielded cubicles are shared amongst other tenants, so factory pre-assembly is not possible. UWAVS components within the North-East shielded cubicles include but are not limited to stepper motor controllers and visible and IR camera power supplies. Refer to [52] for details on cubicle and I&C definition.

12.4.4 Diagnostic Hall

The Diagnostic Hall cubicles will be assembled at manufacturer's facility, shipped to ITER, and installed directly on-site. Cubicle power and signal cabling will plug directly to site receptacles. Refer to [52] for details on cubicle and I&C definition.

12.5 Alignment Method

Successful assembly requires real-time inspection and alignment to precisely locate the position and angle of the mechanical structures during installation. The primary tool used for inspection and alignment will be a laser tracker viewing Spherically Mounted Retroreflectors (SMRs) [FARO] mounted in precisely located nests such as shown in Figure 64. These removable nests will be integrated into locating fiducials in the various structures to provide data on the structures position and orientation relative to similar fiducials located on the DSM, Port Plug, ISS, PCSS, and facility.

Released 2024/12/04
Released 2024/12/04

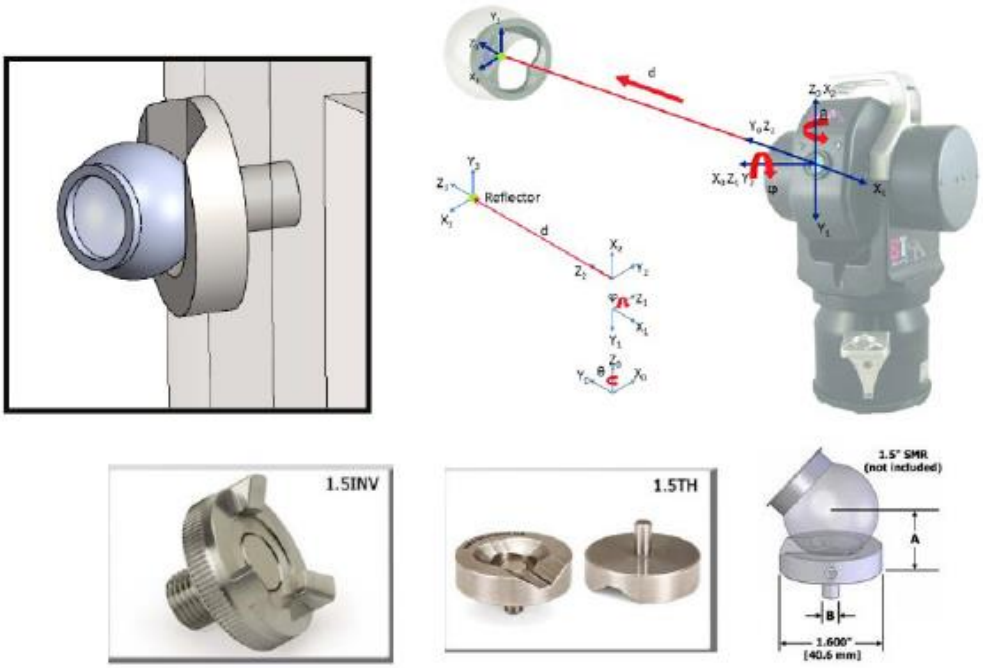

Figure 64. Laser tracker and nest mounted spherical mounted retroreflectors (SMRs)

The locations of the ISS, PCSS, and Port Plug fiducials to be referenced for UWAVS alignment and inspection are shown in Figure 65 from [70]. Removable SMR nests are integrated into the frames.

In some cases, most notably for the larger structures where many sampling points are desirable or line of sight to the laser tracker is questionable, use of a T-probe stylus like that shown in Figure 66 may be preferable to direct observation of SMRs. This facilitates quick and repeatable measurement by placing the ball tip of the stylus in a low-profile integrated fiducial such as a conical hole which can be easily integrated into the structures without compromising the design function. These features are also easily applied to more delicate equipment such as opto-mechanical mounts.

Released 2024/12/04
Released 2024/12/04

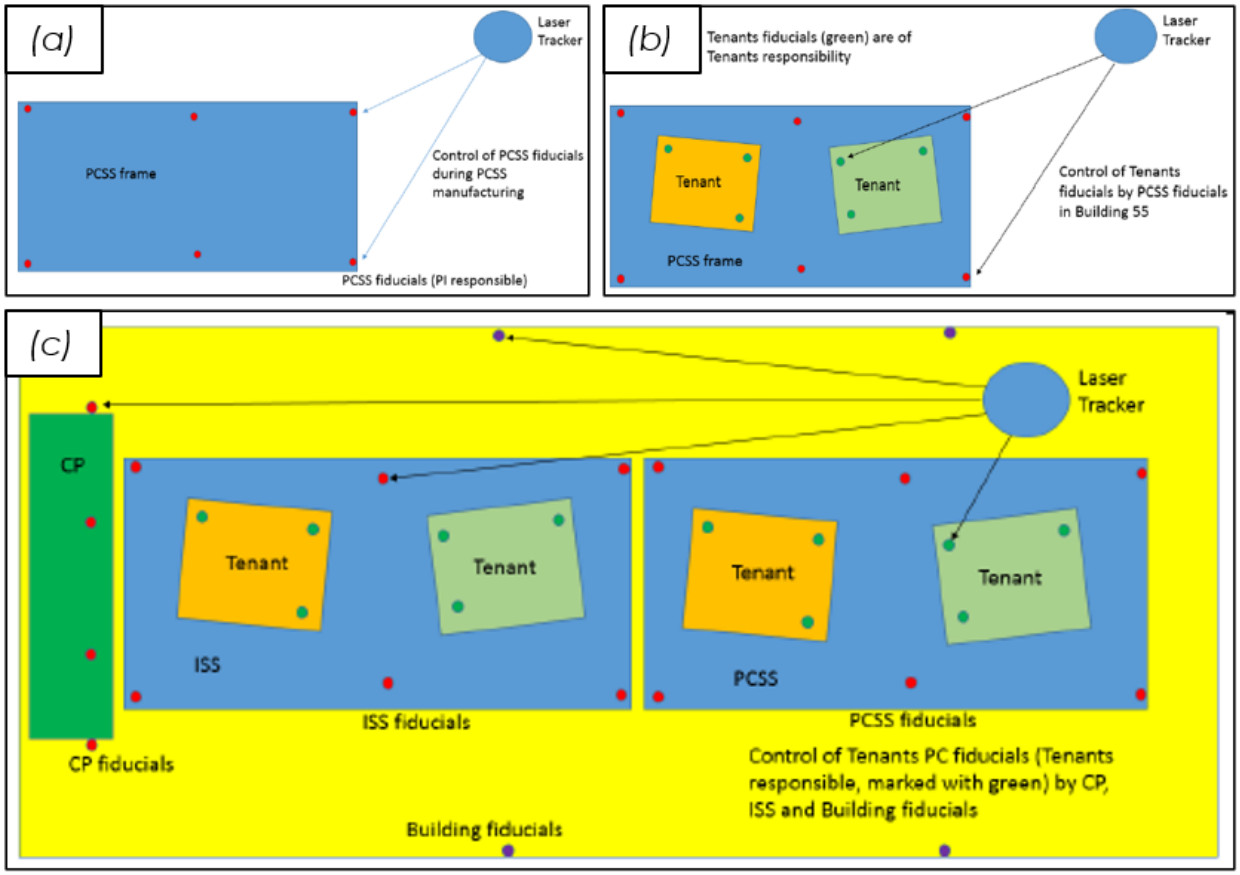

Figure 65. Example laser tracker metrology of (a) PCSS frame, (b) tenant location on PCSS, and (c) ISS and PCSS installed in Upper Port.

Released 2024/12/04

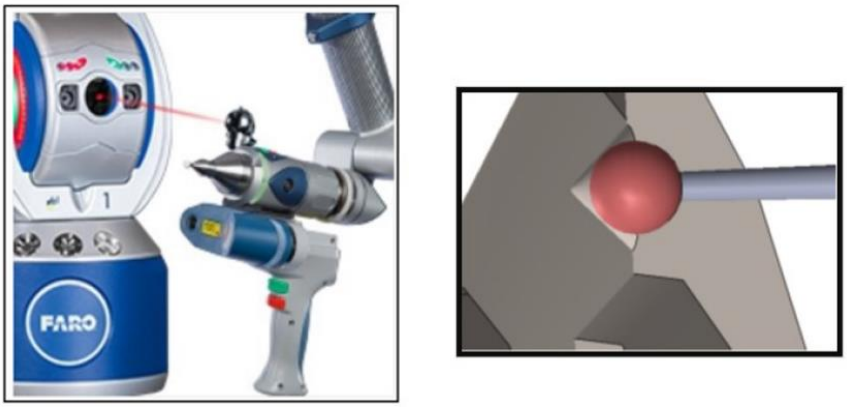

(a) (b)

Figure 66. Laser tracker with (a) T-probe stylus used with (b) integrated fiducials.

Released 2024/12/04

12.6 Alignment Requirement Verification

Final subsystem position requirement verification will be conducted using the laser tracker and the integrated SMRs on trolley as seen in Figure 67 from [70].

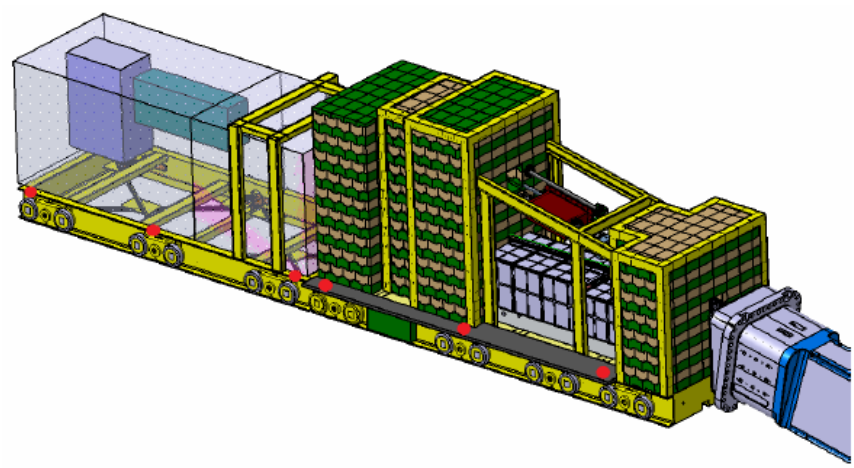

Figure 67. ISS and PCSS trolley SMR locations for final subsystem positional requirements verification.

Final system alignment will be performed in accordance with the On-Site Testing and Commissioning Plan [66]. While the laser tracker verifies CP and trolley position, a series of interferometers, fiber optic lasers and fiducials verify alignment and image performance. Examples of interferometers and fiber lasers used to verify image performance of the FEOMS, IOT, and BEOC are shown in Figure 68 through Figure 70. System performance and alignment verification is performed under the assumption there is a light source available to illuminate the divertor.

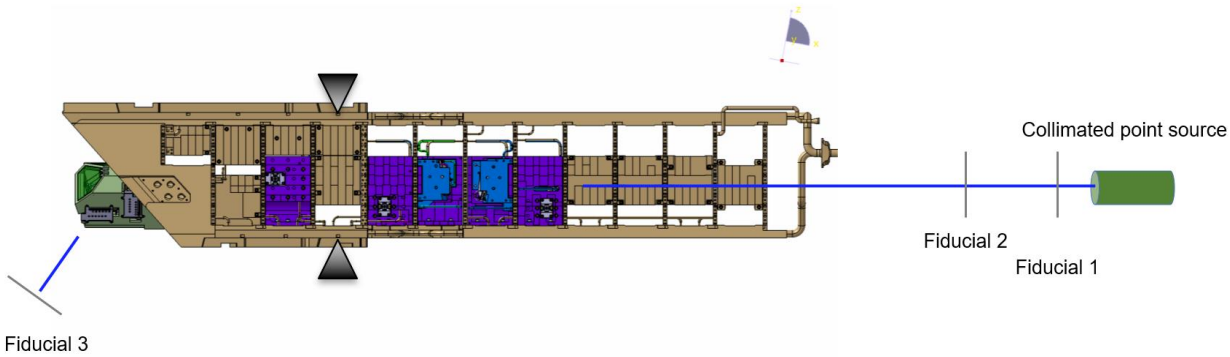

Figure 68. Optical axis alignment test configuration for the installed FEOMS.

Released 2024/12/04
Released 2024/12/04

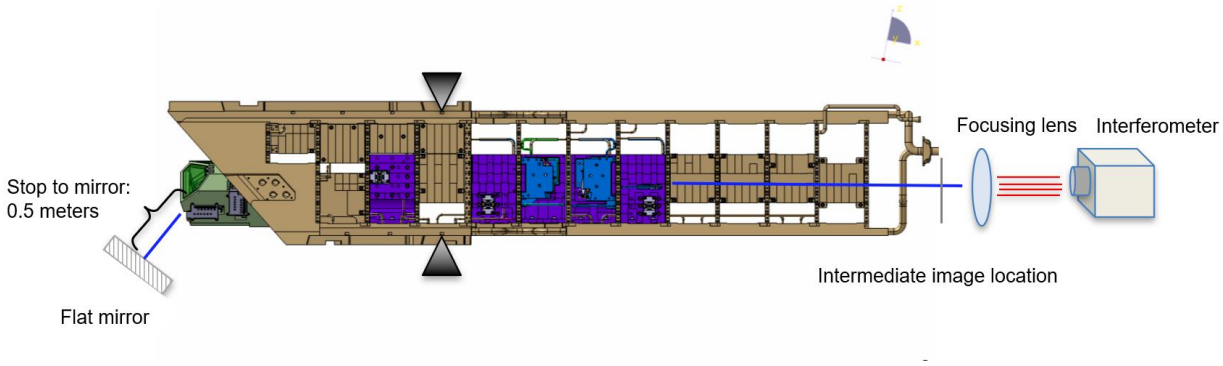

Figure 69. Imaging performance test configuration for the installed FEOMS.

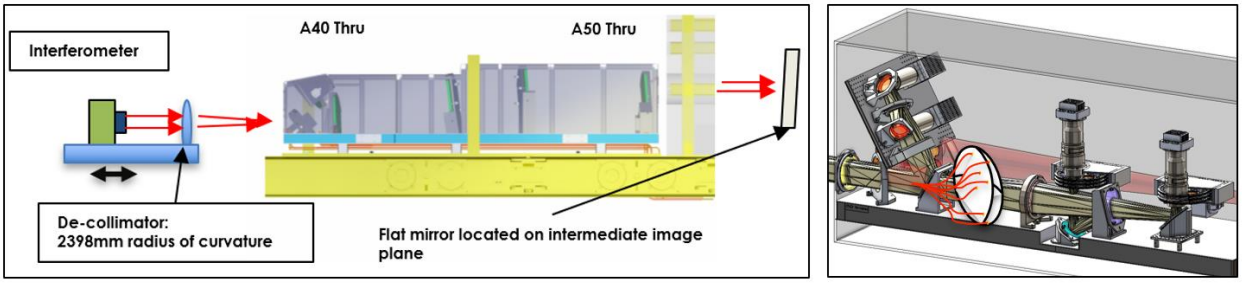

(a) (b)

Figure 70. Image performance verification of (a) IOT using an interferometer and (b) BEOC using fiber lasers mounted to a curved fiducial.

12.7 Port Plug Testing at PPTF

55.GA provides support in developing functional test procedures with the port integrators and a provided a plan to establish acceptance tests [71]. Testing of the system at the Port Plug Testing Facility (PPTF) shall include visual acceptance of components upon receipt at the test facility, environmental tests, and other critical system function tests to ensure the system performs in the future ITER environment. The visual acceptance test includes integrity of the system, basic functioning of the optical system and ensuring no damage occurred during transit. This is followed by environmental tests which include all tests as described in Section 7.5 of [5]. Basic system functionality tests follow the environmental tests to confirm Port Plug integration and system functionality. These include testing thermocouple functionality, mirror cleaning, shutter actuation, mirror and module system alignment, shutter calibration filament, and a final electrical continuity compliance check.

A summary of the PPTF testing sequence and cumulative duration is outlined in Table 33. Anticipated duration times include all testing setup and post-testing activities including but not limited to draining and drying.

Released 2024/12/04
Released 2024/12/04

Table 33. PPTF Test Sequence

Test No.	Test Description	Estimated Duration (days)	Cumulated Duration (days)
1	Visual Inspection Acceptance	15	15
2	Leak Tightness (Environmental Test)	28.5	43.5
3	Thermocouples Functionality	3	46.5
4	Mirror Cleaning	10	56.5
5	Shutter Actuation	15	71.5
6	Alignment	15	86.5
7	Shutter Calibration Filament	5	91.5
8	Check of Electrical Continuity (Electrical Compliance Environmental)	8	99.5

12.8 Onsite Testing and Commissioning

On-site testing and commission activities are covered for Phase 1 (before first plasma) of PBS-55.GA. This includes testing and commission activities between delivery of the pre-integrated and tested hardware to ITER (Turn Over Packages (TOP)) and the first ITER operational phase. For a detailed plan, see 55.GA UWAVS-35 On-Site Testing and Commissiong Plan [66].

There are 5 main Turn Over Packages that define the system. Each Turn Over Package is tested and validated in the factory prior to delivery, and listed below.

- TOP 55GA00-B74/B11-01 (TOP1), the cubicles including all power connectivity, and communications for the instrument from the Diagnostic building up the BEOC.
- TOP 55GA00-B11-02 (TOP2), in-vessel optical system, including imaging optics, in-vessel cooling system, mirror cleaning system, shutter, and transmission monitoring system.
- TOP 55GA00-B11-03 (TOP3), interspace optics, including imaging optics, active alignment system, and bioshield labyrinth optics.
- TOP 55GA00-B11-04 (TOP4), back end optical system, including imaging optics, cameras, and back-end calibration sources/optics.
- TOP 55GA00-B11-05 (TOP5), valve box for Nitrogen and compressed air supply.

There are 5 main phases in the commissioning process as listed below.

Released 2024/12/04
Released 2024/12/04

1. Integrate cubicles with other services.
2. Install and validate in-vessel optical system.
3. Install and validate interspace optical system.
4. Install and validate valve box.
5. Install and validate back end optical system, calibrate BEOC, then calibrate instrument.

In order to start the commissioning, the prerequisites needed are shown in Figure 71.

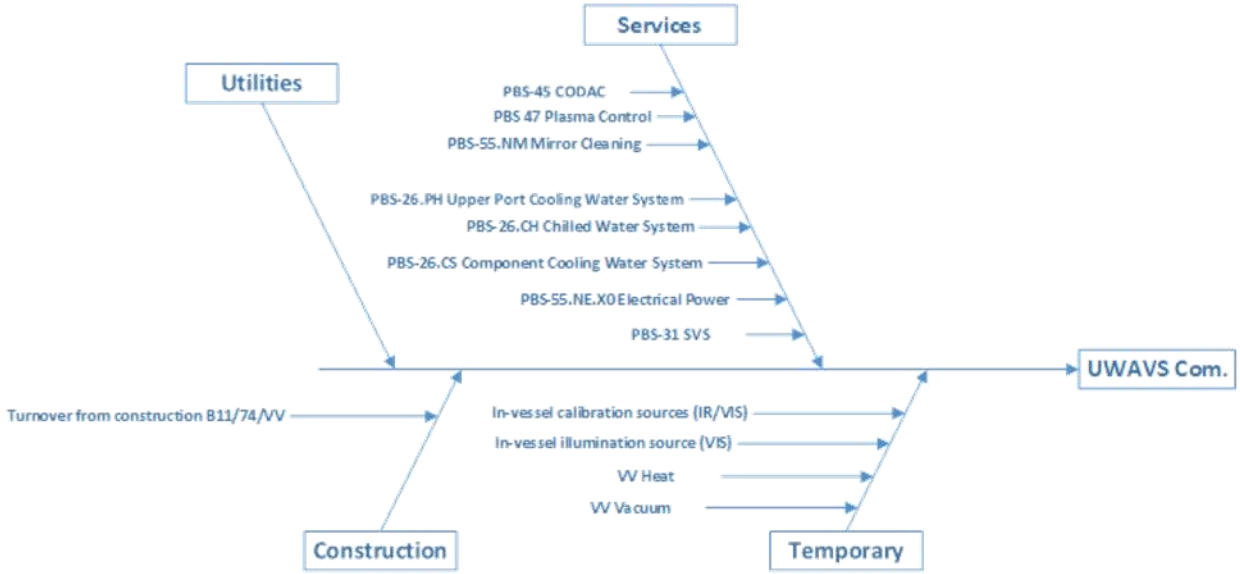

Figure 71. Fishbone diagram of perquisites for System Commissioning

Released 2024/12/04
Released 2024/12/04

13 REMOTE HANDLING

This section provides a high-level overview of the remote handling plans for UWAVS-35.

13.1 Remote Handling Compatibility Assessment

A detailed summary of remote handling operations for UWAVS-35 is given in the 55.GA UWAVS-35 Remote Handling Compatibility Assessment Report [72]. Remote handling operations consist of refurbishment of the Bullnose and FEOMS A20 and A30 Mirror Modules, all taking place after extraction and transportation of the DSM to the Hot Cell Facility (HCF).

The document breakdown structure for UWAVS-35 remote handling is shown in Figure 72.

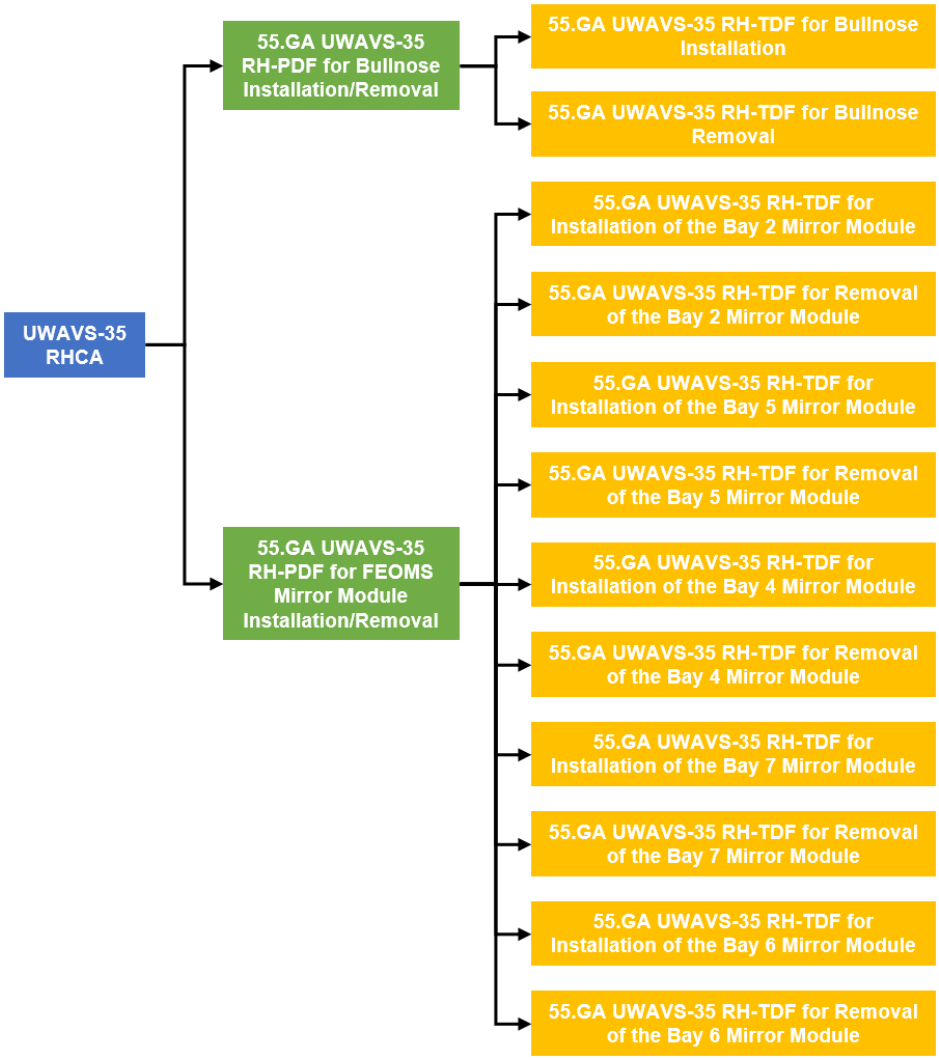

Figure 72. Breakdown of the UWAVS-35 Remote Handling Documents.

Released 2024/12/04
Released 2024/12/04

13.2 Plant Definition

The UWVAS-35 remote handling tasks use equipment standard to the HCF. Including, but not limited to:

- Universal Work Station (UWS) [73]
- Telemanipulator robots [73]
- Visual inspection equipment [73]
- Power Torque Driver [74]
- Pintle Grab System [73]

The remote handling tasks use the generic tools specific to pipe maintenance including:

- Generic Alignment Tool (GAT) [75]
- Generic Pipe Cutting Tool (GCT) [75]
- Generic Pipe Welding Tool (GWT) [75]
- Pipe refurbishment tool [75]
- Pipe cleaning tool [75]

The Bullnose, A20 and A30 Mirror Modules each feature pins for self-alignment during installation operations. Captive screws are used on the modules and their respective modules feature counter-torque slots for the Power Torque Driver. LEVI connectors are used to make electrical connections at installation. The modules feature their own individual interface tools that are installed onto the removable mirror modules after the DSM is in the Universal Work Station. These interface tools allow the Pintle Grab System to grip and manipulate the modules. An example of removal of a mirror module (A20) is shown in Figure 73.

Detailed Plant Definition Forms are given for the FEOMS [76] and Bullnose modules [77].

Released 2024/12/04
Released 2024/12/04

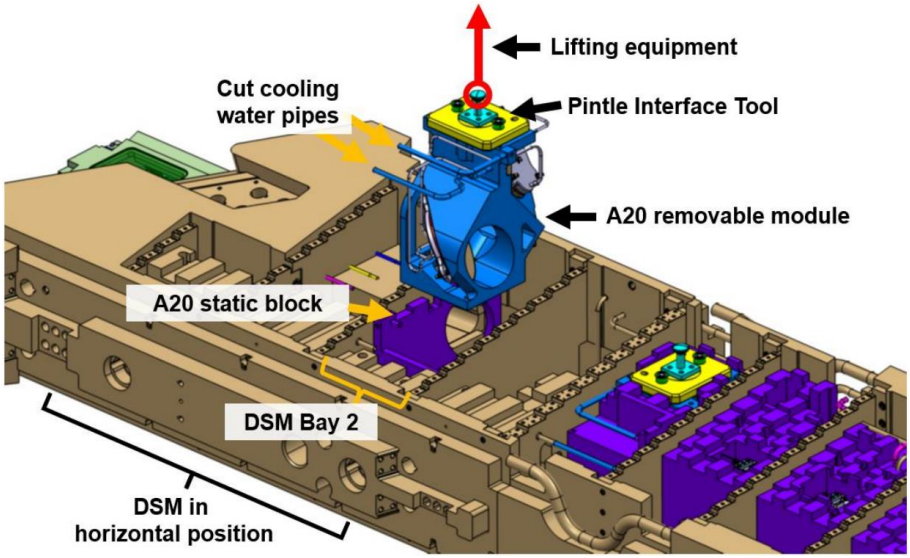

Figure 73. Removal of the A20 mirror module.

13.3 Task Definition Forms

The remote handling tasks for UWAVS-35 are limited to unplanned refurbishment of failed mirror modules. During refurbishment, the removable mirror modules have their pipes cut and are removed. After removal, the cut pipes are refurbished with the pipe refurbishment tool and pipe cleaning tool. The replacement module is installed, and its cooling pipes are welded and inspected.

The list of Remote Handling Task Definition Forms (RH-TDF's) is given in Table 34.

Table 34. List of UWAVS-35 Remote Handling Task Definition Forms

TDF Reference	RH Class	Task Description
ITER_D_AK7F6V [78]	RH-2	55.GA UWAVS-35 RH-TDF for Bullnose Installation
ITER_D_ARTMQW [79]	RH-2	55.GA UWAVS-35 RH-TDF for Bullnose Removal
ITER_D_ARTR43 [80]	RH-2	55.GA UWAVS-35 RH-TDF for Installation of the Bay 2 Mirror Module
ITER_D_ARTSYG [81]	RH-2	55.GA UWAVS-35 RH-TDF for Removal of the Bay 2 Mirror Module
ITER_D_ATQ8Q2 [82]	RH-2	55.GA UWAVS-35 RH-TDF for Installation of the Bay 5 Mirror Module
ITER_D_ATVQ6A [83]	RH-2	55.GA UWAVS-35 RH-TDF for Removal of the Bay 5 Mirror Module

Released 2024/12/04
Released 2024/12/04

TDF Reference	RH Class	Task Description
ITER_D_AS4P23 [84]	RH-2	55.GA UWAVS-35 RH-TDF for Installation of the Bay 4 Mirror Module
ITER_D_AS4XGY [85]	RH-2	55.GA UWAVS-35 RH-TDF for Removal of the Bay 4 Mirror Module
ITER_D_ATXDWX [86]	RH-2	55.GA UWAVS-35 RH-TDF for Installation of the Bay 7 Mirror Module
ITER_D_ATXF5V [87]	RH-2	55.GA UWAVS-35 RH-TDF for Removal of the Bay 7 Mirror Module
ITER_D_ATWLMC [88]	RH-2	55.GA UWAVS-35 RH-TDF for Installation of the Bay 6 Mirror Module
ITER_D_ATX52T [89]	RH-2	55.GA UWAVS-35 RH-TDF for Removal of the Bay 6 Mirror Module

Released 2024/12/04
Released 2024/12/04

14 RISK ANALYSIS

Several risks were identified during the preliminary design phase and at the peer review held in June of 2023. The initial assessment of these risks at PDR are described as follows. If the initial assessment warrants additional attention, a mitigation strategy has been or can be planned in the final design phase.

14.1 Fire Assessment

Per requirement 55.GA SSCs shall comply with the ITER Fire Safety Approach document [22]. Per [90], the Upper Port Cell areas are considered fire sectors, therefore combustible materials (fire loads) must be controlled and accounted for and kept to reasonable minimum. The following criteria is considered for Port Cell subsystem designs. In instances where these criteria cannot be met, combustible materials are quantified and tabulated.

1. No fire loads allowed in 2 m radius at level and beneath DS low flow line suction point (<1 m high).
2. Cable trays in a 1 m radius at level and above ignition source (LAC, junction box, motor) shall be fully enclosed in metallic casing with metallic straps. Cable trays shall not contact ignition source to prevent heat transfer by conduction.
3. Cubicles and motors should be avoided in PC volume, however, if required must have passive fire rated cubicle or active fire protection with internal fire suppression system.
4. No fire loads allowed above 3 m high and unprotected tray or junction box not allowed in Port Cell Interspace (PC-I).
5. The exclusion zone above 3 m height into the PC-I and design principle to route combustible material below this area.
6. Bundle of Cables to be considered as Cable Trays for cumulative fire load equal or higher than 100 MJ/ml (>.44dm2 of bundle section).

Analysis from [90] indicates temperatures within the Port Cell areas after a fire for a duration of 2 hours. Summarized lists of materials and associated melting points in the IOT, BOL, and BEOC are quantified in Table 35, Table 36, and Table 37 respectively. Materials with a lower melting point than temperatures indicated in these areas are highlighted red and must be contained within the subsystem during a fire.

Released 2024/12/04
Released 2024/12/04

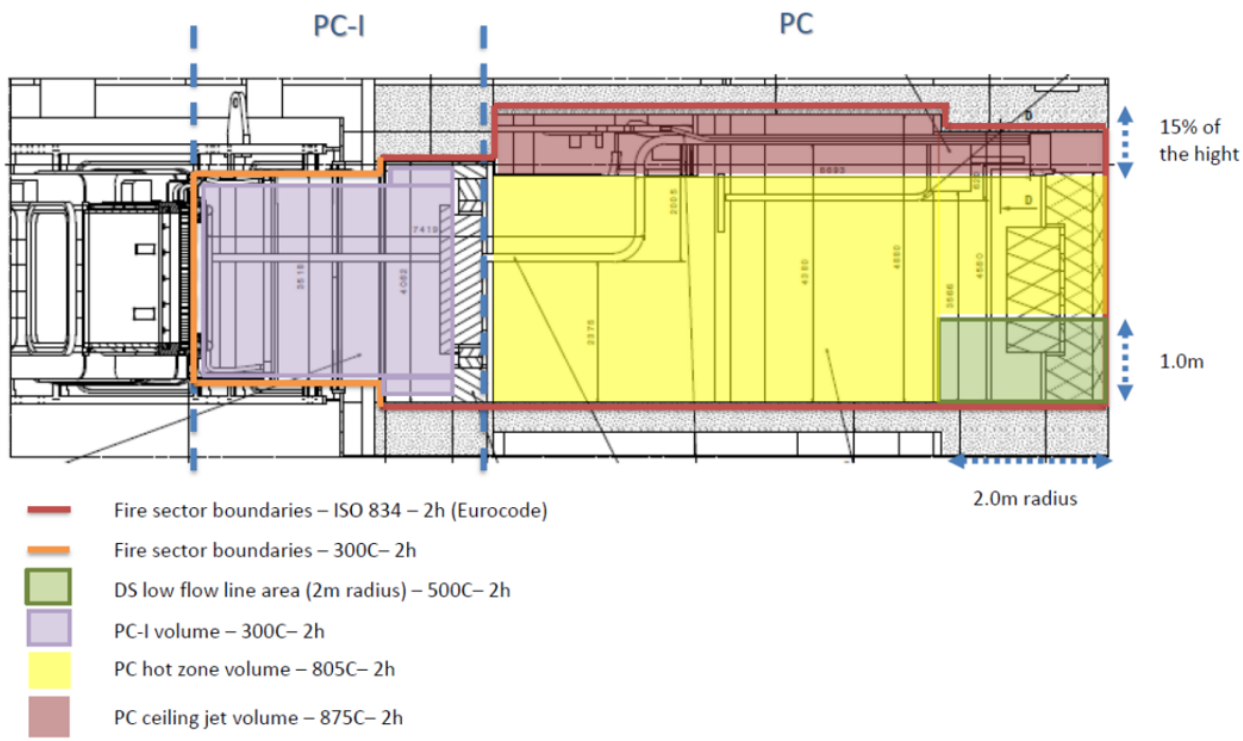

Figure 74. Port Cell loading conditions in case of fire.

Table 35. IOT Quantified Materials and Melting Points

Item	Component	Material	Total Weight (kg)	Total Volume (m^3)	Melting Point (C)
1	Structure and supports, bulk	Stainless Steel	1212.82	0.152	1370
2	Optical mounts, bulk	Stainless Steel	208.22	0.026	1370
3	Optics	Glass (optical)	32.3	0.013	1585
4	Hardware (Bolts, screws, nuts)	Class 10.9 Steel (Medium-High Strength)	16.09	0.002	1420
5	Shroud bushings	Bronze (UNS93200, M02)	3.02	0.000	854

Released 2024/12/04
Released 2024/12/04

Table 36. BOL Quantified Materials and Melting Points

Item	Component	Material	Total Weight (kg)	Total Volume (m^3)	Melting Point
1	Optical Mounts	Stainless Steel	130.17	0.016	1370
2	Stainless Steel structure and supports	Stainless Steel	423.44	0.053	1370
3	Optical mirrors	Glass (NBK-7)	17.79	0.008	719
4	O-ring seals	EPDM	0.006	7.09E-06	175
	M24 Fasteners	Inconel 718	2.034	2.48E-04	1260
	M12 Fasteners	Class 10.9 Steel (Medium-High Strength)	4.537	5.64E-04	1420

Table 37. BEOC Quantified Materials and Melting Points

Item	Component	Material	Total Weight (kg)	Total Volume (m^3)	Melting Point (C)
1	Optical Mounts	Aluminum	90.7	0.034	**582**
2	Stainless Steel structure and supports	Stainless Steel	10276.5	1.285	1370
3	Cadmium Shielding	Cadmium (Cd)	864.2	0.100	**321**
4	Iron shielding	Pure Iron (Fe)	1941.5	0.247	1535
5	Neutronic shielding	Boron Carbide (B4C)	8365.5	3.346	2350
6	Optical lenses and mirrors	Glass (optical)	28	0.011	1585
7	Optical windows	Sapphire (optical)	2.45	0.001	2030

Released 2024/12/04

Released 2024/12/04

As indicated in the aluminum optical mounts and cadmium shielding layers will melt after exposure to a fire at 805°C in the Port Cell. The aluminum will be contained within the stainless steel shielded enclosure and poses no risk to surrounding PCSS tenants. The cadmium shielding however, poses a serious risk as it is not contained within the stainless steel shielded enclosure and cadmium has a boiling point of 767°C. After exposure to temperatures of 805°C for 2 hours, the cadmium shielding layer can melt and boil, resulting in cancer-causing vapors. See Section 14.16 for additional details on risks assumed associated with the use of cadmium.

In addition to tracking materials above, combustible materials are considered fire loads and must be controlled and accounted for. Combustible materials for in the Port Cell Interspace and Port Cell are tabulated for the IOT, BOL, and BEOC in Table 38, and Table 39, respectively.

Table 38. IOT Combustible materials within the Port Cell Interspace

Item	Component	Quantity Each	Unit Qty	Total quantity	Unit
1	Cable insulation	1	50.00	50.00	m
2	Bearing grease	12	3.619E-06	4.343E-05	m^3
3	Gear box grease	5	3.58E-04	1.790E-03	m^3
4	Stepper motors	5	25.92	129.60	W
5	Position sensors	10	1.12E-05	1.12E-04	m^3
6	Flexible Sleeve, Fore Shroud	1	1.52E-04	1.52E-04	m^3

Table 39. BOL Combustible materials within the Port Cell Interspace

Item	Component	Quantity Each	Unit Qty	Total quantity	Unit
1	Cable insulation	1	50.00	50.00	meter
2	Bearing grease	8	1.18E-05	9.44E-05	m^3
3	Gear box grease	4	1.18E-05	4.72E-05	m^3
4	Stepper motors, NEMA-17	2	52	104	W
5	Stepper motors, NEMA-23	2	77	154	W
6	Stepper motor brakes, NEMA-17	2	6	12	W
7	Stepper motor brakes, NEMA-23	2	35	70	W
8	Position sensors	8	1.12E-05	8.96E-05	m^3
9	EPDM O-ring	2	3.55E-06	7.1E-06	m^3

Table 40. BEOC Combustible materials within the Port Cell

Item	Component	Quantity Each	Unit Qty	Total quantity	Unit
1	Cable insulation	1	10	10.000	m
2	Bearing grease	9	9.512E-06	8.561E-05	m^3

Released 2024/12/04
Released 2024/12/04

Item	Component	Quantity Each	Unit Qty	Total quantity	Unit
3	IR blackbody calibration source	1	3000	3000	W
4	Visible integrating sphere	1	4.8	4.8	W
5	RF matchbox	2	90	180	W
6	Visible cameras	2	10	20	W
7	IR cameras	2	27	54	W
8	Filter wheel motors	6	3.47	20.82	W
9	Filter wheel sensors	6	1.438E-05	8.625E-05	m^3
10	Visible camera linear stage	2	10	20	W
11	55.GL assembly (cameras + laser source)	1	TBD	TBD	TBD

Currently 55.GA has no requirement to introduce active fire suppression internal to the subsystem enclosures and it is assumed fire suppression is managed within the fire sector. 55.GA follows fire mitigation by design guidelines of Appendix D of [22].

55.GA follows design guidelines for fire load management and observes exclusion zone restrictions as defined in [90] with one exception. Stepper motors are baselined in the IOT, BOL, and BEOC ex-vessel subsystems.

The IOT, BOL, and BEOC inside the PC do not require a fire barrier to protect adjacent SIC components. The one exception is the valve box that needs to be assessed in final design (located in alcove, not in PDR scope).

55.GA provides a combustible material list inside the BEOC, BOL, IOT that are affected by fire loading condition temperatures and 2h duration in PC and PC. Based on combustible material list solicit fire load impact feedback from IO, to determine need for active fire suppression system. Baseline assumption is NOT required due to limited combustible materials.

Based on this preliminary fire assessment of the 55.GA system, IO can determine additional requirements or changes that need to be made to better mitigate fire risk or associated hazards in final design.

Released 2024/12/04

Released 2024/12/04

14.2 Visible Species Measurements

Producing accurate species concentration measurements is challenging for a number of reasons. Depending on the strength of the plasma, the background Bremsstrahlung radiation can be many orders of magnitude larger than the signal of interest. This is compounded with the spatially dependent distribution of impurities such as more emission at the edges of the field of view rather than the center. The system can only measure an integrated column of light over a small spectral

band. The concentration of ions emitting light in that band does not depend only on impurity concentration, but also electron density, temperature, and temperature dependent apportion cross section. Related to background emission correction challenges, surface reflectivity and emissivity will have a dynamic effect on total integrated signal per pixel. Without quantifiable measurements and accurate models, predicting accuracy is challenging.

14.3 Heat Flux Measurement

A model exists to calculate surface temperature from a heat flux in the divertor but inverting that model to produce heat flux from temperature is not trivial. As of PDR, there is a lack of scope to create the temperature to heat flux model/algorithm needed produce the power load measurement both by default and during disruption.

14.4 Front-to-End Calibration (F2E)

As discussed in Section 8 and the Optical Model Results [44], F2E calibration is an essential final verification step for validating system performance following installation. While the current calibration plan includes comprehensive factory testing and in-situ calibration sources, it cannot account for the full system calibration in the installed state and any unforeseen effects. Failure to provide a means for F2E calibration for both IR and visible channels may result in loss of measurement accuracy in radiance per pixel and wall temperature. If piecewise calibration is necessary, then errors in both absolute and relative measurements of temperature and spectral line strength will result. This includes spatial variation, line-line variation, and port-port variation. As these are the critical measurements provided by UWAVS, failure to accommodate F2E calibration presents a large risk to the ultimate success of UWAVS, as well as other similar diagnostic systems.

At this time, an approach to F2E calibration is not formally confirmed by ITER. Replacing F2E calibration by in factory testing will result in loss of measurement accuracy but is a viable backup option if IO does not provide for the as-installed F2E calibration.

14.5 Ghost Images

For both the visible and infrared imaging systems, surface reflectivity of the divertor can cause large variations in collected light. Wall reflectivity can vary between 0.5 for polished tungsten and 0.9 for rough tungsten in the mid-wave infrared. Researchers have started using machine learning to predict and account for reflections in-vessel. Currently this is a timely and costly process, and not suitable to real time results. Initially, regions of interest to mask out untrustworthy areas in the field of view will be used.

While the two-color temperature measurement scheme can update changes in emissivity in the infrared band, it does not provide emissivity changes in the visible spectrum. Though, thermal

Released 2024/12/04
Released 2024/12/04

emission of the wall in the visible spectrum will be small if the wall temperature is less than ~500C. Unfortunately, the disentanglement of light emitted from the wall, reflected/scatter from the wall, and in the visible case generated by the plasma, is quite complex and out of scope for UWAVS.

14.6 Neutron Damage of Ceramics

Several applications in the bullnose require vacuum rated materials with specific electrical and thermal properties that can withstand the temperatures of bake out. Aluminum Oxide (alumina) and Aluminum Nitride (AlN) are used for their high dielectric constant and thermal conductivity respectively. The components using these materials is summarized in Table 41. Radiation damage from high energy neutrons has been documented [91] [92] [93] for both Alumina and AlN. Both materials are subject to swelling which is somewhat reversed with relatively low temperature annealing. Swelling in alumina is caused by microvoid formation at grain boundaries with almost no change in lattice constants. In AlN the swelling results from interstitial loop formation vertical to the c-axis [93]. At high doses there is degradation of thermal conductivity in AlN [92]. Anticipated neutron fluence with E > 0.1 MeV is approximately 4.86×10^{20} n/cm². Anticipated neutron fluence with E > 0.1 MeV is approximately 4.86×10^{20} n/cm² [94]. Using a summary of available data shown in Figure 75, less than 0.7% swelling is anticipated for the alumina parts. Work by Pornphatdetaudom et. al. [93] found that swelling of AlN was similar to other structural ceramics indicating that swelling will be less than 1% for AlN parts.

There is little data describing the changes in dielectric constant of Alumina and AlN resulting from neutron irradiation. The change in lattice constants is more than an order of magnitude less than the macroscopic length change [92]. This small change in crystal structure implies that there will be a small change in dielectric properties. The ability to tune the frequency of the affected RF circuits can compensate for this change.

Large changes in the thermal conductivity of AlN resulting from neutron damage at high temperatures and flux have been reported [92]. These changes may impact mirror alignment and must be addressed in final design.

Released 2024/12/04
Released 2024/12/04

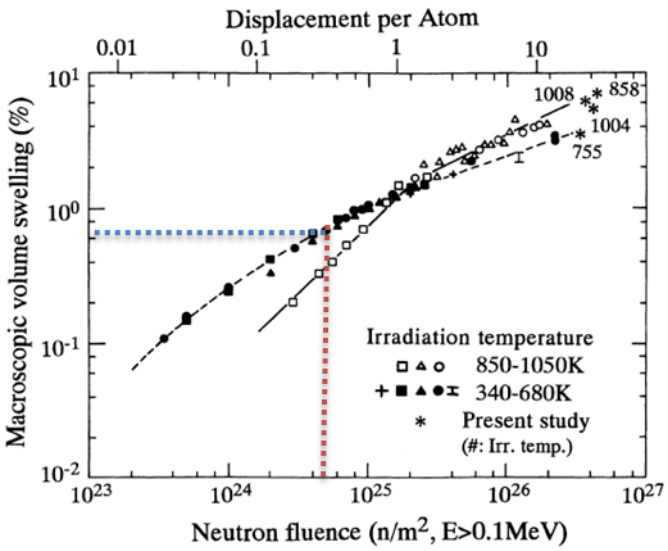

Figure 75. Volumetric swelling in Alumina due to neutron fluence (E > 0.1MeV)

Released 2024/12/04

Released 2024/12/04

Table 41. Ceramic Materials used in Bullnose

Component	Material	Volume (mm^3)	Qty. In Bullnose	Total Volume in BN (mm^3)
Notch Filter Ceramics	Aluminum Oxide	603587	2	1207174
Prematcher PCB	Aluminum Nitride	14130	2	28260
Spherolinder Isolator Ceramics	Aluminum Nitride	3505	6	21030
Mirror Cavity Shield	Aluminum Nitride	109923	2	219846
Transition Pipes Flame Spray Layers	Aluminum Oxide	1823.54	1	1823.54
Oribital Weld Zone Cover Half Cylinder	Aluminum Nitride	226.78	8	1814.24
MIC Cable Insulator	Magnesium Oxide	No More than 215564	Total volume of MIC Cables	215564
Shutter Ceramic Insulator	Aluminum Oxide	104.3	2	208.6

14.7 Stepper Motors Selection

Standard NEMA-17 size stepper motors will be used throughout the UWAVS system for actuated components. Where needed, radiation-tolerant stepper motors from Empire Magnetics will be used (model RH-U17-2) in place of traditional stepper motors, as depicted for the A40M2 mirror assemblies in Figure 76. Such motors have been utilized in similar nuclear radiation applications and have run for years without failure. It is estimated that such motors will be sufficiently hardened to survive the neutron and gamma ray exposure in the Interspace for a minimum of several years, though this will be confirmed during the final design phase. Stepper motors are also present on the A40M1 mirror assembly, on the A60 mirrors in the BOL, and on the filter wheel assemblies and visible camera linear stages in the BEOC. The 55.GL system may also require a stepper motor for the linear stage used to pick off light from the UWAVS system, which will be defined in the final design stage.

Released 2024/12/04
Released 2024/12/04

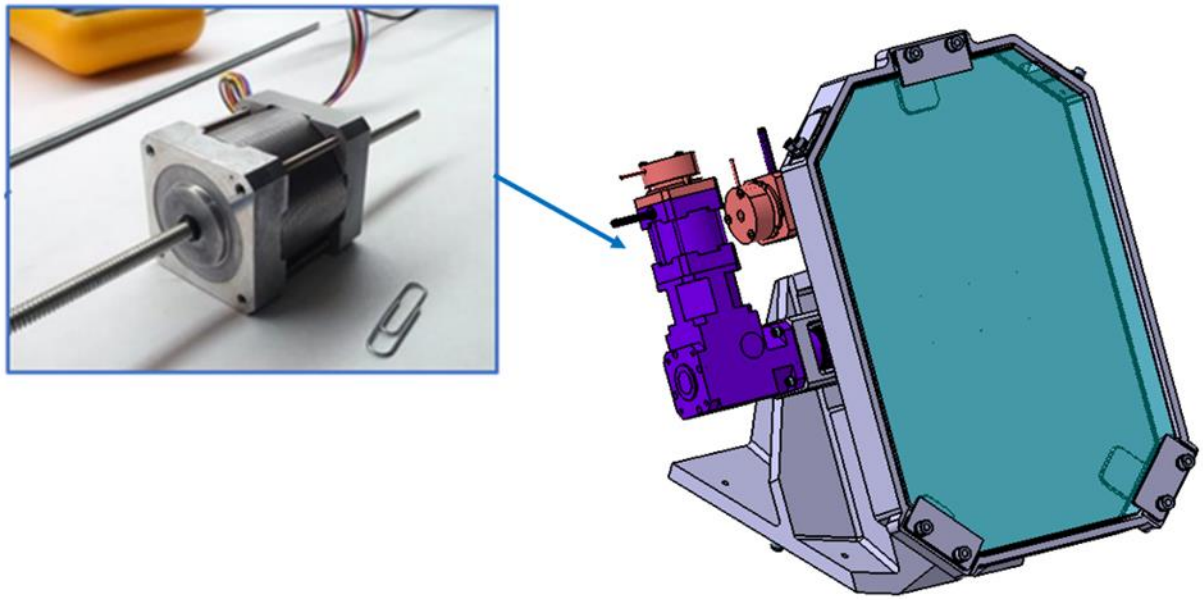

Figure 76. Radiation hardened stepper motors integrated onto the A40M2 mirror assembly.

The stepper motors have the advantage that they can be reliably operated in open-loop, an important requirement as it avoids the need for radiation-sensitive encoder electronics. All stepper motors utilize an associated electromagnetic brake that is itself radiation hardened, and the motors associated with the A40 mirror assemblies in the IOT additionally utilize a 90 degree gearbox.

While the stepper motors selected should be adequately hardened to survive the radiation and thermal environment, it has yet to be confirmed that the stepper motors can be used in the Interspace due to the high magnetic fields present in the area. The IOT A40 alignment mirror subassemblies were identified as high-risk assemblies during preliminary design due to electromechanical components, which are susceptible to body forces within the significant static magnetic field at the fore portion of Interspace (directly outside the CP). These components were not included in the Port Integrator EM analysis. Therefore, a preliminary risk assessment was made using a coarse EM model of the ITER magnet coils to estimate fields and forces in the motors and actuation components. The motors contain various components made from M19 Silicon Iron, 17-4 PH Stainless Steel (SST), and several other magnetic ferrous materials. While it is possible to custom manufacture some motor elements such as the housings and bearings from non-magnetic substitute materials such as 316 SST, others, such as the rotor and stator, cannot be replaced without compromising the function of the motor. In addition, the associated brakes and gearboxes are themselves made from magnetic materials which either cannot be substituted or would involve significant development to do so.

Released 2024/12/04

Released 2024/12/04

Figure 77 displays the results of the EM analysis, which gives a maximum body force of as high as 195 N for the A40 motor assemblies at the front of the IOT. Note that this plot contains datapoints for the motor itself, the brakes, and the gearboxes when applicable. The orientation of the components relative to the magnetic field results in considerable variability even at similar locations as components perpendicular to the field lines are less effected. Also, since the gearboxes are 90 degree bends, the forces on the motor/brake are often in different directions than the gearbox within the same assembly. The forces on the components in the BOL and BEOC are almost negligible, with extreme magnitudes of 1.79 N and 0.60 respectively, and so not a concern for electromagnetic loading. Note the BEOC components are also contained within a magnetic shield not considered in this analysis.

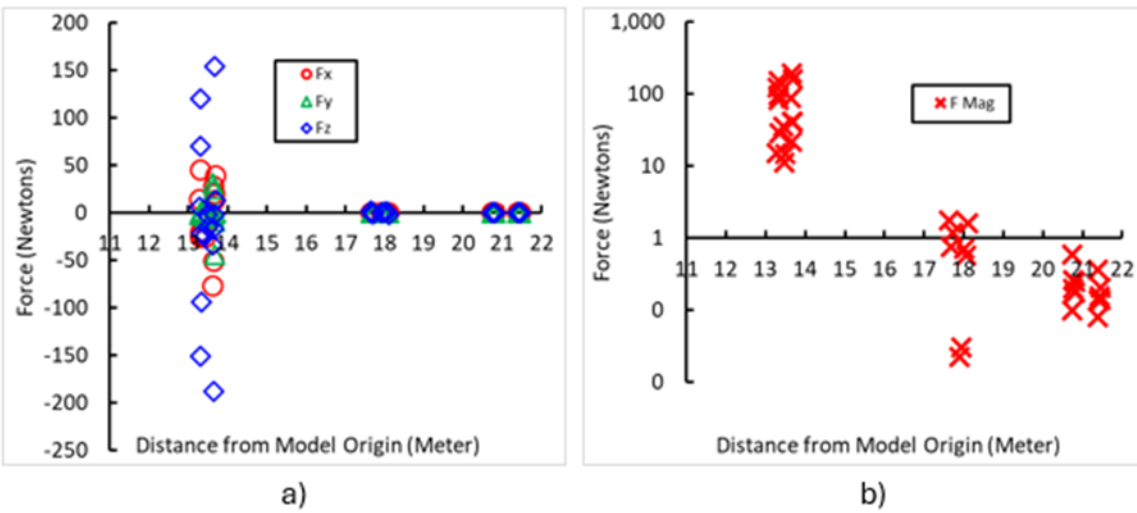

Figure 77. Max body forces imposed on magnetic components due to the ITER magnetic field during a plasma shot (17MA-DINA2019-01). a) X,Y, Z components b) magnitude

To determine if these body forces represent a concern for the structural integrity, performance, and function of the A40 mirror assemblies, a mechanical analysis was performed on the extreme case quantified in Table 10, the A40-M1 tilt axis motor. This analysis included a bolted joint calculation and a finite element analysis of the bolted joint/bracket. Calculations showed that the minimal required preload for the assembly's four bolts to achieve a stable design under these EM loads along with an SL-2 seismic event and gravity was 678 N, corresponding to a minimal bolt size of M2.5 X 0.45 if made from class 10.9 /8.8 steel or M4 X 0.7 if made from 316L SST. The present design utilizes four M3 X 0.5 class 10.9 bolts loaded to 1200 N preload and so is adequate to withstand such loading. The subsequent FEA model confirmed all stress levels in both the bolts and other members are below design allowable limits and deflection is limited to less than 0.06 mm. Some concern remains about the robustness of the motor components themselves, the interiors of which were not modeled in detail. However, the vendor asserts that these motors have been utilized in static fields of 10 kilogauss (1.0 Tesla), compared to the 0.8 Telsa max field in the

Released 2024/12/04
Released 2024/12/04

area of interest in this model. It is expected subsequent qualification during the final design stage will confirm the motor's viability.

Table 42. Body forces on the A40 mirror actuator assemblies

ID	Distance from Machine Axis [meter]	Fx	Fy	Fz	FMAG
IS_M1	13.67730794	12.55231	-44.0314	153.7266	160.4001
IS_B1	13.68850011	38.86841	0.161437	12.85777	40.94022
IS_GB1	13.65242057	-51.2576	-3.08386	-188.142	195.0235
IS_M2	13.65077122	28.36079	24.53843	-16.6793	41.04472
IS_B2	13.66381668	20.01276	-8.69909	-1.80935	21.89654
IS_GB2	13.62753106	-76.5786	31.34794	-33.7739	89.37361
IS_M3	13.47468437	-11.1802	1.037768	-1.83029	11.37645
IS_B3	13.49113647	0.033222	2.798306	-14.6368	14.9019
IS_GB3	13.43458426	-25.4851	-5.00301	-24.1034	35.43295
IS_M4	13.29657345	-26.3989	-1.74936	119.9921	122.8742
IS_B4	13.28548147	13.60472	-2.33472	6.12327	15.10079
IS_GB4	13.31741376	-21.1195	0.379613	-151.114	152.5827
IS_M5	13.33101804	-21.8986	2.089222	-93.529	96.08116
IS_B5	13.3429013	-19.1026	-0.7528	-21.8423	29.0269
IS_GB5	13.31561989	45.16623	0.029616	70.34087	83.59323

The present analysis is very conservative, and it is expected more detailed analysis will give magnetic fields and forces within the current results. The magnetic saturation limits of the various magnetic materials were not considered in this model leading to unrealistically high magnetic fields and forces for the A40 group, as the ability to sustain an internal magnetic field is limited above a certain threshold. Additionally, the motors in the EM model utilized simplified and conservative geometries not accounting for discontinuities, interior gaps, and multiple materials many of which have lesser magnetic permeability than the conservative values used. Despite these factors, the current A40 designs are adequate to withstand the calculated loads, which will be confirmed with more detailed models in the final design stage.

An additional concern with the use of the radiation hardened stepper motors in the Interspace is the presence of Cobalt in the SmCo5 alloy permanent magnets of the stepper motors. Cobalt is heavily restricted within the VV as it is typically in the form of Co-59 which transmutes to Co-60 upon capturing a neutron, a strong gamma emitter with a half-life of 5.27 years. The amount of Cobalt material is limited as it is contained only within the small permanent magnets in the interior of the motors, however, the amount of Cobalt allowed Ex-Vessel is presently unknown. The estimated mass of Cobalt expected in each area is given in Table 43. Radiation levels in the BOL and BEOC are significantly lower than in the IOT due to being behind the Bioshield, and all motors

Released 2024/12/04
Released 2024/12/04

in the BEOC are contained within the radiation shielded cabinet. Alternate permanent magnet alloys have been investigated to replace the Co, most notably various AlNiCo alloys which range from 0-40% Co by composition, however the reduction comes with an associated reduction in motor performance which is unacceptably high for the A40 assemblies. The acceptability of small amounts of Co in these areas and the potential replacement with alternate magnet alloys or motor technologies will be further investigated in the final design phase.

Table 43. Estimated mass of Co in UWAVS system due to stepper motors

Area	Qty. Magnets	Model	Co Mass per Motor Assy. (g)	Total Co Mass (g)
IOT	5	RH-U17-2	21.3	106.5
BOL	4	RH-U17-2	21.3	85.2
BEOC	9	RH-U17-2	21.3	191.7

14.8 MIC Coax Thermo-nuclear Load

As mentioned in section 6.1.1, MIC9 coaxial cables deliver RF power from the LEVI connector to both A10-M1 and A10-M2 mirrors for RF plasma mirror cleaning as shown in Figure 78. The length of the coax internal to the bullnose are to be bent to shape and installed without additional restraint or provisions for active cooling. Additionally, no guidance has been given on the maximum exposure temperature nor the nuclear loading of the coax or connectors. Heating form mirror cleaning RF operation is not expected to generate significant component heating and will be assessed during the prototype activities. However, no calculations have been made to estimate the steady state temperature during ITER operation. There is currently a risk that the coaxial cables and connectors are at risk to damage should they overheat. Provisions could be made during the FDR phase to provide additional cooling by mating them to the bullnose body, but additional guidance from ITER is necessary.

Released 2024/12/04
Released 2024/12/04

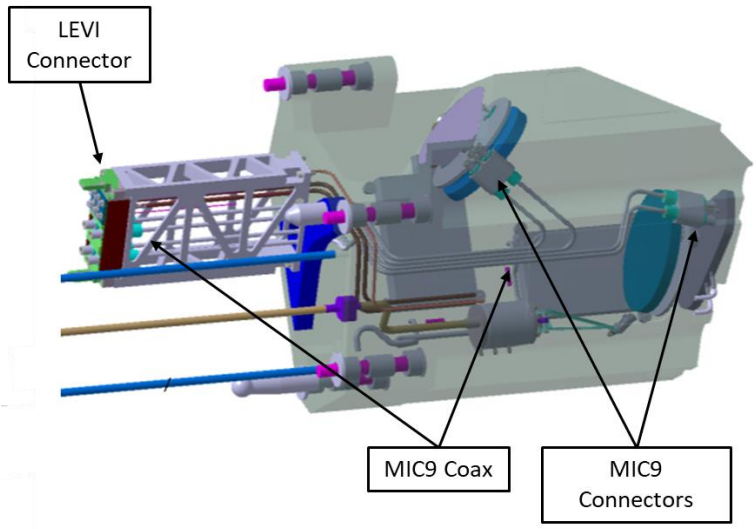

Figure 78. Bullnose with MIC9 coax

14.9 Mirror Cleaning Long-term Redeposition

Extensive research and development have demonstrated the effectiveness of plasma mirror cleaning which includes a variety of parameters (mirror type, contaminant type, gas species, RF frequency and power, presence of B-field, mirror grounding strategy, etc.). To date most of these studied have applied a small amount of material (~100 nm) to the mirror surface or coupons installed at the mirror surface. Effort has been taken to show that mirror cleaning can be repeated many times, each time successfully removing contaminants and returning the mirror surface to acceptable quality (reflectivity, roughness, etc.). To achieve this the mirrors must be kept in a net erosion regime during cleaning, where the rate of material removal exceeds the rate of redeposition. There are two risks associated with the long-term redeposition of material within the bullnose: downstream contamination of optics and increased redeposition rates as the contamination accumulates within the system.

The first two mirrors of UWAVS will experience the highest levels of contamination because they both exist within a volume exposed to the ITER plasma and A10-M1 has uninterrupted line-of-sight exposure to the ITER plasma. This is precisely why both mirrors have provisions for in-situ RF cleaning. However, optics downstream in the system, most notably A20-M1, will experience some contaminate deposition at lower rate, resulting from either the ITER plasma or redeposition of material removed during mirror cleaning operation. Presently, there is no mitigation taken to reduce the degradation of downstream optics. Studies will be performed during mirror cleaning prototype activities to estimate contamination rates during mirror cleaning, however actual rates experience at ITER may differ substantially.

Released 2024/12/04
Released 2024/12/04

The other risk associated with redeposition is the accumulation of contaminants within the bullnose volume and a rise of redeposition rates over time. As mentioned above, most studies to date have looked at removing contaminants which are intentionally applied to the mirror surface or witness coupons. The contamination experienced by the bullnose during ITER operation will not be limited to the mirror surfaces, as some contaminants will be deposited on the interior surfaces. In addition, material removed from the mirror surface during mirror cleaning will redeposit within the bullnose structure. As the presence of contaminants continues to rise in the environment, the rate of redeposition of those contaminants will also rise. Should the redeposition rate exceed the erosion rate, the mirror cleaning activity will fail to restore the full reflectivity of the mirror.

14.10 RF Transmission Loss

The estimated RF power losses due attenuation in the transmission lines are also shown in Table 27, using an assumed attenuation of 3dB per 100 m at 60 MHz. The greatest impact is on ports UP02 and UP17 with an estimated power loss of up 76%. This has a considerable impact on the design as it would require significantly larger RF generators than would otherwise be needed. Moreover, if the RF generators in the DH are upsized then additional cables would be required to handle the increased power since the Ecoflex10 cable type is only rated for 1250W at 60MHz. While this represents conservative estimates of cable length and the association attenuation, it does not account for any additional transmission loss resulting from connecters and feedthroughs or matching network, notch filter, and prematcher performance.

The prohibitive RF power loss to ports UP02 and UP17 warrants re-consideration of the current design. One solution is to relocate the RF generators serving ports UP02 and UP17 to powered cubicles located in the Shielded Corners. This approach is described in the next section.

14.10.1 Risk Mitigation via Relocation of UP02 and UP17 RF Generators

UWAVS is currently assigned space in a shared cubicle located in the North-East shielded corner (11-L2-02E) managed by 55.NEX0, as shown in Figure 79. The current UWAVS design has the camera power supplies and step motor controllers for UP02 and UP17 located in this cubicle. The RF generators for these ports were not placed in this cubicle to due to the limited space, power, and cooling allowable by the interface with 55.NEX0.

However, this limitation deserves reconsideration given the impact of distance on the critical RF generator performance. Therefore, UWAVS will seek priority placement of the RF generators in the shielded and table corners during final design. The impact on performance and risk reduction can readily be seen in Table 44 where estimated power loss to UP02 is reduced from 76% to 28%, and UP17 is reduced from 72% to 38%.

Released 2024/12/04
Released 2024/12/04

Additional improvements to the overall design can be realized if space is made available to re-locate the RF generators for UP14 to the South-East Shielded Corner. This would cut the losses to that port from 57% to only 33%. (UP14 changes not reflected in Table 44).

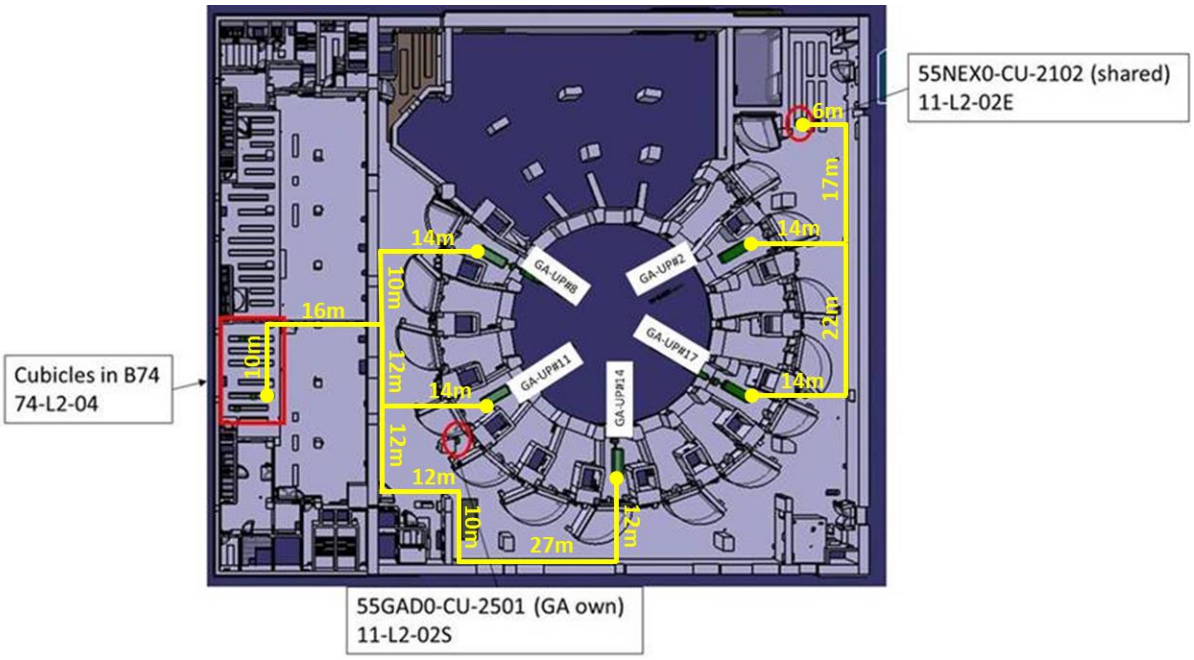

Figure 79. Illustration showing benefit of relocating UP02 and UP17 RF generators to NE Shielded Corner.

Table 44. Improvement to Cable Runs by Relocating RF Generators

Port #	Est. Cable Length (m)			Atten. (dB)	Power Loss
	DH to BEOC	BEOC to EFT	Total		
UP08	50	10	**60 m**	1.80dB	34%
UP11	52	10	**62 m**	1.86dB	35%
UP14	111	10	**121 m**	3.63dB	57%
UP17	59	10	**69 m**	2.07dB	38%
UP02	37	10	**47 m**	1.41dB	28%

Released 2024/12/04
Released 2024/12/04

14.11 DSM Surface Tolerances

55.GA initially proposed using the kinematic mounts to adjust for larger profile tolerances in the DSM bay interfaces. This is problematic for several reasons. Logistically, it is challenging to adjust the modules to unique DSM interfaces and verify performance as an optical subsystem. This requires interface data prior to factory assembly, detailed management of data, and the

development of unique scripts or optical modules to define optimal mirror positions. It is not practical for IO, Port Integrators, or 55.GA to manage this complexity.

However, initial tolerance analysis made this assumption, and the DSM profile interface tolerance was not indicated as a worst offender. The design approach has shifted to controlling interfaces to nominal. 55.GA plans to do a sensitivity analysis to establish the maximum profile tolerances bay to bay that meets system performance. These tolerances shall be agreed upon with port integrators or a performance loss will be quantified prior to final design.

14.12 In-Vessel Mirror Fabrication

All the in-vessel mirrors aim to share a common design architecture and manufacturing approach. The initial architecture proposed leverages a backing plate machined with spiral channels that is furnace brazed to mirror top plate. A full penetration weld around the perimeter provides the VQC-1A boundary weld (water to vacuum boundary). Final surface and prescription of each mirror will be machined, or diamond turned after braze, weld, and stress relief. Initial manufacturability assessment determined the inspection process will be critical, and the adjacent weld to braze joints risk manufacturing and inspection challenges.

Preliminary design and analysis of the first mirrors show very tight temperature uniformity across the light reflecting surface. This high level of thermal performance is achieved through a series of gun drilled holes which are plug welded, following the same design as other ITER diagnostics and DSM port plugs.

Several alternative manufacturing approaches evolved during preliminary design and prototype activities are planned to evaluate performance and costs benefits to aid in down selection. The goal is to have a common approach for all in-vessel mirrors but also address VQC-1 vacuum welds and inspection challenges early in final design.

Released 2024/12/04

Released 2024/12/04

14.13 In-Vacuum Mirror Module Fabrication

Preliminary design and analysis of the in-vessel mirror modules highlighted a complex design requiring an intricate water cooling circuits that require deep hole drilling and weld plugs on a lightweight structures supporting critical optics. Although this manufacturing approach is a proven method for ITER in-vessel components, the complexity lies within the material removal process to ensure internal residual stresses from welding and machining do not cause instability for mirror alignment. It also provides assessment of VQC-1 vacuum welds and inspections.

14.14 In-Vessel Mirror Module Stability

The unique requirements for in-vessel components, as well as restrictive space and specific geometric constraints, lead to custom mirror mounts and optic retention mechanisms. These

designs introduce the risk of mirror mount drift after thermal cycling. Testing is the best approach to establish thermal set requirements for factory assembly. Early testing provides feedback into the design. Prototype activities are planned (see Section 14.13) that provide the opportunity to verify design retention and establish thermal cycling requirements during factory assembly as required.

14.15 Ex-Vessel Condensation

Condensation is a potential risk due to elevated air temperatures in the Port Cell interfacing with cooling pipes transferring 6°C water from the Chilled Water Supply (CHWS) in the BEOC. To mitigate this risk, the use of 28°C water from the Component Cooling Water Supply (CCWS) will be evaluated as well as passive air cooling solutions for the IR cameras and IR blackbody calibration source.

14.16 Blackbody Heat Management

The increase in air temperature caused by the 3 kW black body source during IR calibration exceeds the limitations of electronics in BEOC. Various configurations of active and passive cooling concepts were analyzed to determine an efficient and effective cooling method, however were inconclusive. Large assumptions in the analysis resulted in a wide range of air temperatures from 54°C to 104°C, all of which are outside the max operating range of 44°C for the black body source. Best case analysis temperature plots taken at the IR blackbody source and cameras are shown in Figure 80 and Figure 81. The upper red area of the temperature scales in are set to 50°C which corresponds with the maximum allowable temperature of the IR cameras. Note that temperatures are for IR calibration case where only the IR black body source and IR cameras are on. Temperatures for normal operation are within limits of all electronics.

Released 2024/12/04

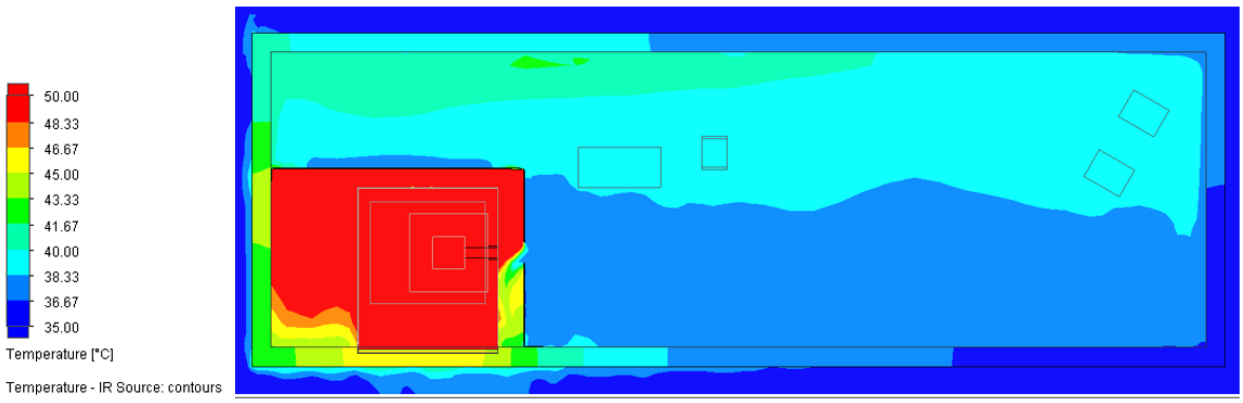

Figure 80. Thermal calibration temperature plot of internal ambient air temperature taken at IR blackbody source location.

Released 2024/12/04

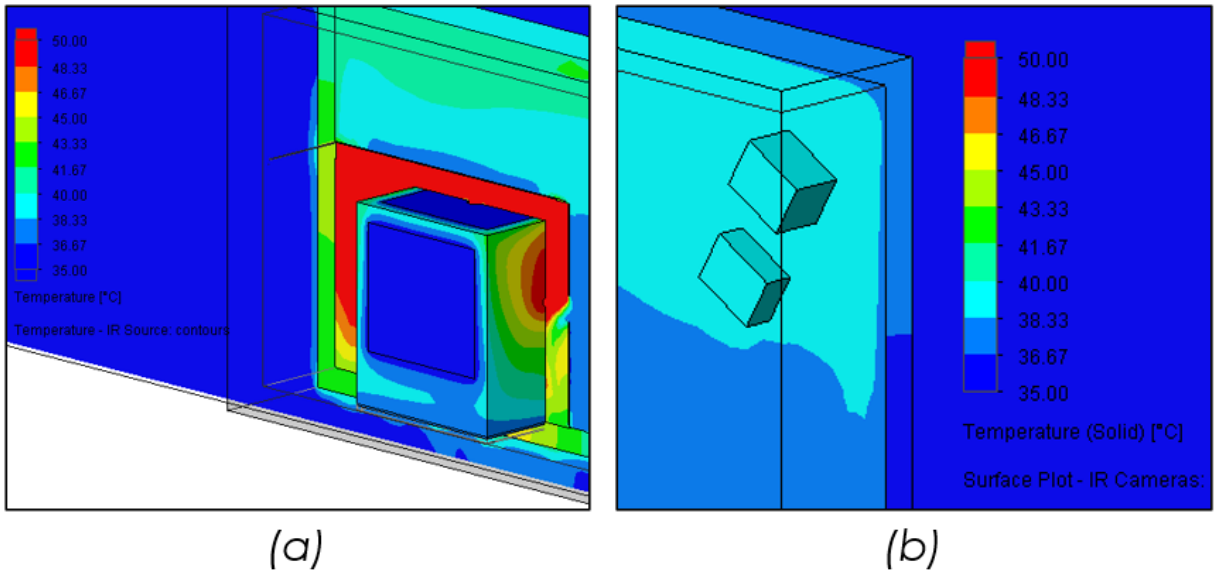

Figure 81. Surface temperature plots for thermal calibration of (a) IR blackbody source and (b) IR cameras.

Due to the inconclusive preliminary analysis, prototype testing of the black body source to identify heat loads and flux will be conducted in final design. The results of which will be used in final analysis to determine an effective cooling solution. This prototype effort will also explore repackaging of the black body source and its standard controls aiming to move electronics out of the Port Cell.

14.17 Use of Cadmium

Cadmium is often used for nuclear shielding because it provides high neutron and gamma ray attenuation with low thickness. 55.GA leveraged existing diagnostic designs and analysis to shield critical electronics and cameras in the BEOC. However, Cadmium was identified as a health risk in the draft HIRA. Cadmium components carry a multitude of risks that necessitate careful consideration and management throughout all phases of the project. Furthermore, Cadmium has low melting temperature and adds significant risk in the event of a fire.

Using cadmium for shielding in ITER, poses several risks:

- Toxicity: Cadmium is highly toxic to humans and the environment.
- Environmental Impact: Cadmium is a persistent pollutant that can long-lasting environmental consequences.
- Operational Hazards: Handling Cadmium during fabrication, installation, maintenance, and decommissioning of ITER presents risks to workers' health and requires strict safety protocols.

Released 2024/12/04
Released 2024/12/04

- Regulatory Challenges: The use of Cadmium in large-scale projects like ITER may face regulatory hurdles due to environmental and health concerns. Strict adherence to safety standards and regulations is necessary to mitigate these risks.

Considering the risks associated with Cadmium, finding and implementing safer alternatives for shielding in ITER is expected. Alternate materials or composite layers with similar or better radiation shielding properties but lower toxicity will be explored.

14.18 Dust Protection

55.GA UWAVS has a specific requirement that ex-vessel optics shall be protected from dust. However, without a clear specification on the cleanliness of the interspace and port cell, it is difficult to quantity the level or protection required. Assuming the levels of cleanliness are ISO Class 7 (or better) per ISO 14644 1:2015 [95], optics should stay relatively clean and the risk of dust contamination is low. The ex-vessel optics are protected by enclosures for the IOT, BOL, and the BEOC. However, the enclosures do not provide hermetic seals with the environment. Telescopic shrouds are designed between all subsystems of the IOT, BOL, and BEOC to further prevent dust ingress. An example of a telescopic shroud in shown in Figure 82.

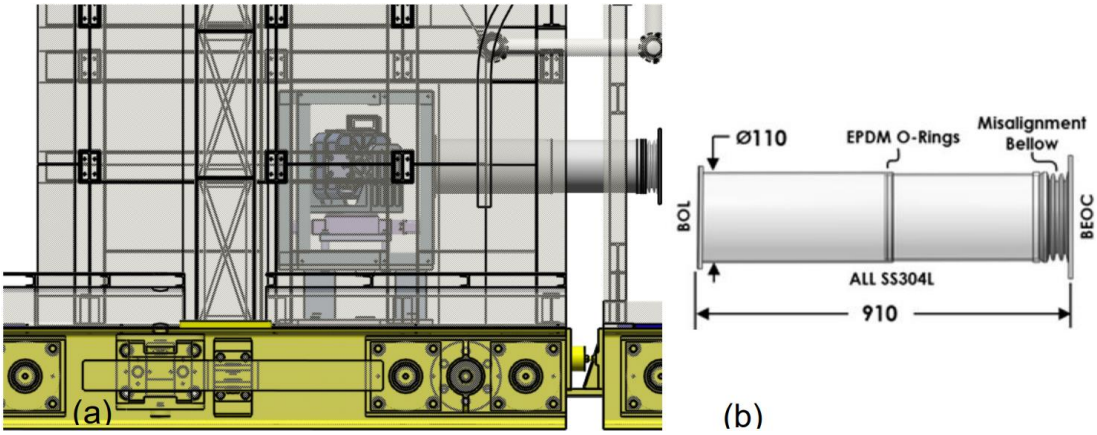

Figure 82. UWAVS ISS-PCSS shroud (a) in bioshield (b) components and size.

Dust on optics generally has a more noticeable effect on visible light compared to infrared light. Dust particles are typically larger than the wavelength of visible light but smaller than infrared wavelengths. This means they can scatter and block visible light more effectively because they interact more readily with the shorter visible wavelengths. The primary temperature measurement is lower risk than the visible light species measurements and the protective measures seem adequate at this time. As visible measurements and requirements mature the level of protection from dust may need to evolve in final design.

A stronger mitigation strategy is to use a light positive clean dry air (CDA) purge inside each enclosure to prevent the ingress of dust. However, this may require design efforts to hermetically

Released 2024/12/04
Released 2024/12/04

seal the enclosures due to possible limitations on air leak rates in the port cells. Seals will need to be added to the designs and the enclosures will need to be strengthened to accommodate a slight over-pressure.

Released 2024/12/04

Released 2024/12/04

15 PROTOTYPES

15.1 Mirror Cleaning Prototype

The UWAVS mirror cleaning system integrates several components which must be validated through measurement. A prototype and test activity will evaluate the mirror cleaning hardware and process with a fully representative UWAVS design with expected mirror contaminants, or proxies, in a representative ITER environment. While plasma cleaning is a well-established technique for industrial and scientific applications, ITER requirements and the UWAVS design results in several unique challenges to the mirror cleaning process. Extensive research has been performed to show challenges are individually solvable, but they have also demonstrated that the effectiveness of the cleaning process is highly dependent on system design and geometry. The highly coupled nature of the cleaning process and UWAVS design drives a need to test and develop the mirror cleaning process on the integrated system hardware that captures all the relevant aspects of the final system. This effort will mature the mirror cleaning process and recipes for UWAVS as well as validate the performance of the integrated RF system.

The prototype tests will be performed without a magnetic field at GA's Diagnostic Center. The prototype will be installed within a vacuum chamber, which includes all the necessary viewports, feedthroughs, and peripherals for the proposed testing (see Figure 83).

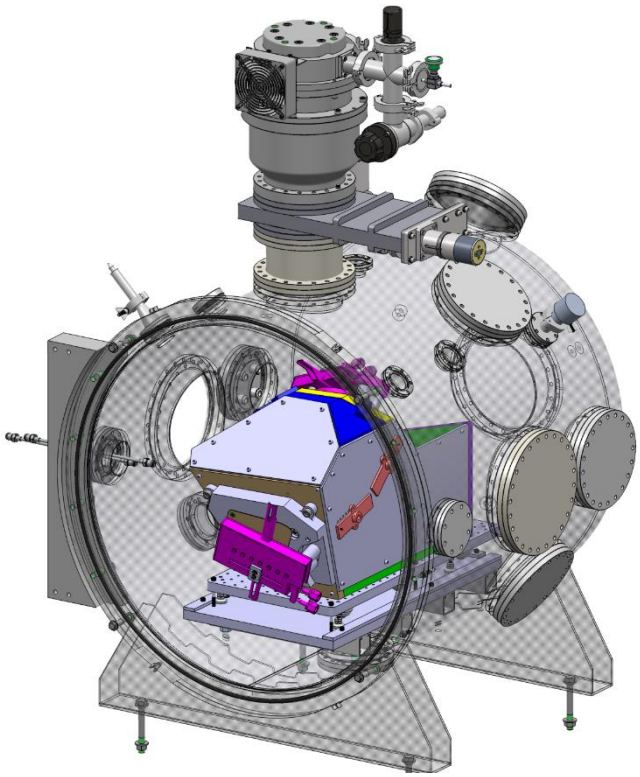

Figure 83. Mirror Cleaning Prototype hardware.

Released 2024/12/04
Released 2024/12/04

Many of the components of the bullnose require long-lead materials and complex manufacturing processes. To expedite the work, reduce the cost, and provide additional flexibility, the prototype will not be an exact match to the full bullnose assembly, but it will be functionally equivalent for mirror cleaning activities. This includes a water-cooled bullnose structure with the correct internal geometry, mirror size and mounting, water cooling of the housing and mirrors, and RF transmission network (prematcher, notch filter, generator, active matcher, etc.).

Notable differences between the prototype design and final bullnose include the following:

Bullnose Body: The prototype bullnose body will be manufactured from 316 Stainless steel with a simplified cooling scheme to reduce complexity and cost. It will represent the correct internal geometry and mounting of the RF components, prematcher, notch filter, connectors, cables and feedthroughs. The bullnose will be designed for easy assembly, disassembly, removal of the mirrors, electrical connections, cooling lines, etc. Figure 84 and Figure 85 show a comparison of the prototype bullnose with the UWAVS-35 bullnose design and identify key changes.

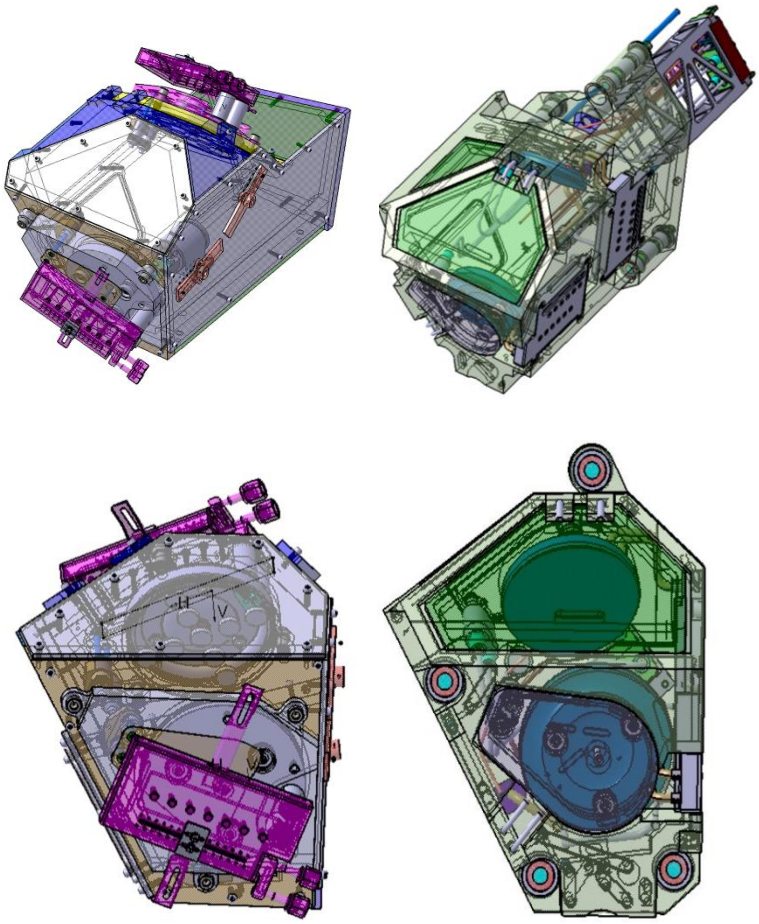

Figure 84. Comparison of the Prototype Bullnose (left) to the UWAVS-35 Bullnose (right).

Released 2024/12/04

Released 2024/12/04

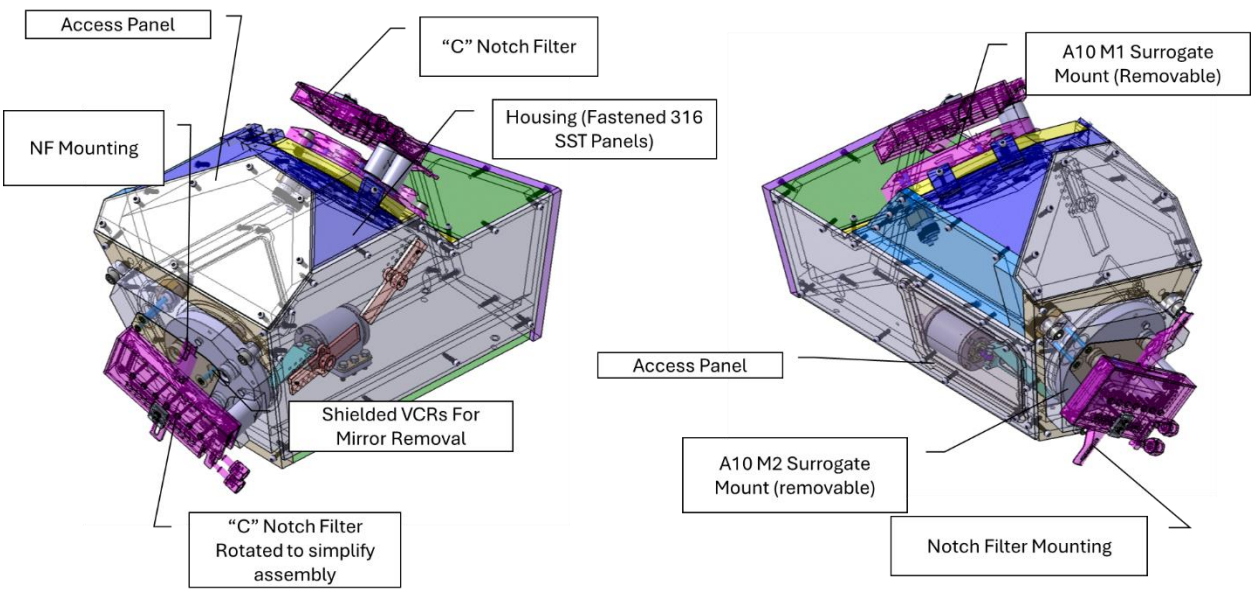

Figure 85. The prototype Bullnose with key elements identified.

Mirror Substrate: Testing with the final mirror design is not envisioned to be cost effective to fulfill mirror cleaning prototype objectives. Thus, representative mirror size, attachment, and surface quality are the prime considerations for the prototype. As such, the prototype mirror substrate will be manufactured with the correct size but with a simplified coolant path. The mirror substrate will be made to accept coated coupons/witnesses for testing purposes. The use of coupons allows for many cleaning test and characterization cycles. These coupons will also be designed for easy removal from the assembly and metrology. To avoid cross-contamination between the mirror substrate and coupons, the substrate will be coated with the mirror coating material (Pt). Figure 86 show key changes to the prototype mirror and Figure 87 shows the prototype mirror in its removable assembly for easy assembly and removal during testing.

The cross sectional view in Figure 88 shows includes the internal components of the mirror cleaning assembly including the central connector and electrical insulators around the conductive fasteners. A closer view of the RF connection between the mirror and the prematcher PCB is shown in Figure 89.

Released 2024/12/04
Released 2024/12/04

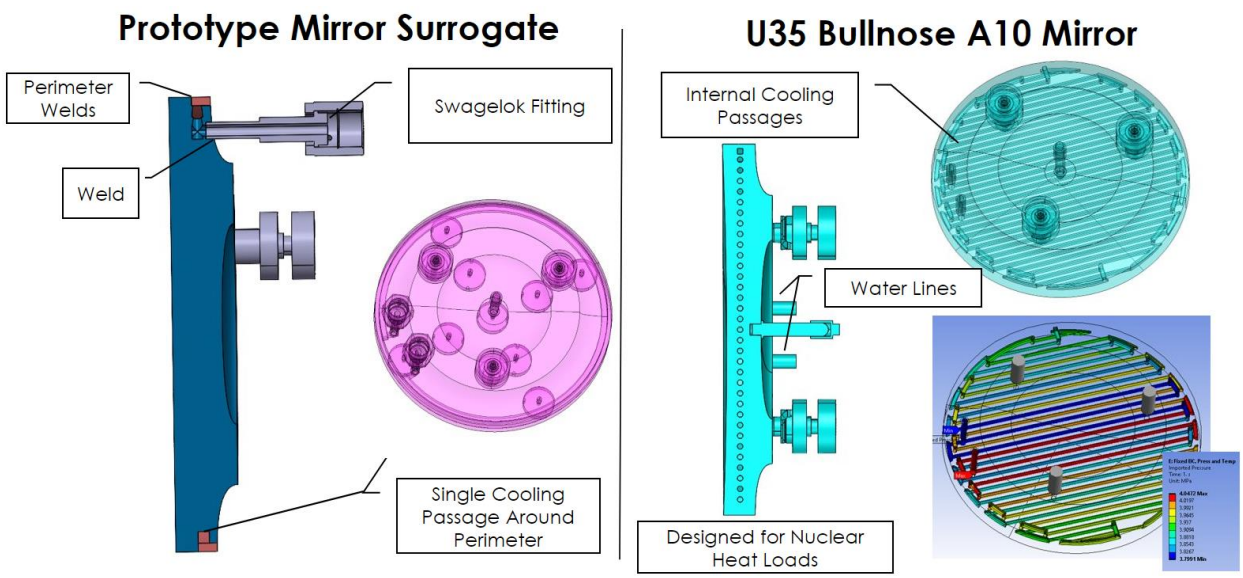

Figure 86. Comparison of the prototype mirror (left) with the UWAVS-35 A10 mirror (right).

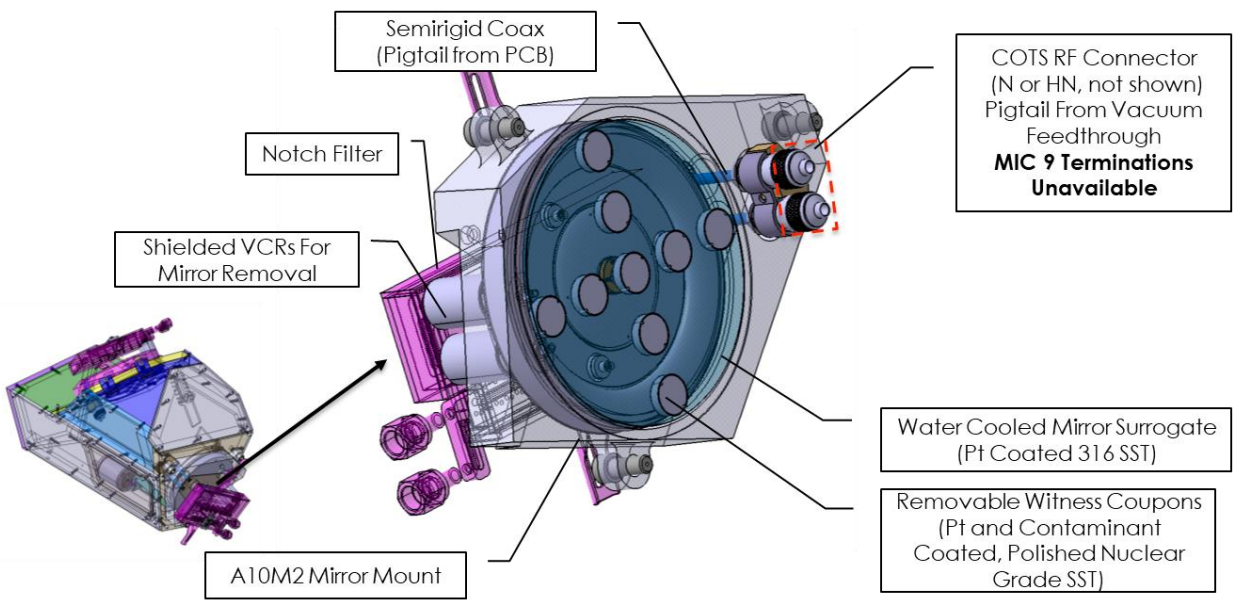

Figure 87. Detailed view of the prototype mirror assembly.

Released 2024/12/04
Released 2024/12/04

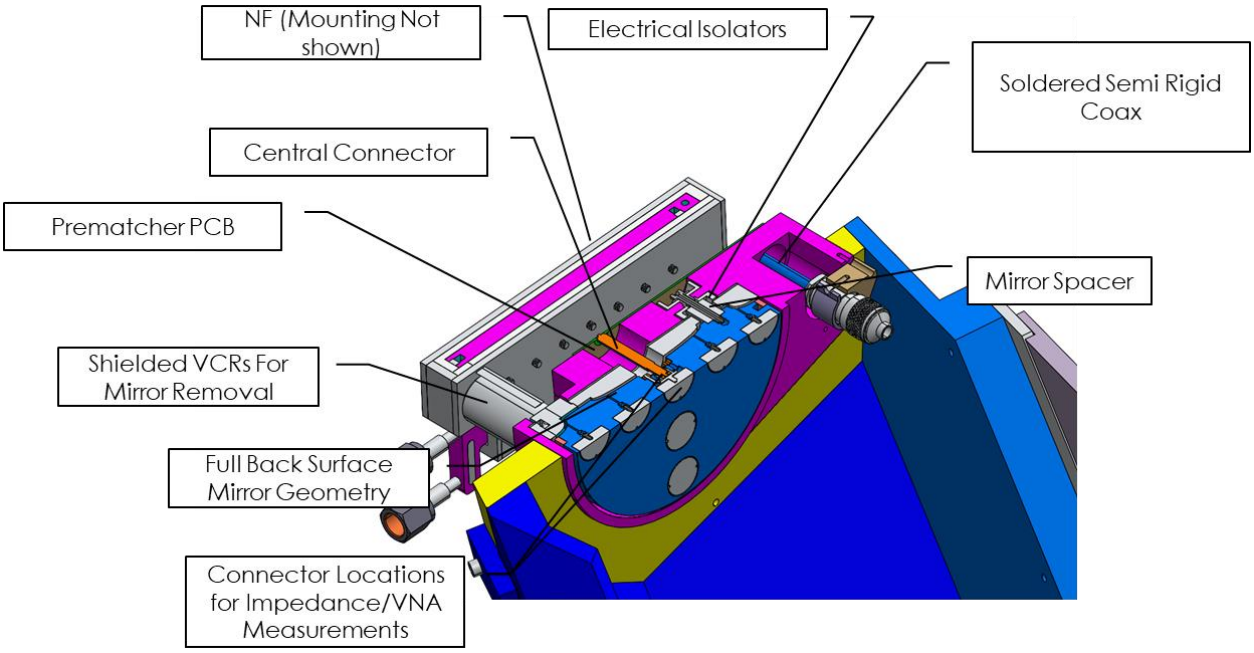

Figure 88. Cross-section view of the prototype mirror assembly.

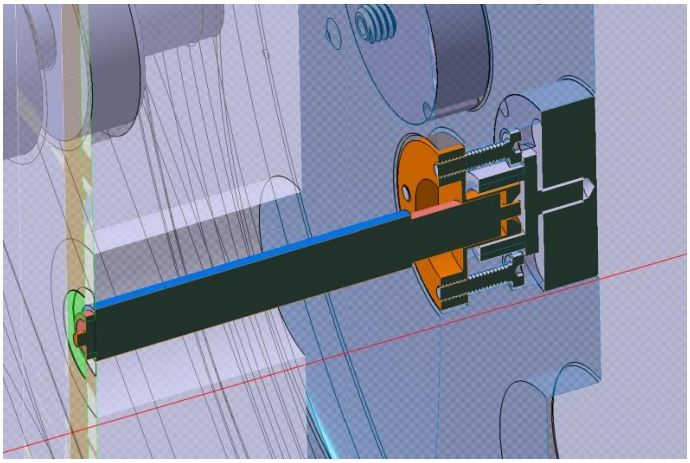

Figure 89. RF connection between the mirror and the prematcher PCB.

- RF Transmission Network: The RF transmission network will include all the functional components and characteristics of the UWAVS design. During initial tests simplified, commercially available coaxial lines and connectors are used, and the length of the transmission lines may be reduced. However, the goal will be to test the UWAVS design (full length mineral insulated cables and MIC9 connectors) once those components become available.

Released 2024/12/04
Released 2024/12/04

- Notch Filter: The notch filter has been shortened to match the notch frequency to 60 MHz. However, the UWAVS-35 “S-shape” design resulted in only ±3 MHz of adjustability. To increase the range, the prototype NF has been changed to a “C-shape” which increases the range to 60±6 MHz, shown in Figure 90. This additional range will accommodate any inaccuracy in the RF simulation, or modifications made to the prototype assembly. Additionally, the UWAVS-35 design includes welded and captive connections between the NF and the mirror. Periodic disassembly is expected to be necessary for the prototype activity, so removable VCR fittings have been added to make the plumbing connection. Shielding has also been added to prevent the electrified portions (between the NF and the mirror) from radiating. These fittings are expected to degrade the performance slightly. It should be noted that the prototype still shows an estimated 95% coupling efficiency, shown in Figure 91.To accommodate the VCR connection the NF has been rotated in the assembly and is now position behind the mirror assembly, shown in Figure 92.

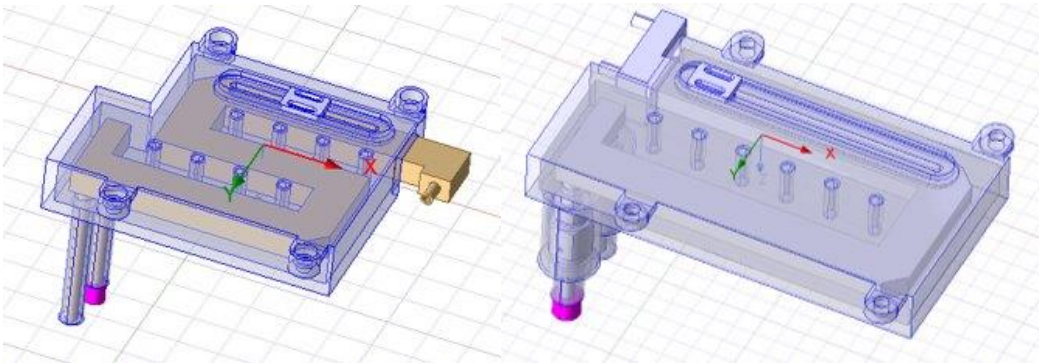

Figure 90. S-Shaped NF (left) and C-Shaped NF with VCR fittings (right).

Released 2024/12/04

Released 2024/12/04

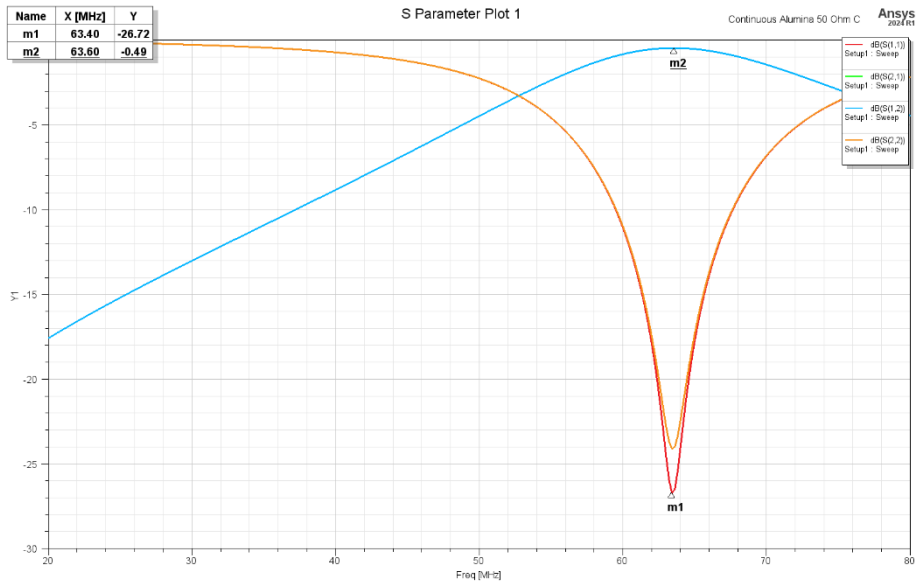

Figure 91. NF performance when tee onto a 50 ohm transmission line.

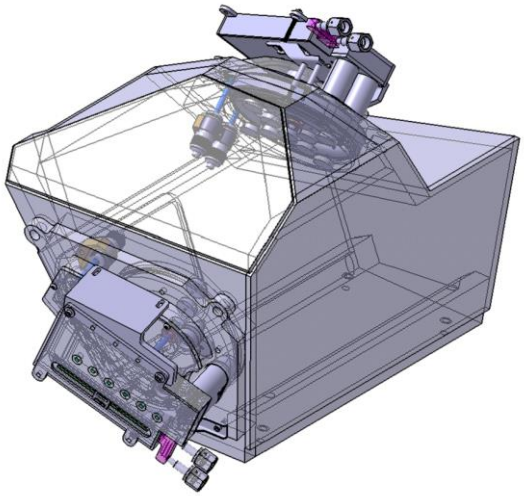

Figure 92. Prototype bullnose with the NF in its rotated orientation.

- Prematcher: As discussed previously the plasma/load impedance are currently unknown in the UWAVS configuration. To allow maximum flexibility in the prototype design the area behind the mirror has been left clear to allow for development of a fixed prematcher board based on the measured impedance. Once the prematcher board is proven to meet design specifications, integration into the UWAVS-35 bullnose design will be considered in a separate activity.

Released 2024/12/04
Released 2024/12/04

- Other: Unnecessary components will be removed to reduce cost. This includes, certain exterior features, and interfaces (e.g., Remote Handling) which are not involved in the mirror cleaning process. Additional modifications may be made to the prototype to increase flexibility during the testing phase. For instance, the design will be modified to enable use with or without a prematcher or with a simplified notch filter, but this will not preclude the use of the final system hardware.

The full-scale mirror substrates (~165 mm diameter) will be made to accept witness samples. The witness samples will be 22 mm disks constructed of nuclear grade stainless steel and polished to meet the UWAVS specification for surface roughness. These witnesses will then be prepared and coated with the mirror coating material. The current plan is to deposit several microns of polycrystalline platinum (Pt) with either DC magnetron sputtering or high-power impulse magnetron sputtering (HiPIMS). A 5 nm titanium or chromium (Ti or Cr) adhesion layer will be used between the substrate and Pt coating. The Pt mirror witnesses will be coated with different materials to replicate the expected impurities of the ITER tokamak environment. Aluminum (Al) and aluminum oxide (Al2O3) coatings will be used as a proxy for light-atomic weight impurities (beryllium (Be), beryllium oxide (BeO), carbon, boron, etc) Tungsten (W) and tungsten oxides (WxOy) will be used as heavy-atomic weight impurities. Additional impurities may be added if necessary.

The prototype system will first be tested with a single powered mirror, but eventually both mirrors will be powered simultaneously for cleaning tests. The basic test procedure will be as follows: First, approximately 50-100 nm of impurity material will be deposited on the polished Pt mirror witnesses, either by sputter deposition (for Al, W, and W_xO_y) or by atomic layer deposition (for Al_2O_3). Characterization of the layer thickness/areal density of each deposited material will be performed after each deposition using x-ray fluorescence (XRF), energy dispersive X-ray analysis (EDX), or ellipsometry. In addition, SEM, AFM, optical reflectivity, and / or interferometry analysis will be used to observe the crystal size, and surface quality, and reflectivity. The coated witnesses will be serialized and arranged across the mirror surface in an orientation to provide measurements across two perpendicular axes intersecting at the mirror's center. The witnesses will then undergo a mirror cleaning process under RF plasma bombardment within the vacuum chamber using a specified cleaning recipe. This recipe will include either helium (He) or Argon (Ar) as the process gas, with a pressure in the range of 1-10 pascals and a delivered RF power of up to 300 W.

Throughout the cleaning process gas pressure and component temperatures will be measured and recorded. The plasma's electron temperature, ion temperature, and potential will be measured via a Langmuir probe, and the ion flux and energy distribution will be measured via a retarding field energy analyzer (RFEA). Broad scans of system parameters will be performed to characterize the relationship between the plasma parameters and operating conditions (gas

Released 2024/12/04
Released 2024/12/04

pressure, gas species, RF power). Once the general parameter space is established, the most promising sets of conditions will be further investigated using iterative optimization.

The performance and adequacy of the mirror-cleaning process will be assessed using a number of metrics. As these mirrors will be used for visible and infrared imaging, this generally requires the removal of layers any thicker than $\lambda_{min}/20$, or approximately 20 nm (where $\lambda_{min} \approx 400$ nm for visible light). In addition, the surface roughness must be maintained at a value below ~ $\lambda_{min}/4$. An exact requirement for material removal rate has not been specified by the customer, but it is generally considered that at least 10-20 nm of material needs to be removed during an 8-hour Test and Conditioning State (TCS). The entire active portions of A10M1 and A10M2 (i.e., the entire front surface) must be in a net erosion zone and become clear of deposits after the conclusion of a conditioning cycle. The Pt witnesses at the A10M1 and A10M2 locations will be removed from the bullnose assembly after each RF mirror cleaning cycle, and the thickness and composition of deposits on each mirror will again be characterized using the appropriate technique (e.g., XRF, EDX, ellipsometry, etc.) as a function of location along the mirror surface. From this analysis the relative sputtering/removal rates will be determined for each recipe and each material (e.g., Pt, Al, W, etc.). The redeposition rates will also be assessed by looking for the presence of the vessel materials (primarily the components of stainless steel, Fe, Ni, Cr, etc.). In addition, SEM analysis and optical reflectivity will be performed on a subset of witness samples to characterize changes to the mirror surface and optical performance. The full characterization procedure is still under development at this time.

15.1.1 Mockup Notch Filter Testing

The RF notch filter has evolved to a compact design to accommodate both the UWAVS-17 and UWAVS-35 commonality of parts. Additionally, 3D modeling of the preceding mockup notch filter showed that it was too low in frequency (adjustable from 50-58 MHz) to support the 60 MHz design frequency. However, the mockup notch filter was fabricated and tested to validate the 3D RF models and design performance [96]. The measurements show good agreement to the RF models and indicate the mockup notch filter acts as a high impedance open circuit at the notch frequency. A single measurement is shown in Figure 93. It is estimated that the mockup notch filter would allow from ~96% power coupling to the load. These results serve as verification of the RF models and the current compact NF design approach.

Released 2024/12/04
Released 2024/12/04

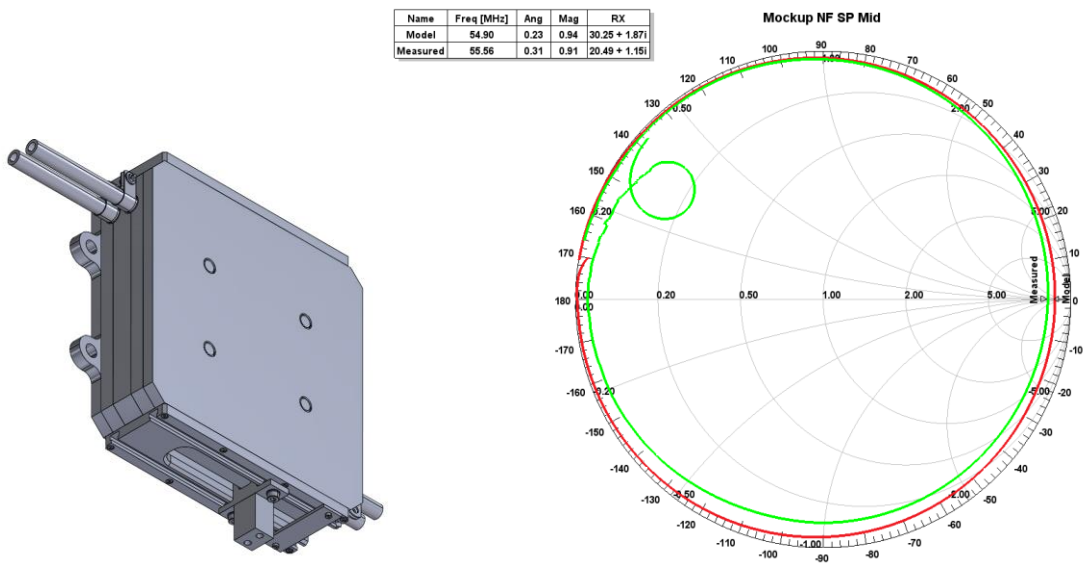

Figure 93. Measured smith chart of mockup notch filter (red line) with HFSS results overlayed (green line). Note impedance values are given normalized to 50 ohms.

15.1.2 Prototype Impedance Measurement

The load or combined mirror and plasma impedance is a critical input parameter to the RF transmission circuit for proper mirror cleaning operation. The impedance value dictates the design of the prematcher and the overall performance of the RF circuit. Achieving a proper impedance match limits reflected RF power and delivers maximum power transmission to the plasma. This reduces the total input RF power required and the voltage seen by each of the system components, thereby reducing the potential for failures of connectors and components.

The best current estimate of the load impedance was determined from JADA reports (55262TS000/5RVGU4). This report calculated the impedance based on a simple physical model and measurements from 2016 and a much larger mirror size. It should not be assumed correct without proper benchmarking. The report itself states, “hard to get accurate/ real numbers for Zpl at the moment, measurements planned.” To date, no additional measurements have been made to increase the accuracy of the impedance value. In addition, the calculation results were strong functions of the RF frequency, power, gas type, and gas pressure. Since no calculations were made at 60 MHz, the current best estimate of the load impedance was taken from the nearest frequency, 50 MHz. The combined impedance (mirror+plasma) is also expected to be a strong function of the mirror and mirror housing geometry, as stray capacitance must be considered.

While the current UWAVS RF system includes an active matching network to account for some discrepancy between the assumed and actual impedance value, a poor match from the prematcher to the load may severely restrict the range over which the active matcher can compensate. This could result in a reduced range of powers, pressures, and gasses for which the

Released 2024/12/04
Released 2024/12/04

circuit will achieve suitable transmission losses. A poor match of the prematcher to the load will also result in increased reflected power and voltage standing wave ratio (VSWR) between the active matcher and prematcher, increasing the failure potential of the cables and connectors in that region.

The prototype strategy involves the use the prototype bullnose to measure the plasma and mirror impedances. The system will be instrumented with plasma diagnostics, and measurements of the true mirror and plasma impedances will be made. These measurements will be made with an RF frequency of 60 MHz and with the correct process gasses (He and Ar) and pressure ranges. To measure the plasma impedance the system will initially be assembled without a prematcher and with a single 50 Ω RF connection. This system allows for direct determination of the combined mirror and plasma impedance by determining the active matching network parameters. However, it will be advantageous to determine the independent mirror and plasma impedances. The basic procedure for measurement of the plasma impedance of each mirror is as follows:

- A plasma is generated and sustained for a given gas species, pressure and RF power, then active matching network settings are recorded and fixed. This allows for determination of the combined mirror + plasma impedance.
- Replace RF generator with 50 ohm load and connect VNA to connector at mirror surface, measure circuit impedance. This allows for determination of the mirror impedance.
- Connect VNA at rear mirror surface connector. This allows for determination of the impedance up stream of the mirror. This should not be necessary in the simplified circuit shown in Figure 94 (as it represents a simple 50 ohm transmission line). However, it would be necessary should this test be performed with a splitter or prematcher installed.
- Optional: Connect VNA to active matching network and measure the circuit impedance. This confirms the output impedance of the active matching network.

Released 2024/12/04
Released 2024/12/04

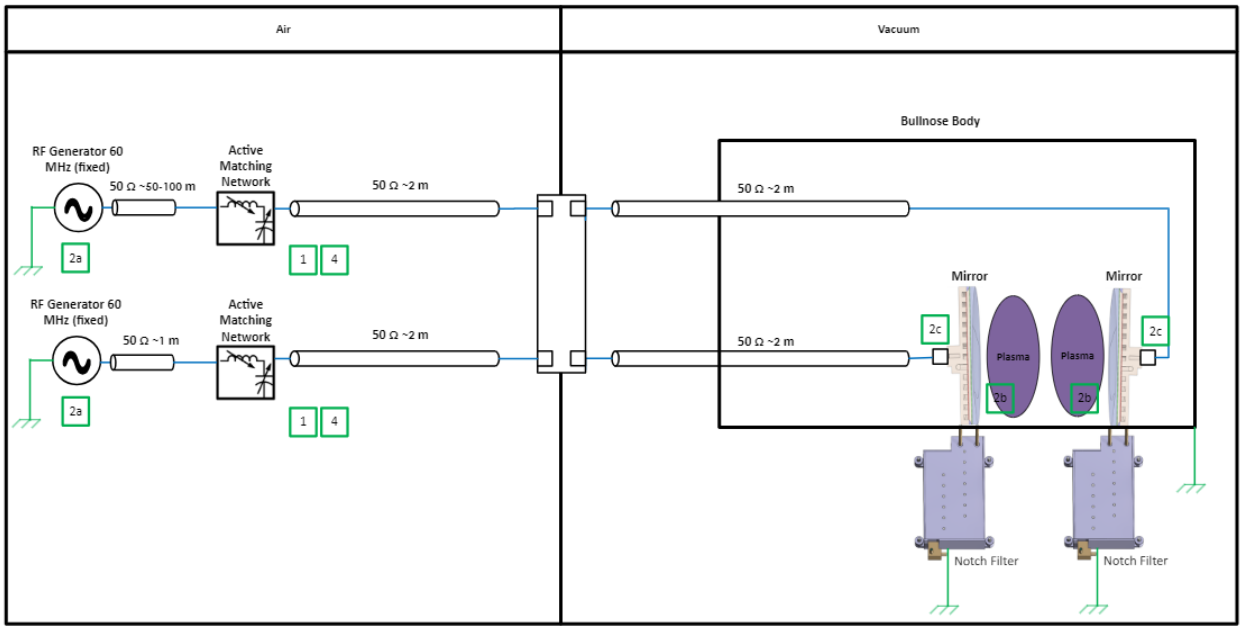

Figure 94. Plasma Impedance measurement diagram

15.2 First Mirror Prototype

Fabricating the first mirrors using a mosaic of relatively large single crystals of molybdenum (Mo) was the baseline at the start of preliminary design This approach is expensive and technically challenging. A trade study to evaluate the performance, cost and technical risk of the baseline and several other approaches to fabricate first mirrors was conducted. The most desirable approaches were rhodium (Rh) or platinum (Pt) coatings applied to stainless steel mirrors.

A substantial effort was made to develop an affordable technique to apply Rh coatings with adequate thickness to survive the multiple RF cleaning events required. Previous work using magnetron sputtering demonstrated excellent performance but scale up was deemed cost prohibitive. Efforts to apply Rh coatings via electroplating showed promise but were not capable of producing adequately thick coatings with good surface adhesion.

With no viable process to apply Rh coatings, focus was shifted to Pt coatings. Small mirror coupons were machined form ITER grade stainless steel (316L(N)-IG) and polished to meet optical specifications. The coupons were coated with Pt using two variations of magnetron sputtering: DC magnetron sputtering and Bipolar High Power Impulse Magnetron Sputtering (BP-HiPIMS). Both approaches were evaluated using various SEM techniques to characterize surface structure and adherence to the substrate. BP-HiPIMS created a slightly smaller grain structure which appears to be more desirable. Samples from both coating techniques were submitted to ITER for inclusion in steam ingress and RF cleaning tests. Reflectivity was measured before and after both events. Results from the tests performed at University of Basil, shown in

Released 2024/12/04
Released 2024/12/04

Figure 95 and Figure 96 demonstrate that there little change in reflectivity resulting from either exposure test. These positive results justified moving forward with efforts to demonstrate coating a full-scale mirror with Pt using the BP-HiPIMS process. Additional prototype testing is planned to subject the witness coupons to thermal cycling events which simulate the bakeout process for installation in ITER and confirm that no delamination or surface degradation is observed. Full scale (~165mm) prototype mirrors will also be procured to validate the the Pt coatings of appropriate thickness (7 µm) can be uniformly applied across the optical clear aperture.

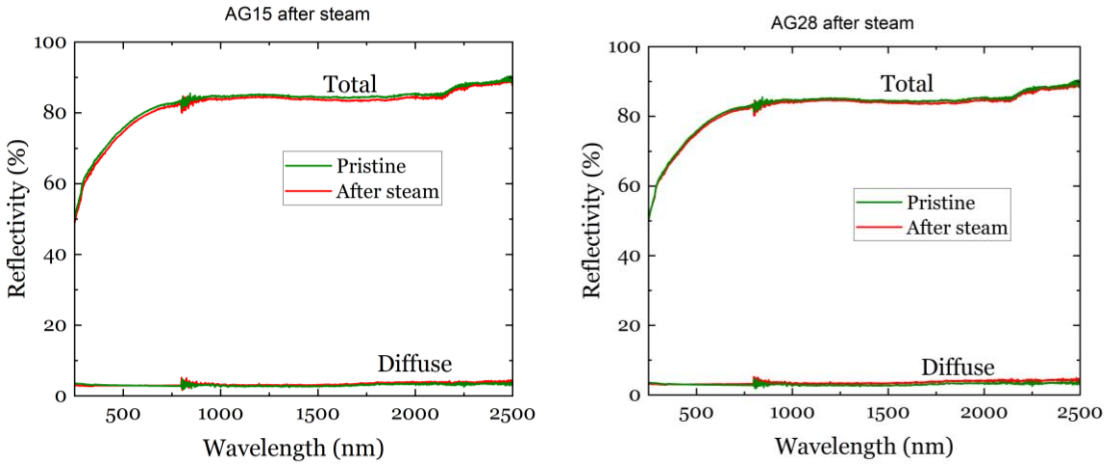

Figure 95. Reflectivity of Pt coated specimens before and after simulated steam ingress event showing minimal loss of reflectivity.

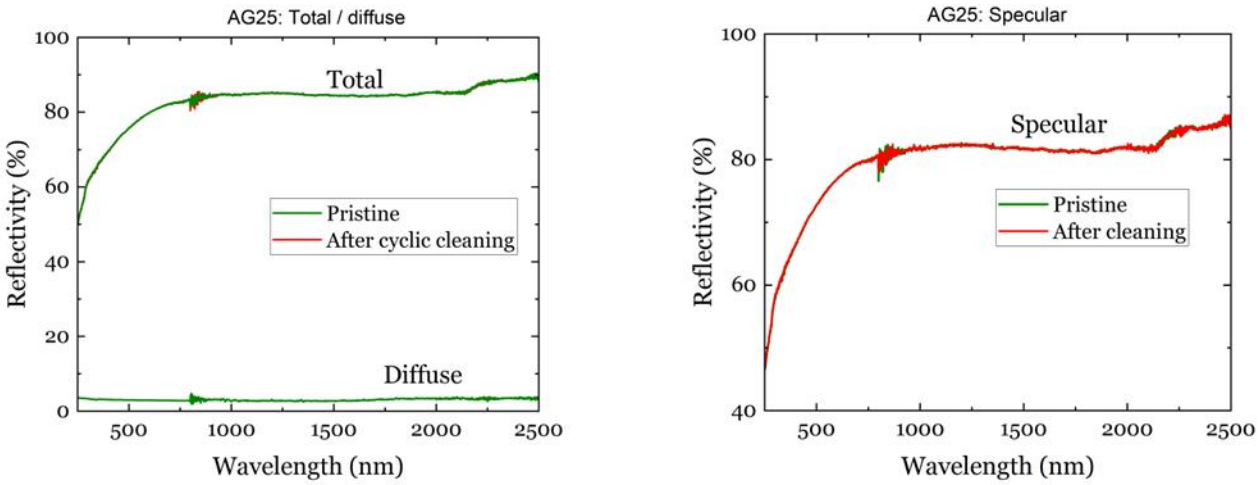

Figure 96. Diffuse and specular reflectivity of Pt coated samples before and after mirror cleaning showing minimal degradation.

Released 2024/12/04
Released 2024/12/04

15.3 Transmission Filament Prototype

The unique high temperature heater is leveraging a staged process development. A prototype is currently under development during preliminary design that includes detailed design and prototype hardware. The initial prototype heater characterization will include testing to measure the following parameters:

- Resistance of each element at room temperature both before and after characterization testing.
- Plots of radiator plate temperature as a function of voltage and current for at least 3 excursions to temperature for each of the operational modes.
- Measurement of temperature uniformity of the radiator plate at steady state conditions for all three operational modes. (for operational modes see design specifications details in Section 8.3)

Subsequent functional testing and characterization is planned for final design leveraging existing test hardware and instrumentation as shown in Figure 97.

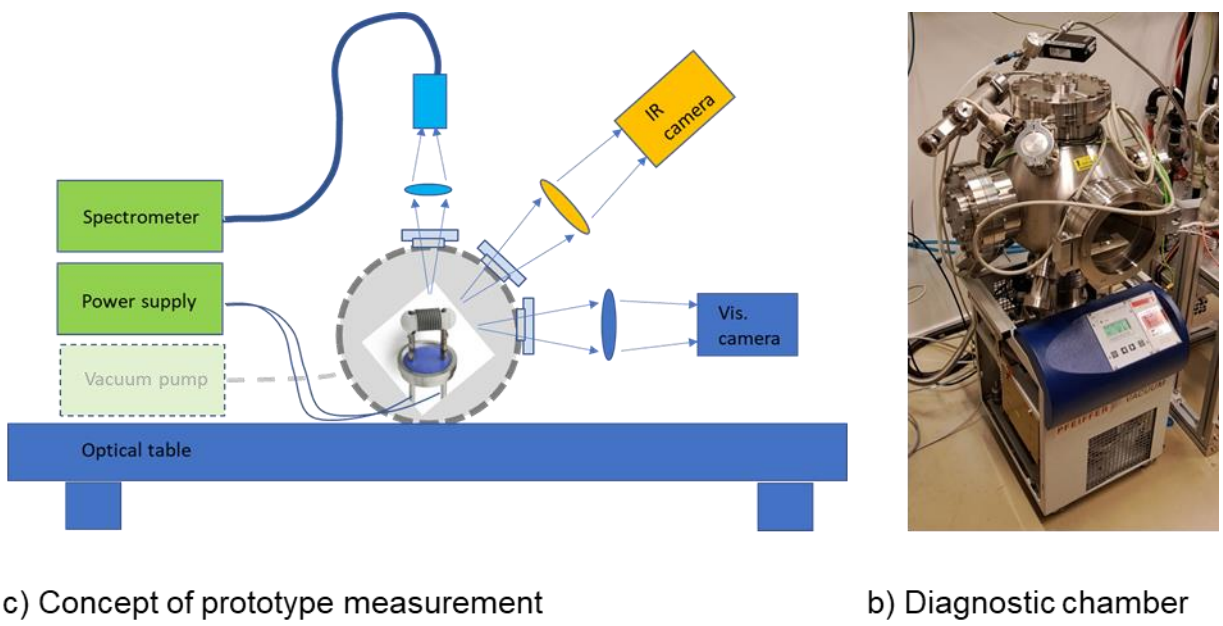

Figure 97. Prototype test apparatus a) conceptual layout b) existing hardware.

Released 2024/12/04
Released 2024/12/04

The additional functional tests will be performed in final design. The details of the test plan are in development.

- I-V characterization with power increase in steps
  - Current voltage and temperature
  - Spectral distribution
  - Spatial intensity distribution
- Post test inspection
  - Surface properties
  - Electrical contacts

After characterization studies are complete, at least one test article will be cycled to failure to determine margin in the design as conceptually illustrated in Figure 98.

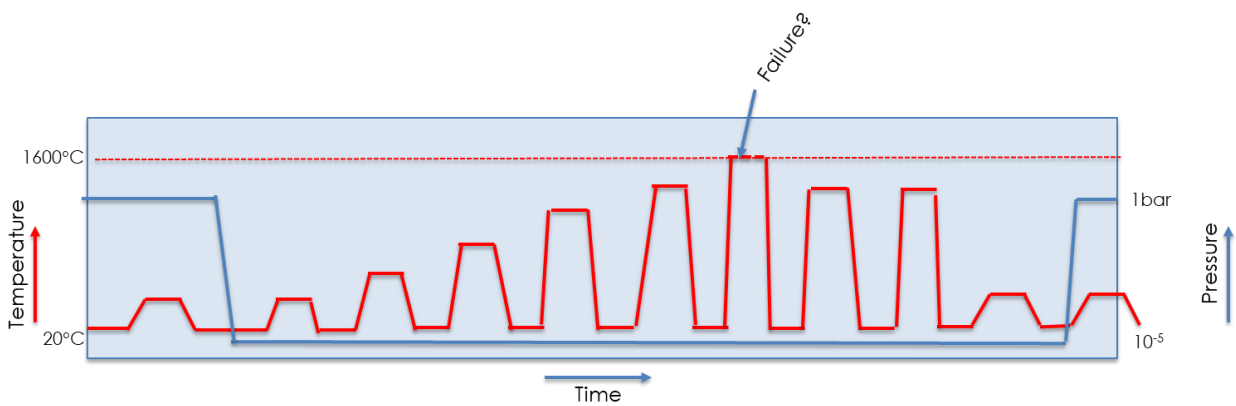

Figure 98. Representation of filament life cycle test.

15.4 Shutter Prototype

The in-vessel shutter requires prototype testing to validate the design. A test plan has been created prior to testing. Full details of the test plan are documented in [97] Hardware is currently in procurement. The following test objectives from the test plan are listed below for reference.

1. Verify form, fit and function of the shutter assembly on a test bench.
2. Confirm full open of shutter aperture blade is achievable in vacuum environment.
3. Confirm shutter aperture blade can achieve full close state under normal operating pressure within a vacuum environment.

Released 2024/12/04
Released 2024/12/04

4. At vacuum and elevated heat loading (per in-vessel thermal analysis), cycle shutter assembly 100,000 cycles (this means 100,000 open operations and 100,000 close operations) through its full range of motion to determine lifecycle.
5. Measure the aperture blade open area every 10,000 cycles and upon completion of 100,000 cycles.
6. Inspect and document any wear, fretting, galling or cold welding of all kinematic joints every 10,000 cycles.

Released 2024/12/04

Released 2024/12/04

REFERENCES

[1] "55.GA (UWAVS-35) Structural Integrity Report: In-Vessel, 304243-R00015, ITER_D_WL5TZ6, v2.0".

[2] "55.GA UWAVS Structural Integrity Report: Ex-Vessel, 304243-R00016, ITER_D_APHWM7, v2.0".

[3] ITER Coordinate Systems, ITER_D_2A9PXZ, v3.7.

[4] Sub-System Requirement Document sSRD-55.GA: IR Cameras: Vis/IR TV (Upper), ITER_D_WYWS36, v1.2.

[5] 55.GA PA Annex B, ITER_D_3UT2WX, v2.8.

[6] 55.GA UWAVS-35 System Detailed Performance Definition, 304243-R00018, Rev. A, ITER_D_WL6RMF, v1.0.

[7] ITER Project Requirements, ITER_D_27ZRW8, v6.3.

[8] Safety Requirement Roombook, ITER_D_KF63PB, v2.11.

[9] PBS 55 Global PIC list, ITER_D_3G2T8J, v2.7.

[10] IS-55.NW-55.GA-001, ITER_D_SZRKME, v6.2.

[11] SRJ54E, 55.NW-System-Loads-Specifications-For-Sapphire-Windows, ITER_D_XLCJWV, v1.3.

[12] ITER Vacuum Handbook, ITER_D_2EZ9UM, v2.5.

[13] 55-GA-A0 IR Cameras: VIS/IR TV (Upper) UPP02 PID, ITER_D_PJ4JFG, v2.0.

[14] 55-GA-B0 IR Cameras: VIS/IR TV (Upper) UPP08 PID, ITER_D_PJAC7P, v1.0.

[15] 55-GA-C0 IR Cameras: VIS/IR TV (Upper) UPP11 PID, ITER_D_PJCAT5, v1.0.

[16] 55-GA-EO IR Cameras: Vis/IR TV (Upper) UPP14 PID, ITER_D_PJB95T, v1.0.

[17] 55-GA-A0 IR Cameras: VIS/IR (Upper) UPP02 Cabling, ITER_D_3QQP6T, v2.2.

[18] 55-GA-B0 IR Cameras: VIS/IR (Upper) UPP08 Cabling, ITER_D_3QSJ6B, v2.4.

[19] 55-GA-C0 IR Cameras: VIS/IR (Upper) UPP11 Cabling, ITER_D_596WA5, v2.0.

[20] 55-GA-D0 IR Cameras: VIS/IR (Upper) UPP14 Cabling, ITER_D_3QSD6R, v2.0.

[21] Electrical Power Cabling Table, ITER-D-WKS6M6, v2.1.

[22] ITER Fire Safety Approach, ITER_D_25SDBD, v3.1.

[23] 55.GA UWAVS-35 Decommissioning Plan, 304243-N00016, Rev A, ITER_D_APHWM7, v1.0.

[24] Design Compliance Matrix, ITER_D_WL7E9X, v1.0.

[25] ITER Materials Properties Handbook, Introduction,, ITER_D_2NRCSB, v1.3.

[26] In-Vessel Components, SDC-IC, ITER_D_222RHC, v3.0.

[27] SDC-IC Appendix A, Materials Design Limit Data, ITER_D_222RLN, v3.3.

[28] RCC-MRx, 2018 Edition, Design and Construction Rules for Mechanical Components of Nuclear Installations: High Temperature, Research, and Fusion Reactors.

[29] IO Cable Catalogue, 355QX2, v6.11.

[30] Technical Description for LEVI RH Connectors, ITER_D_5FKEX9, v2.0.

[31] CAD Manual 04-3 Mechanical Design Methodologies, ITER_D_33XVW6, v2.1.

[32] 55.GA UWAVS-35 Technical Design Description for Bullnose, 304243-R00024, Rev A, ITER_D_ATY3SB, v1.0.

Released 2024/12/04

Released 2024/12/04

[33] 55.GA UWAVS-35 Engineering Calculation Note for Bullnose, 304243-R00021, Rev A, ITER_D_ATYNR5, v1.0.

[34] 55.GA UWAVS-35 Technical Design Description In-Vessel Shutter, 304243-R00022, Rev A, ITER_D_AJWKF7, v1.0.

[35] 55.GA UWAVS-35 Engineering Calculation Note for In-vessel Shutter, 304243-R00014, Rev A, ITER_D_ATYMDG, v1.0.

[36] 55.GA UWAVS-35 Technical Design Description for Front End Optical Modular System A20-A30, 304243-R00025, Rev A, ITER_D_AU4VZT, v1.0.

[37] 55.GA UWAV-35 Engineering Calculation Note for FEOMS A20-A30, 304243-R00020, Rev A, ITER_D_WL7LFH, v1.0.

[38] 55.GA UWAVS Technical Design Description for Interspace Optics Tube, 304243-R00026, Rev A, ITER_D_AU4LBU, v1.0.

[39] 55.GA UWAVS Engineering Calculation Note for Interspace Optics Tube, 304243-R00013, Rev A, ITER_D_ATYL9E, v1.0.

[40] 55.GA UWAVS Engineering Calculation Note for Bioshield Optical Labyrinth, 304243-R00012, Rev A, ITER_D_ATYJVY, v1.0.

[41] 55.GA UWAVS Technical Design Description for Bioshield Optical Labyrinth, 304243-R00027, Rev A, ITER_D_ATYDUW, v1.0.

[42] 55.GA UWAVS Technical Design Description for Back End Optics and Cameras, 304243-R00028, Rev A, ITER_D_ATYFD5, v1.0.

[43] 55.GA UWAVS Engineering Calculation Note for Back End Optics and Cameras, 304243-R00011, Rev A, ITER_D_ATYL5C, v1.0.

[44] 55.GA UWAVS-35 Optical Model Results, 304243-R00029, Rev A, ITER_D_AQLWZW, v1.0.

[45] UWAVS Mechanical Tolerance Stack Summary, 304243-V00034, Rev B, ITER_D_C8DFNH, V1.0.

[46] D1 – Building of the Tolerance chain of the contents of the, ITER_D_2PGZ53, v1.1.

[47] System Design Description for Interspace Support Structure (ISS), Port Cell Support Structure (PCSS) for Lower, Equatorial and Upper Ports, ITER_D_7M5RVG, v1.2.

[48] 55.GA UWAVS-35 On-Site Assembly Plan, 304243-N00007, Rev A, ITER_D_AK7KBE, v1.0.

[49] Oberg, Franklin, Horton, & Ryffel, "Machinery's Handbook," 29th Edition, 2012.

[50] Interspace Temperature Estimation, ITER_D_R3L9HK, v1.0.

[51] UWAVS Calibration Plan, 304243-V00057, Rev A, ITER_D_C8HP3D, V1.0.

[52] 55.GA UWAVS Instrumentation and Control Architecture, 304243-R00030, Rev A, ITER_D_AU4W6P, v1.0.

[53] 55-GA-D0 IR Cameras: VIS/IR TV (Upper) UPP14 PID, ITER_D_PHUE63, v1.0.

[54] Reponse Engagement 31.4 : Zonage Dechets, ITER_D_PLFVHE.

[55] 55-GA-A0 IR Cameras: VIS/IR TV (Upper) UPP02 SLD, ITER_D_RF429Q, v1.0.

[56] 55-GA-B0 IR Cameras: VIS/IR TV (Upper) UPP08 SLD, ITER_D_RMEANB, v1.0.

[57] 55-GA-C0 IR Cameras: VIS/IR TV (Upper) UPP11 SLD, ITER_D_RRE4X9, v1.0.

[58] 55-GA-D0 IR Cameras: VIS/IR TV (Upper) UPP14 SLD, ITER_D_RY67QS, v1.0.

[59] 55-GA-A0 IR Cameras: Vis/IR TV (Upper) UPP02 PFD, ITER_D_3QRZQ8, v1.0.

[60] 55-GA-B0 IR Cameras: Vis/IR TV (Upper) UPP08 PFD, ITER_D_FA247Z, v1.0.

Released 2024/12/04

Released 2024/12/04

[61] 55-GA-C0 IR Cameras: Vis/IR TV (Upper) UPP11 PFD, ITER_D_FA49ZM, v1.0.

[62] 55-GA-D0 IR Cameras: Vis/IR TV (Upper) UPP14 PFD, ITER_D_FAA8Y4, v1.0.

[63] 55.GA UWAVS I&C System Requirement Specification, 304243-S00024, Rev A, ITER_D_ARRY56, v1.0.

[64] 55.GA UWAVS I&C System Design Specification, 304243-S00025, Rev A, ITER_D_ARS734, v1.0.

[65] 55.GA UWAVS-35 Factory Qualification Test Plan, 304243-N00004, Rev A, ITER_D_WL65RC, v1.0.

[66] 55.GA UWAVS-35 Onsite Testing and Commissioning Plan, 304243-N00011, Rev A, ITER_D_WL7A5Y, v1.0.

[67] Anthoine, D, "UWAVS2 FAT Test Plan", 24400-400-PR002, Rev A, Bertin, 2024, ITER_D_AU4385, V1.0.

[68] 55.GA UWAVS-35 Port Integrator Assembly Plan for the FEOMS, 304243-N00006, Rev A, ITER_D_WL6CDG, v1.0.

[69] 55.U2/U8/UB/UE - On site Assembly Plan(s), ITER_D_9T2D2M, v1.0.

[70] 55.U2 - On site Assembly Plan(s), ITER_D_VQ9Q2Z, v1.2.

[71] 55.GA UWAVS-35 Test Plan in Port Plug Test Facility, 304243-N00008, Rev A, ITER_D_WL76ZM , v1.0.

[72] 55.GA UWAVS-35 Remote Handling Compatibility Assessment Report, 304243-R00019, Rev. A, ITER_D_WL6SN7, v1.0.

[73] Refurbishment Process in HCC - High Level Description, ITER_D_2CTTT8, v1.0.

[74] DDD 23-05 APPENDIX H Design of Generic Tools, ITER_D_A2HS4L, v1.0.

[75] PBS 23.06.CM - Tool Specification Sheet for Pipe Maintenance, ITER_D_9PQ86C, v1.4.

[76] 55.GA UWAVS-35 RH-PDF for FEOMS Mirror Module Installation/Removal, 304243-S00009, Rev A, ITER_D_AK7F5C, v1.0.

[77] 55.GA UWAVS-35 RH-PDF Bullnose Installation/Removal, 304243-S00010, Rev A, ITER_D_WL7LHG, v1.0.

[78] 55.GA UWAVS-35 RH-TDF for Bullnose Installation, 304243-S00011, Rev A, ITER_D_AK7F6V, v1.0.

[79] 55.GA UWAVS-35 RH-TDF for Bullnose: Removal, 304243-S00012, Rev A, ITER_D_ARTMQW, v1.0.

[80] 55.GA UWAVS-35 RH-TDF for Installation of the Bay 2 Mirror Module, 304243-S00013, Rev A, ITER_D_ARTR43, v1.0.

[81] 55.GA UWAVS-35 RH-TDF for Removal of the Bay 2 Mirror Module, 304243-S00014, Rev A, ITER_D_ARTSYG, v1.0.

[82] 55.GA UWAVS-35 RF-TDF for Installation of the Bay 5 Mirror Module, 304243-S00015, Rev A, ITER_D_ATQ8Q2, v1.0.

[83] 55.GA UWAVS-35 RH-TDF for Removal of the Bay 5 Mirror Module, 304243-S00016, Rev A, ITER_D_ATVQ6A, v1.0.

[84] 55.GA UWAVS-35 RH-TDF for Installation of the Bay 4 Mirror Module, 304243-S00017, Rev A, ITER_D_AS4P23, v1.0.

[85] 55.GA UWAVS-35 RH-TDF for Removal of the Bay 4 Mirror Module, 304243-S00018, Rev A, ITER_D_AS4XGY, v1.0.

[86] 55.GA UWAVS-35 RH-TDF for Installation of the Bay 7 Mirror Module, 304243-S00019, Rev A, ITER_D_ATXDWX, v1.0.

Released 2024/12/04

Released 2024/12/04

[87] 55.GA UWAVS-35 RH-TDF for Removal of the Bay 7 Mirror Module, 304243-S00020, Rev A, ITER_D_ATXF5V, v1.0.

[88] 55.GA UWAVS-35 RH-TDF for Installation of the Bay 6 Mirror Module, 304243-S00021, Rev A, ITER_D_ATWLMC, v1.0.

[89] 55.GA UWAVS-35 RH-TDF for Removal of the Bay 6 Mirror Module, 304243-S00022, Rev A, ITER_D_ATX52T, v1.0.

[90] Guideline for implementation of the PCR-1103 related to the fire loads management in the Port Cells, ITER_D_WM7PYF, v2.2.

[91] Pells, George P., “Radiation Damage Effects in Alumina,” Science of Alumina, J. Am. Ceram. Soc. 77, 1994.

[92] Yano, Ichikawa, Akiyoshi, Tachi, “Neutron irradiation damage in aluminum oxide and nitride ceramics,” 226, Journal of Nuclear Materials, 1995.

[93] T. Y. K. Y. Thanataon Pornphatdetaudom, "Physical property changes of neutron-irradiated aluminum nitride and their recovery behavior by annealing using a step-heating dilatometer," *Nuclear Materials and Energy,* vol. 16, pp. 24-28, 2018.

[94] Interfacing Loads with TN in UP17, IDOM Corp., F4E_D_2RUEMA, v1.0.

[95] ISO 14644-1:2015, Cleanrooms and associated controlled environments - Part 1: Classification of air cleanliness by particle concentration.

[96] 55.GA UWAVS RF Notch Filter Prototype Low Power Test Report, 304242-R00031, Rev A, C8HGL8, V1.0.

[97] 55.GA UWAVS In-Vessel Shutter Test Plan,304242-N00009, Rev A, ITER_D_AW4WFF, v1.0.

[98] F4E, "F4E_D_2RUEMA v1.0 Interfacing Loads with TN in UP17".

[99] 55.GA (UWAVS-35) RAMI Analysis Report, ITER_D_WL78K6, v1.0.

[100] A. Ciampichetti and J. Guirao, IS-26.PH-55-001 Interface between Cooling Water System (PBS 26.PH) and Upper Port Systems (PBS 55.U0), ITER_D_33VYYN, v4.0.

[101] *Load Specifications, ITER-D-222QGL, v6.2.*

Released 2024/12/04

Released 2024/12/04

APPENDIX A
UWAVS SYSTEM DIAGRAMS

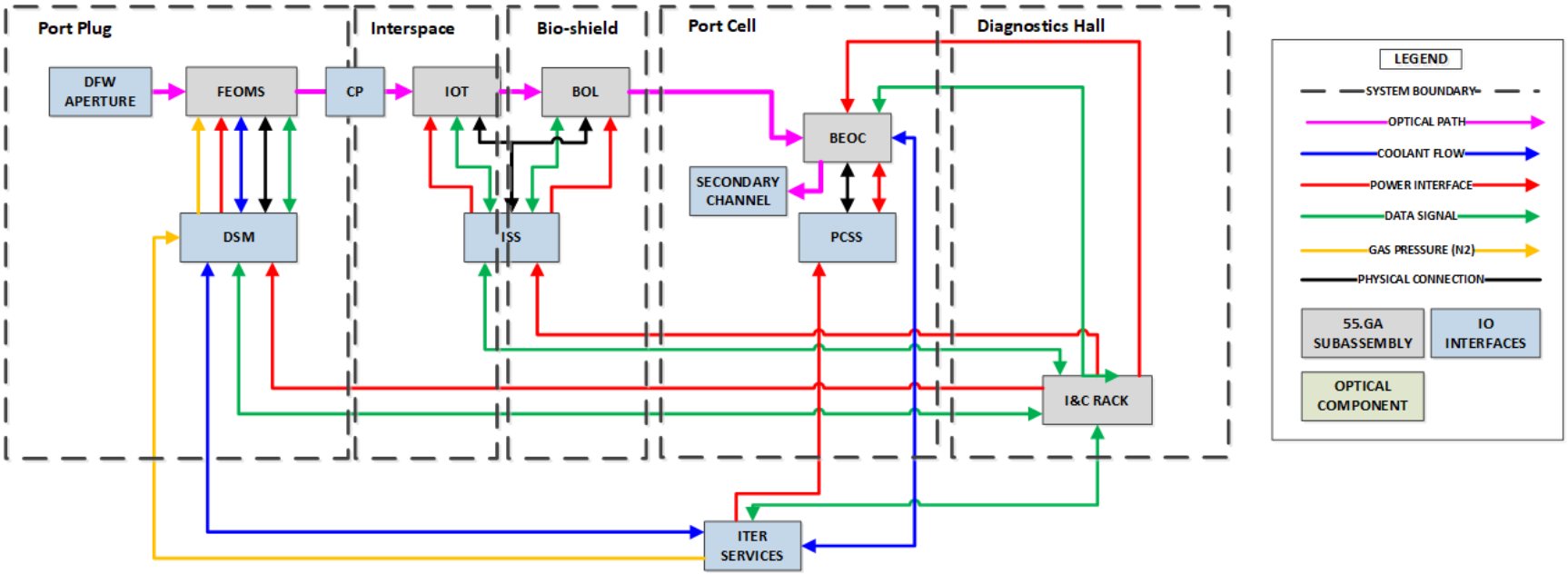

Figure 99. UWAVS system architecture.

Released 2024/12/04

Released 2024/12/04

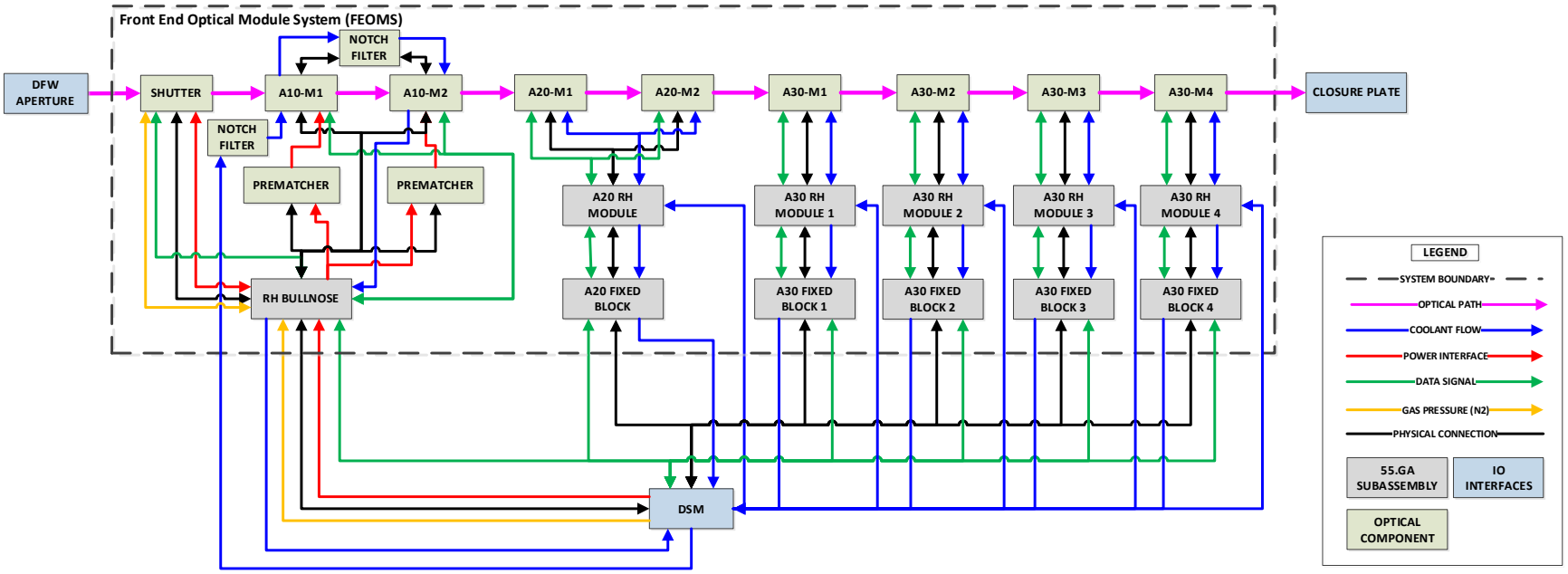

Figure 100. FEOMS decomposition and functional interfaces.

Released 2024/12/04

Released 2024/12/04

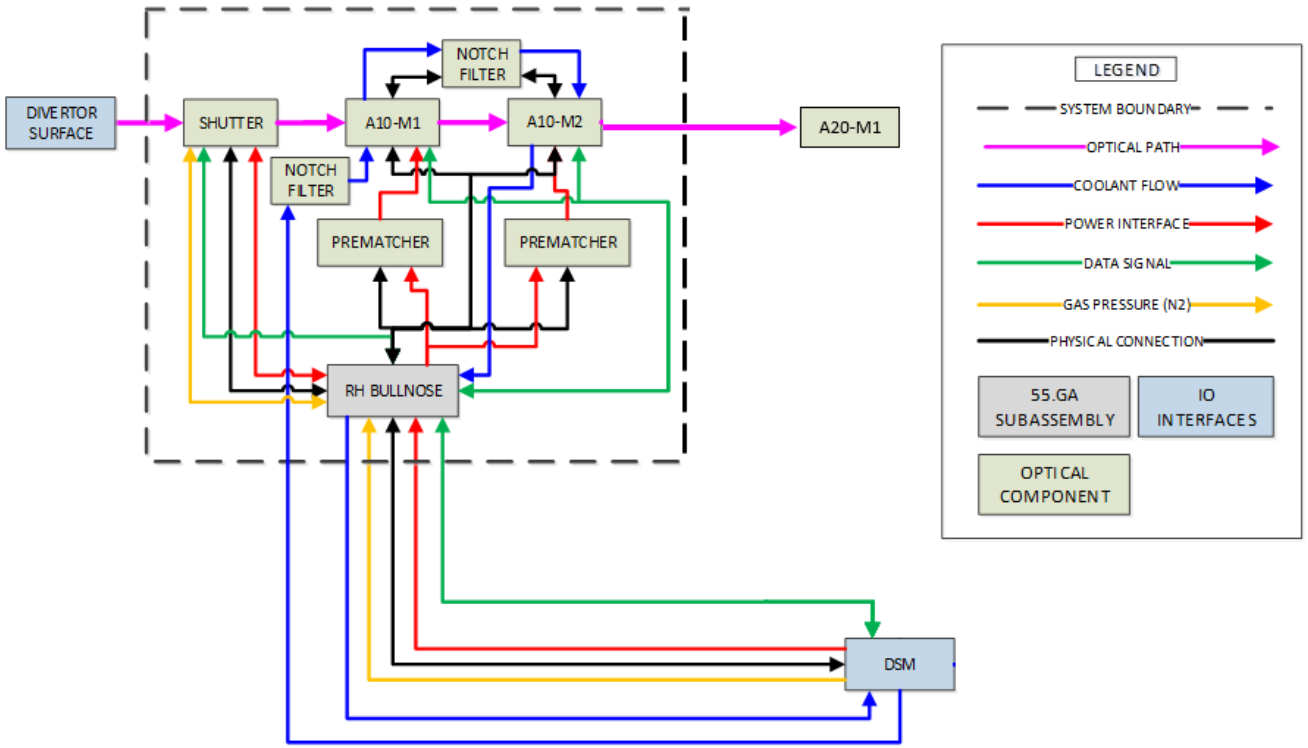

Figure 101. Bullnose decomposition and functional interfaces.

Released 2024/12/04

Released 2024/12/04

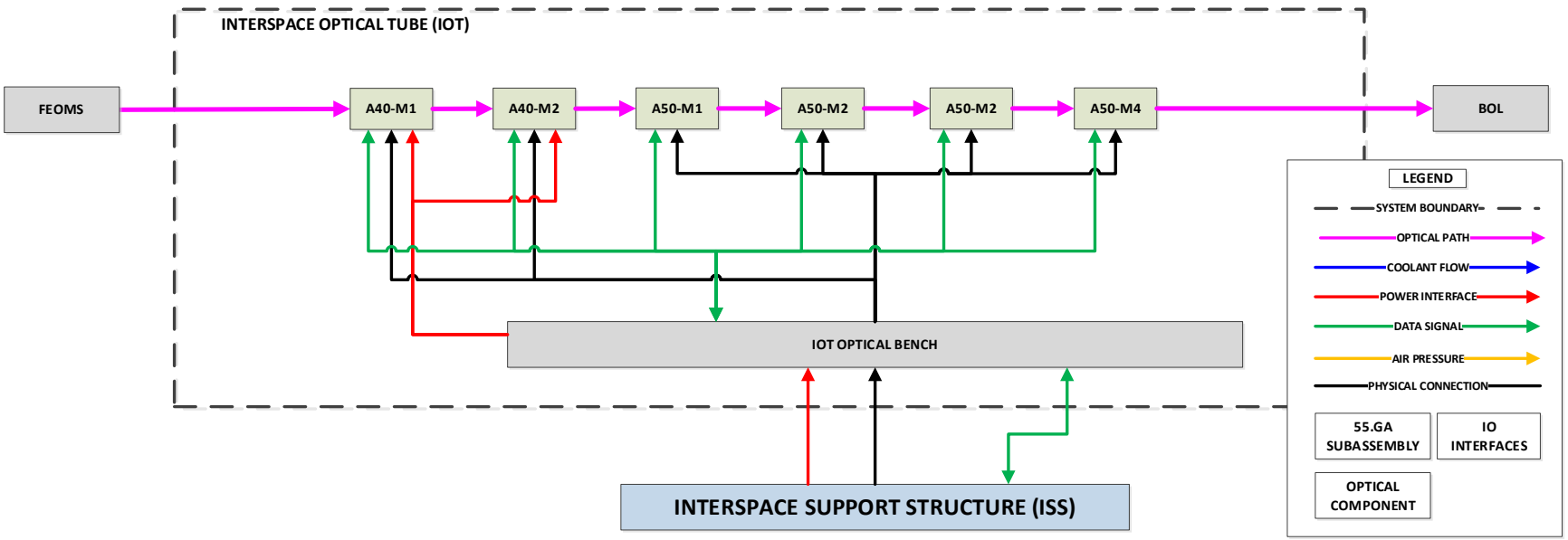

Figure 102. IOT decomposition and functional interfaces.

Released 2024/12/04

Released 2024/12/04

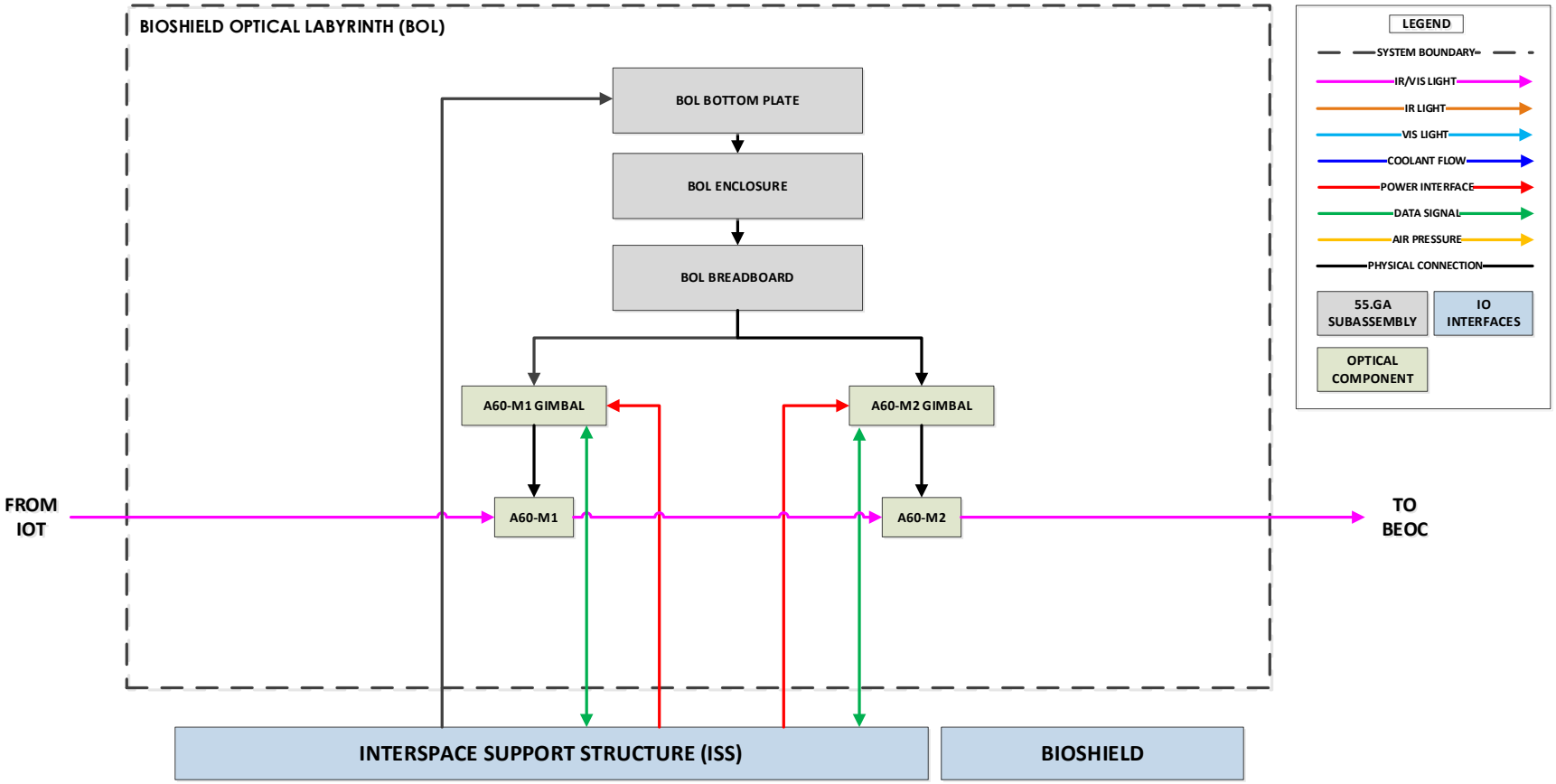

Figure 103. BOL decomposition and functional interfaces.

Released 2024/12/04

Released 2024/12/04

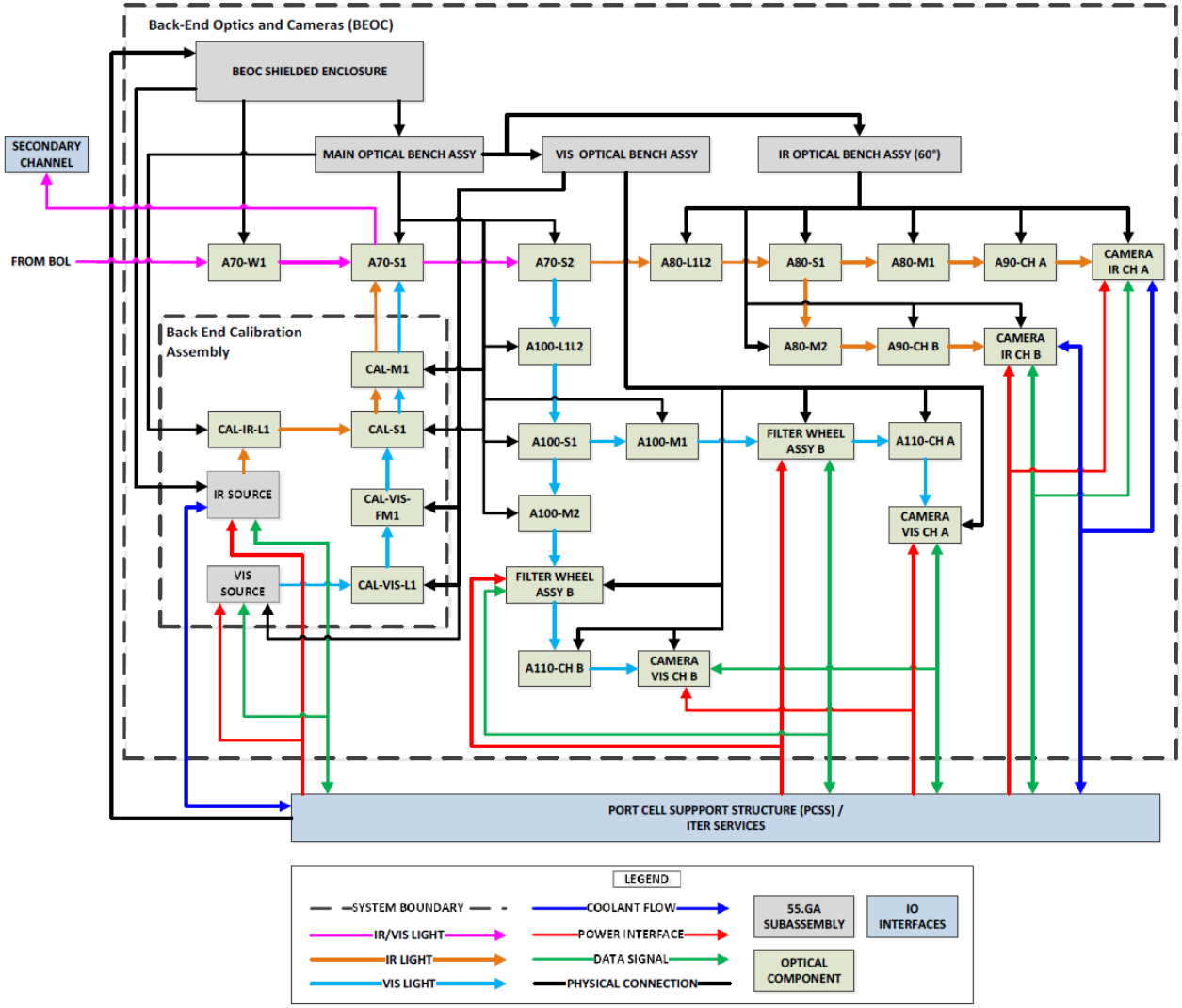

Figure 104. BEOC decomposition and functional interfaces.

Released 2024/12/04

Released 2024/12/04

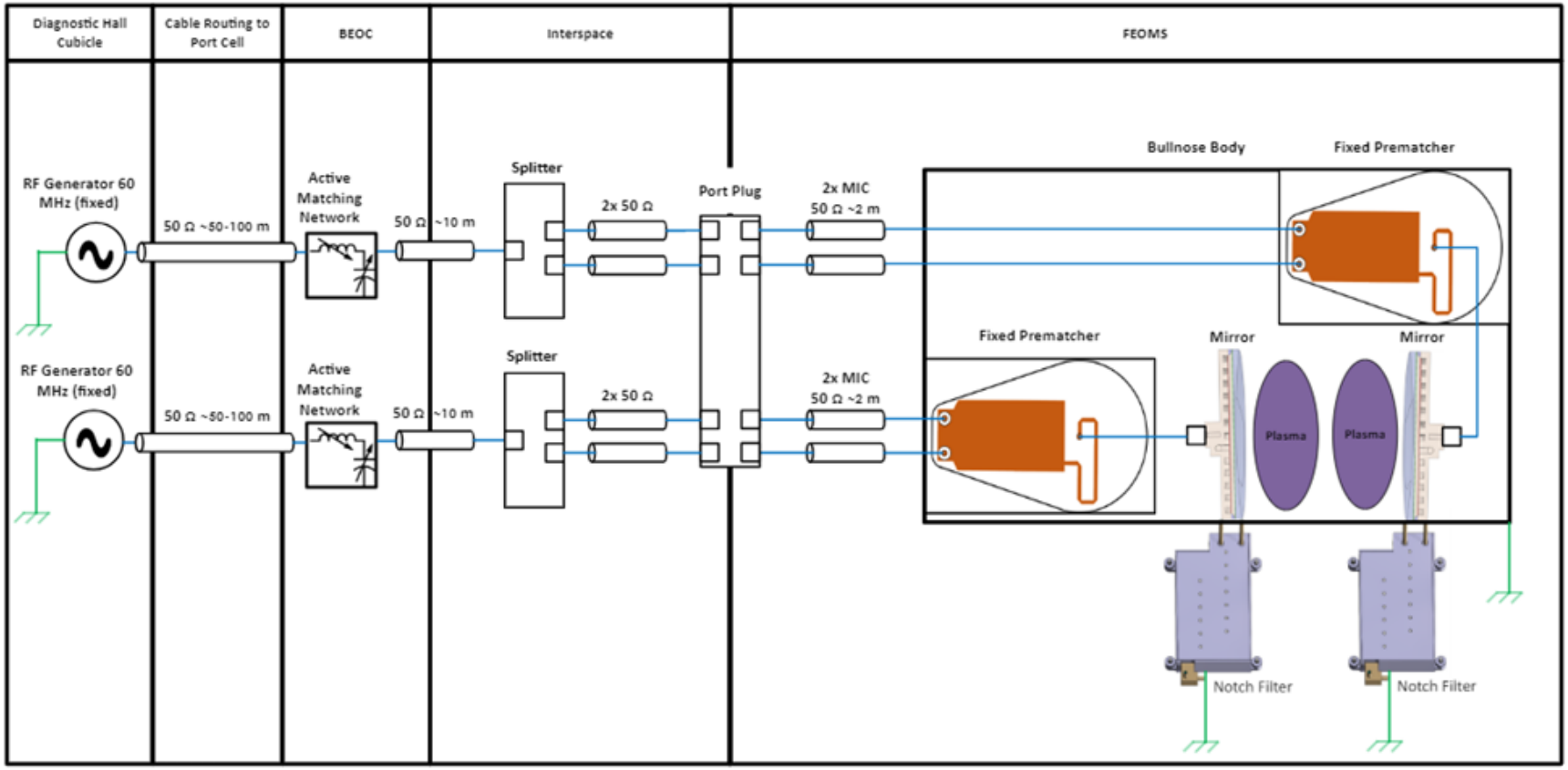

Figure 105. Simplified RF mirror cleaning system schematic.

✓Released 2024/12/04

✓Released 2024/12/04

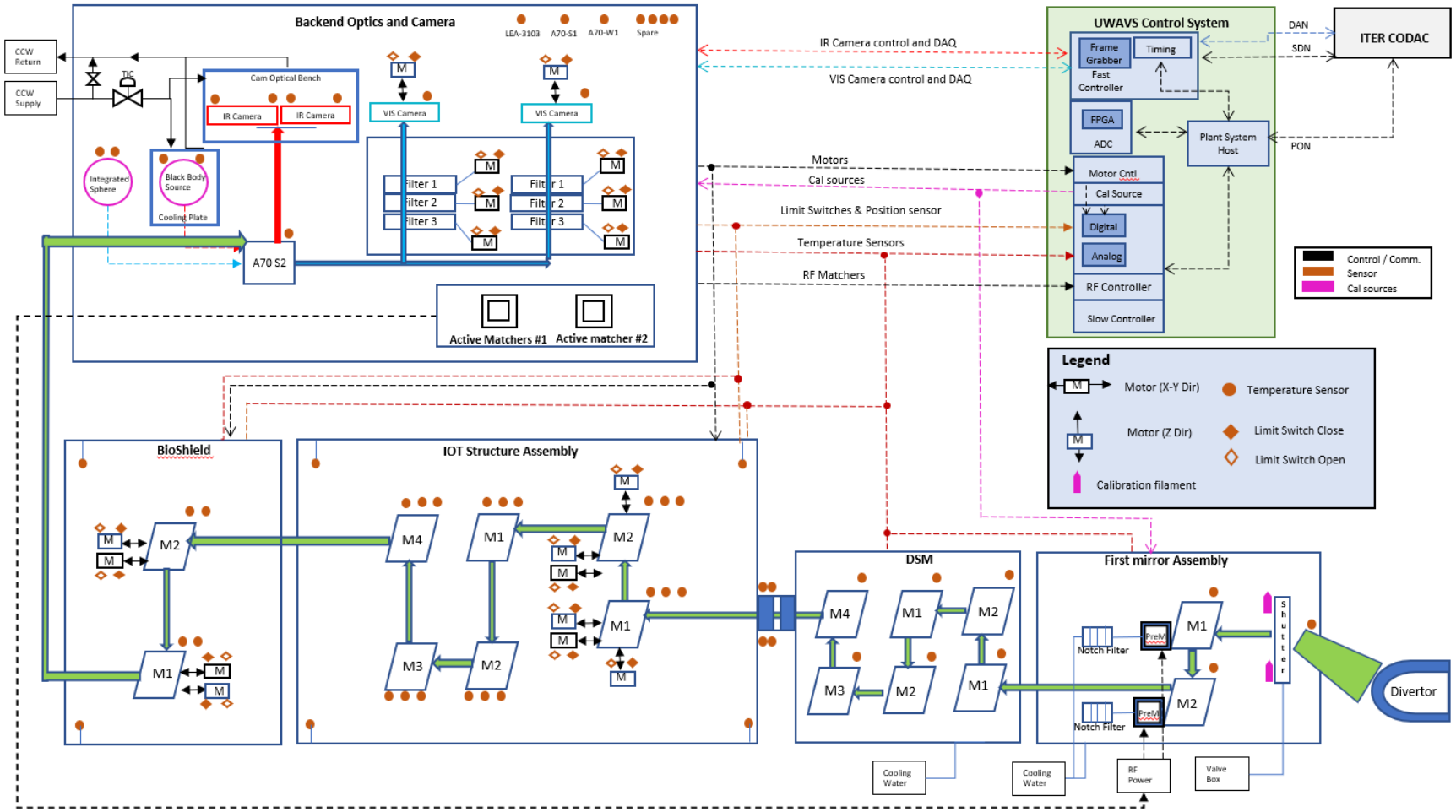

Figure 106. Illustration of the instrumentation and controls for 55.GA single port

Released 2024/12/04

Released 2024/12/04

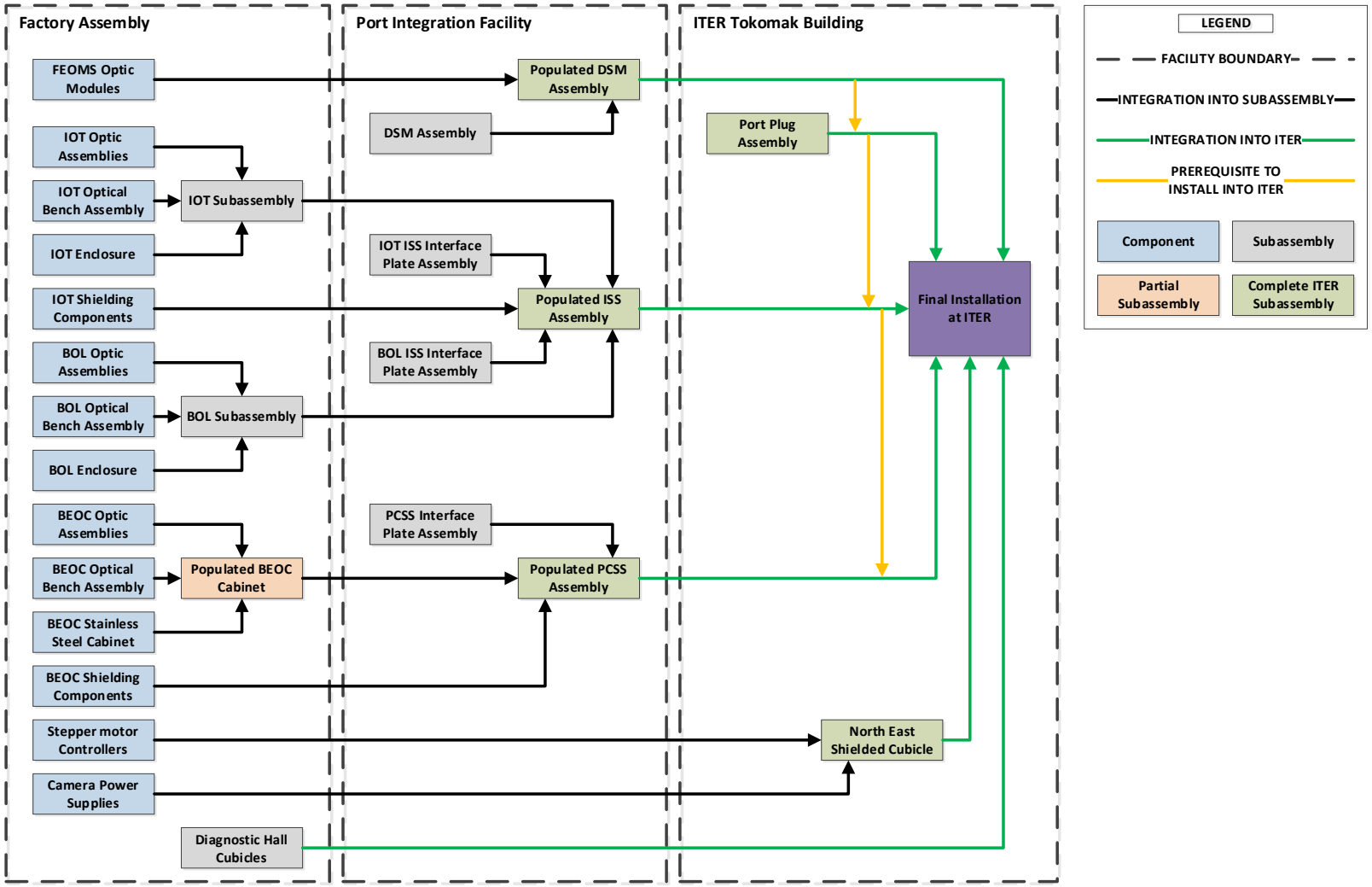

Figure 107. UWAVS installation process sequence.

Released 2024/12/04

Released 2024/12/04

APPENDIX B
OPTICALLY SIGNIFICANT INTERFACES

Table 45. Optically significant interfaces of the FEOMS

I/F #	INTERFACE DESCRIPTION
0	*ITER TGCS origin*
3	*UPP origin 1 to DSM origin*
A10.1	*DSM to A10 fixed module (FMU)*
A10.3	A10M1 Carrier Plate to A10M1 Mirror Weldment
A10.5	A10M1 Mirror Optical Surface tolerance
A10.8	A10M2 Carrier Plate to A10M2 Mirror Weldment
A10.10	A10M2 Mirror Optical Surface tolerance
A10.11	A10 Fixed Module (Starboard Side Bullnose Housing) to Aperture
A20.1	*DSM to A20 fixed module*
A20.2	A20 fixed module to removable module
A20.3	A20 removable module to A20M1 mirror mount
A20.6	A20M1 mirror optical surface tolerance
A20.7	A20 removable module to A20M2 mirror mount
A20.10	A20M2 mirror optical surface tolerance
A30M1.1	*DSM to A30M1 fixed module*
A30M1.2	Fixed module to removable module
A30M1.3	Removable module to mirror mount
A30M1.6	Mirror optical surface tolerance
A30M2.1	*DSM to A30M2 fixed module*
A30M2.2	Fixed module to removable module
A30M2.3	Removable module to mirror mount
A30M2.6	Mirror optical surface tolerance
A30M3.1	*DSM to A30M3 fixed module*
A30M3.2	Fixed module to removable module
A30M3.3	Removable module to mirror mount
A30M3.6	Mirror optical surface tolerance
A30M4.1	*DSM to A30M4 fixed module*
A30M4.2	Fixed module to removable module
A30M4.3	Removable module to mirror mount
A30M4.6	Mirror optical surface tolerance

Released 2024/12/04
Released 2024/12/04

Table 46. Optically significant interfaces of the IOT

I/F #	INTERFACE DESCRIPTION
ITER_TGCS_0	**ITER TGCS origin**
ISS_4	**IOT plate to IOT table top**
A40_M1_1	**Frame to assy bracket**
A40_M1_3	Piston bracket to tilt_y axis
A40_M1_4	Tilt_y axis to tilt_x axis
A40_M1_5	Tilt_x axis to mirror S2
A40_M1_6	Surface 1 tolerance
A40_M2_1	**Frame to assy bracket**
A40_M2_2	Assy bracket to piston bracket
A40_M2_3	Piston bracket to tilt_y axis
A40_M2_4	Tilt_y axis to tilt_x axis
A40_M2_5	Tilt_x axis to mirror S2
A40_M2_6	Surface 1 tolerance
A50M1_1	**Table to mount**
A50M1_3	KM groove to mirror mount pads
A50M1_4	Mirror mount pads to mirror S2
A50M1_5	Mirror S1 tolerance
A50M2_1	**Table to mount**
A50M2_3	KM groove to mirror mount pads
A50M2_4	Mirror mount pads to mirror S2
A50M2_5	Mirror S1 tolerance
A50M3_1	**Table to mount**
A50M3_3	KM groove to mirror mount pads
A50M3_4	Mirror mount pads to mirror S2
A50M3_5	Mirror S1 tolerance
A50M4_1	**Table to mount**
A50M4_3	KM groove to mirror mount pads
A50M4_4	Mirror mount pads to mirror S2
A50M4_5	Mirror S1 tolerance

Released 2024/12/04
Released 2024/12/04

Table 47. Optically significant interfaces of the BEOC

I/F #	INTERFACE DESCRIPTION
0	***ITER TGCS origin***
PCSS.1.1	***PPAD origin***
BEOC.1.5	***BEOC pedestal to main optical bench surface***
BEOC.1.6	***Main optical bench to angled IR bench surface***
BEOC.1.7	***Main optical bench to A100-M2 lower level bench surface***
BEOC.1.8	***Main optical bench to second level VIS bench surface***
A70-W1.1	***Shielding to window mount***
A70-W1.2	Window mount to optic
A70-W1.3	Mirror optical surface tolerance
A70-S1.1	***Optical bench to optic mount***
A70-S1.2	Optic mount to optic
A70-S1.3	Mirror optical surface tolerance
A70-S2.1	***Optical bench to optic mount***
A70-S2.2	Optic mount to optic cell
A70-S2.3	Optic cell to optic
A70-S2.4	Mirror optical surface tolerance
A80-L1L2.1	***Optical bench to optic mount***
A80-L1L2.2	Optic mount to lens stube
A80-L1L2.3	Optic mount to L1 surface 1 (L1S1)
A80-L1L2.4	Optic mount to L2 surface 1 (L2S1)
A80-L1L2.5	Mirror optical surface tolerance
A80-S1.1	***Optical bench to optic mount***
A80-S1.2	Optic mount to optic cell
A80-S1.3	Optic cell to optic
A80-S1.4	Mirror optical surface tolerance
A80-M1.1	***Optical bench to optic mount***
A80-M1.2	Optic mount to optic cell
A80-M1.3	Optic cell to optic
A80-M1.4	Mirror optical surface tolerance
A80-M2.1	***Optical bench to optic mount***
A80-M2.2	Optic mount to optic
A80-M2.3	Mirror optical surface tolerance
A90-L.1_A	***Optical bench to optic mount base***
A90-L.2_A	Mount base to lens tube
A90-L.3_A	Lens 1 to lens tube

Released 2024/12/04
Released 2024/12/04

I/F #	INTERFACE DESCRIPTION
A90-L.4_A	Lens 2 to lens tube
A90-L.5_A	Lens 3 to lens tube
A90-L.6_A	Lens 4 to lens tube
A90-L.7_A	Lens 5 to lens tube
A90-L.8_A	Lens 6 to lens tube
A90-L.9_A	Lens 7 to lens tube
A90-L.10_A	Lens 8 to lens tube
A90-L.11_A	Lens 9 to lens tube
A90-L.12_A	Lens 10 to lens tube
A90-L.1_B	***Optical bench to optic mount***
A90-L.2_B	Mount base to lens tube
A90-L.3_B	Lens 1 to lens tube
A90-L.4_B	Lens 2 to lens tube
A90-L.5_B	Lens 3 to lens tube
A90-L.6_B	Lens 4 to lens tube
A90-L.7_B	Lens 5 to lens tube
A90-L.8_B	Lens 6 to lens tube
A90-L.9_B	Lens 7 to lens tube
A90-L.10_B	Lens 8 to lens tube
A90-L.11_B	Lens 9 to lens tube
A90-L.12_B	Lens 10 to lens tube
A100-L1L2.1	***Optical bench to optic mount***
A100-L1L2.2	Optic mount to lens cell
A100-L1L2.3	Optic mount to L1 surface 1 (L1S1)
A100-L1L2.4	Optic mount to L2 surface 1 (L2S1)
A100-L1L2.5	Mirror optical surface tolerance
A100-S1.1	***Optical bench to optic mount***
A100-S1.2	Optic mount to optic cell
A100-S1.3	Optic cell to optic
A100-S1.4	Mirror optical surface tolerance
A100-M1.1	***Optical bench to optic mount***
A100-M1.2	Optic mount to optic cell
A100-M1.3	Optic cell to optic
A100-M1.4	Mirror optical surface tolerance
A100-M2.1	***Optical bench to optic mount***
A100-M2.2	Optic mount to optic cell
A100-M2.3	Optic cell to optic
A100-M2.4	Mirror optical surface tolerance

Released 2024/12/04
Released 2024/12/04

I/F #	INTERFACE DESCRIPTION
A110-L.1_A	***Optical bench to optic mount base***
A110-L.2_A	Mount base to lens tube
A110-L.3_A	Lens 1 to lens tube
A110-L.4_A	Lens 2 to lens tube
A110-L.5_A	Lens 3 to lens tube
A110-L.6_A	Lens 4 to lens tube
A110-L.7_A	Lens 5 to lens tube
A110-L.8_A	Lens 6 to lens tube
A110-L.9_A	Lens 7 to lens tube
A110-L.10_A	Lens 8 to lens tube
A110-L.11_A	Lens 9 to lens tube
A110-L.1_B	***Optical bench to optic mount***
A110-L.2_B	Mount base to lens tube
A110-L.3_B	Lens 1 to lens tube
A110-L.4_B	Lens 2 to lens tube
A110-L.5_B	Lens 3 to lens tube
A110-L.6_B	Lens 4 to lens tube
A110-L.7_B	Lens 5 to lens tube
A110-L.8_B	Lens 6 to lens tube
A110-L.9_B	Lens 7 to lens tube
A110-L.10_B	Lens 8 to lens tube
A110-L.11_B	Lens 9 to lens tube

Released 2024/12/04
Released 2024/12/04

APPENDIX C
RESPONSES TO COMMENTS ON REV A

Page	Comment	Reviewer	Response	Document update
8	i recommend this version for PDR. For the next update, please consider this following comments: table4, I suppose the double barriers window assembly will be used. The IO design is a PIC/SIC-1 window assembly. Outer barrier is not separately classified as SIC-2. For window seismic classification, please define it as "SC1(S)" For safety valve seismic classification, please define it as "SC1(SF)"	Liu	Updated Table 4 per comments to align with latest guidance.	Section 3
86	Figure 71 refers to in-vessel calibration and illumination sources as one of the pre-requisites for the UWAVS commissioning. While this in-vessel vis/IR illumination/calibration source will be probably available at some point, it is currently much less certain that it will be available for before the start of Research Operation, and UWAVS should prepare alternative commissioning strategy.	Kocan	Understood on the availability of an in-vessel VIS/IR calibration source at the time of system commissioning. An alternate strategy will be evaluated in final design as required.	Comment Only
91	i recommend this version for PDR. For the next update, please consider this following comments: chap14.1, for the fire load from 55.GA, please assess if the fire load density and fire load design are complying with the requirements in Guideline for implementation of the PCR-1103 related to the fire loads management in the Port Cells (WM7PYF)	Liu	Section 14.1 will be updated in final design to include fire load densities per WM7PYF(v2.2) Section 6.1.1. Specifically tables 35 through 37 can be updated to quantify densities are with allowable limits.	Comment Only

✓Released 2024/12/04
✓Released 2024/12/04

Page	Comment	Reviewer	Response	Document update
110	Section 14.18: the assumption that interspace and port cell are at ISO Class 7 cleanliness level is not realistic as these areas (as well as the hot cell) are not designed as cleanrooms. So the pre-requisites made in the design to limit the dust ingress in the optical path, combined with periodic/opportunistic maintenance (i.e. dust removal from the ISS/PCSS optics by a portable clean dry air) look reasonably well justified to mitigate the risk.	Kocan	Understood and thank you for the clarification on the cleanliness levels expected in the PC/IS/HC. Efforts will be made in final design to prevent dust ingress by either CDA, hermetically sealed enclosures, dust blocks, or a combination of all. In addition, dust mitigation will be considered in detail for installation and maintenance in the PIF and hot cell.	Comment Only
General	Below are IO IDM UID references to documents listed in the Reference section: 1. Reference-1, In-vessel SIR: 55.GA (UWAVS-35) Structural Integrity Report for UP2, 8, 11, and 14 for In-Vessel (WL5TZ6 v2.0) (current) 2. Reference-2, Ex-vessel SIR: 55.GA (UWAVS-35) Structural Integrity Report for UP2, 8, 11, and 14 for Ex-Vessel (APHWM7 v2.0) 3. Reference-45, Tolerance Stack Summary: 55.GA UWAVS Mechanical Tolerance Stack Summary (C8DFNH v1.0) 4. Reference-51, Calibration Plan ppt: 55.GA UWAVS PDR Presentation - Temperature Measurement Approach and Calibration Strategy (C8HP3D v1.0) (current) 5. Reference-67, UWAVS2 FAT Test Plan : 55.GA UWAVS Bertin Factory Acceptance Test (FAT) Plan (AU4385 v1.0) (current) 6. Reference-96. Notch Filter Low Power Test Report: 55.GA UWAVS Test Report for Radio Frequency (RF) Notch Filter Prototype Low Power (C8HGL8 v1.0) (current)	Martin	Updated reference table with IO IDM UID numbers.	References

✓Released 2024/12/04
✓Released 2024/12/04

Page	Comment	Reviewer	Response	Document update
General	Mature enough for PDR level. Proposed updates in fast change mode: - No information on camera model pre-selection, please clarify what are the current assumptions and specifications for selection of cameras or provide a reference to a support design specification document if existing. - Please provide IO IDM UIDs for all refenced documents. For next phase: - Some tables with numbers without units, please check and update when needed. - Details of calculations, etc. to be put in annexes, just keep key results, conclusions and references to support documents in the main text.	Martin	Document will be updated in final design to implement changes per comments. - Added preliminary camera models to I&C Section 10. - References have been updated with IO IDM UIDs. - Will review and revise tables with units. - Will update format moving detailed calculations to appendices, keeping key results in main content.	Section 10 References Comment Only

✓Released 2024/12/04

✓Released 2024/12/04

✓Released 2024/12/04

✓Released 2024/12/04

GENERAL ATOMICS